LIBRARY Michigan State University

PLACE IN RETURN BOX to remove this checkout from your record. TO AVOID FINES return on or before date due.

DATE DUE	DATE DUE	DATE DUE

MSU Is An Affirmative Action/Equal Opportunity Institution ctclrctdatedus.pm3-p.;

NEW SYNTHETIC APPROACHES TO REACTIVE MIXED-LIGAND COMPLEXES AT THE INTERFACE OF COORDINATION AND ORGANOMETALLIC CHEMISTRY

Ву

Sue-Jane Chen

A DISSERTATION

submitted to
Michigan State University
in partial fulfillment of the requirement
for the degree of

DOCTOR OF PHILOSOPHY

Department of Chemistry
1991

ABSTRACT

NEW SYNTHETIC APPROACHES TO REACTIVE MIXED-LIGAND COMPLEXES AT THE INTERFACE OF COORDINATION AND ORGANOMETALLIC CHEMISTRY

bу

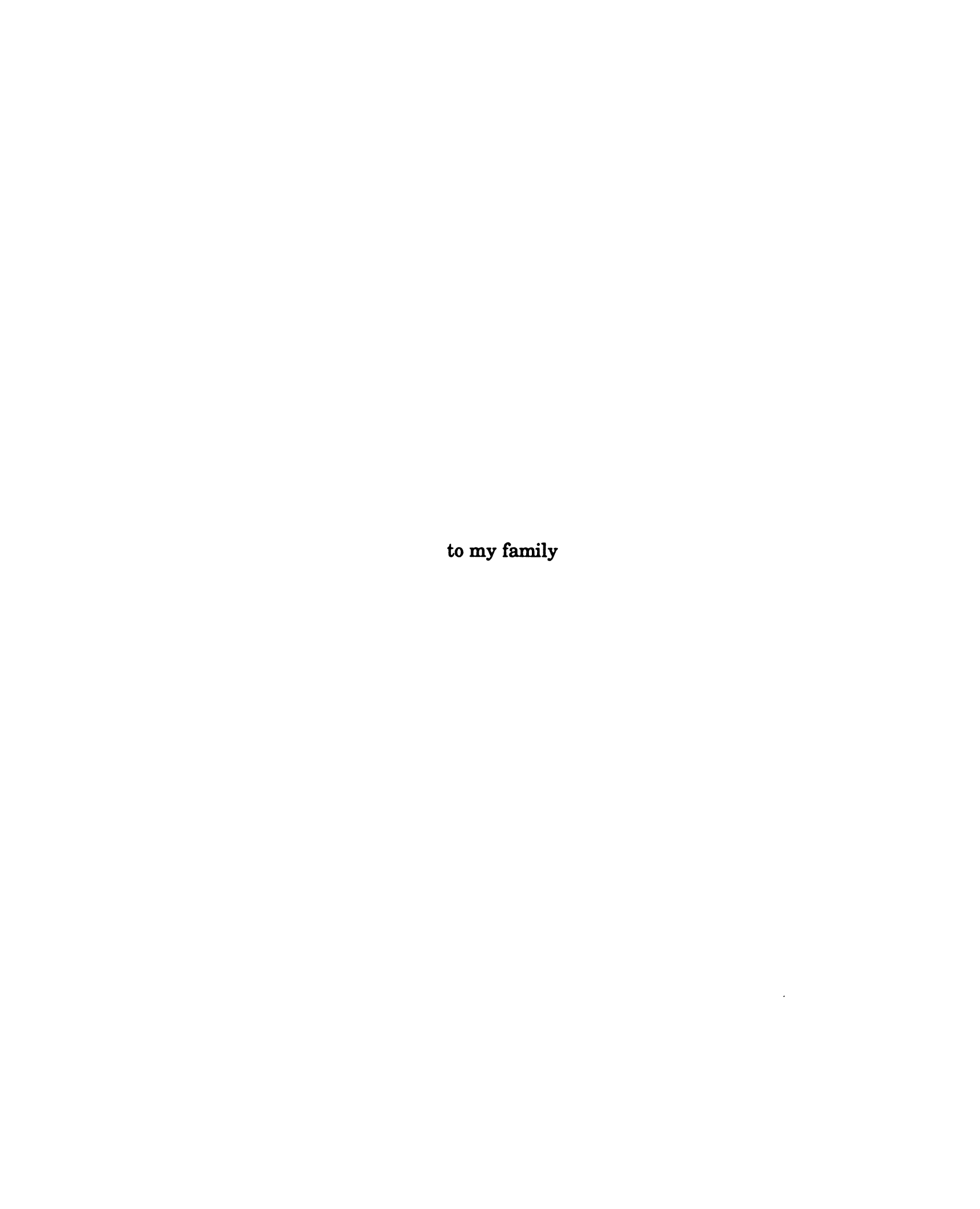
Sue-Jane Chen

The historic distinction between organometallic and coordination chemistry is becoming less clear, and links between 'classical' organometallic and coordination chemistry have recently emerged in the form of organometallic compounds with ancillary donor ligands such as halides, nitrenes and alkoxide ligands. These new classes of compounds demonstrate the ability of soft π -acceptor ligands such as CO to bond to a metal in the presence of relatively extreme ligand environments.

In an effort to unite the two areas of chemistry, we investigated reactions between multiply bonded metal-metal $(M^{\underline{n}}M)$ dinuclear complexes, namely, 'highly early transition metals' and trinuclear carbonyl clusters, namely low valent late transition metals'. We initiated these studies by the reaction between $Re_2Cl_4(dppm)_2$ ($Re^{\underline{3}}Re$) (dppm =

Ph₂PCH₂PPh₂) and the electronically and coordinatively unsaturated molecule $H_2Os_3(CO)_{10}$ in the presence H_2 , work that resulted in the isolation of the novel bridging hydride dirhenium species $Re_2(\mu-H)(\mu-Cl)Cl_2(CO)_2(dppm)_2$. The compound $Re_2(\mu-H)(\mu-Cl)Cl_2(CO)_2(dppm)_2$ exhibits a rich redox activity, with four redox couples representing two oxidations and two reductions being observed in the cyclic voltammegram. A new carbonyl halide cluster, $Ru_3(CO)_8(Cl)_2(PBu_3^n)_2$, was synthesized from the reaction between the multiply bonded dirhenium complex $Re_2Cl_6(PBu_3^n)_2$ (Re^4 Re) and $Ru_3(CO)_{12}$. These results demonstrate the feasibility of preparing mixed ligand complexes by ligand transfer reactions between two entirely different metal systems; this new synthetic approach provides a promising opportunity for the syntheses of unusual coordination and organometallic compounds.

In a second area of investigation, our study of TMPP chemistry with dinuclear metal-metal bonded systems led to the discovery of unsymmetrical complexes containing an unusual bridging phenoxy-phosphine ligand. The phosphine ligand, TMPP also exhibits novel chemistry with trinuclear cluster complexes. In the chemistry of Group 8 carbonyls of Fe, Ru and Os, we observed facile cluster transformations under extraordinarily mild conditions compared to all previously reported phosphine reactions of these systems. Key results such as facile P-C bond activation by intramolecular oxidative addition and cyclometallation in the triruthenium system, and demethylation of the phosphine to give an open trinuclear phenoxy-phosphine cluster in the triosmium system are presented and discussed.



ACKNOWLEDGES

I woulk like to express my sincere gratitude to my research advisor, Professor Kim R. Dunbar, for her guidance, support and assistance during my graduate study; as the first group member, I especially appreciate the experience of growing up with the group under her inspiration, encouragement and hard work throughout these years. In particular, I wish to say many thanks for her time and patience in helping me with my project and the accomplishment of dissertation.

To all of my group members, Steve Haefner, Anne Quillevéré, Alice Sun, Stuart Bartley, Stacey Berstein, Garry Finniss, John Matonic, Julia Clements, Helen Chifotides, I woulk like to say many thanks for sharing lots of good time with me, and enduring my 'mood shits' in these years.

('Hi, Dudes, I love you!')

In particular, I wish to express my deep appreciation to John Matonic and 'TMPP patrol' (Steve Haefner, Anne Quillevéré and Alice Sun) for their assistance in my work.

Finally, I would like to thank my parents, my sister and brother; their love, concerns and understanding have always been the radiant support for me on this way.

TABLE OF CONTENTS

	Page
LIST OF TABLES	xiv
LIST OF FIGURES	xviii
LIST OF ABBREVIATIONS	xxvii
CHAPTER I. INTRODUCTION	1
CHAPTER II. REACTIONS OF TRIPLY BONDED DIRHENIUM	
COMPLEXES WITH TRINUCLEAR CARBONYL	
CLUSTERS	28
1. Introduction	29
2. Experimental	30
A. Synthesis	30
(1) Preparation of $Re_2(\mu-H)(\mu-Cl)Cl_2(CO)_2(dppm)_2$	30
(i) Reaction of $Re_2Cl_4(dppm)_2$ with $(\mu-H)_2Os_3(CO)_{10}$	
in the presence of H ₂	30
(ii) Reaction of Re ₂ Cl ₄ (dppm) ₂ with Os ₃ (CO) ₁₂ in the	
presence of H ₂	31
(iii) Reaction of Re ₂ Cl ₄ (dppm) ₂ with Ru ₃ (CO) ₁₂ in the	
presence of H ₂	31
(iv) Reaction of Re ₂ Cl ₄ (dppm) ₂ with an H ₂ /CO gas	
mixture	32

		1	Page
		(v) Reaction of $Re_2Cl_4(dppm)_2$ with $(\mu-H)_2Os_3(CO)_{10}$	
		in the absence of H ₂	32
		(vi) Reaction of Re ₂ Cl ₄ (dppm) ₂ with NaBH ₄ in the	
		presence of CO	33
		(vii) Reaction of Re2Cl4(dppm)2 with NaH in the	
		presence of CO	33
		(2) Reaction of $Re_2(\mu-H)(\mu-Cl)Cl_2(CO)_2(dppm)_2$ with one	
		equivalent of NOBF ₄	34
		(3) Reaction of $Re_2(\mu-H)(\mu-Cl)Cl_2(CO)_2(dppm)_2$ with an	
		excess of NOBF ₄	34
		(4) Reaction of $Re_2(\mu-H)(\mu-Cl)Cl_2(CO)_2(dppm)_2$ with	
		cobaltocene	34
		(5) Electrochemical Oxidation of	
		$Re_2(\mu\text{-H})(\mu\text{-Cl})Cl_2(CO)_2(dppm)_2 $	35
		(6) Electrochemical Reduction of	
		$Re_2(\mu\text{-}H)(\mu\text{-}Cl)Cl_2(CO)_2(dppm)_2 $	36
	B.	X-ray Crystal Structures	36
		(1) $Re_2(\mu-H)(\mu-Cl)Cl_2(CO)_2(dppm)_2$	36
		(2) $[Re_2(\mu-H)(\mu-Cl)Cl_2(CO)_2(dppm)_2](BF_4)$	38
		(3) $[Re_2(\mu\text{-CO})(\mu\text{-Cl})Cl_2(CO)(NO)(dppm)_2](BF_4)$	39
		(4) $Re_2(\mu\text{-Cl})(\mu\text{-CO})Cl_2(CO)_2(dppm)_2$	40
3.	Res	ults and Discussion	41
	A.	Synthesis	41
	B.	Spectroscopic Studies	46
	C.	Redox Chemistry	53

			Page
		(i) Electrochemical and Chemical Oxidation	62
		(ii) Electrochemical and Chemical Reduction	68
	D.	Molecular Structures	69
		(1) $\operatorname{Re}_2(\mu-H)(\mu-Cl)\operatorname{Cl}_2(CO)_2(\operatorname{dppm})_2$	69
		(2) $[Re_2(\mu-H)(\mu-Cl)Cl_2(CO)_2(dppm)_2](BF_4)$	70
		$(3) [Re_2(\mu\text{-CO})(\mu\text{-Cl})Cl_2(CO)(NO)(dppm)_2](BF_4) $	71
		$ (4) [Re_2(\mu\text{-}Cl)_2Cl_2(CO)_2(dppm)_2](BF_4) \\$	71
4.	Sur	nmary	72
CHAP	rer	III. REACTIONS OF QUADRUPLY BONDED	
		DINUCLEAR HALIDE COMPLEXES WITH	
		TRINUCLEAR CARBONYL CLUSTERS	98
1.	Inti	roduction	99
2.	Exp	perimental	100
	A.	Synthesis	100
		(1) Reaction of $Ru_3(CO)_{12}$ with $Re_2Cl_6(PBu_3^n)_2$	100
		(2) Reaction of $(\mu-H)_2Os_3(CO)_{10}$ with $(n-Bu_4N)_2Re_2Cl_8$	100
	B.	X-ray Crystal Structure of $Ru_3(CO)_8(\mu-Cl)_2(PBu_3^n)_2$	101
3.	Res	ults and Discussion	102
	A.	Synthetic Methods	102
	B.	Molecular Structure	104
4.	Sun	nmary	109

				Page
СНАРТ	ER	IV.	REACTIONS OF THE MULTIFUNCTIONALIZED	
			PHOSPHINE LIGAND TRIS(2,4,6-	
			TRIMETHOXYPHENYL)PHOSPHINE WITH	
			DINUCLEAR METAL CARBOXYLATE	
			COMPLEXES	110
1.	Inti	rodu	ction	111
2.	Exp	erin	nental	115
	Α.	Syı	nthesis	115
		(1)	Reaction of Rh ₂ (O ₂ CCH ₃) ₄ (MeOH) ₂ with TMPP	115
			(i) Synthesis of Rh ₂ (O ₂ CCH ₃) ₃ (TMPP-O)(MeOH)	115
			(ii) Chemical Oxidation of	
			$Rh_2(O_2CCH_3)_3(TMPP-O)(MeOH)$	116
		(2)	Preparation of Mo ₂ (O ₂ CCF ₃) ₄	116
		(3)	Reaction of Mo ₂ (O ₂ CCF ₃) ₄ with TMPP	117
		(4)	Preparation of Rh ₂ (O ₂ CCF ₃) ₄	117
		(5)	Reaction of Rh ₂ (O ₂ CCF ₃) ₄ with TMPP	118
	B.	X-1	ray Crystal Structure of	
		Rh	₂ (O ₂ CCH ₃) ₃ (TMPP-O)(MeOH)	118
3.	Res	ults	and Discussion	119
	(1).	Rea	action of Rh ₂ (O ₂ CCH ₃) ₄ (MeOH) ₂ with TMPP	119
		A.	Synthesis	119
		B.	Spectroscopic Studies	120
		C.	Molecular Structure of	
			Rh ₂ (O ₂ CCH ₃) ₃ (TMPP-O)(MeOH)	129
		n	Rodow Chomistry	130

			Page
	(2).	Reactions of $M_2(O_2CCF_3)_4$ (M = Mo, Rh) with TMPP	155
	(3).	Reactions of $[M_2(O_2CCH_3)_2(NCMe)_6](BF_4)_2$ (M = Mo, Rh)	
		with TMPP	165
	(4).	Reactions of [Mo ₂ (NCMe) ₁₀](BF ₄) ₄ with TMPP	166
4.	Sur	nmary	166
CHAP	rer	V. REACTIONS OF TRIS(2,4,6-TRIMETHOXY-	
		PHENYL)PHOSPHINE WITH TRINUCLEAR	
		CARBONYL CLUSTERS	167
1.	Int	roduction	168
2.	Exp	perimental	170
	A.	Synthesis	170
		(1) Reaction of Fe ₃ (CO) ₁₂ with TMPP	170
		(2) Preparation of Ru ₃ (CO) ₁₁ (NCMe)	171
		(3) Reaction of Ru ₃ (CO) ₁₁ (NCMe) with TMPP	171
		(4) Preparation of Ru ₃ (CO) ₁₀ (NCMe) ₂	172
		(5) Reaction of Ru ₃ (CO) ₁₀ (NCMe) ₂ with TMPP	172
		(6) Preparation of $(\mu-H)_2Os_3(CO)_{10}$	173
		(7) Reaction of $(\mu-H)_2Os_3(CO)_{10}$ with TMPP	173
		(8) Preparation of Os ₃ (CO) ₁₁ (NCMe)	174
		(9) Reaction of Os ₃ (CO) ₁₁ (NCMe) with TMPP	174
		(10) Preparation of Os ₃ (CO) ₁₀ (NCMe) ₂	175
		(11) Reaction of Os ₃ (CO) ₁₀ (NCMe) ₂ with TMPP	175
	B.	X-ray Crystal Structure	176
		(1) [HFe ₃ (CO) ₁₁][HTMPP]	176

	Page
(2) $Ru_3(\mu\text{-CO})_2(CO)_6[\mu_3-\eta^2\text{-C}_6H_2(OMe)_3][\mu$ -	
$P{C_6H_2(OMe)_3}_2$]	177
(3) $Os_3(\mu\text{-OH})_2(CO)_9(TMPP)$	178
(4) $Os_3(\mu\text{-OH})(CO)_9(\mu\text{-}\eta^2\text{-TMPP-}O)$	179
3. Results and Discussion	180
(1) Triiron carbonyl clusters	180
A. Synthesis and Characterization	180
B. Molecular Structure	182
(2) Triruthenium carbonyl clusters	193
A. Synthesis and Characterization	193
B. Molecular Structure	207
(3) Reactions of Triosmium Carbonyl Clusters	217
A. Synthesis and Characterization	217
B. Molecular Structure	233
(i) $Os_3(\mu\text{-OH})_2(CO)_9(TMPP)$	233
(ii) $Os_3(\mu\text{-OH})(CO)_9(\mu\text{-}\eta^2\text{-TMPP-}O)$	238
4. Summary	238
CHAPTER VI. CONCLUDING REMARKS	245
REFERENCES	248
APPENDICES	263

LIST OF TABLES

		Page
1.	¹ H NMR data of phosphine (TMPP) and phosphonium salts (in	
	CDCl ₃)	22
2.	Various synthetic approach in the preparation of	
	$Re_2(\mu\text{-H})(\mu\text{-Cl})Cl_2(CO)_2(dppm)_2. \qquad$	43
3.	Crystal data for $Re_2(\mu-H)(\mu-Cl)Cl_2(CO)_2(dppm)_2$ (1) and $Re_2(\mu-H)(\mu-Cl)Cl_2(CO)_2(dppm)_2$	
	H)(μ -Cl)Cl ₂ (CO) ₂ (dppm) ₂ ·MeCN (2)	78
4.	Selected bond distances (Å) and angles (deg) for	
	$Re_2(\mu-H)(\mu-Cl)Cl_2(CO)_2(dppm)_2$ (1) and	
	$Re_2(\mu-H)(\mu-Cl)Cl_2(CO)_2(dppm)_2\cdot MeCN \ \ \textbf{(2)}.$	79
5.	Crystal data for $[Re_2(\mu-H)(\mu-Cl)Cl_2(CO)_2(dppm)_2](BF_4)$ (3) and	
	$[Re_2(\mu\text{-CO})(\mu\text{-Cl})Cl_2(CO)(NO)(dppm)_2](BF_4)$ (4)	86
6.	Selected bond distances (Å) and angles (deg) for	
	$[Re_2(\mu-H)(\mu-Cl)Cl_2(CO)_2(dppm)_2](BF_4). \qquad$	87
7.	Selected bond distances (Å) and angles (deg) for	
	[Re ₂ (μ -CO)(μ -Cl)Cl ₂ (CO)(NO)(dppm) ₂](BF ₄)	94

		Page
8.	Crystal data for the disordered structure formulated as "Re ₂ Cl ₄ (CO) ₂ (dppm) ₂ ".	95
9.	Crystal data for Ru ₃ (μ-Cl) ₂ (PBu ₃ ⁿ) ₂ (CO) ₈	105
10.	Selected bond distances (Å) and angles (deg) for	106
	$Ru_3(\mu-Cl)_2(PBu_3^n)_2(CO)_8.$	106
11.	Crystal data for Rh ₂ (O ₂ CCH ₃) ₃ (TMPP-O)(MeOH)	141
12.	Selected bond distances (Å) and angles (deg) for	1.40
	$Rh_2(O_2CCH_3)_3(TMPP-O)(MeOH).$	142
13.	Bridging v(CO) stretches for various $[HFe_3(CO)_{11}]^-$ salts	183
14.	Crystal data for [HTMPP][Fe $_3(\mu$ -H)(μ -CO)(CO) $_{10}$]	187
15.	Selected bond distances (Å) and angles (deg) for [HTMPP][Fe $_3$ (μ -	
	H)(μ-CO)(CO) ₁₀]	188
16.	Crystal data for $Ru_3(\mu - CO)_2(CO)_6\{\mu_3 - \eta^2 - C_6H_2(OMe)_3\}[\mu - G_6H_2(OMe)_3]$	
	$P\{C_6H_2(OMe)_3\}_2].$	209
17.	Selected bond distances (Å) and angles (deg) for	
	$Ru_3(\mu-CO)_2(CO)_6\{\mu_3-\eta^2-C_6H_2(OMe)_3\}[\mu-P\{C_6H_2(OMe)_3\}_2].$	210

		Page
18.	Crystal data for $Os_3(\mu\text{-OH})_2(CO)_9(TMPP)$ (1) and	
	$Os_3(\mu-OH)(CO)_9(\mu-\eta^2-TMPP-O)$ (2).	234
19.	Selected bond distances (Å) and angles (deg) for	
	$Os_3(\mu\text{-OH})_2(CO)_9(TMPP)$.	235
20.	Selected bond distances (Å) and angles (deg) for	
	$Os_3(\mu\text{-OH})(CO)_9(\mu\text{-}\eta^2\text{-TMPP-}O).$	240
21.	Atomic positional parameters (\mathring{A}^2) and their estimated standard	
	deviations for $Re_2(\mu-H)(\mu-Cl)Cl_2(CO)_2(dppm)_2$	266
22.	Atomic positional parameters (\mathring{A}^2) and their estimated standard	
	deviations for $[Re_2(\mu-H)(\mu-Cl)Cl_2(CO)_2(dppm)_2](BF_4)$	267
23.	Atomic positional parameters (\mathring{A}^2) and their estimated standard	
	deviations for [Re $_2(\mu\text{-CO})(\mu\text{-Cl})\text{Cl}_2(\text{CO})(\text{NO})(\text{dppm})_2](BF_4)$	270
24.	Atomic positional parameters (\mathring{A}^2) and their estimated standard	
	deviations for $Ru_3(\mu-Cl)_2(PBu_3^n)_2(CO)_8$	272
25.	Atomic positional parameters (\mathring{A}^2) and their estimated standard	
	deviations for Rh ₂ (O ₂ CCH ₃) ₃ (TMPP-O)(MeOH)	273

		Page
26.	Atomic positional parameters (\mathring{A}^2) and their estimated standard	
	deviations for [HTMPP][Fe $_3(\mu\text{-H})(\mu\text{-CO})(CO)_{10}$]	276
27.	Atomic positional parameters (\mathring{A}^2) and their estimated standard	
	deviations for $Ru_3(\mu\text{-CO})_2(CO)_6\{\mu_3\text{-}\eta^2\text{-}C_6H_2(OMe)_3\}[\mu\text{-}$	
	$P\{C_6H_2(OMe)_3\}_2].$	279
28.	Atomic positional parameters (\mathring{A}^2) and their estimated standard	
	deviations for $Os_3(\mu\text{-OH})_2(CO)_9(TMPP)$	284
29.	Atomic positional parameters (\mathring{A}^2) and their estimated standard	
	deviations for $Os_3(\mu\text{-OH})(CO)_9(\mu-\eta^2\text{-TMPP-}O)$	287

LIST OF FIGURES

		Page
1.	Schematic diagram depicting the five nonzero d-d overlaps	
	between two metal atoms.	5
2.	Conversion of quadruply bonded d ⁴ -d ⁴ dinuclear complexes with	
	$\sigma^2\pi^4\delta^2$ configurations to electron-rich (d^5-d^5) and electron-	
	deficient (d ³ -d ³) triply bonded dinuclear complexes via a two-	
	electron transfer reduction and oxidation, respectively	8
3.	Schematic representation of the chemistry occurring during the	
	decomposition of $Os_3(\mu\text{-Cl})_2(CO)_{10}$ on phosphine–functionalized	
	silica, showing the formation of an unsaturated mononuclear	
	compound OsCl(CO) ₂ which exhibits catalytic activity due to its	
	coordinative unsaturation.	13
4.	A plot of cone angles versus the $v(CO)_{A_1}$ stretch for various	
	Ni(CO) ₃ (L) complexes (L = phosphine)	20
5.	A 500 MHz ¹ H NMR spectrum of Re ₂ (μ-H)(μ-Cl)Cl ₂ (CO) ₂ (dppm) ₂	
	in CD ₂ Cl ₂ at 22 °C.	49

		Page
6.	A 500 MHz 1H NMR spectra of the methylene region for $Re_2(\mu\text{-}$	
	$H)(\mu\text{-Cl})Cl_2(CO)_2(dppm)_2$ in (a) CD_2Cl_2 and (b) acetone- d_6 at	
	22 °C	52
7.	T_1 measurements in CD_2Cl_2 and at 200 MHz 1H NMR with	
	variable temperatures for the bridging hydride of $Re_2(\mu\text{-}H)(\mu\text{-}$	
	Cl)Cl ₂ (CO) ₂ (dppm) ₂ .	55
8.	Positive ion FABMS spectrum of $Re_2(\mu-H)(\mu-Cl)Cl_2(CO)_2(dppm)_2$.	57
9.	Cyclic voltammogram of $Re_2(\mu-H)(\mu-Cl)Cl_2(CO)_2(dppm)_2$ in a	
	CH ₂ Cl ₂ solution with 0.2 M TBAPF ₆ at 200 mV/s using a Pt-disk	
	electrode.	59
10.	Infrared spectra of (a) $Re_2(\mu-H)(\mu-Cl)Cl_2(CO)_2(dppm)_2$ (———)	
	and the corresponding oxidation product () and (b) $Re_2(\mu)$	
	$H)(\mu-Cl)Cl_2(CO)_2(dppm)_2$ (———) and the corresponding	
	reduction product ().	61
11.	Electronic absorption spectral changes during electrochemical	
	oxidation of $Re_2(\mu-H)(\mu-Cl)Cl_2(CO)_2(dppm)_2$ in 0.1 M $TBABF_4-$	
	CH ₂ Cl ₂ solution. The total reaction time at ambient temperature	
	was two hours.	65

		Pa
12.	Positive ion FABMS spectrum of the decomposition product	
	Re ₂ Cl ₄ (CO) ₂ (dppm) ₂ isolated from the electrochemical oxidation	
	of $Re_2(\mu-H)(\mu-Cl)Cl_2(CO)_2(dppm)_2$ in 0.1 M $TBABF_4-CH_2Cl_2$	
	solution, showing (a) the molecular ion peak [M] =	
	$Re_2Cl_4(CO)_2(dppm)_2$, (b) [M-CO] = $Re_2Cl_4(CO)(dppm)_2$ and (c)	
	[M-2CO] = Re2Cl4(dppm)2	67
13.	An X-band EPR spectrum taken on a solid sample of	
	$[Cp_2Co][Re_2(\mu-H)(\mu-Cl)Cl_2(CO)_2(dppm)_2]$ at -150 °C	75
14.	Schematic diagram depicting the redox reactions of $Re_2(\mu\text{-}H)(\mu\text{-}$	
	Cl)Cl ₂ (CO) ₂ (dppm) ₂	77
15.	ORTEP drawing of Re ₂ (µ-H)(µ-Cl)Cl ₂ (CO) ₂ (dppm) ₂ , showing the	
	atom labeling scheme. All phenyl-group carbon atoms are	
	represented as small circles for clarity, and all other atoms are	
	represented by their 50% probability ellipsoids. Unlabeled atoms	
	are related to labeled ones by an inversion center at the midpoint	
	of the Re—Re' bond.	81
16.	A skeletal ORTEP plot of Re ₂ (μ-H)(μ-Cl)Cl ₂ (CO) ₂ (dppm) ₂ view	
	down the Re—Re vector.	83
17.	ORTEP drawing of the [Re ₂ (µ-H)(µ-Cl)Cl ₂ (CO) ₂ (dppm) ₂] ⁺ cation	
	showing the atom labeling scheme. All phenyl-group carbon	

		Page
	atoms are represented as small circles for clarity, and all other	
	atoms are represented by their 40% probability ellipsoids	85
18.	ORTEP drawing of $[Re_2(\mu\text{-CO})(\mu\text{-Cl})Cl_2(CO)(NO)(dppm)_2][BF_4]$.	
	showing the atom labeling scheme. All phenyl-group carbon	
	atoms are represented as small circles for clarity	89
19.	Stereoview of the unit cell of the molecule [Re ₂ (µ-CO)(µ-	
	Cl)Cl ₂ (CO)(NO)(dppm) ₂][BF ₄] along the a axis.	91
20.	Pluto drawing emphasizing the main features of the cations in	
	the structures of (a) [Re ₂ (μ -CO)(μ -Cl)Cl ₂ (CO)(NO)(dppm) ₂][BF ₄]	
	and (b) $[Re_2(\mu-H)(\mu-Cl)Cl_2(CO)_2(dppm)_2][BF_4]$	93
21.	Comparison of a series of edge-sharing bioctahedral dirhenium	
	complexes with the syn-Re ₂ Cl ₃ (dppm) ₂ core	97
22.	ORTEP drawing of Ru ₃ (µ-Cl) ₂ (PBu ₃ ⁿ) ₂ (CO) ₈ showing the atom	
22.		
	labeling scheme. All n-butyl carbon atoms are represented as	
	small circles for clarity, and all other atoms are represented by	
	their 50% propability ellipsoids.	108
23.	A graph of ligand size versus basicity. The ligand size and	
	basicity are expressed by the cone angle and v(CO) value,	
	respectively. The cone angles and v(CO) values (smaller values	

		Page
	indicating greater σ -donor and poorer π -acceptor properties)	
	were taken from Tolman's work [22].	114
24.	Schematic diagram of various approaches to the synthesis of	
	$Rh_2(O_2CCH_3)_3(TMPP-O)(MeOH).$	122
0 =	A con less last last last last last last last la	
25.	A 300 MHz ¹ H NMR spectrum of Rh ₂ (O ₂ CCH ₃) ₃ (TMPP-	
	O)(MeOH) in CD ₃ CN at 22 °C.	124
26	A 500 MHz ¹ H NMR spectra of the meta proton region of	
20.		
	Rh ₂ (O ₂ CCH ₃) ₃ (TMPP-O)(MeOH) in CD ₃ CN at 22 °C with (a) ³¹ P	
	decoupling (b) ³¹ P undecoupling	126
07	The dimensional DOCOSY enactures of Ph (O. CCII.) (TMPP	
21.	Two-dimensional DQCOSY spectrum of Rh ₂ (O ₂ CCH ₃) ₃ (TMPP-	
	O)(MeOH).	128
28	¹ H NMR spectra of the meta proton of Rh ₂ (O ₂ CCH ₃) ₃ (TMPP-	
20.		
	O)(MeOH), measured in various solvents (a) THF-d ₈ (b) CD ₃ CN	
	(c) acetone- d_6 (d) $CDCl_3$ (e) CD_2Cl_2	134
90	(a) Simulated and (b) experimental ¹ H NMR spectra of meta-	
4 J.		124
	protons of Rh ₂ (O ₂ CCH ₃) ₃ (TMPP-O)(MeOH).	136
30	A ³¹ P(¹ H) NMR spectrum of Rh ₀ (O ₀ CCH ₀) ₀ (TMPP-O)(MeOH).	138
·MJ.	A FIGINALA SUCCERUM DE AMALVACIO DO DA LAMERA CONTRECTA.	130

		Page
31.	Positive ion FABMS spectrum of Rh ₂ (O ₂ CCH ₃) ₃ (TMPP-	
	O)(MeOH).	140
32.	An ORTEP drawing of Rh ₂ (O ₂ CCH ₃) ₃ (TMPP-O)(MeOH),	
 .	showing the atom labeling scheme. All phenyl-group and	
	MeOH carbon atoms are represented as small circles for clarity,	
	and all other atoms are represented by their 50% propability	
	ellipsoids.	144
33.	Cyclic voltammogram of Rh ₂ (O ₂ CCH ₃) ₃ (TMPP-O)(MeOH) in	
	0.2 M TBAPF ₆ -CH ₃ CN at 200 mV/s using a Pt-disk electrode.	146
34.	Varible scan speed cyclic voltammograms of	
	Rh ₂ (O ₂ CCH ₃) ₃ (TMPP-O)(MeOH) in 0.2 M TBAH-CH ₃ CN	148
35.	An X-band EPR spectrum (-150 °C) of a 2-MeTHF/CH ₃ CN	
	frozen solution containing 0.1 M TBAPF6 of	
	Rh ₂ (O ₂ CCH ₃) ₃ (TMPP-O)(MeOH).	150
36.	Positive ion FABMS spectrum of $Rh_2(O_2CCH_3)_3(TMPP-2O)(NO)$.	152
37.	X-band EPR spectra in (a) the solid state and in (b) solution for	
	Rh ₂ (O ₂ CCH ₂) ₂ (TMPP ₂ 2O)(NO)	154

		Page
38.	A 300 MHz ¹ H NMR spectrum of Mo ₂ (O ₂ CCH ₃) ₂ (TMPP-O) ₂	158
39.	A 300 MHz 19 F NMR spectrum of $Mo_2(O_2CCH_3)_2(TMPP-O)_2$	160
4 0.	A positive ion FABMS spectrum of $Mo_2(O_2CCH_3)_2(TMPP-O)_2$.	162
41.	Schematic diagram of a proposed reaction scheme for the formation of Mo ₂ (O ₂ CCH ₃) ₂ (TMPP-O) ₂ .	164
42.	Infrared spectrum in the $v(CO)$ region for [HTMPP][HFe ₃ (CO) ₁₁]. The $v(CO)$ stretch at 1748 cm ⁻¹ is a bridging mode.	185
43 .	An ORTEP diagram of [HTMPP][HFe ₃ (CO) ₁₁], showing the atom labeling scheme. All atoms are represented by their 40% probability ellipsoids.	190
44.	A packing diagram of [HTMPP][HFe ₃ (CO) ₁₁], showing there is no ion-pairing interaction present in the molecule	192
4 5.	Infrared spectral changes in the $\nu(CO)$ region for (a) initial product $Ru_3(CO)_{11}(TMPP)$ and (b) transformed product with	
	bridging $v(CO)$ bands observed at 1790 and 1800 cm ⁻¹	195

		Page
46.	Infrared spectrum in THF for the molecule $Ru_3(\mu\text{-CO})_2(CO)_6\{\mu_3\text{-}$	
	$\eta^2\text{-}C_6H_2(OMe)_3][\mu\text{-}P\{C_6H_2(OMe)_3\}_2].$ The $\nu(CO)$ stretches at 1807	
	and 1866 cm ⁻¹ are bridging modes.	197
47.	A 300 MHz 1H NMR spectrum in THF–d $_8$ at 22 oC for $Ru_3(\mu\text{-}$	
	$CO)_2(CO)_6\{\mu_3-\eta^2-C_6H_2(OMe)_3\}[\mu-P\{C_6H_2(OMe)_3\}_2]. Resonances$	
	denoted by (a) and (b) are assigned to both ortho-methoxy groups	
	and two meta protons, respectively, in the cyclometallated ring.	200
48.	Proposed reaction pathway for the formation of	
	$Ru_3(\mu\text{-CO})_2(CO)_6\{\mu_3-\eta^2\text{-}C_6H_2(OMe)_3\}[\mu\text{-}P\{C_6H_2(OMe)_3\}_2].$	203
49.	Computer generated space-filling model of molecule B of	
	$Ru_3(\mu\text{-CO})_2(CO)_6\{\mu_3-\eta^2\text{-}C_6H_2(OMe)_3\}[\mu\text{-}P\{C_6H_2(OMe)_3\}_2].$	
	The Ru atoms are denoted by the black balls.	205
50.	ORTEP drawings of (a) molecule A and (b) molecule B of $\mathrm{Ru}_3(\mu$ -	
	$CO)_2(CO)_6[\mu_3-\eta^2-C_6H_2(OMe)_3][\mu-P\{C_6H_2(OMe)_3\}_2]$, showing the	
	atom labeling scheme with all atoms represented by their 40%	
	probability ellipsoids.	212
51.	Main features of both enantiomers A and B in the structure of	
	$Ru_3(\mu\text{-CO})_2(CO)_6\{\mu_3-\eta^2\text{-}C_6H_2(OMe)_3\}[\mu\text{-}P\{C_6H_2(OMe)_3\}_2]. Chiral$	
	carbon atoms in both molecules are denoted by *	214

		Page
52.	Selected bond distances for molecules A and B in the structure of	
	$Ru_{3}(\mu\text{-CO})_{2}(CO)_{6}\{\mu_{3}\text{-}\eta^{2}\text{-}C_{6}H_{2}(OMe)_{3}\}[\mu\text{-}P\{C_{6}H_{2}(OMe)_{3}\}_{2}].$	216
53.	Positive ion FABMS spectrum of $Os_3(\mu-H)(H)(CO)_{10}(TMPP)$	220
54 .	Variable-temperature 500 MHz ¹ H NMR spectra of	
	Os ₃ (μ-H)(H)(CO) ₁₀ (TMPP) recorded in CDCl ₃	222
55.	Positive ion FABMS spectrum of Os ₃ (CO) ₁₁ (TMPP)	225
56.	A 300 MHz ¹ H NMR study depicting spectral changes during the	
	transformation of Os ₃ (CO) ₁₁ (TMPP). (a) Initial product	
	$Os_3(CO)_{11}(TMPP)$ with terminal $v(CO)$ stretches only, and (b)	
	transformed product with bridging v(CO) stretches present	228
57 .	A 300 MHz ¹ H NMR spectrum of Os ₃ (μ-OH)(TMPP-O)(CO) ₉ in	
	CDCl ₃ at room temperature. The doublet denoted by * is due to	
	an impurity of a methyl phosphonium salt.	230
58.	Schematic diagram outlining a proposed reaction sequence in	
	the formation of $Os_3(\mu\text{-OH})_2(TMPP)CO)_9$ and $Os_3(\mu\text{-OH})(TMPP\text{-}$	
	O)(CO) ₉	232
59 .	An ORTEP diagram of Os ₃ (µ-OH) ₂ (TMPP)(CO) ₉ , showing the	
	atom labeling scheme. All phenyl-group carbon atoms of TMPP	

		Page
	are represented as small circles for clarity, and all other atoms	
	are represented by their 40% propability ellipsoids.	237
60.	ORTEP diagram of Os ₃ (µ-OH)(TMPP-O)(CO) ₉ , showing the atom	
	labeling scheme. All phenyl-group carbon atoms of TMPP are	
	represented as small circles for clarity.	242
61.	Main features of the molecular structures of (a) $Os_3(\mu$ -	
	OH) ₂ (TMPP)(CO) ₉ and (b) Os ₃ (μ-OH)(TMPP-O)(CO) ₉	244

LIST OF ABBREVIATIONS

Å angstrom

Ag/AgCl silver-silver chloride reference electrode

Buⁿ n-butyl group

Calcd calculated

cm⁻¹ wavenumber

CV cyclic voltammetry

d deuterated

dppm bis(diphenylphosphine)methane

DQCOSY Double-Quantum Correlation Spectroscopy

 $E_{1/2}$ half-wave potential

ESR electron spin resonance

ε molar extinction coefficient

FABMS fast atom bombardment mass spectroscopy

g grams, ESR g-value

Hz hertz

IR infrared

M—M metal-metal

Me methyl group

ml milliliter

min minutes

mmol millimoles

MSU Michigan State University

nm nanometer

NMR nuclear magnetic resonance

NTU National Taiwan University

obs observed

ox oxidation

Ph phenyl group

PR₃ tertiary phosphine ligand

red reduction

sh shoulder

TBAH tetra-n-butylammonium hexafluorophosphate

TBABF₄ tetra-n-butylammonium tetrafluoroborate

TMPP tri(2,4,6-trimethoxyphenyl)phosphine, $P[C_6H_2(OMe)_3]_3$

TMPP-O P[C₆H₂(OMe)₃]₂[C₆H₂(OMe)₂(O)]

TMPP-2O $P[C_6H_2(OMe)_3]_2[C_6H_2(OMe)(O)_2]$

V volts

CHAPTER I

INTRODUCTION

Transition metal organometallic and coordination complexes comprise a remarkably diverse group of compounds, and among them, polynuclear clusters with two or more metals in close proximity are of great interest [1]. The electronic properties of these compounds reflects the subtle interplay of not only the metal-ligand bonding but also the metal-metal bonding, and the system can display, through mutual metal-metal interactions, chemical and physical properties different from those of the corresponding mononuclear moieties.

There are two main classes of polynuclear cluster complexes in transition metal chemistry. One subdivision is "low valent clusters" which typically involve transition metals with π -acceptors such as isocyanides, NO and CO ligands, and 'classical' organometallic compounds; metal carbonyl clusters are common members of this family. The dominant role of carbon monoxide as a ligand for stabilizing low oxidation state clusters arises, in part, from the fact that CO is a very flexible ligand which can occupy terminal, edge-bridging, or face-capping locations in a cluster. Furthermore, this ligand functions as a two-electron donor in each of these bonding situations, and therefore terminal to bridging intramolecular exchange processes frequently have very low activation energies. The second class of cluster compounds is the "high valent clusters" which are formed by early transition metal elements and contain classical donor ligands such as O⁻², S⁻², Cl⁻, Br⁻, I⁻, and OR⁻. Geometrically these clusters show a strong preference for triangular and octahedral metal skeletal geometries such as Re₃Cl₉L₃ and [Mo₆Cl₆L₆]⁴⁺. An important feature of this class of complexes is that it includes lower nuclearity π donor clusters that exhibit extensive bonding between the metal atoms. The

multiply bonded metal-metal (M - M) dinuclear complexes have contributed significantly to the development of inorganic chemistry.

The past decade has seen remarkable progress towards a broad and deeper understanding of multiply bonded metal-metal dinuclear complexes [2]. The majority of these complexes have been found with the transition metals V, Nb, Ta, Cr, Mo, W and Re, but other metals such as Ru, Os and Rh have also been involved. In these systems, the assignment of a formal metal-metal bond order usually rests on the collective data from structural, spectroscopic, and magnetic measurements. For clusters of the earlier transition metals, multiple bonds are frequently observed in compounds without bridging ligands; in these cases, the structural and spectroscopic data are completely consistent with the assignment of a formal bond order on the basis of the number of d electrons associated with each metal atom (one σ , two π , and two δ bonds) as shown in Figure 1, but the maximum bond order in molecular clusters is generally considered to be four because one of the d^{δ} orbitals is required for metal-ligand bonding. The filling of metal-based orbitals in M-4M complexes renders a $\sigma^2\pi^4\delta^2$ ground state configuration. Of importance to note in such systems is that the HOMO and LUMO with δ-symmetries are formed from the weak interaction between two adjacent dxy orbitals from each metal center. The lowest energy absorption band of quadruply bonded dinuclear complexes therefore corresponds to a ${}^{3}(\delta \to \delta^{*})$ transition with the retention of a strong metal-metal interaction.

The M^nM (n = 1-4) dinuclear complexes often exhibit rich redox activity and electronic flexibility, as the presence of two metal atoms united by a multiple bond provides an electron source or sink for multielectron redox reactions [3]. These reactions lead to stepwise changes in M—M

Figure 1. Schematic diagram depicting the five nonzero d-d overlaps between two metal atoms.

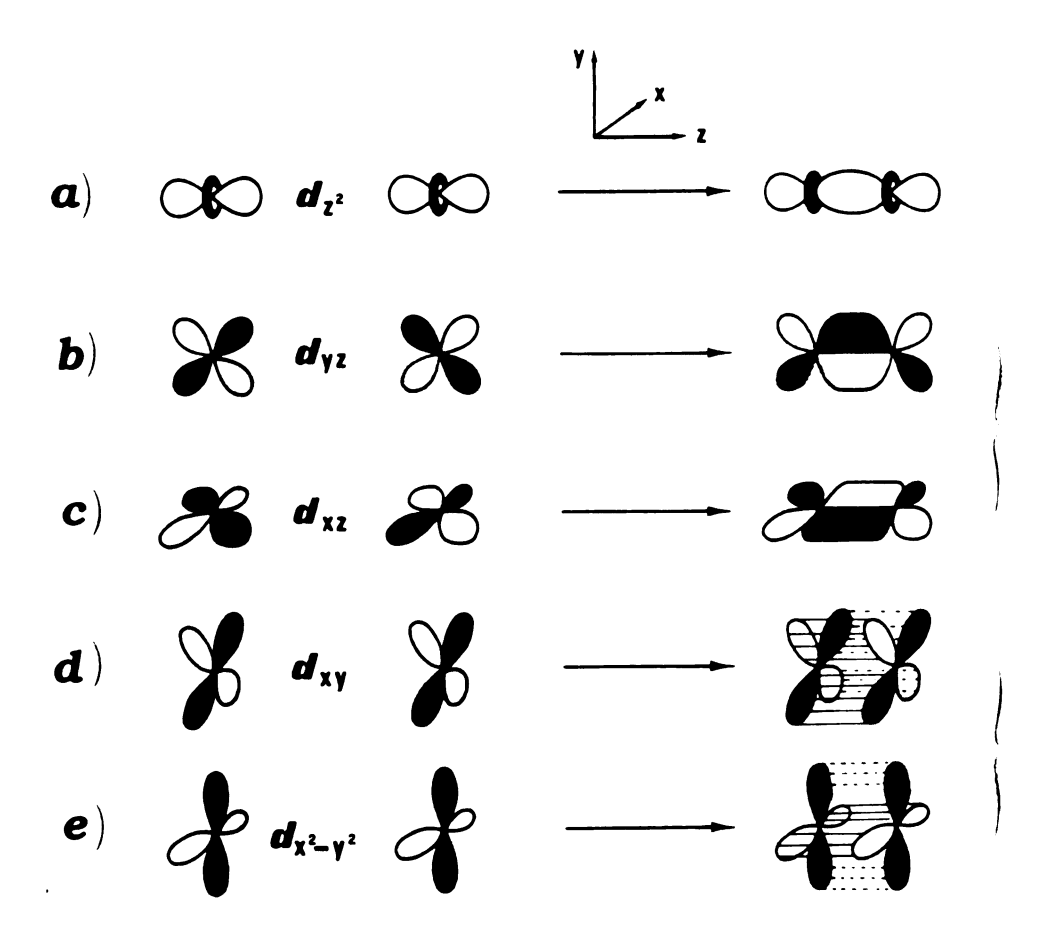


Figure 1

bond order by removing and adding electrons to the metal-metal bond. Figure 2 demonstrates how M-4M complexes can either convert to electron-rich $M^{\frac{3}{2}}M$ species by two one-electron reduction, or to electrondeficient $M ext{-} M$ compounds by two-electron oxidation processes. In theory, the unique structural and electronic properties of M - M complexes can be tailored to promote multielectron transformations by coupling the oneelectron redox chemistry of individual metal cores in sequential steps or by exploiting the two-electron activity of a discrete metal core in an effective single step. The redox reactions of these complexes are significantly influenced by coordination geometry and the nature of the coordinated ligands, both of which determine whether such processes are accompanied by ligand rearrangements. For example, the dinuclear complex $Re_2Cl_4(dppm)_2$ undergoes reversible oxidations by electrochemistry that suggest major structural rearrangement does not take place. On the other hand, two electron oxidized $M_2X_4L_4$ (M = Mo(II), W(II), Rh(III); X = halide; L = donor ligand including halide) species are best stabilized by adopting a confacial [4] or edge-sharing bioctahedral configuration [5], which enforces octahedral coordination about the oxidized metal core.

Finally, the ligands in many multiply bonded molecules exhibit high substitutional lability, thus the coordinatively unsaturated M^n core has the ability to serve as a template for substrate assembly and coupling [6]. In recent years, some organometallic ligands such as alkynes and ethylene have been introduced to the M^n systems, especially in the metal alkoxide compounds [7], and some important reactions such as carbon–carbon and carbon–hydrogen bond activations were observed [8]. For example, 1,2– $R_2W_2(OR)_4$ ($W^3W)^{6+}$ (R = alkyl group) compounds have been shown to undergo either reductive elimination reactions with loss of alkane and

Figure 2. Conversion of quadruply bonded d^4-d^4 dinuclear complexes with $\sigma^2\pi^4\delta^2$ configurations to electron-rich (d^5-d^5) and electron-deficient (d^3-d^3) triply bonded dinuclear complexes via a two-electron transfer reduction and oxidation, respectively.

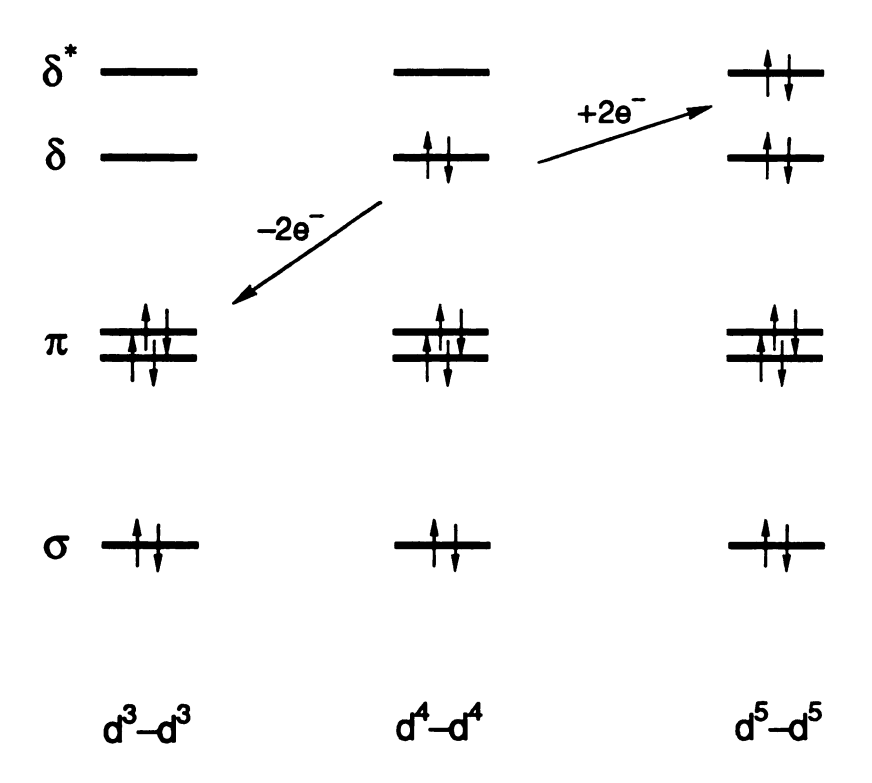


Figure 2

alkene reactio contain

> includi finante finante

respect

nu the

umple socyar

Imred

such as

such as

The fair

and 8 destabl

> ganda Na Cl

ंग्रेप्टि

is prese

alkene and formation of d^4-d^4 (W-4W) compounds, or oxidative addition reactions with elimination of alkane and formation of d^1-d^1 (W-W) containing compounds supported by hydrido and alkylidyne ligands; these competing pathways involve β - and α -CH activation processes, respectively [9].

In direct contrast to the π -donor ligands, the strong π -acid ligands including CO, NO, and isocyanides only rarely occur in multiply bonded dinuclear complexes; to date, none have been found in quadruply bonded dinuclear complexes. In most cases, the introduction of π -acceptor ligands into the MⁿM framework results in M—M bond cleavage, and leads to the formation of mononuclear complexes [10]. For example, reductive or nonreductive Re-Re bond cleavage to afford mononuclear isocyanide complexes of Re(I) and Re(III) was observed in the reactions of alkyl isocyanides with dirhenium(III) complexes containing quadruple bonds such as $\text{Re}_2(\text{O}_2\text{CR})_4\text{Cl}_2$ (R = CH₃ or C_6H_5), $\text{Re}_2\text{X}_8^{2-}$, and $\text{Re}_2\text{X}_6(\text{PR}_3)_2$ (X = Cl or Br, PR₃ = monodentate phosphine ligands) or triply bonded complexes, such as $Re_2X_4(PR_3)_4$ (X = Cl or Br, PR_3 = monodentate phosphine ligands). The facile bond cleavage reactions induced by π -acceptors is presumably because the metal d electrons necessary for the formation of the M-M π and δ bonds are involved in π -backbonding with the ligands, thus destablizing the M—M bond.

In contrast to the facile cleavage of the Re 3 Re bond in Re $_2$ X $_4$ (PR $_3$) $_4$ (X = Cl or Br, PR $_3$ = monodentate phosphine ligands) by CO and isocyanide ligands, the analogous phosphine-bridged species Re $_2$ X $_4$ (dppm) $_2$ (Re 3 Re) (dppm = Ph $_2$ PCH $_2$ PPh $_2$) reacts to give adducts in which a metal-metal bond is preserved [11]. As the scheme below shows, the resulting dinuclear

compounds consist of A-frame-like structures or edge-sharing bioctahedral geometries [12].

In an effort to unite the two areas of cluster chemistry, we investigated reactions between multiply bonded metal-metal $(M^{\frac{n}{m}}M)$ dinuclear complexes, namely 'high valent early transition metals', and 'classical' organometallic compounds with π -acceptor CO groups, namely 'low valent late transition metals'. One predicted outcome of this research was a mild approach to the synthesis of new π -acceptor-containing dinuclear compounds via ligand transfer reactions between the different metal systems. Since the coordinatively unsaturated $M^{\frac{n}{-}}M$ core is known to behave as a template for substrate assemply and coupling, several other plausible modes of reaction such as mixed-metal assembly via a direct interaction of the early and late transition metal atoms, and redox reactions through outer sphere interactions might also be anticipated. Our initial experiment in this study was the reaction of the phosphine-bridged species $Re_2X_4(dppm)_2$ ($Re^{3}Re$) ($dppm = Ph_2PCH_2PPh_2$) with some reactive organometallic molecules such as H₂Os₃(CO)₁₀, and the results and discussion are presented in Chapter II.

The aforementioned approach describes a possible route for bridging the areas of 'classical' organometallic and coordination chemistry. Along this line, we know that the historic distinction between organometallic chemistry and coordination chemistry is becoming less clear, and links between 'classical' organometallic and coordination chemistry have recently emerged in the form of organometallic compounds with ancillary donor ligands such as halides, nitrides and alkoxide ligands. These new classes of compounds demonstrate the ability of soft π -acceptor ligands such as CO to bond to a metal in the presence of relatively extreme ligand environments. Some of the new organometallic compounds have been found to exhibit unique electronic properties induced by the combined presence of the dramatically different donor ligands. For example, the chemistry of carbonyl halide clusters has attracted much research interest because facile CO dissociation reactions in these complexes provide a good opportunity to study catalytic applications under mild condition. One example shown in Figure 3 demonstrates the use of an edge double-bridged osmium complex Os₃(µ-Cl)₂(CO)₁₀ in surface organometallic chemistry [13]. In this case, $Os_3(\mu-Cl)_2(CO)_{10}$ is rendered coordinatively unsaturated by taking advantage of the labile character of CO ligands induced by the bridging chloride atoms, which allows it to be attached to the phosphinefunctionalized silica to make the supported osmium catalyst. In general, these complexes with combined 'hard' π -donor ligands and 'soft' π acceptor CO groups were derived from simple ligand substitution reactions of metal carbonyls with π -donor ligands. Often these reactions are not easy to effect, however, and simple substitution of one for another is usually not possible. We postulated that an alternative approach to such compounds via ligand transfer reactions between 'classical' organometallic

Figure 3. Schematic representation of the chemistry occurring during the decomposition of $Os_3(\mu-Cl)_2(CO)_{10}$ on phosphine–functionalized silica, showing the formation of an unsaturated mononuclear compound $OsCl(CO)_2$ which exhibits catalytic activity due to its coordinative unsaturation.

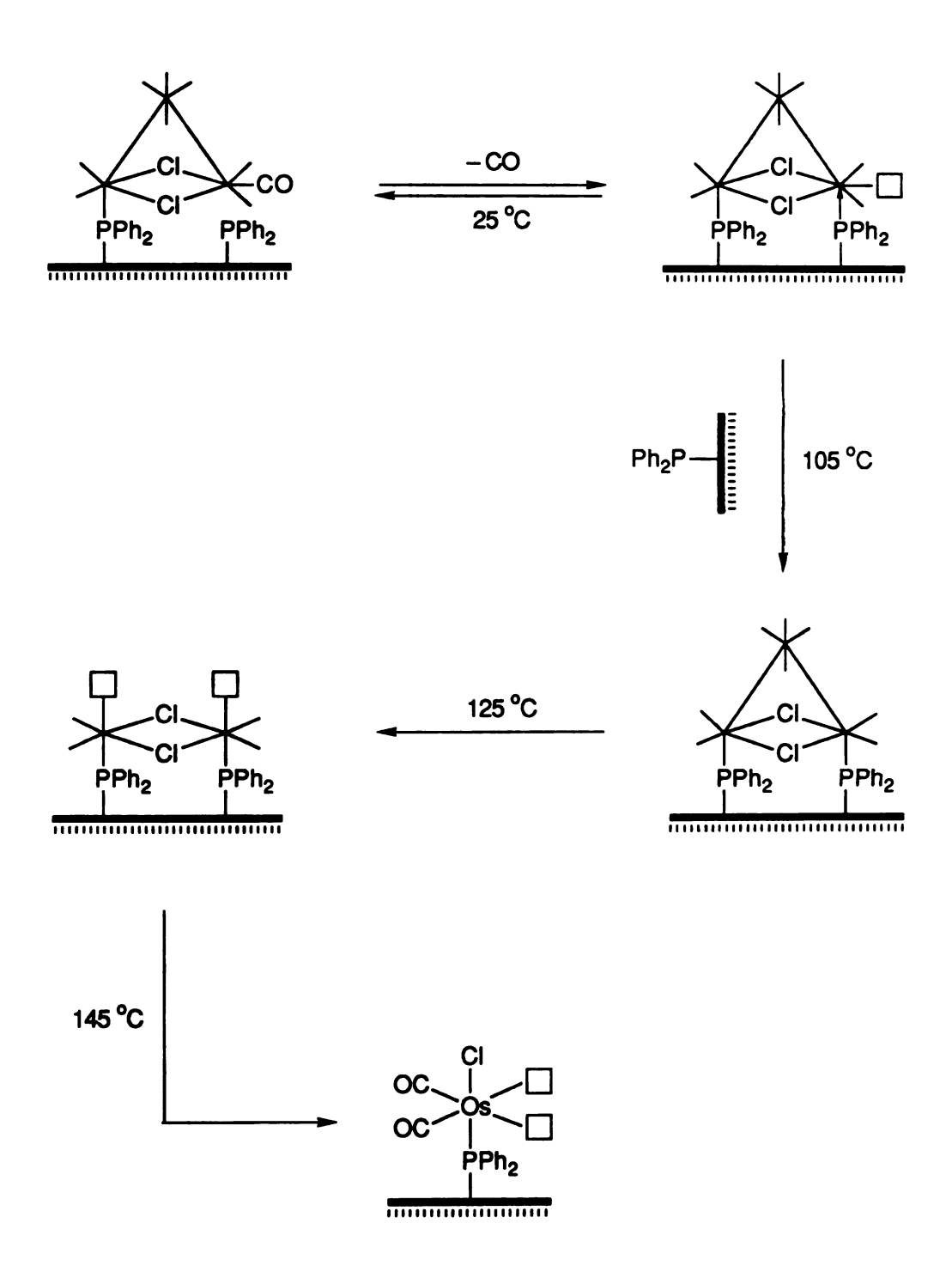


Figure 3

compounds, namely metal carbonyl clusters, and metal halide complexes might be useful. In Chapter III, we report the syntheses of a new class of halide carbonyl clusters derived from the reactions between Re—Re halide complexes with metal carbonyl clusters.

An entirely different approach to uniting the distinct properties of 'high valent early transition metals' and 'low valent late transition metals' involves the use of functionalized ligands. Ligands bearing mixed donor atoms have received special attention because "soft" and "hard" donor ligands complement each other in their preferences for metals [14]. The soft donors stabilize electron-rich metal centers in low oxidation states, whereas the hard donor ligands stabilize electron-poor metals in high oxidation states. These ligands, with the potential to form weak chelate interactions due to these two inherently different coordination abilities. strongly influence the activity, selectivity and stability of a catalytic system via electronic and steric effects. Furthermore, metal chelates containing "hard" and "soft" donors exhibit catalytic potential due to the ligand flexibility and lability. For example, ligands containing P~O chelates exhibit high activity and selectivity in a catalytic process for the manufacture of α -olefins [15]; this process is currently one of the most important applications of homogeneous catalysis in industry.

The study of phosphines, especially tertiary phosphines, with the capacity to stabilize a wide range of oxidation states in transition metal complexes, continues to be a field of intense research area in both fundamental and applied chemistry [16]. One of the primary reasons for this interest is that metal phosphine complexes have been found to be good homogeneous catalysts. Recent work has focused on the preparation of new phosphine ligands which may enhance the reactivity of key industrial

reactions such as hydrogenation, hydroformylation and hydrosilation. To date, there are two main catagories of heteroatom phosphine ligands bearing both "hard" and "soft" donors that have been investigated:

(1) Nitrogen-containing functionalized phosphines, denoted as P~N [17]: Amino-phosphines contain a 'soft' phosphorus atom and a 'hard' primary aromatic amine donor, both of which participate in bonding to the metal as shown below [17(b)].

$$\begin{array}{c|c} Ph_2P & & & \\ \hline \\ H_2N & & & \\ \hline \end{array}$$

(2) Oxygen-containing functionalized phosphines, denoted as P~O [18]: Ether-phosphines are one of the most extensively studied class of oxygen-containing functionalized phosphines [18(a)]. In addition to imparting high reactivity to the metal center, the ligand itself can undergo deprotonation or dealkylation to form rigid unsymmetrical chelates or bridges. Examples of phenoxy-phosphine chelates have been reported in the chemistry of remarkably stable Rh(II) and Ir(II) complexes as shown below [18(j)-(1)]:

$$R_2P$$
 MeO
 R_2
 R_2
 R_2
 R_2
 R_2
 R_2
 R_3
 R_4
 R_2
 R_2

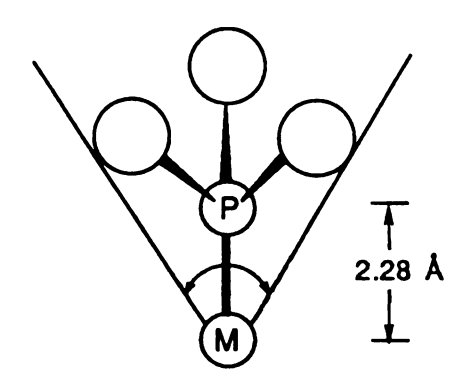
In the investigation of the chemistry of functionalized ligands with transition metal complexes, our interest was sparked by a functionalized tertiary phosphine, tris(2,4,6-trimethoxyphenyl)phosphine (TMPP) which is depicted below.

Tris(2,4,6-trimethoxyphenyl)phosphine
(TMPP)

Since both oxygen and phosphorus are good donors, the presence of nine potentially interacting pendant methoxy groups renders TMPP a versatile ligand. The phosphorus atom promotes the formation of stable low valent metal complexes, in which the metal binds strongly to the soft phosphorus and more weakly to the harder oxygen donors. Finally, the ligand is quite flexible, and provides sites of high lability thereby inducing desirable conditions for increasing the rates of small molecule activation reactions.

The synthesis of tris(2,4,6-trimethoxyphenyl)phosphine (TMPP) was first reported in 1957 by the reaction of 2,4,6-trimethoxybenzene, $ZnCl_2$ and PCl_3 [19]. A more recent synthesis involves a two step reaction of 1,3,5-trimethoxybenzene and n-butyllithium followed by coupling with

triphenylphosphine, giving 60–70% yields [20-21]. The TMPP phosphine ligand exhibits unusually high steric bulk which significantly dominates its reactivity toward metal complexes. A quantitative measurement of the steric bulk of phosphines, developed by Tolman [22], was used to define the size of TMPP in the context of other PR₃ ligands. The method is based on a CPK model by measuring the cone angle (θ) defined by the cylindrical cone containing a metal atom bound to a P atom with a fixed M—P distance of 2.28 Å and extending outward to the van der Waals radii of the outermost atoms of the model as shown below. The cone angle concept has proved a useful approach to the understanding of steric effects of the phosphorus ligands.



The cone angle of the new tertiary phosphine TMPP was measured to be approximately 184° by Wada [21]; this was confirmed in our laboratories. Phosphine ligands with large cone angles have played an important role in the development of new coordination chemistry. For example, bulky tertiary PR₃ ligands such as P(mesityl)₃, P(o-tolyl)₃ or P(Cy₃)₃ have been used to design complexes with unusual geometries and properties. In some cases, stable, coordinatively unsaturated 14 electron ML₂ palladium

compl. We ar

report

and w

behar based

> ralue phis

(<u>34)</u>]

the Fig.

ion:

tha

0.T gelt

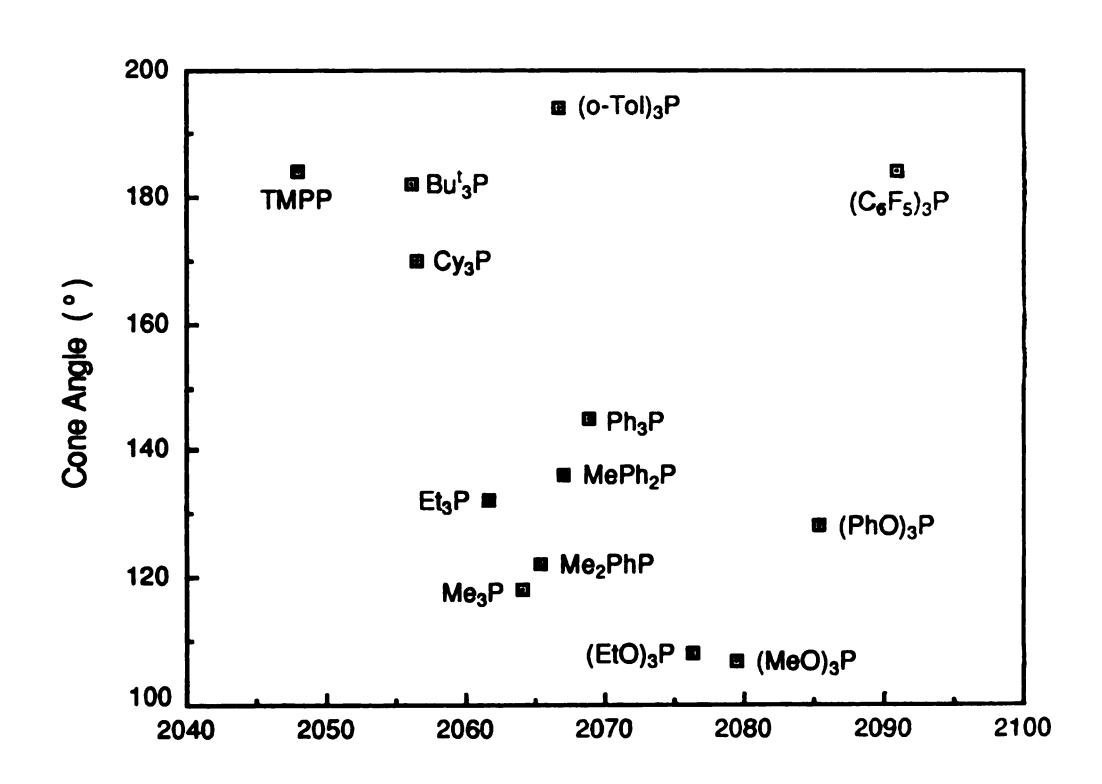
E : 24

ŝÿ

complexes have been synthesized with $P(Cy_3)_3$ and $P(t-Bu_3)_3$ as ligands [23]. We anticipated that TMPP would have also a rich and unusual chemistry, and were surprised to learn that no metal complexes of the ligand were reported at the time of our beginning this project.

Electronic effects also influence transition metal-phosphorus bonding [24]. The M—P bond is a donor covalent bond with the phosphorus behaving as a Lewis base; the measure of phosphine basicity is usually based on the proton affinity (i.e. Bronsted basicity) and represented by a pKa value. A second method for the determination of the nucleophilicity of phosphine ligands toward transition metal complexes is to measure the value of the $v_{A_1}(CO)$ stretching for the $Ni(CO)_3(L)$ (L = phosphine) complex [22]. A graph of the $v_{A_1}(CO)$ for various $Ni(CO)_3(L)$ complexes plotted versus the cone angle (θ) for various tertiary phosphine ligands is shown in the Figure 4. This is a good indication of the combined contribution of σ and π bonding to the metal complex. This, of course, is in the absence of other effects which would be expected to shift the v(CO) bands, such as geometry changes of Ni(CO)₃(L) with phosphines of greatly different sizes. In general, electron-releasing substituents will increase the electron density on the phosphorus center, resulting in a greater nucleophilicity towards a In this vein, a series of methoxy-substituted metal atom. triphenylphosphines including PPh_2R , $PPhR_2$, and PR_3 with R = (2,4,6) (i.e. (2,4,6)-trimethoxyphenyl) or R = (2,6) (i.e. (2,6)-trimethoxyphenyl) have been synthesized and reported in the literature [21].

Figure 4. A plot of cone angles versus the $\nu(CO)_{A_1}$ stretch for various $Ni(CO)_3(L)$ complexes (L = phosphine).



$$v_{A1}(CO)$$
 for LNi(CO)₃ (cm⁻¹)

Figure 4

The el

the phospi

of me

55F 5

of the

ins 2

basici

The h

as a s

high,

:H:

Phos CDC

TPfie

L'E

Steri al e

۸.

QD.

$$R = \frac{\text{MeO}}{\text{MeO}}$$

$$R = \frac{\text{MeO}}{\text{MeO}}$$

$$R = (2,4,6)$$

$$R = (2,6)$$

The electron-donating methoxy groups in the ortho and para positions of the phenyl rings have an enhancing effect on the nucleophilicity of the phosphorus atoms. The basicities of the phosphines decrease as the extent $PPh(2,6)_2 > PPh_2(2,4,6) > PPh_2(2,6) > PPh_3$ (pKa ≈ 2.3). The mesomeric effect of the multi-methoxy substituents in the trisubstituted phosphine P(2,4,6)₃ [tris(2,4,6-trimethoxy)phenylphosphine (TMPP)] results in the highest basicity of any known arylphosphine, on the order of piperdine (pKa ≈ 11.0). The high basicity of TMPP suggested to us that the phosphine would behave as a strong Lewis base. To verify this hypothesis, the value of $\nu_{\mbox{\scriptsize A}_{\mbox{\scriptsize 1}}}(\mbox{\scriptsize CO})$ in Ni(CO)₃(TMPP) was measured and found to be 2048 cm⁻¹ which reveals the highest nucleophilicity ever reported for a phosphine ligand. Furthermore, ¹H NMR studies in CDCl₃ of the phosphine TMPP and several phosphonium salts were measured (Table 1). ³¹P (¹H) NMR studies in CDCl₃ revealed a singlet at $\delta = -68$ ppm versus 85% H₃PO₄. The extreme upfield position of the resonance is in agreement with the high basicity of TMPP. When taken together with the fact that the ligand exhibits a large steric bulk with a cone angle (θ) of 184°, we concluded that TMPP would be an excellent ligand for the preparation of coordinatively unsaturated metal complexes.

Table 1. ¹H NMR data of phosphine (TMPP) and phosphonium salts (in CDCl₃).

Compound	3,5-Н	4-MeO	4-MeO 2,6-MeO	P-H	Р-СН3	P-CH ₂ Cl
(2,4,6)3P	6.03 (d) $(J_{HP} = 3 Hz)$	3.76 (s)	3.47 (s)			
[(2,4,6) ₃ P–H] ⁺	6.17 (d) $(J_{HP} = 5 Hz)$	3.89 (s)	3.69 (s)	$8.35 (d)$ $(J_{HP} = 541 Hz)$		
[(2,4,6) ₃ P-CH ₃] ⁺	6.13 (d) $(J_{HP} = 5 \text{ Hz})$	3.89 (s)	3.58 (s)		$2.45 (d)$ ($J_{HP} = 15 Hz$)	
$[(2,4,6)_3\mathrm{P-CH}_2\mathrm{Cl}]^+$	6.14 (d) $(J_{HP} = 5 \text{ Hz})$	3.88 (s)	3.63 (s)			$4.25 (d)$ $(J_{HP} = 7.5 Hz)$

In (Rh TMP

with [Ri

namely PC₆H₂

characte

with bot

älferent

Unsymm

inducing consider

spite of

dinucle

with so

E

trimeth

a syste

metal-

11⁵.0⁵

ærdid

1, Cardue to

form

puggi

thelati

higher Here In our laboratory, some unique metal chelate TMPP complexes $[Rh(TMPP)_2]^n$ (n = +1, +2, or +3) were discovered in the chemistry of TMPP with $[Rh_2(NCMe)_{10}]^{4+}$ [25]; recently a demethylated TMPP complex, namely the phenoxy-phosphine chelate Ni(II)(TMPP-O)₂ [(TMPP-O) = $P(C_6H_2(OMe)_3)_2(C_6H_2(OMe)_2(O)]$ was isolated and structurally characterized [26]. Besides chelation, heteroatom functionalized ligands with both "soft" and "hard" donors are capable of coordinating to two different metal centers to form unsymmetrically bridged metal complexes. Unsymmetrical bridging ligands may form mixed-valence complexes by inducing an electronic polarity to the metal-metal bond; these are of considerable interest to synthetic chemists and spectroscopists alike. In spite of the promising nature of this chemistry, the designed synthesis of dinuclear metal complexes containing heteroatom functionalized ligands with "soft" and "hard" donor atoms is still in an early stage.

Based on these considerations, we extended our studies of tris(2,4,6-trimethoxyphenyl)phosphine to M^n complexes in the hopes of providing a systematic synthetic route for the formation of unsymmetrically bridged metal-metal bonded complexes. Metal tetracarboxylate compounds $M_2(O_2CR)_4$ with "paddlewheel" structures were regarded as attractive candidates for the chemistry of TMPP for the following reasons:

(1) Carboxylate ligands are important in inorganic and biological chemistry due to their versatile coordination ability [27]. This manifests itself in the form of a wide range of metal bonding modes such as monodentate bridging, bidentate bridging, as well as symmetric and asymmetric chelating; therefore these metal carboxylate complexes in general exhibit higher chemical reactivity due to their ligand flexibility.

- (2) The complexes $M_2(O_2CR)_4$ (M = Mo(II), W(II) or Rh(II), R = alkyl or aryl) have been extensively studied from the viewpoints of synthesis, spectroscopy, electrochemistry, and chemical reactivity [28]. In particular, theoretical studies of dirhodium (II,II) compounds confirm the existence of a single σ bond designated as $\sigma^2\pi^4\delta^2\delta^{*2}\pi^{*4}$ for the electronic configuration of the Rh_2^{4+} unit, and $M_2(O_2CR)_4$ (M = Mo(II) or W(II), R = alkyl or aryl) compounds contain quadruply bonded metal-metal cores with the $\sigma^2\pi^4\delta^2$ configuration.
- (3) These types of molecules are symmetrical, but if a carboxylate group is substituted by a hetero-bridging ligand such as a phenoxy-phosphine, the electronic environment in the equatorial plane will be altered not only because of the presence of ligands with different field strengths, but because of symmetry changes; the result therefore is a degree of electronic polarity in the metal-metal core which may give rise to mixed-valence complexes that are of considerable interest [29].

To this end, Chapter IV reports our investigation of reactions of the functionalized phosphine TMPP with dirhodium and dimolydenum carboxylate metal complexes; in these studies, we discovered several unique molecules containing unsymmetrical phenoxy-phosphine bridges as shown below.

$$\begin{array}{c|c}
 & M^{\delta^+} & M^{\delta^-} \\
 & & \\
 & & \\
 & & \\
 & & \\
 & & \\
 & & \\
 & & \\
 & & \\
 & & \\
 & & \\
 & & \\
 & & \\
 & & \\
 & & \\
 & & \\
 & & \\
 & & \\
 & & \\
 & & \\
 & & \\
 & & \\
 & & \\
 & & \\
 & & \\
 & & \\
 & & \\
 & & \\
 & & \\
 & & \\
 & & \\
 & & \\
 & & \\
 & & \\
 & & \\
 & & \\
 & & \\
 & & \\
 & & \\
 & & \\
 & & \\
 & & \\
 & & \\
 & & \\
 & & \\
 & & \\
 & & \\
 & & \\
 & & \\
 & & \\
 & & \\
 & & \\
 & & \\
 & & \\
 & & \\
 & & \\
 & & \\
 & & \\
 & & \\
 & & \\
 & & \\
 & & \\
 & & \\
 & & \\
 & & \\
 & & \\
 & & \\
 & & \\
 & & \\
 & & \\
 & & \\
 & & \\
 & & \\
 & & \\
 & & \\
 & & \\
 & & \\
 & & \\
 & & \\
 & & \\
 & & \\
 & & \\
 & & \\
 & & \\
 & & \\
 & & \\
 & & \\
 & & \\
 & & \\
 & & \\
 & & \\
 & & \\
 & & \\
 & & \\
 & & \\
 & & \\
 & & \\
 & & \\
 & & \\
 & & \\
 & & \\
 & & \\
 & & \\
 & & \\
 & & \\
 & & \\
 & & \\
 & & \\
 & & \\
 & & \\
 & & \\
 & & \\
 & & \\
 & & \\
 & & \\
 & & \\
 & & \\
 & & \\
 & & \\
 & & \\
 & & \\
 & & \\
 & & \\
 & & \\
 & & \\
 & & \\
 & & \\
 & & \\
 & & \\
 & & \\
 & & \\
 & & \\
 & & \\
 & & \\
 & & \\
 & & \\
 & & \\
 & & \\
 & & \\
 & & \\
 & & \\
 & & \\
 & & \\
 & & \\
 & & \\
 & & \\
 & & \\
 & & \\
 & & \\
 & & \\
 & & \\
 & & \\
 & & \\
 & & \\
 & & \\
 & & \\
 & & \\
 & & \\
 & & \\
 & & \\
 & & \\
 & & \\
 & & \\
 & & \\
 & & \\
 & & \\
 & & \\
 & & \\
 & & \\
 & & \\
 & & \\
 & & \\
 & & \\
 & & \\
 & & \\
 & & \\
 & & \\
 & & \\
 & & \\
 & & \\
 & & \\
 & & \\
 & & \\
 & & \\
 & & \\
 & & \\
 & & \\
 & & \\
 & & \\
 & & \\
 & & \\
 & & \\
 & & \\
 & & \\
 & & \\
 & & \\
 & & \\
 & & \\
 & & \\
 & & \\
 & & \\
 & & \\
 & & \\
 & & \\
 & & \\
 & & \\
 & & \\
 & & \\
 & & \\
 & & \\
 & & \\
 & & \\
 & & \\
 & & \\
 & & \\
 & & \\
 & & \\
 & & \\
 & & \\
 & & \\
 & & \\
 & & \\
 & & \\
 & & \\
 & & \\
 & & \\
 & & \\
 & & \\
 & & \\
 & & \\
 & & \\
 & & \\
 & & \\
 & & \\
 & & \\
 & & \\
 & & \\
 & & \\
 & & \\
 & & \\
 & & \\
 & & \\
 & & \\
 & & \\
 & & \\
 & & \\
 & & \\
 & & \\
 & & \\
 & & \\
 & & \\
 & & \\
 & & \\
 & & \\
 & & \\
 & & \\
 & & \\
 & & \\
 & & \\
 & & \\
 & & \\
 & & \\
 & & \\
 & & \\
 & & \\
 & & \\
 & & \\
 & & \\
 & & \\
 & & \\
 & & \\
 & & \\
 & & \\
 & & \\
 & & \\
 & & \\
 & & \\
 & & \\
 & & \\
 & & \\
 & & \\
 & & \\
 & & \\
 & & \\
 & & \\
 & & \\
 & & \\
 & & \\
 & &$$

$$M = Mo(II), Rh(II)$$

The discussion of the formation of phenoxy-phosphine bridging dinuclear complexes, characterization of these newly synthesized compounds, and the electrochemistry of the dirhodium product are detailed.

As part of the investigation of the chemistry of TMPP with various transition metal complexes, we included the study of metal carbonyl clusters. A number of cluster-assisted ligand transformations have been investigated in recent years [30]. Reactions involving transition metal carbonyl clusters and functionalized ligands containing phosphorus, sulfur, oxygen or nitrogen have provided some interesting models. For example, cluster complexes containing oxygen donor ligands are good models for oxide grafted species, and in some cases, they display a comparable chemical reactivity. Alkoxo groups are of particular interest as ancillary ligands due to the stability of the carbon-oxygen bond. The intrinsic properties of coordinated oxygen can facilitate the activation of various ligands including unsaturated hydrocarbons. In other cases, metal-mediated transformations of coordinated phosphines are typical reactions that are facilitated by a cooperative effect of several metal centers. They proceed through sequential oxidative addition reactions (P-C, P-H bond cleavage and/or acitvation of the C-H bond of the phosphorus substituents) and reductive eliminations involving migration of the phosphorus substituents to other coordinated substrates, generally ending with the stabilization of bridging phosphido or phosphinidene groups.

A major problem in cluster chemistry in terms of useful applications is their tendency to undergo thermal or photochemical fragmentation which often involves a preliminary heterolytic or homolytic metal-metal bond cleavage to generate a polynuclear metal unit containing an

unsatu

a meta

The fra za:bon;

> breakir arbony

duster

at high

1.g010u €cond

greater

I

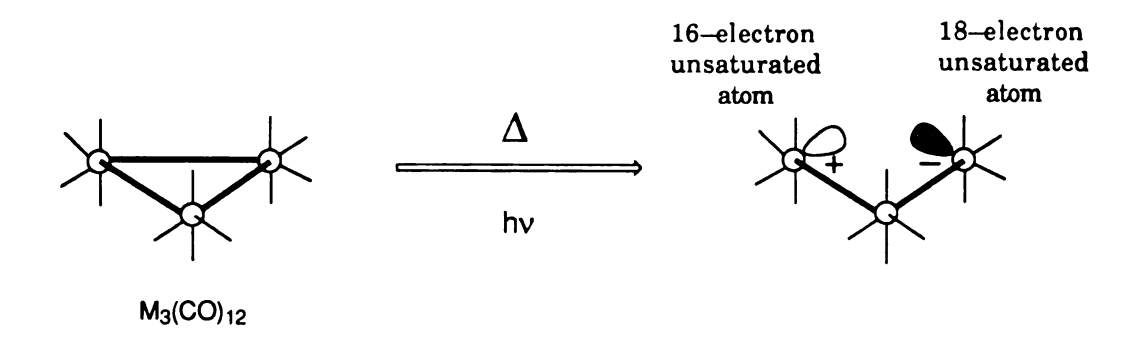
activate themist

uncjeo k

activati dusters

have be

unsaturated, 16-electron metal center. For example, a heterolytic fission of a metal-metal bond in a trinuclear carbonyl cluster is represented below.



The fragmentation arises from the fact that metal-metal and metal carbonyl bond energies are often comparable and hence metal-metal bond breaking is competitive with substitution processes. In the metal cluster carbonyls of Group 8, it is found that reactions of Fe₃(CO)₁₂ often lead to cluster break-up, while substitution of CO groups in Ru₃(CO)₁₂ occurs only at higher temperatures (ca. 80–100 °C), and in Os₃(CO)₁₂ under even more vigorous conditions. The activation of metal cluster complexes of the second and third row metals to permit milder reaction conditions and greater control of kinetic pathway is therefore essential.

In order to solve the problem of cluster fragmentation, the use of activated clusters as presursors has provided a breakthrough in cluster chemistry. Recent advances in the chemistry of activated clusters include nucleophilic activation, electron—induced nucleophilic substitution, activation by unsaturated metal clusters, and lightly stabilized metal clusters [31]. The lightly stabilized metal clusters with coordinated solvents have been proven to be excellent precursors in numerous reactions.

An M

×

ton;

000!

va-

ph.os

Among them, the most common solvated clusters are $M_3(CO)_{12-n}(NCMe)_n$ (M = Os, Ru; n = 1,2) which can be synthesized as following.

$$Me_3NO$$
 $Me_3N + CO_2$
 $M_3(CO)_{12}$
 $M_3(CO)_{11}$
 $M_3(CO)_{11}$
 $M_3(CO)_{11}$
 $M_3(CO)_{11}$
 $M_3(CO)_{11}$

Chapter V reports our investigation of the tertiary phosphine TMPP toward Group 8 metal carbonyl clusters. By taking advantage of the flexible coordination ability of the functionalized ligand TMPP, we demonstrated a variety of coordination modes in clusters. Cluster transformations of the phosphine complexes are also observed and discussed therein.

CHAPTER II

REACTIONS OF TRIPLY BONDED DIRHENIUM COMPLEXES WITH TRINUCLEAR CARBONYL CLUSTERS

l Intr

devel(

struct activi

987VB

the li latili

CO, :

comp

form from

Ph.₂I

Meta

oom abb

COE

\$0<u>u</u>

de: ar.c

H₂

•

1. Introduction

Multiply bonded dinuclear $(M^{\frac{n}{-}}M)$ complexes have been well developed in the past decade [2]. These compounds exhibit interesting structural and spectroscopic properties, ligand substitution and redox activity. The coordinatively unsaturated $M^{\frac{n}{-}}M$ core has been proven to serve as a template for substrate assemply and coupling [6]. Furthermore, the ligands in many multiply bonded molecules exhibit high substitutional lability. However, one major point is that strong π -acid ligands including CO, NO, and isocyanides only rarely occur in multiply bonded dinuclear complexes; in most cases, the introduction of π -acceptor ligands into the $M^{\frac{n}{-}}M$ framework results in M—M bond cleavage, and leads to the formation of mononuclear complexes [10]. Only a few complexes derived from phosphine-bridged species $Re_2X_4(dppm)_2$ ($Re^{\frac{3}{-}}Re$) ($dppm = Ph_2PCH_2PPh_2$) react with strong π -acid ligands to give adducts in which a metal-metal bond is preserved [11].

In this respect, we are interested in investigating an alternative approach to the synthesis of the π -acceptor containing metal-metal bonded complexes by the reaction between multiply bonded metal-metal dinuclear complexes with metal carbonyl clusters with the ability to serve as a CO source.

In this chapter we describe our work in the study of reactions between the multiply bonded dirhenium complex $Re_2X_4(dppm)_2$ ($Re^{-3}Re$) and the carbonyl clusters $H_2Os_3(CO)_{10}$ and $M_3(CO)_{12}$ (M=Ru, Os) and with H_2/CO mixtures. These reactions produce the unusual μ -hydrido carbonyl species $Re_2(\mu-H)(\mu-Cl)Cl_2(CO)_2(dppm)_2$.

2. Experimental

A. Synthesis

(1) Preparation of Re₂(µ-H)(µ-Cl)Cl₂(CO)₂(dppm)₂

The following methods involve refluxing a toluene solution of $Re_2Cl_4(dppm)_2$ in the presence of various carbonyl clusters $(\mu-H)_2Os_3(CO)_{10}$, $Os_3(CO)_{12}$ and $Ru_3(CO)_{12}$ with a constant flush of H_2 passing through the solution. $Os_3(CO)_{12}$ and $Ru_3(CO)_{12}$ were obtained from commercial sources. $Re_2Cl_4(dppm)_2$ [39] and $(\mu-H)_2Os_3(CO)_{10}$ [40] were prepared by literature methods.

(i) Reaction of $Re_2Cl_4(dppm)_2$ with $(\mu-H)_2Os_3(CO)_{10}$ in the presence of H_2

A mixture of $(\mu\text{-H})_2\text{Os}_3(\text{CO})_{10}$ (0.10 g, 0.117 mmol) and $\text{Re}_2\text{Cl}_4(\text{dppm})_2$ (0.15 g, 0.12 mmol) was placed in a 50 mL Schlenk tube equipped with a condenser and a stir bar. Toluene (20 mL) was added, and the solution was refluxed with a slow stream of H_2 bubbling through the solution. During the course of the reaction, the solution color changed from dark purple to green-brown. The progress of the reaction was monitored by infrared spectroscopy and was judged to be complete after 12 h on the basis of the disappearance of $(\mu\text{-H})_2\text{Os}_3(\text{CO})_{10}$. The solvent was removed to give a green-brown residue which was further separated by column chromatography (packed with unactivated silica gel), and the first light yellow band was collected by using hexane/CH₂Cl₂ (1:1, v/v) as the eluent, and was identified as $H_4\text{Os}_4(\text{CO})_{12}$ by a comparison of its infrared and ¹H NMR spectroscopy to that reported in the literature [41]; yield: 0.05 g (39%). IR (CH₂Cl₂): v(CO) = 2085 (m), 2067 (s), 2019 (s), 1995 (m) cm⁻¹. ¹H NMR

CD :92₍

and

spec

v () 401

130 C. 4

(ii)

g. () of H

> spe Os

> :es

ch: sol:

of c

:he

Œ

iii

g. (

(CD₂Cl₂): $\delta = -20.44$ (s) ppm. EI–MS spectrum: parent ion, m/z = 1101.9 (¹⁹²Os). The second green band was collected with CH₂Cl₂ as the eluent, and characterized as Re₂(μ -H)(μ -Cl)Cl₂(CO)₂(dppm)₂ on the basis of spectroscopic and crystallographic data; yield: 0.10 g (70%). IR (Nujol): v(CO) = 1890 (vs), 1854 (s) cm⁻¹. ¹H NMR (CD₂Cl₂): δ = 12.75 (1H, s), 7.35 (40H, m), 4.70 (2H, m), 4.27 (2H, m). FABMS spectrum: parent ion, m/z = 1304.5 (¹⁸⁷Re). Anal. Calcd for C₅₂H₄₅Cl₃O₂P₄Re₂: C, 47.87; H, 3.50. Found: C, 48.34; H, 4.10.

(ii) Reaction of Re₂Cl₄(dppm)₂ with Os₃(CO)₁₂ in the presence of H₂

A mixture of $Os_3(CO)_{12}$ (0.10 g, 0.110 mmol) and $Re_2Cl_4(dppm)_2$ (0.14 g, 0.110 mmol) in toluene (20 mL) was refluxed with a constant slow stream of H_2 passing through the solution. The reaction was monitored by infrared spectroscopy and stopped after 8 h on the basis of the disappearance of $Os_3(CO)_{12}$. The resulting solution was evaporated to dryness, and the residue was redissolved in CH_2Cl_2 (5 mL), and purified by column chromatography. Elution with hexane/ CH_2Cl_2 (1:3, v/v) gave a pale yellow solution containing 0.020 g of $H_4Os_4(CO)_{12}$ (yield \approx 20%) and a small amount of compound (1) (yield \approx 10%). A brown intractable material was retained at the top of the column. The IR, ¹H NMR and mass spectral data for both compounds are given in section A(i).

(iii) Reaction of $Re_2Cl_4(dppm)_2$ with $Ru_3(CO)_{12}$ in the presence of H_2

A mixture of $Ru_3(CO)_{12}$ (0.10 g, 0.156 mmol) and $Re_2Cl_4(dppm)_2$ (0.21 g, 0.16 mmol) in toluene (20 mL) was refluxed with a constant slow stream of H_2 bubbling through the solution. The reaction was monitored by infrared spectroscopy and was stopped after 8 h on the basis of the

disappearance of $Ru_3(CO)_{12}$. The reaction solution was worked-up in the same manner as reaction A(ii). The main product that was isolated is the known compound $H_4Ru_4(CO)_{12}$ [42]; yield: 0.018 g (\approx 15%). IR (CH_2Cl_2): v(CO) = 2080 (s), 2066 (vs), 2022 (s), 2010 (w) cm⁻¹, along with a small amount of compound (1) (yield < 5%).

(iv) Reaction of Re₂Cl₄(dppm)₂ with an H₂/CO Gas Mixture

A solution of $Re_2Cl_4(dppm)_2$ (0.10 g, 0.08 mmol) in toluene (20 mL) was refluxed for 20 h with a rapid stream of H_2 and a slow stream of CO passing through the solution. The resulting cloudy green solution contained a small amount of olive green precipitate, which was collected by filtration and identified as $Re_2Cl_4(CO)_2(dppm)_2$ by its infrared spectrum (Nujol) (v(CO) = 1958 (vs), 1946 (vs), 1722 (m) cm⁻¹); yield: 0.011 g (17%). The green filtrate was characterized as compound (1) on the basis of IR and ¹H NMR spectroscopies; yield 0.050 g (48%).

(v) Reaction of $Re_2Cl_4(dppm)_2$ with $(\mu-H)_2Os_3(CO)_{10}$ in the absence of H_2

The reaction was performed under the same manner as section A(i) but without the constant flush of H_2 through the solution. During the reaction, the solution color changed from dark purple to cloudy greenbrown, and after 68 h of reflux, infrared spectroscopy indicated that very little $(\mu$ -H)₂Os₃(CO)₁₀ remained. After removal of the solvent, the residue was extracted with diethyl ether (20 mL) and filtered to yield a brown precipitate and a brown solution. The brown solid was dissolved in THF (20 mL) and chilled to -10° C to give a green solid that did not contain carbonyl ligands as judged by infrared spectroscopy. The compound was not further investigated. There was no evidence for the presence of the title compound

in the r

starting

(vi) Rea

e. 0.08

stream

green j

Nujol

contin

mmol

Was st

r::C0

produ

(vii)

0.08 Strea

:esu

Re₂(

exce

COUC

(CH

ľ(ę

in the remaining brown THF solution or the diethyl ether solution. The only identifiable $\nu(CO)$ band in these solutions may be attributed to the starting material $(\mu-H)_2Os_3(CO)_{10}$.

(vi) Reaction of Re₂Cl₄(dppm)₂ with NaBH₄ in the presence of CO

A suspension of $Re_2Cl_4(dppm)_2$ (0.10 g, 0.08 mmol) and $NaBH_4$ (0.003 g, 0.08 mmol) was refluxed in toluene (20 mL) for 3 h with a constant slow stream of CO passing through the solution. During this time, an olive green precipitate formed which was identified as $Re_2Cl_4(CO)_2(dppm)_2$. IR (Nujol): v(CO) = 1958 (vs), 1944 (s), 1721 (m) cm⁻¹. The reaction was then continued after the addition of an excess amount of $NaBH_4$ (0.015 g, 0.4 mmol) into the suspension of $Re_2Cl_4(CO)_2(dppm)_2$ in toluene. The solution was stirred for 6 h to give a soluble green compound which exhibits a single v(CO) stretch at 1857 cm⁻¹. No attempt was made to characterize the product. There was no evidence for the presence of (1) in the reaction.

(vii) Reaction of Re₂Cl₄(dppm)₂ with NaH in the presence of CO

A mixture of $Re_2Cl_4(dppm)_2$ (0.10 g, 0.08 mmol) and NaH (0.002 g, 0.08 mmol) was refluxed in CH_2Cl_2 (20 mL) for 24 h with a constant slow stream of CO passing through the solution. An infrared spectrum of the resulting yellow-green solution revealed that the product is $Re_2Cl_4(CO)_2(dppm)_2$. The reaction was continued after addition of an excess amount of NaH (0.10 g, 0.4 mmol) into the reaction solution containing $Re_2Cl_4(CO)_2(dppm)_2$. The solution was stirred for 24 h to give a dark green solution which exhibits a complicated v(CO) region. IR (CH₂Cl₂): 1955 (s), 1945 (s), 1925 (s), 1845 (m), and 1724 (m) cm⁻¹. There was no evidence for the formation of (1) in this reaction.

(2) Reaction of $Re_2(\mu-H)(\mu-Cl)Cl_2(CO)_2(dppm)_2$ with one equivalent of $NOBF_4$

Acetonitrile (10 mL) was added into a mixture of $Re_2(\mu-H)(\mu-Cl)Cl_2(CO)_2(dppm)_2$ (0.050 g, 0.220 mmol) and $NOBF_4$ (0.008 g, 0.220 mmol), and the green solution turned brown immediately. The mixture was stirred for 15 min with constant pumping to remove NO gas. A green solid was collected on a medium-porosity frit under argon and dried *in vacuo*. The product was recrystallized by slow diffusion of diethyl ether into a CH_2Cl_2 solution of the compound; yield ≈ 90 %. IR (Nujol): v(CO) = 2007 (vs), 1851 (w) cm⁻¹. λ_{max} (CH_2Cl_2) = 401 nm.

(3) Reaction of Re₂(μ-H)(μ-Cl)Cl₂(CO)₂(dppm)₂ with an excess of NOBF₄

Acetonitrile (10 mL) was added into a mixture of $Re_2(\mu-H)(\mu-Cl)Cl_2(CO)_2(dppm)_2$ (0.050 g, 0.220 mmol) and an excess of NOBF₄ (0.016 g, 0.440 mmol), and the green solution turned brown. After the mixture was stirred for 8 h in a close system under argon, a green solid was collected on a medium-porosity frit under argon and dried *in vacuo*. The product was recrystallized by slow diffusion of diethyl ether into a CH_2Cl_2 solution of the compound. The compound was further characterized by X-ray diffraction study and revealed to be $Re_2(\mu-Cl)(\mu-CO)Cl_2(CO)(NO)(dppm)_2$.

(4) Reaction of $Re_2(\mu-H)(\mu-Cl)Cl_2(CO)_2(dppm)_2$ with Cobaltocene

Acetone (5 mL) was added to the mixture of $Re_2(\mu-H)(\mu-Cl)Cl_2(CO)_2(dppm)_2$ (0.025 g, 0.11 mmol) and cobaltocene (0.005 g, 0.11 mmol) whereupon the green solution turned blue-green. The solution was stirred for 15 min after which time a fine blue-green precipitate was

filtered from a clear solution. The solid was collected on a fine-porosity frit under argon and dried in vacuo; yield $\approx 90\%$. IR (Nujol): v(CO) = 1823 (vs), 1805 (w) cm⁻¹.

(5) Electrochemical Oxidation of Re₂(μ-H)(μ-Cl)Cl₂(CO)₂(dppm)₂

A four compartment electrochemical cell was used for the bulk electrolysis experiment. The working electrode is constructed of Pt mesh approximately 1 cm² in area. The counter electrode (Pt wire) is separated from the working elctrode by two medium porosity glass frits, and the Ag/AgCl reference electrode is separated from the working electrode by a fine porosity glass frit. A dichloromethane solution containing 0.1 M [n- Bu_4N [BF₄] as a supporting electrolyte was added to all four compartments, and a small amount of Re₂(μ-H)(μ-Cl)Cl₂(CO)₂(dppm)₂ (≈ 0.005 g) was added to the working electrode compartment. The potential of the working electrode was set to +1.0 V and the solution was stirred rapidly. The green solution slowly turned yellow-green, and the oxidation process was monitored by UV-visible spectroscopy. During the electrolysis, the original intense absorption band at 423 nm due to the neutral species diminished and an absorption band appeared at 404 nm. After the bulk oxidation proceeded for 2 h, the yellow-green solution was transferred via syringe to a Schlenk tube, and crystallized by slow diffusion of hexane into the solution. IR (Nujol): v(CO) = 1999 (vs), 1973 (vs) cm⁻¹. λ_{max} (CH₂Cl₂) = 404 nm. The compound was structurally characterized as the salt [Re₂(μ-H)(μ- $C1)Cl_2(CO)_2(dppm)_2](BF_4).$

Prolonged bulk electrolysis at +1.0 V resulted in a decomposition of the yellow-green product to give a brown solution after ca. 2 days. The brown product was worked-up in the same manner as above, and recrystallized by slow diffusion of hexane into the $[n\text{-Bu}_4N][BF_4]$ – CH_2Cl_2 solution. Brown crystals appeared after 2 days. IR (Nujol): $\nu(CO) = 2007$ (vs), 1851 (w) cm⁻¹. FABMS spectrum: parent ion, m/z = 1338 (^{187}Re). An X-ray diffraction study of one of the brown crystal revealed the compound to be $Re_2(\mu\text{-Cl})(\mu\text{-CO})Cl_2(CO)_2(dppm)_2$.

(6) Electrochemical Reduction of Re₂(μ-H)(μ-Cl)Cl₂(CO)₂(dppm)₂

The same electrochemical cell described in the previous section was also used for bulk reduction. A dichloromethane solution containing 0.1 M $[n-Bu_4N][BF_4]$ as the supporting electrolyte was added to all four compartments, and a small amount of $Re_2(\mu-H)(\mu-Cl)Cl_2(CO)_2(dppm)_2$ (\approx 0.005 g) was added to the working electrode compartment with an applied potential of -1.0 V accompanied by rapid stirring of the solution. The green solution slowly turned blue-green. After the bulk reduction had proceeded for 2 h, the blue-green solution was transferred to a Schlenk tube and recrystallized by slow diffusion of diethyl ether (or hexane) into the solution. The reduction species is very air-sensitive, and it underwent oxidation to the neutral complex during the recrystallization process. IR (Nujol): v(CO) = 1823 (vs), 1805 (w) cm⁻¹.

B. X-ray Crystal Structures

(1) $Re_2(\mu-H)(\mu-Cl)Cl_2(CO)_2(dppm)_2$

(i) Data Collection and Reduction

A green crystal of dimensions $0.40 \times 0.30 \times 0.25 \text{ mm}^3$ was covered with epoxy cement and mounted at the end of a glass fiber. Geometric and intensity data were obtained on a Nicolet P3/F diffractometer equipped with graphite monochromated MoK α radiation. A rotation photograph indicated that the crystal diffracted well. An automatic search routine was used to locate 25 reflections in the range $20 \le 20 \le 30^\circ$. The reduced cell dimensions indicated that the crystal belongs to the tetragonal crystal system; axial photographs revealed that the Laue class is 4/mmm.

Data reduction was carried out by standard methods with the use of well-established computational processures. Systematic absences from the data led to the space group choices of $P4_12_12$ and $P4_32_12$. An ω -20 motion was used to scan 8125 data points in the range of $4.5 \le 20 \le 45^{\circ}$. Structure factors were obtained after Lorentz and polarization corrections. During intensity data collection three check reflections were measured at regular intervals; an average loss in intensity of 4.8% was observed. The program CHORT was applied to correct for this. Azimuthal scans of reflections with Eulerian angle χ near 90° (3 curves) were used as a basis for an empirical absorption correction. After avaraging of the equivalent reflections, there remained 4834 unique data and 3319 reflections with $F_0^2 > 3 \sigma(F_0^2)$.

(ii) Structure Solution and Refinement

The position of the unique Re atom was obtained by the application of MULTAN 11/82. A sequence of successive difference Fourier maps and least-squares cycles led to full development of the coordination sphere. The final full-matrix refinement involved 289 variable parameters and 3319 data, for a data-to-parameter ratio of 11.5. The refinement converged with residuals of R = 0.0304, $R_w = 0.0368$ and quality-of-fit 0.643. A comparison

of the refinement in the two enantiomorphs revealed that P4₁2₁2 is the correct choice for the space group.

(2) $[Re_2(\mu-H)(\mu-Cl)Cl_2(CO)_2(dppm)_2](BF_4)$

(i) Data Collection and Reduction

A plate-like green crystal of approximate dimensions 0.48 x 0.15 x 0.26 mm³ was mounted on a glass fiber with vacuum grease, and data collection was carried out at -98°C on a Nicolet P3/F diffractometer upgraded to a Siemens P3/V equipped with graphite-monochromated CuKa radiation and a low temperature device. A rotation photograph was used to locate 15 reflections from which a preliminary cell was indexed. The reduced cell dimensions indicated that the crystal was triclinic which was confirmed by axial photography. An accurate cell for data collection was measured based on 25 reflections with $40 \le 20 \le 60^{\circ}$. Intensity data were collected using the ω -20 scan mode in the range of $4 \le 20 \le 106^{\circ}$ with variable scan speed from 3 to 10 min^{-1} in ω . Three standard reflections measured at constant intervals showed no significant decay in intensities. Data were corrected for Lorentz and polarization effects. The linear absorption coefficient for CuKa was 112.510° cm⁻¹, and an empirical absorption correction was applied based on ψ scan of three reflection with χ near 90°C.

(ii) Structure Solution and Refinement

The structure was solved by direct methods using the program in SHELXS-86. The heavy atoms were located by a sequence of successive difference Fourier maps, and least-squares cycles led to full development of

th 75 the coordination sphere. The final full–matrix refinement involved 334 variable parameters and 4841 observed reflections with $F_o^2 > 3\sigma(F_o^2)$. The refinement converged with residuals of R = 0.161 and $R_w = 0.146$.

(3) $[Re_2(\mu\text{-CO})(\mu\text{-Cl})Cl_2(CO)(NO)(dppm)_2](BF_4)$

(i) Data Collection and Reduction

A small green crystal of approximate dimensions 0.20 x 0.18 x 0.05 mm³ was mounted on a glass fiber with vacuum grease, and cooled to -95 °C in a nitrogen cold stream on a Nicolet P3/F diffractometer upgraded to a Siemens P3/V equipped with graphite—monochromated CuK α radiation and a low temperature device. Cell parameters were determined from 25 reflections with $40 \le 20 \le 60^{\circ}$. Intensity data were collected using the ω -20 scan mode in the range of $4 \le 20 \le 106^{\circ}$ with variable scan speed 1.5 – 3.0 min⁻¹ in ω . Three standard reflections measured at constant intervals showed no significant decay in intensities. Data were corrected for Lorentz and polarization effects. The linear absorption coefficient for CuK α was 90.628 °cm⁻¹, and an empirical absorption correction was applied based on ψ scans of three reflection with χ near 90°C.

(ii) Structure Solution and Refinement

The structure was solved by direct methods using SHELXS. The positions of heavy atoms were located, and a sequence of successive difference Fourier maps and least-squares cycles led to the location of the remaining non-hydrogen atoms. The final full-matrix refinement involved 326 variable parameters and 5904 observed reflections with F_0^2 >

 $3\sigma(F_o^2)$. The refinement converged with residuals of R = 0.167 and $R_w = 0.214$.

(4) $Re_2(\mu\text{-Cl})(\mu\text{-CO})Cl_2(CO)_2(dppm)_2$

(i) Data Collection and Reduction

A brown crystal with approximate dimensions of 0.26 x 0.13 x 0.05 mm³ was mounted on a glass fiber. All measurements were made on a Nicolet P3/F diffractometer upgraded to a Siemens P3/V equipped with graphite monochromated MoK α radiation and a low temperature device. A rotation photograph was used to locate 16 reflections from which a preliminary cell was indexed. Accurate cell constants and an orientation matrix for data collection were obtained from a least–squares refinement using the setting angles of 25 reflections in the range of $20 \le 20 \le 25^{\circ}$. The cell is monoclinic (C centered) with dimensions : a = 22.945 (5) Å, b = 11.322 (3) Å, c = 23.406 (8) Å and V = 5968 (3) Å³. The data were collected using an omega scan mode in the range $4 \le 20 \le 45^{\circ}$ with a scan speed of 4 min⁻¹. The diameter of the incident beam collimator was 1.5 mm.

Three standard reflections were measured at constant intervals with no significant loss in intensity. The linear absorption coefficient for MoK α was 43.996 cm⁻¹. An empirical absorption correction, based on azimuthal scans of three reflections with χ near 90°, was applied which resulted in transmission factors ranging from 1.000 to 0.226. The data were corrected for Lorentz and polarization effects.

(ii) Structure Solution and Refinement

All calculations were performed using the TEXSAN crystallographic software package of Molecular Structure Corporation.

The structure was solved by direct methods using SHELXS-86. The positions of heavy atoms were obtained from peaks with the highest electron density. A sequence of successive difference Fourier maps and least-squares cycles led to full development of the coordination sphere. The final cycle of full-matrix least-squares refinement involved 121 variable parameters and 2163 observed reflections with $F_o^2 > 3\sigma(F_o^2)$. The refinement converged with residuals of R = 0.210 and $R_w = 0.241$.

3. Results and Discussion

A. Synthetic Methods

Our study of the reaction between $(\mu\text{-H})_2\text{Os}_3(\text{CO})_{10}$ and $\text{Re}_2\text{Cl}_4(\text{dppm})_2$ in the presence of H_2 provides a high yield synthetic route for the preparation of a halide carbonyl dinuclear complex that also contains a bridging hydride ligand $\text{Re}_2(\mu\text{-H})(\mu\text{-Cl})\text{Cl}_2(\text{CO})_2(\text{dppm})_2$. The source of the hydride ligand is of considerable interest to us; two plausible reaction routes for the synthesis of the hydride–bridged dirhenium complex are postulated: (a) the bridging hydride ligand was derived from $(\mu\text{-H})_2\text{Os}_3(\text{CO})_{10}$ via metal hydride coupling, followed by H—Os bond scission [43], and (b) the bridging hydride ligand was derived directly from molecular hydrogen through oxidative addition as shown on the following page.

$$\begin{bmatrix} \text{Re} = \text{Re} \end{bmatrix}$$

$$H_2\text{Os}_3(\text{CO})_{10}$$

$$\begin{bmatrix} \text{Re} = \text{Re} \end{bmatrix}$$

$$H_2$$

$$\begin{bmatrix} \text{Re} = \text{Re} \end{bmatrix}$$

$$\begin{bmatrix} \text{Re} = \text{Re} \end{bmatrix}$$

$$H_2$$

A second important question is whether the CO ligands in (1) were obtained by ligand transfer reaction from $(\mu\text{-H})_2\text{Os}_3(\text{CO})_{10}$ without any interaction between both metal systems, or via an intermediate with the interaction between the complexes $\text{Re}_2\text{Cl}_4(\text{dppm})_2$ and $(\mu\text{-H})_2\text{Os}_3(\text{CO})_{10}$ followed by ligand exchange reaction. These points are important for the understanding of possible formation of heteronuclear complexes in this reaction. In order to probe the role of $(\mu\text{-H})_2\text{Os}_3(\text{CO})_{10}$ and H_2 in the reaction and to further understand the reaction pathway, two alternative reactions were designed (Table 2). One involves the use of carbonyl clusters as precursors to provide the sources of CO, and another one involves the use of CO gas along with various potential hydride sources including molecular hydrogen and hydride reagents such as NaH and NaBH₄. In the latter of the two approaches, a significant result was obtained from the direct reaction of $\text{Re}_2\text{Cl}_4(\text{dppm})_2$ with an H_2/CO gas mixture at atmospheric pressure. The yield of (1) by this method critically depends on the relative

Table 2. Various synthetic approach in the preparation of $Re_2(\mu\text{-}H)(\mu\text{-}Cl)Cl_2(CO)_2(dppm)_2.$

Con	Condition		
СО	+	H_2	≈ 40
СО	+	NaH	0
СО	+	NaBH ₄	0
(μ-H) ₂ Os ₃ (CO) ₁₀	+	H_2	≈ 7 0
(μ-H) ₂ Os ₃ (CO) ₁₀			0
$\mathrm{Os_3(CO)_{12}}$	+	H_2	≈ 1 0
Ru ₃ (CO) ₁₂	+	H ₂	≈ 10

concentrations of H₂ and CO in the reaction. If the CO concentration is in excess, one obtains a high yield of the previously reported compound Re₂Cl₄(CO)₂(dppm)₂ but very little of (1). It is known that the reaction of Re₂Cl₄(dppm)₂ with CO is facile, and it will form an A-frame-like monocarbonyl adduct first, and react further to form an edge-sharing bioctahedral complex Re₂Cl₄(CO)₂(dppm)₂. The reactions of Re₂Cl₄(dppm)₂ under a CO atmosphere with sodium borohydride and sodium hydride led to product mixtures which contained Re₂Cl₄(CO)₂(dppm)₂ and some polyhydride complexes, but no evidence for the formation of (1), as determined by IR and ¹H NMR spectroscopy

(i) H₂ (ii) NaH or NaBH₄

From the aforementioned discussion, it can be ascertained that the control of the CO concentration in these reactions is essential, and higher levels of H₂ are necessary in order to favor the formation of (1). This finding suggests that the molecular hydrogen reacts with Re₂Cl₄(dppm)₂ first, which prevents the formation of the highly unreactive product Re₂Cl₄(CO)₂(dppm)₂. Based on this consideration, we postulate that the product (1) may initially form an edge-sharing bioctahedral dihydride complex via an oxidation addition by molecular hydrogen, followed by a subsequent reductive elimination of HCl as shown on the following page.

Attempts to isolate the intermediate dihydride by reaction of Re₂Cl₄(dppm)₂ with H₂ resulted in intractable mixtures, so we believe that it is an unstable compound that is trapped by CO. Unlike the reaction with main group hydrides described above, the reaction of (μ-H)₂Os₃(CO)₁₀ and $Re_2Cl_4(dppm)_2$ provides a good yield of (1) ($\approx 70\%$). In order to determine the importance of (µ-H)₂Os₃(CO)₁₀ as the source of the hydrogen atom in our original synthesis, several additional reactions with clusters were carried In one approach, $Os_3(CO)_{12}$ and H_2 gas was used instead of (μ - $H_{2}Os_{3}(CO)_{10}$ as a starting material; this produced (1) in a very low yield (5– 10%). Since the initial formation of $(\mu-H)_2Os_3(CO)_{10}$ from the reaction of H_2 and $Os_3(CO)_{12}$ is facile, the following reaction of $(\mu-H)_2Os_3(CO)_{10}$ with Re₂Cl₄(dppm)₂ may occur. If this were the case, one would expect a yield that is comparable to that obtained when starting directly from (µ- $H_{2}Os_{3}(CO)_{10}$ (\approx 70%). Furthermore, there is no dihydride analogue in a triruthenium cluster system which could act as an intermediate, yet one still obtains a small amount of (1).

It is important to note that if the reaction between $(\mu-H)_2Os_3(CO)_{10}$ and $Re_2Cl_4(dppm)_2$ is performed under an atmosphere of argon instead of hydrogen, the resulting reaction solution contains a mixture of products including the osmium starting material and an intractable brown

compound but none of (1). The result, when taken together with the above observations, suggests that the presence of H_2 facilitates the reaction, presumably by assisting in the formation of an intermediate(s).

Moreover, the result suggests that a hydrido-cluster intermediate formed by metal hydride coupling might not be an essential requirement in the formation of (1), but the best yield of compound (1) derived from the reaction between $H_2Os_3(CO)_{10}$ and $Re_2Cl_4(dppm)_2$ in the presence of H_2 indicates that $H_2Os_3(CO)_{10}$ might play an important role as a source of a controlled amount of CO in the reaction. The discovery of the formation of the novel complex (1) from the gaseous starting materials H_2 and CO appears to provide a promising opportunity. The result demonstrated an alternative synthetic route for the synthesis of multiply bonded halide carbonyl complexes, and the success in the synthesis of the hydride containing compound under an ambient pressure of H_2 paves the way for an exciting research area, namely, the activation of molecular hydrogen in the presence of multiply bonded dinuclear systems [35].

B. Spectroscopic Studies

¹H NMR spectroscopy is the most widely used spectroscopic tool for the study of hydride complexes, with resonances for diamagnetic complexes usually appearing in the range from 0 to -40, and exceptional examples occurring in the range +30 to -60ppm [44]. In our study, the observation of sharp signals in the ¹H NMR spectrum supports the formulation of the compound (1) as a diamagnetic Re₂⁴⁺ species and not a paramagnetic complex derived from an Re₂³⁺ core. The diamagnetism was further demonstrated by a magnetic susceptibility measurement that was carried out in solution by the Evans method [45]. The absence of a

shifte A roo

of the

methy

appro

= +12

atter

some .

open l

should

for ot

transit

R = 1them10

Ppm (4

due to

by sele

nethy:

Pinter

ritual

simmet when th

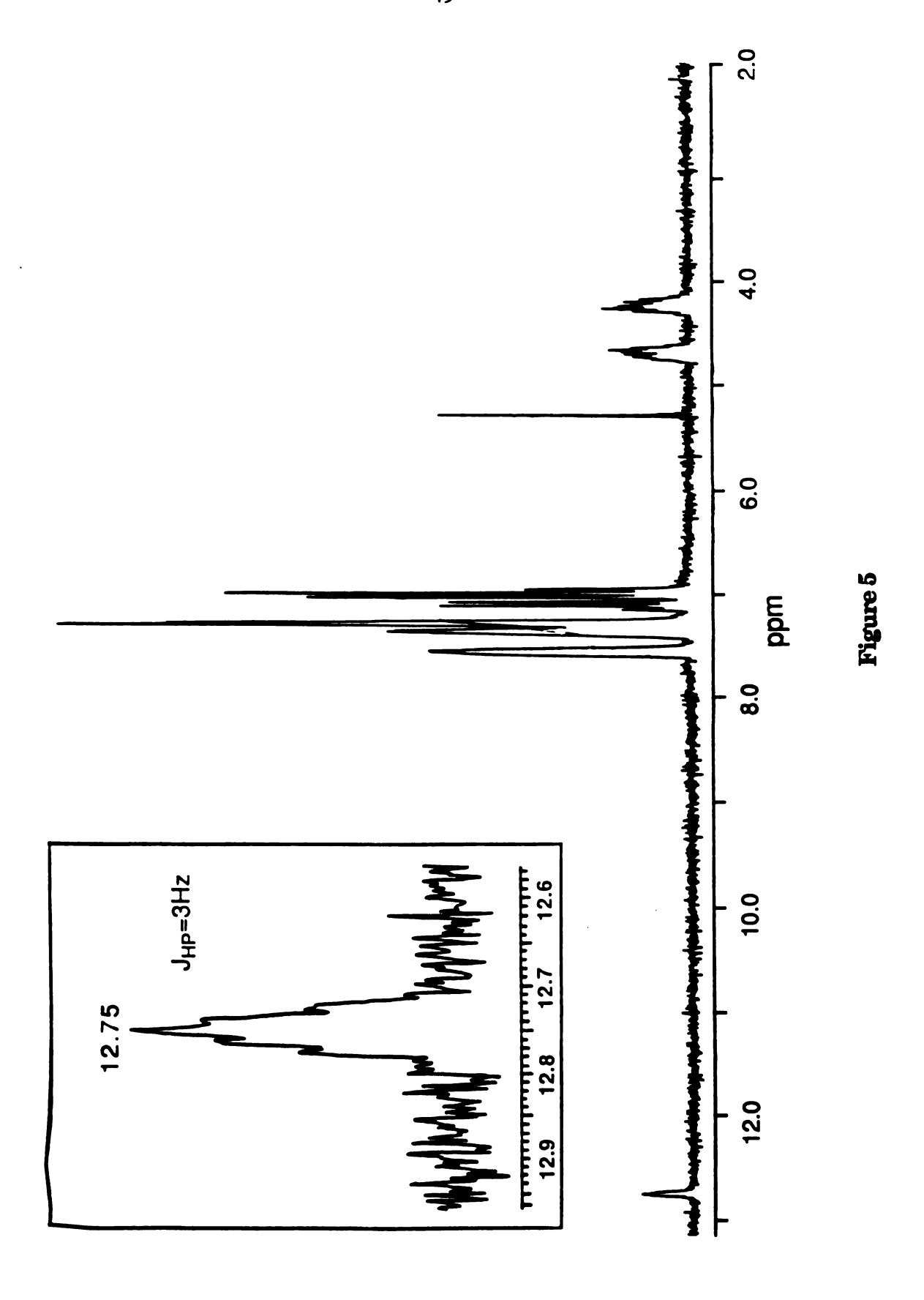
resonan

excips i

shifted solvent resonance rules out the presence of a paramagnetic species. A room-temperature ¹H NMR spectrum of (1) in CD_2Cl_2 (Figure 5) consists of the phenyl proton resonances as a multiplet centered at $\delta = 7.50$ ppm, the methylene resonances of the dppm located at $\delta = 4.70$ and 4.27 ppm, which approximates to an ABX₄ pattern, and surprisingly, a broad resonance at δ = +12.75 ppm, which integrates as one proton. As the reproducibility of the latter signal for several different samples of (1) was excellent, we concluded that the resonance is due to a hydride ligand in the compound and not to some anomalous impurity. Indeed, the X-ray structure of (1) reveals an open bridging site where a hydrogen atom may be expected to reside. It should be noted that unusual downfield chemical shifts have been reported for other hydrido-bridged metal-metal bonded dimers of the early transition metals. For example, the hydride resonances of NaW₂(μ -H)(OR)₈ $(R = i-Pr, CH_2-t-Bu)$ appear as sharp singlets ca. $\delta = +9$ ppm [46] and the chemical shift of the μ -H groups for $Ta_2Cl_6(PMe_3)_4(\mu$ -H)₂ occurs at $\delta = +8.52$ ppm [47]. The unusual chemical shift of the bridging hydride is probably due to the diamagnetic anisotropy of the multiple metal-metal bond [48].

The presence of the bridging hydride ligand was further confirmed by selective decoupling experiments. As shown in Figure 5, when the methylene resonances of the dppm ligand are decoupled, a symmetrical quintet is observed for the signal at $\delta = +12.75$ ppm ($J_{PH} = 3$ Hz) due to virtual coupling to the four trans phosphorous atoms, which are symmetrically situated with respect to the bridging hydgide. Furthermore, when the resonance at $\delta = +12.75$ ppm is decoupled, both sets of methylene resonances are affected, thereby establishing that the coupling to these groups is not an NOE effect but a through-bound coupling phenomenon. If

Figure 5. A 500 MHz 1 H NMR spectrum of Re $_2(\mu$ -H)(μ -Cl)Cl $_2$ (CO) $_2$ (dppm) $_2$ in CD $_2$ Cl $_2$ at 22 o C.



an NOE effect were responsible, only one methylene proton (the one closest to the bridging hydride) would be affected.

We have also observed a solvent effect on the ¹H NMR spectrum of $Re_2(\mu-H)(\mu-Cl)Cl_2(CO)_2(dppm)_2$. The methylene resonances, which exhibit a closely spaced ABX_4 pattern in CD_2Cl_2 , appear as an AM pattern ($\delta=4.47$, 5.35 ppm) with superimposed phosphorous coupling in acetone– d_6 (Figure 6). Also, the chemical shift of the μ -H ligand is different in the two oxygen–donor solvents. In acetone– d_6 and THF– d_8 , the μ -H resonance occurs at $\delta=+12.89$ and +12.91 ppm, respectively. These observations are consistent with the formation of a weak solvent interaction with $Re_2(\mu-H)(\mu-Cl)Cl_2(CO)_2(dppm)_2$ species. The $\nu(CO)$ bands are also solvent–dependent, which further supports the notion that oxygen donors are capable of interacting with the complex.

A room-temperature ³¹P NMR spectrum (without decoupling ¹H) in CD_2Cl_2 displays a broad singlet at $\delta = -14$ ppm, which is shifted downfield from free dppm ($\delta = 22.7$ ppm) as expected. The broad nature of the signal is due to the unresolved coupling to the dppm methylene protons and to the bridging hydride.

The " T_1 criterion" [49] for distinguishing between "classical" and "nonclassical" hydrides, originally proposed by Crabtree [49(i)], was based on the distinction of whether $T_1(\min)$ (i.e., the minimum value of T_1 when the temperature is varied) was shorter than 80 ms (nonclassical) or greater than 150 ms (classical) at 250 MHz (Note: $T_1(\min)$ is proportional to the magnetic field strength, so that these values correspond to 160 and 300 ms at 500 MHz, etc.). Recent studies have revealed several examples of polyhydrides that apparently violate this criterion [49(g)-(h)]. In order to further understand the variation of the T_1 values for metal hydride

Figure 6. A 500 MHz 1 H NMR spectra of the methylene region for Re $_2$ (μ -H)(μ -Cl)Cl $_2$ (CO) $_2$ (dppm) $_2$ in (a) CD $_2$ Cl $_2$ and (b) acetone-d $_6$ at 22 $^{\circ}$ C.

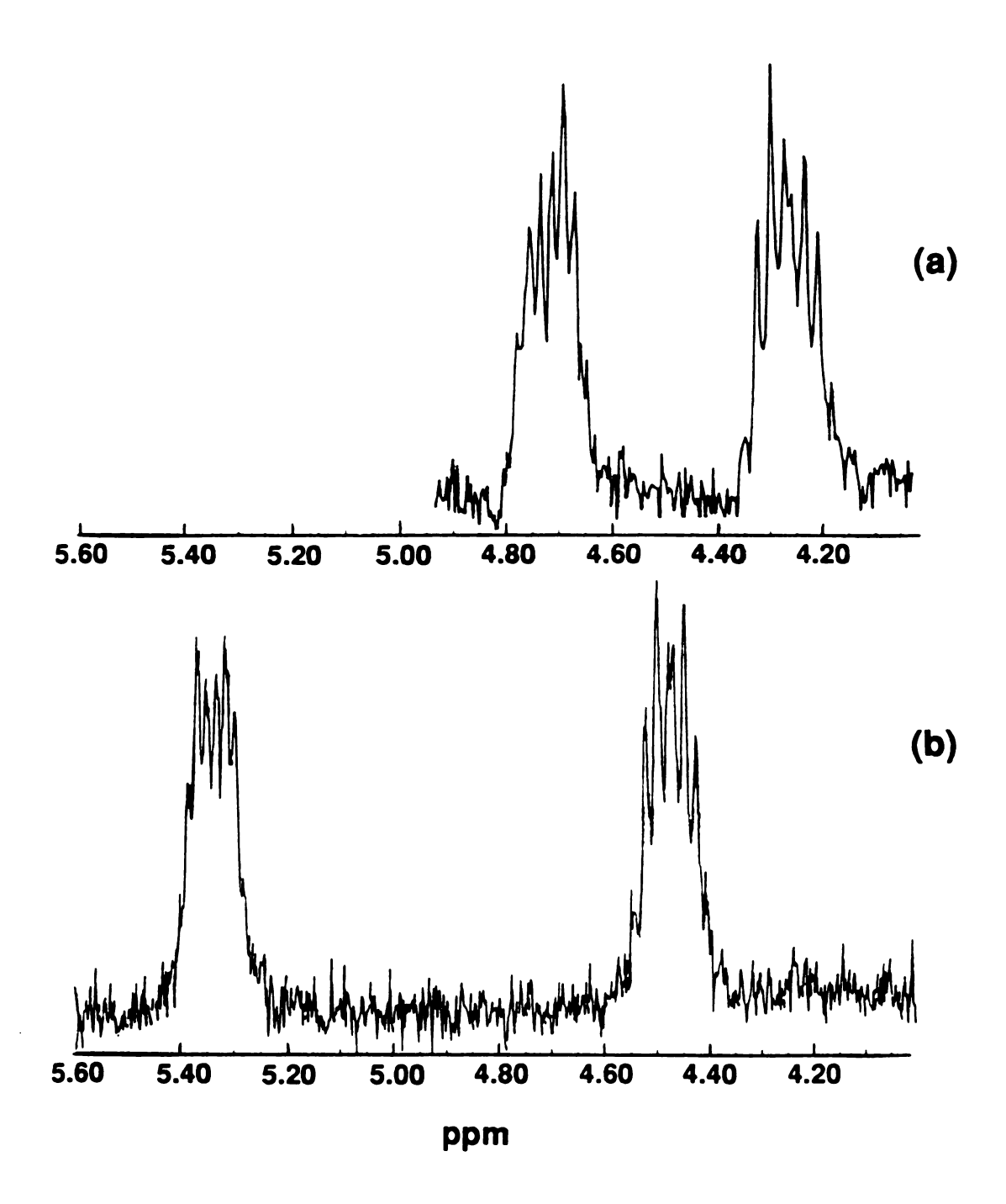


Figure 6

complexes, varible-temperature T_1 measurements on the dirhenium monohydride compound $Re_2(\mu-H)(\mu-Cl)Cl_2(CO)_2(dppm)_2$ (1) have been carried out at 200 MHz ¹H NMR in CD_2Cl_2 . The data showed a decrease in T_1 with temperature to ca. 85 ms at 200 MHz and -50°C but no increase or decrease as the temperature was lowered further as shown in Figure 7. The result indicated that the scalar coupling mechanism might contribute to the low T_1 value in this complex instead of a dipole-dipole relaxation [49(d)].

Fast atom bombardment (FAB) mass spectrometry has been recently developed to provide a powful tool for the characterization of organometallic and coordination compounds [50]. In our study, an anlysis of (1) by positive fast atom bombardment (FAB) mass spectrometry gave a spectrum with well—resolved peaks (Figure 8). In order to further substantiate that the highest mass peak at m/z = 1304.5 corresponding to $C_{52}H_{45}Cl_3O_2P_4Re_2$ is due to the molecular ion (M⁺) rather than the pseudo molecular ion peak (M + H)⁺; the related compound $Re_2Cl_4(CO)_2(dppm)_2$ was examined by the same technique. The highest mass peak of the sample (m/z = 1339; ^{187}Re) corresponded to the correct molecular formula, i.e. to M⁺ and not to (M + H)⁺. It is reasonable to expect that very similar compounds will exhibit analogous behavior under identical FABMS experimental conditions. This analysis combined with the NMR data (vide supra) strongly supports the presence of the hydride ligand.

C. Redox Chemistry

Electrochemistry of $\text{Re}_2(\mu\text{-H})(\mu\text{-Cl})\text{Cl}_2(\text{CO})_2(\text{dppm})_2$ studied by cyclic voltammetry reveals the compound is of a high redox activity, as evidenced by the presence of four redox processes between +2.0 and -2.0 V. The cyclic

Figure 7. T_1 measurements in CD_2Cl_2 and at 200 MHz 1H NMR with variable temperatures for the bridging hydride of $Re_2(\mu-H)(\mu-Cl)Cl_2(CO)_2(dppm)_2$.

T, °C	T ₁ , ms	T, °C	T ₁ , ms
22	343 (62)	-50	87.4 (16)
0	279 (99)	–60	99.6 (22)
-20	257 (33)	-80	83.9 (2)
–30	139 (15)	-100	80.9 (15)
-4 0	107 (9)		

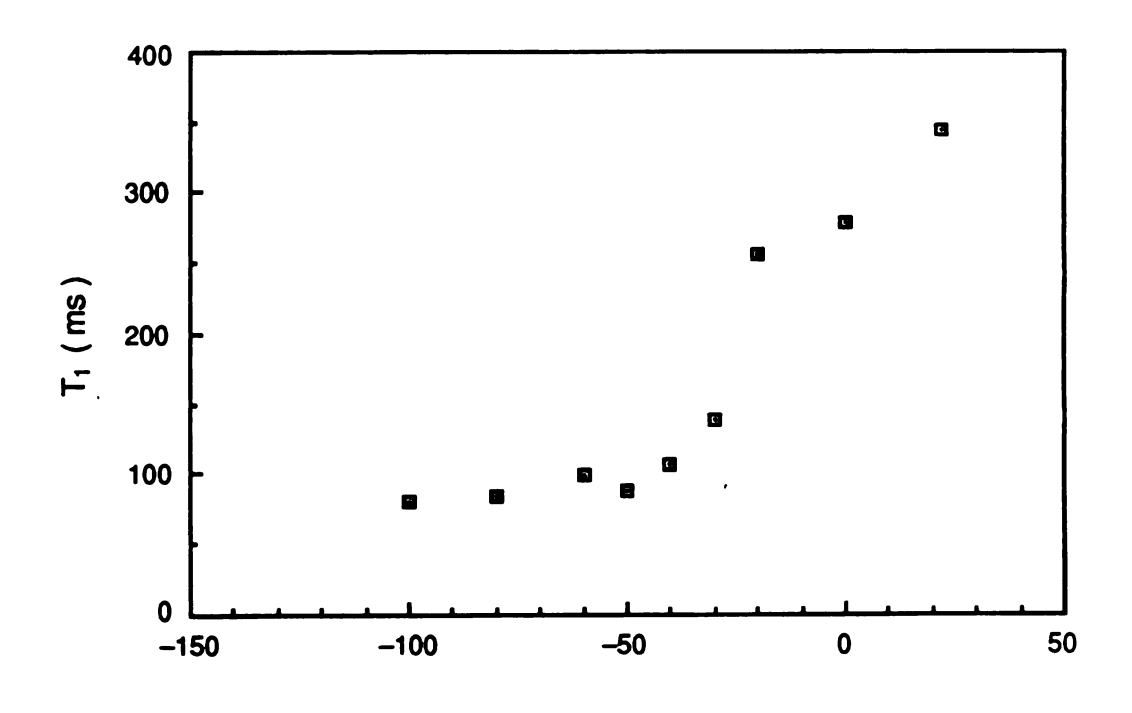


Figure 7

Temperature (°C)

Figure 8. Positive ion FABMS spectrum of $Re_2(\mu-H)(\mu-Cl)Cl_2(CO)_2$ - $(dppm)_2$.

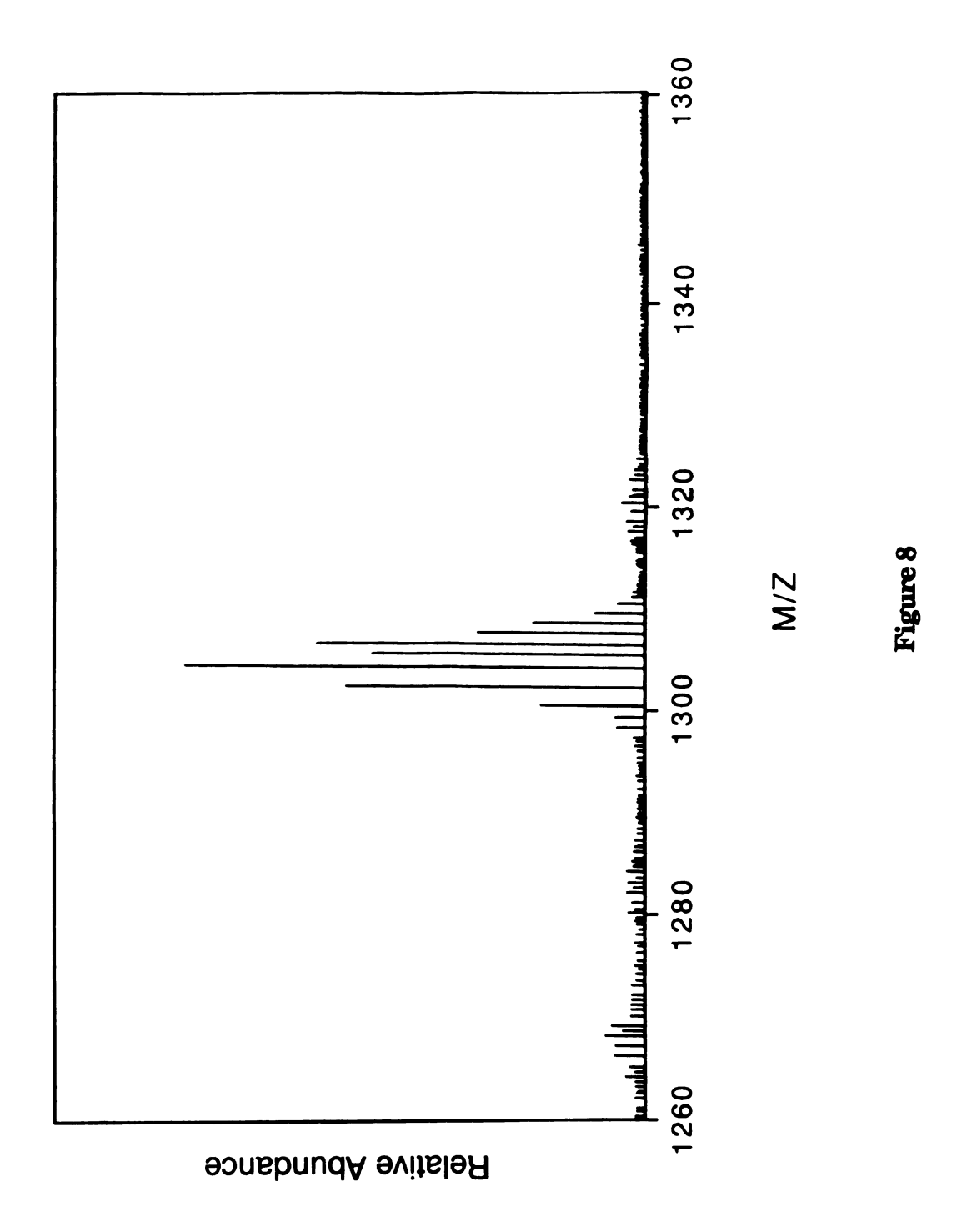
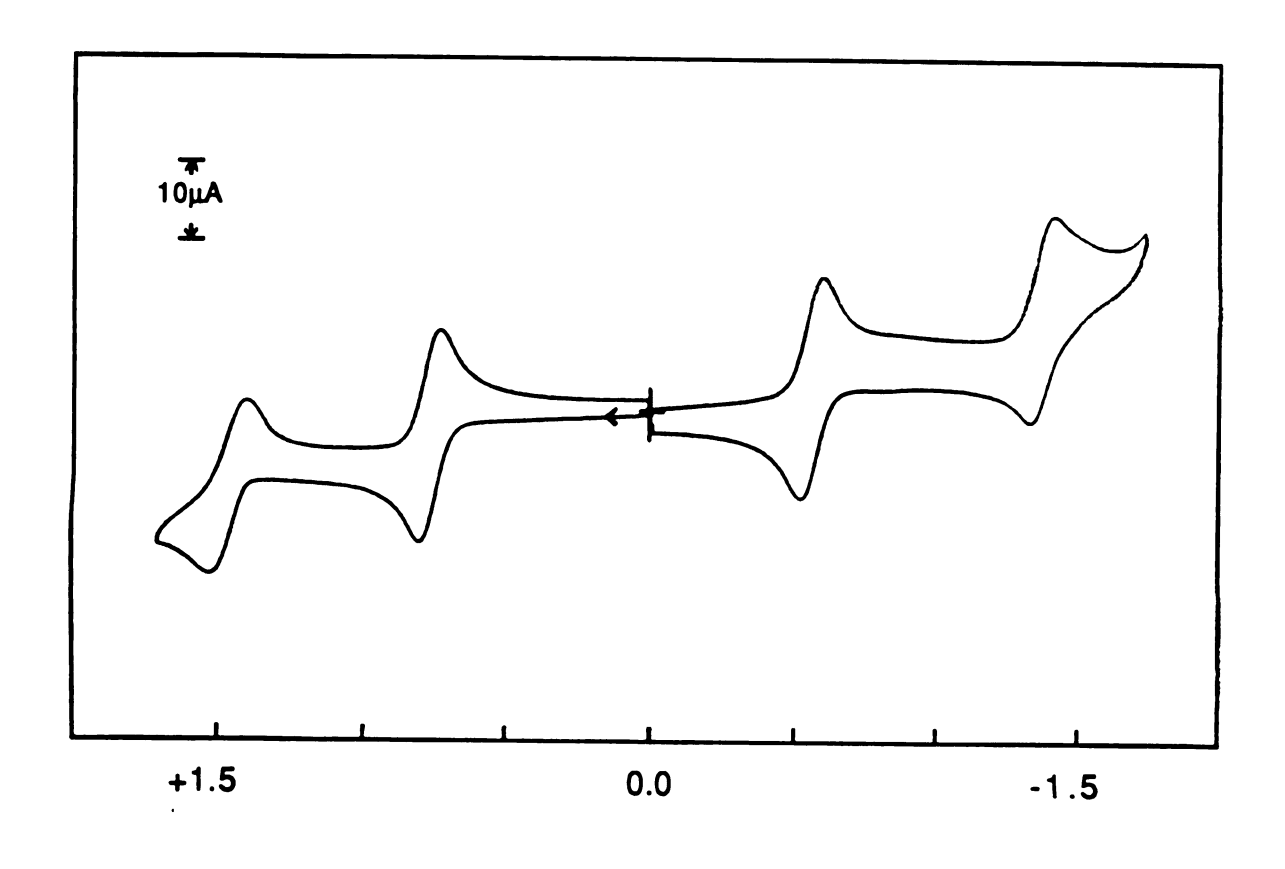


Figure 9. Cyclic voltammogram of $Re_2(\mu-H)(\mu-Cl)Cl_2(CO)_2(dppm)_2$ in a CH_2Cl_2 solution with 0.2 M TBAPF $_6$ at 200 mV/s using a Ptdisk electrode.



VOLTS vs Ag/AgCI

Figure 9

Figure 10. Infrared spectra of (a) $Re_2(\mu-H)(\mu-Cl)Cl_2(CO)_2(dppm)_2$ (——) and the corresponding oxidation product (-----) and (b) $Re_2(\mu-H)(\mu-Cl)Cl_2(CO)_2(dppm)_2$ (——) and the corresponding reduction product (-----).

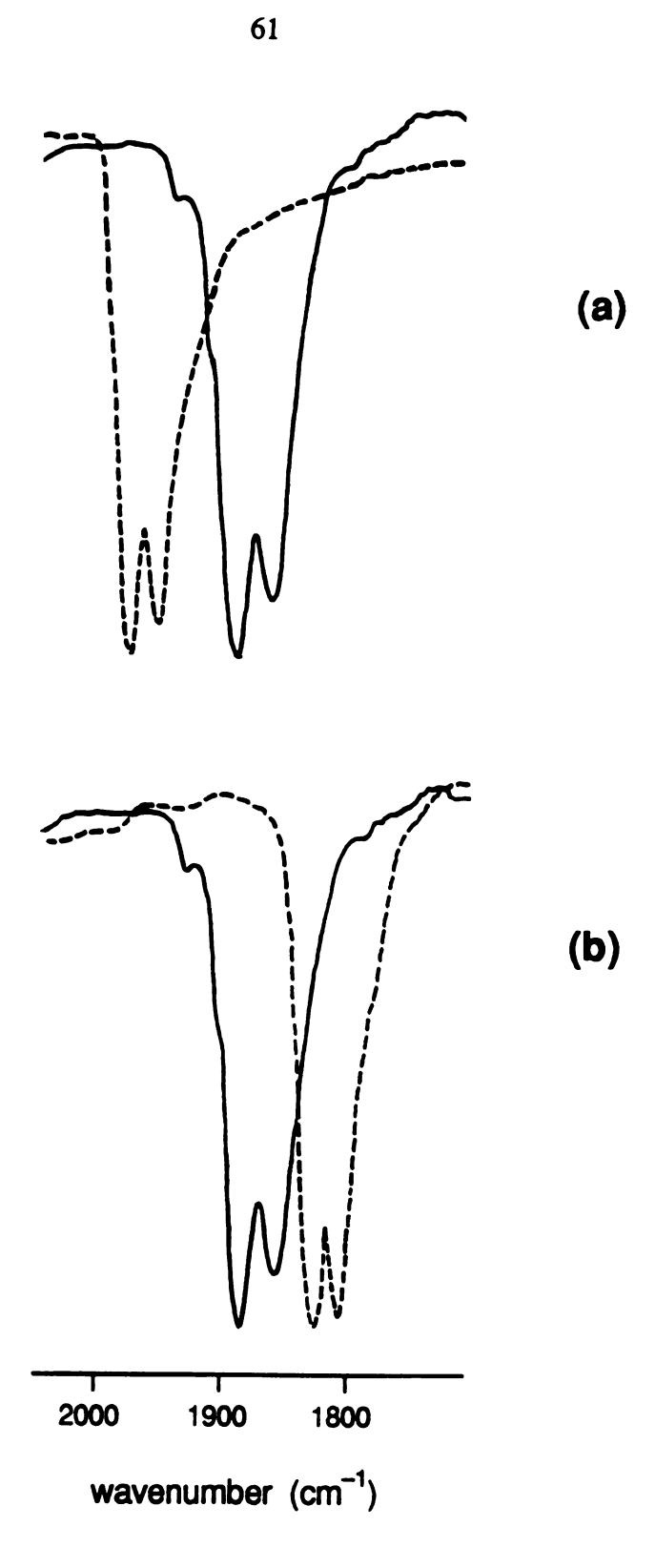


Figure 10

voltammogram of the compound (1) in a dicholoromethane solution containing 0.1 M [n-Bu₄N][BF₄] as a supporting electrolyte shows a one-electron reduction couple at $E_{1/2} = -0.80$ V with a peak-to-peak separation of 70 mV at 200 mV/sec which confirms the reduction process is reversible. A one-electron reversible oxidation at $E_{1/2} = +0.57$ V with a peak-to-peak separation of 70 mV is also observed. In addition, a quasi-reversible reduction couple at $E_{1/2} = -1.53$ V with the peak-to-peak separation of the couple is ca. 160 mV and an irreversible oxidation near the solvent limit at $E_{p,a} = +0.96$ V vs Ag/AgCl are observed (Figure 9). This extensive redox behavior is characteristic of edge-sharing bioctahedral dirhenium complexes [36, 51-52].

(i) Electrochemical and Chemical Oxidation

The oxidation process at $E_{1/2} = +0.57$ V vs Ag/AgCl is accessible and can be achieved chemically by using the salts NO+Y- or Ag+Y-(Y= BF₄, PF₆, etc) as oxidants. Upon addition of one equivalent of [NO][BF₄] to an acetonitrile solution of compound (1), an instant color change of the solution from green to green-brown was observed, indicating a facile oxidation had occurred. The infrared spectrum of the oxidation product shows essentially the same pattern for the CO stretching region as the neutral species, Re₂(μ -H)(μ -Cl)Cl₂(CO)₂(dppm)₂ but at a lower energy of \approx 60 cm⁻¹ (Figure 10). This result may be taken as an indication of a lesser M—CO π -backbonding upon oxidation from an Re₂⁴⁺ to an Re₂⁵⁺ dimetal core.

It should be mentioned, that oxidation reactions with nitrosonium salts such as NO^+Y^- (Y= BF₄, PF₆, etc) often result in coordination of the NO group to the meatl to form nitrosyl complexes. In the present study, reaction with excess [NO][BF₄] with (1) indeed produced the nitrosyl

product Re₂Cl₃(CO)₂(NO)(dppm)₂ which was also characterized by an X-ray diffraction study.

Another approach to the synthesis of the oxidized species is by an electrochemical method. A controlled-potential bulk oxidation of (1) in a 0.1 M $[n\text{-Bu}_4N][BF_4]$ - CH_2Cl_2 solution, at an applied potential of +1.0 V, resulted in the formation of a dark green solution after ca. 30 min. The electrochemical generation of the cation was monotored by UV-visible spectroscopy, and the original strong absorption band at 416 nm was replaced by the electrogenerated cation with an absorption band at 396 nm (Figure 11). The cyclic voltammogram of the electrolyzed solution was idential to (1) except that the wave at +0.57 V vs Ag/AgCl corresponded to a reduction process, indicating the oxidation product is isostructural to the neutral compound (1). Recrystallization of the product by slow diffusion of hexane into the electrolyzed solution gave a suitable X-ray quality crystal which was confirmed as $[Re_2(\mu\text{-H})(\mu\text{-Cl})Cl_2(CO)_2(dppm)_2](BF_4)$ by a crystallographic study.

In the course of prolonged bulk oxidation, the green solution gradually turned brown, and the brown decomposition product was analyzed by FABMS spectrum which showed the highest mass peak at m/z = 1338 corresponding to the dirhenium complex $Re_2Cl_4(CO)_2(dppm)_2$. The result is in a good agreement with an analysis of isotope distributions for the compound (Figure 12). We rationalize the formation of $Re_2Cl_4(CO)_2(dppm)_2$ as arising from loss of the bridging hydride followed by abstraction of a chloride ligand from the CH_2Cl_2 solvent.

Figure 11. Electronic absorption spectral changes during electrochemical oxidation of $Re_2(\mu-H)(\mu-Cl)Cl_2(CO)_2(dppm)_2$ in 0.1 M TBABF₄– CH_2Cl_2 solution. The total reaction time at ambient temperature was two hours.

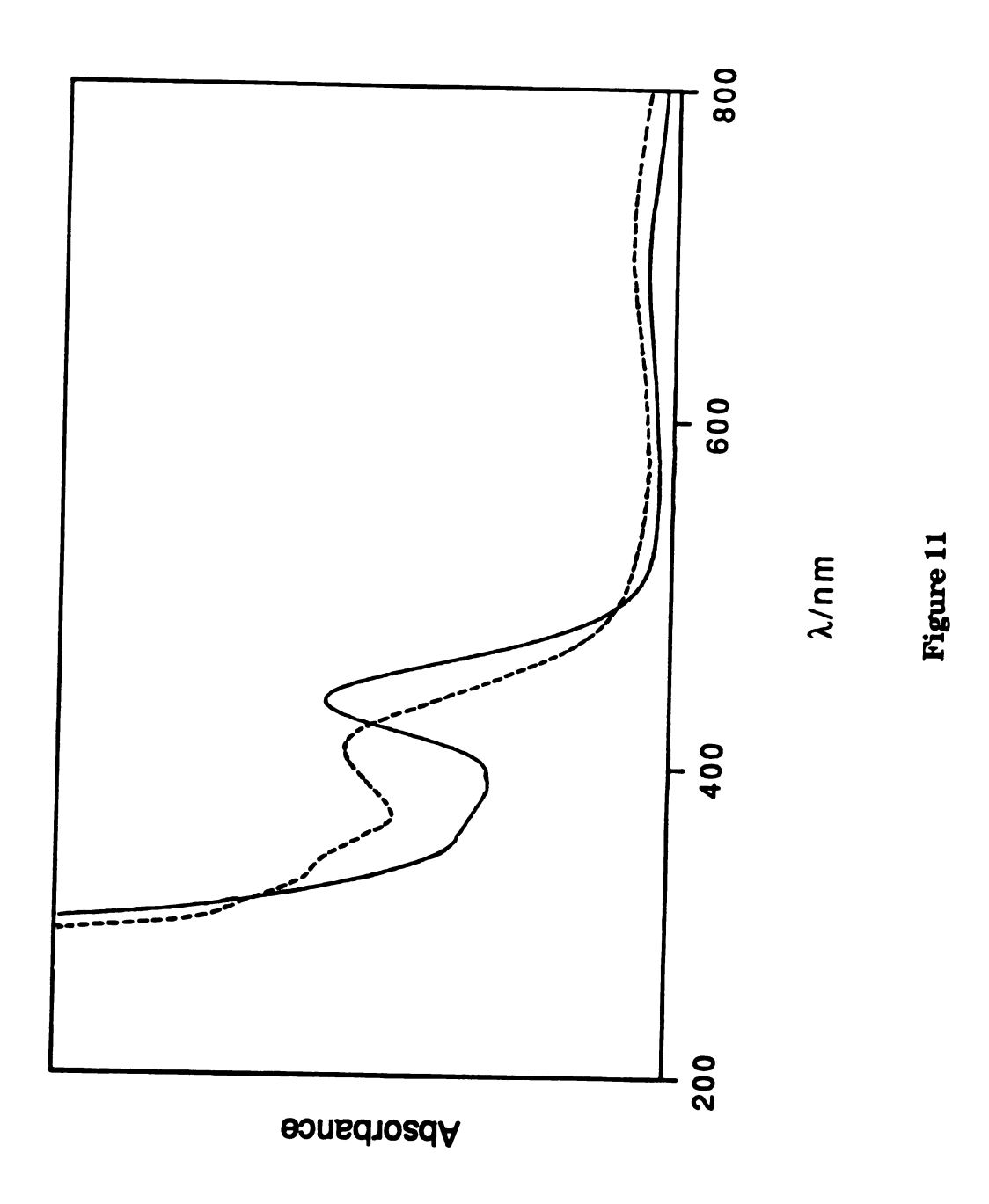
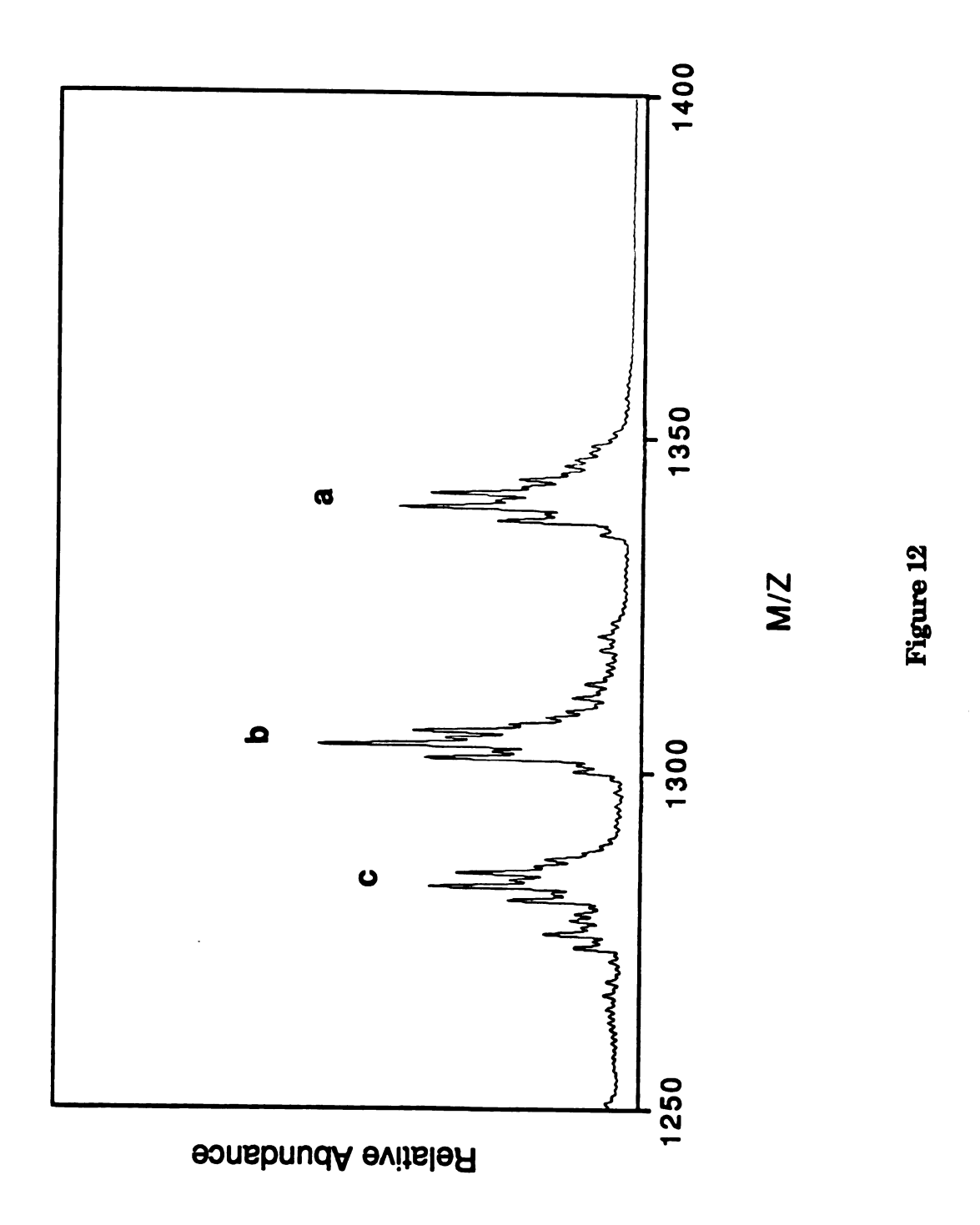


Figure 12. Positive ion FABMS spectrum of the decomposition product $\operatorname{Re_2Cl_4(CO)_2(dppm)_2}$ isolated from the electrochemical oxidation of $\operatorname{Re_2(\mu-H)(\mu-Cl)Cl_2(CO)_2(dppm)_2}$ in 0.1 M TBABF₄- $\operatorname{CH_2Cl_2}$ solution, showing (a) the molecular ion peak [M] = $\operatorname{Re_2Cl_4(CO)_2(dppm)_2}$, (b) [M-CO] = $\operatorname{Re_2Cl_4(CO)(dppm)_2}$ and (c) [M-2CO] = $\operatorname{Re_2Cl_4(dppm)_2}$.



(ii) Electrochemical and Chemical Reduction

The compound (1) exhibits an accessible reduction couple at -0.8 V vs Ag/AgCl, a process which was chemically achieved by using cobaltocene [Cp₂Co] as the reductant. Treatment of an acetone solution of (1) with one equivalent of cobaltocene produced an instantaneous color change from The blue-green salt $[Cp_2Co][Re_2(\mu-H)(\mu-H)]$ green to blue-green. Cl)Cl₂(CO)₂(dppm)₂] is very air-sensitive, and underwent reoxidation back to the neutral species (1) in the presence of a trace amount of water and oxygen present in the solution. The infrared spectrum of the anion product shows the same v(CO) pattern as (1) with a shift to lower energies of ≈ 100 cm⁻¹ (Figure 10). This is consistent with the expected increase in M—CO π -backbonding upon reduction of the dimetal core. The product is nearly insoluble in all organic solvents, which is a severe drawback in the study of its solution behavior. Fortunately, the solid state EPR spectrum at -170 °C showed a well-defined signal with hyperfine coupling to the rhenium (187 Re, I = 5/2) and phosphorus (31 P, I = 1/2) atoms (Figure 13), thereby establishing the compound as a one-electron reduction product as expected. The complex EPR behavior has been noted previously in related dirhenium phosphine complexes and is not unexpected considering the presence of two I = 5/2 nuclei for 187 Re and 185 Re [53].

Our efforts to isolate the reduction species extended to electrochemical methods as well. A controlled-potential bulk reduction of (1) in a 0.2 M $[n\text{-Bu}_4N][BF_4]$ — CH_2Cl_2 solution was carried out with an applied potential of -1.0 V. The electrogenerated monoanion $[n\text{-Bu}_4N][Re_2(\mu\text{-H})(\mu\text{-Cl})Cl_2(CO)_2(dppm)_2]$ was highly air sensitive which caused difficluty in monitoring the electrochemical process by UV-visible

spectroscopy and also prevented recrystallization. Studies of the redox chemistry of $Re_2(\mu-H)(\mu-Cl)Cl_2(CO)_2(dppm)_2$ are summarized in Figure 14.

D. Molecular Structures

(1) $Re_2(\mu-H)(\mu-Cl)Cl_2(CO)_2(dppm)_2$

Crstallographic data for (1) are listed in Table 3, and the important bond distances and angles for (1) are given in Table 4. An ORTEP plot of the molecular structure with the atom-labeling scheme is shown in Figure 15. The bridging hydrogen atom was not located; thus, it does not appear in the plot.

The structure of the dinuclear complex consists of two trans diphosphine ligands bisecting a plane containing the rhenium atoms, two cis terminal CO groups, and the three chloride ligands. The structure is similar to those found for other carbonyl complexes of the $[Re_2(dppm)_2]^{4+}$ unit in that the π -acceptor ligands are situated on the same side of the molecule [51]. Also, the conformation of the Re—P—C—P—Re five-membered ring formed by the metal atoms and the dppm ligand is that of a half-chair with the two methylene carbon atoms in a syn rather than anti configuration, in keeping with the 2-fold symmetry of the molecule.

As in previously characterized dirhenium complexes containing CO or CNR ligands, the bridgehead carbon atoms are folded to the side of the molecule containing the π -acceptor ligands. The syn structure is preserved in solution, as evidenced by the ¹H NMR spectrum in the -CH₂-regions of the dppm ligands (vide supra). As the side view of the molecule (Figure 16) clearly shows, the diphosphine ligands are twisted from an

eclipsed conformation ($\chi = 8.5^{\circ}$), resulting in a molecular symmetry of C_2 rather than C_{2v} .

The distances and angles in the molecule are within expected ranges. The metric parameters for (1) are very similar to those exhibited by other edge-sharing bioctahedral molecules such as $Re_2Cl_6(dppm)_2$ and $Re_2Cl_4(CO)_2(dppm)_2$. In $Re_2Cl_4(CO)_2(dppm)_2$, the Re—Re—C_t angle is 125 (2)° and Re—Re—Cl_t = 141.3 (7)°. In the present molecule, Re—Re'—C_t = 112.2 (3)° and Re—Re'—Cl_t = 146.23 (5)°. The unusually small angle that the CO ligand in (1) assumes with respect to the metal-metal bond axis suggests that some attractive interaction may be occurring between the bridging hydride ligand and the CO groups.

The Re—Re bond length of 2.605 (1) Å is quite long for a complex formally derived from the Re_2^{4+} core. In fact, this distance is close to those values found in Re_2^{6+} compounds such as $\text{Re}_2\text{Cl}_6(\text{dppm})_2$ (Re—Re = 2.616 (1) Å). The long metal-metal distance in $\text{Re}_2(\mu\text{-H})(\mu\text{-Cl})\text{Cl}_2(\text{CO})_2(\text{dppm})_2$ is even more surprising considering that it contains a $\mu\text{-H}$ group, which is known to have the effect of drawing metal atoms closer together. Clearly, more examples of these types of carbonyl-hydrido dinuclear complexes are required to explain the structural parameters of the molecule.

(2) $[Re_2(\mu-H)(\mu-Cl)Cl_2(CO)_2(dppm)_2](BF_4)$

Crstallographic data for this compound are listed in Table 5. Bulk oxidation of a dichloromethane solution of (1) yields $[Re_2(\mu-H)(\mu-Cl)Cl_2(CO)_2(dppm)_2](BF_4)$ (3), as determined by X-ray crystallography. The ORTEP diagram of (3) (Figure 17) shows that the cation $[Re_2(\mu-H)(\mu-Cl)Cl_2(CO)_2(dppm)_2]^+$ is isostructural to the neutral species. Both compounds exhibit an edge-sharing bioctahedral geometry with a $[Re_2(\mu-H)(\mu-L)]$

H)(μ-Cl)Cl₂(CO)₂(dppm)₂] core which consists of two dppm ligands in trans position, three chloride ligands located on the same side and two terminal CO trans to the bridging chloride with one bridging hydride occupying the other bridging position. The bond lengths and bond angles for (3) listed in Table 6, compare favorably to those for (1).

(3) $[Re_2(\mu-CO)(\mu-Cl)Cl_2(CO)(NO)(dppm)_2](BF_4)$

Crystallographic data for this compound are listed in Table 5. Chemical oxidation of compound (1) with the use of NOBF₄ led to the isolation of a nitrosyl complex $[Re_2(\mu\text{-CO})(\mu\text{-Cl})Cl_2(CO)(NO)(dppm)_2](BF_4)$ confirmed by an X-ray diffraction study. The dinuclear complex consists of an edge sharing bioctahedral ligation sphere. The molecular structure of (2) represented by the ORTEP diagram is shown in Figure 18. A stereoview of the molecule (2) is illustrated in Figure 19. A listing of selected bond distances and angles are given in Table 7. The good π -accepting properties of the NO and CO ligands reduces the electron density at the metal center, thereby enhancing the Re—Cl π -donating interaction. The synergistic effect between the π -accepting and terminal π -donor ligands may well explain the short terminal bond distances.

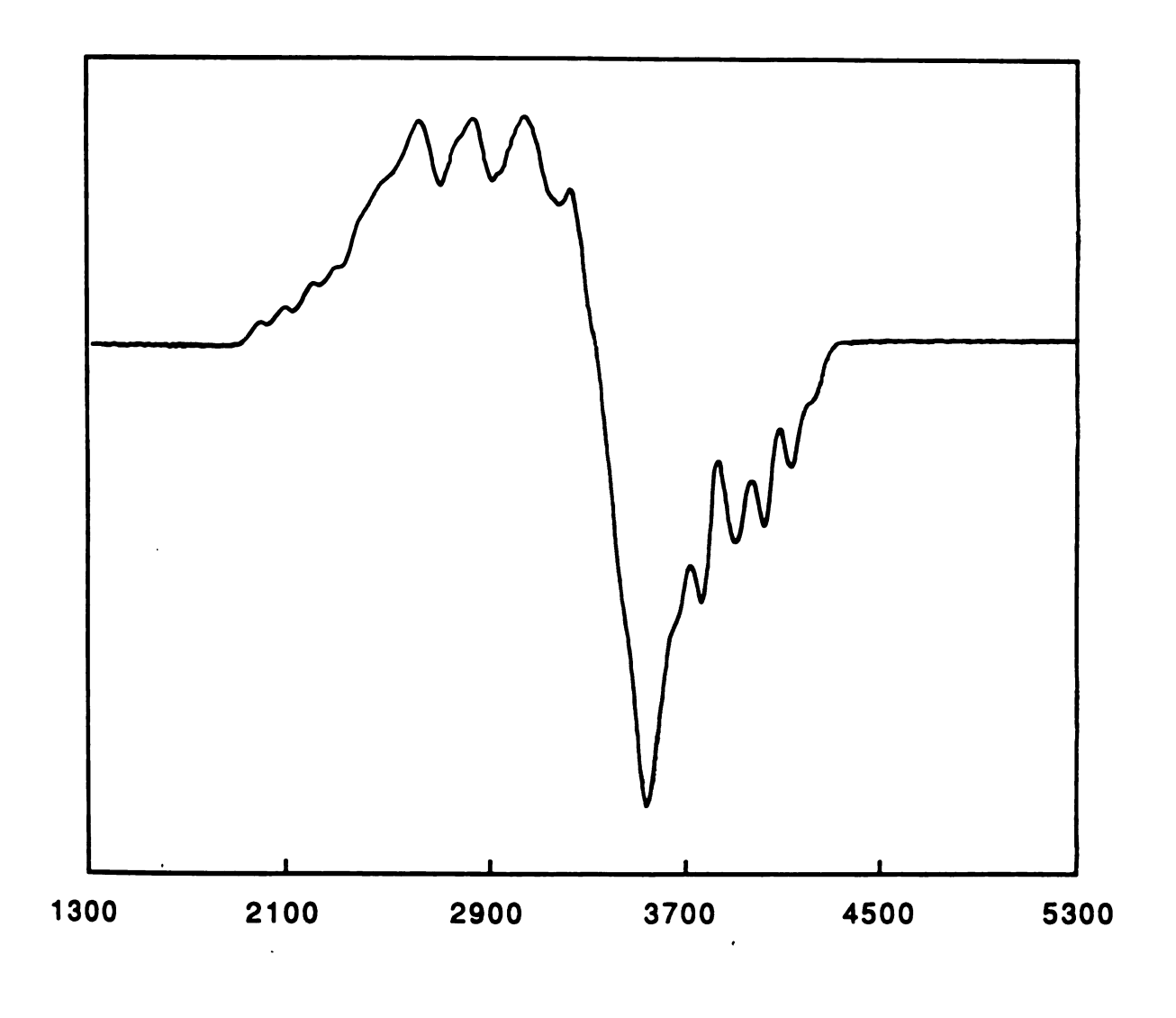
A comparison of the main features of molecular structres (2) and (3) is shown in Figure 20, and a comparison of a series of edge-sharing bioctahedral dirhenium complexes with "Re₂Cl₃" ccores is shown in Figure 18.

5. SUMMARY

The studies described herein were undertaken to gain a more complete understanding of the formation of an unusual hydrido-dirhenium complex. We have verified that the compound $Re_2(\mu-H)(\mu-Cl)Cl_2(CO)_2(dppm)_2$ can be prepared by reactions of with carbonyl clusters under an H_2 atmosphere and the direct reaction of $Re_2(\mu-H)(\mu-Cl)Cl_2(CO)_2(dppm)_2$ with a CO/H_2 gas misture at atmospheric pressure. The role of $H_2Os_3(CO)_{10}$ as a cluster presursor appears to be an important one in the high-yield synthesis of $Re_2(\mu-H)(\mu-Cl)Cl_2(CO)_2(dppm)_2$. We have also noted the behavior of H_2 in assisting the reaction to form the complex. Attempts to stabilize reactive intermediates might also provide an interesting mixed-metal complex in this reaction.

Furthermore, the compound $Re_2(\mu-H)(\mu-Cl)Cl_2(CO)_2(dppm)_2$ exhibits a high redox activity, and an intensive effort has been made to isolate both oxidation and reduction products, namely $[Re_2(\mu-H)(\mu-Cl)Cl_2(CO)_2(dppm)_2]^+$ and $[Re_2(\mu-H)(\mu-Cl)Cl_2(CO)_2(dppm)_2]^-$; successful attempts were achieved by electrochemical and chemical methods.

Figure 13. An X-band EPR spectrum taken on a solid sample of $[Cp_2Co][Re_2(\mu-H)(\mu-Cl)Cl_2(CO)_2(dppm)_2] \ at \ -150 \ ^oC.$



Field (Gauss)

Figure 13

Figure 14. Schematic diagram depicting the redox reactions of ${\rm Re}_2(\mu-H)(\mu-Cl)Cl_2(CO)_2(dppm)_2$.

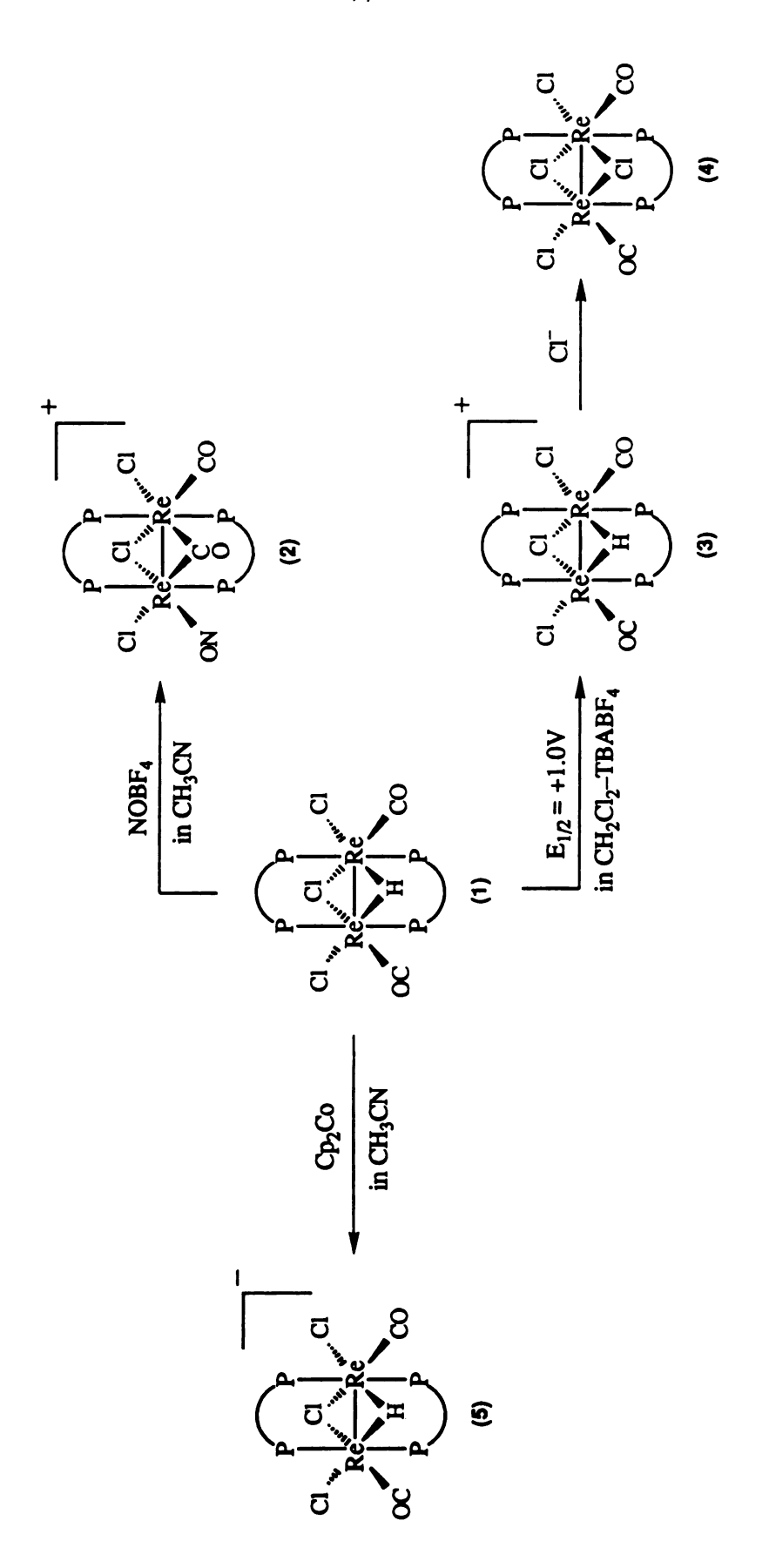


Figure 14

Table 3. Crystal Data for $Re_2(\mu-H)(\mu-Cl)Cl_2(CO)_2(dppm)_2$ (1) and $Re_2(\mu-H)(\mu-Cl)Cl_2(CO)_2(dppm)_2\cdot MeCN$ (2)

	(1)	(2)
Formula	Re ₂ Cl ₃ P ₄ O ₂ C ₅₂ H ₄₅	$Re_2Cl_3P_4O_2N_1C_{54}H_{48}$
Formula weight	1304.59	1345.65
Crystal system	Tetragonal	Tetragonal
Space group	P4 ₁ 2 ₁ 2	P4 ₂ /n
а, Å	14.935 (2)	16.561 (2)
b, Å	14.935 (2)	16.561 (2)
с, Å	25.804 (7)	20.294 (5)
α, deg	90	90
β, deg	90	90
γ, deg	90	90
V, Å ³	5755 (4)	5564 (2)
Z	4	4
d _{calc} , g/cm ³	1.545	1.605
Crystal size, mm	0.40 x 0.30 x 0.25	0.30 x 0.15 x 0.08
Radiation	Mo $K_{\alpha}(\lambda = 0.71073 \text{ Å})$	Mo K_{α} (λ = 0.71073 Å)
μ, cm ⁻¹	45.90	47.07
Data collection instrument	Nicolet P3/F	Siemens P3/V
Temperature, °C	22 ± 2	-100 ± 2
Scan method	ω – 2θ	ω
Data col. range, 20, deg.	4.4 – 40	4 – 45
R ^a	0.030	0.040
R _w ^b	0.036	0.051

 $aR = \Sigma | |F_o| - |F_c||/\Sigma |F_o|$

$$b R_w = [\Sigma w | F_o| - |F_c|)^2 / \Sigma w |F_o|^2]^{1/2}; w = 1/\sigma^2 (|F_o|)$$

Selected Bond Distances (Å) and Angles (deg) for $\text{Re}_2(\mu\text{-H})(\mu\text{-Cl})\text{Cl}_2(\text{CO})_2(\text{dppm})_2$ (1) and $\text{Re}_2(\mu\text{-H})(\mu\text{-Cl})\text{Cl}_2(\text{CO})_2(\text{dppm})_2$. MeCN (2). Table 4.

		Dis	Distance			Die	Distance
Atom 1	Atom 1 Atom 2	(1)	(2)	Atom 1	Atom 1 Atom 2	(1)	(2)
Re(1)	Re'(1)	2.605 (0)	2.626 (3)	P(1)	C(2)	1.833 (8)	1.81 (2)
Re(1)	Cl(1)	2.526 (3)	2.50 (1)	P(1)	C(11)	1.832 (7)	1.88 (3)
Re(1)	CI(2)	2.449 (2)	2.437 (6)	P(1)	C(21)	1.847 (8)	1.85 (3)
Re(1)	C(1)	1.833 (2)	1.83 (2)	P(2)	C'(2)	1.846 (6)	1.81 (2)
Re(1)	P(1)	2.456 (2)	2.46 (8)	P(2)	C(31)	1.840 (7)	1.78 (3)
Re(1)	P(2)	2.435 (7)	2.445 (8)	P(2)	C(41)	1.843 (8)	1.83 (2)
C(1)	0(1)	1.112 (12)	1.20 (2)				

			Ang	ngle				Angle	gle
Atom 1	Atom 1 Atom 2 Atom 3	Atom 3	(1)	(2)	Atom 1	Atom 1 Atom 2 Atom 3	Atom 3	(1)	(2)
Re'(1) Re(1)	Re(1)	Cl(1)	58.93 (1)	59.3(5)	CI(1)	Re(1)	Cl(2)	87.76 (5)	89.5 (5)
Re'(1)	Re(1)	CI(2)	146.23 (5)	148.8 (2)	CI(1)	Re(1)	C(1)	170.2 (3)	173.7 (7)
Re'(1)	Re(1)	C(1)	112.2 (3)	114.6 (7)	CI(2)	Re(1)	C(1)	101.4 (3)	96.7 (7)
Re'(1)	Re(1)	P(1)	94.22 (6)	94.2 (2)	Re(1)	Cl(1)	Re'(1)	62.11 (5)	62.7(2)
Re'(1)	Re(1)	P(2)	95.11 (7)	95.1 (2)	Re(1)	C(1)	0(1)	175.9 (8)	176 (2)

Figure 15. ORTEP drawing of Re₂(μ-H)(μ-Cl)Cl₂(CO)₂(dppm)₂, showing the atom labeling scheme. All phenyl-group carbon atoms are represented as small circles for clarity, and all other atoms are represented by their 50% probability ellipsoids. Unlabeled atoms are related to labeled ones by an inversion center at the midpoint of the Re—Re' bond.

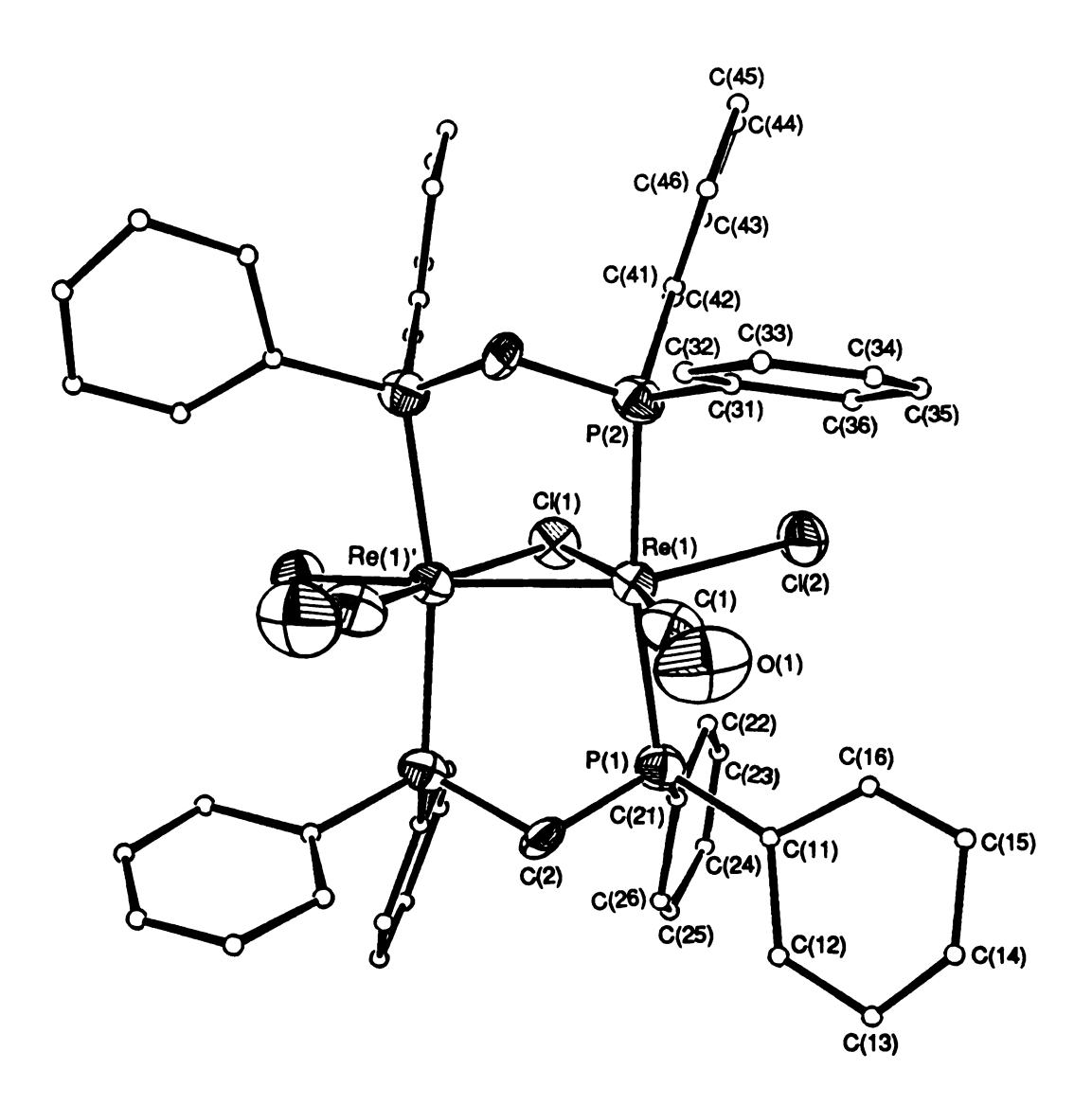


Figure 15

Figure 16. A skeletal ORTEP plot of $Re_2(\mu\text{-H})(\mu\text{-Cl})Cl_2(CO)_2(dppm)_2$ view down the Re—Re vector.

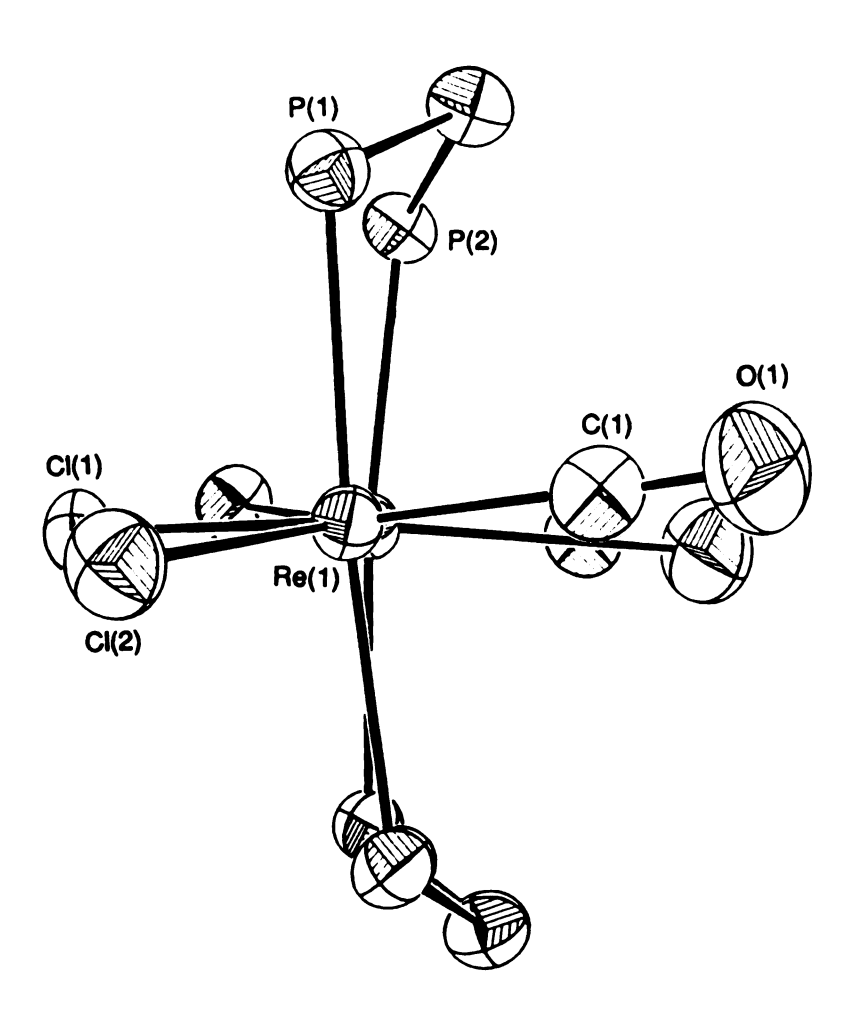


Figure 16

Figure 17. ORTEP drawing of the $[Re_2(\mu-H)(\mu-Cl)Cl_2(CO)_2(dppm)_2]^+$ cation showing the atom labeling scheme. All phenyl-group carbon atoms are represented as small circles for clarity, and all other atoms are represented by their 40% probability ellipsoids.

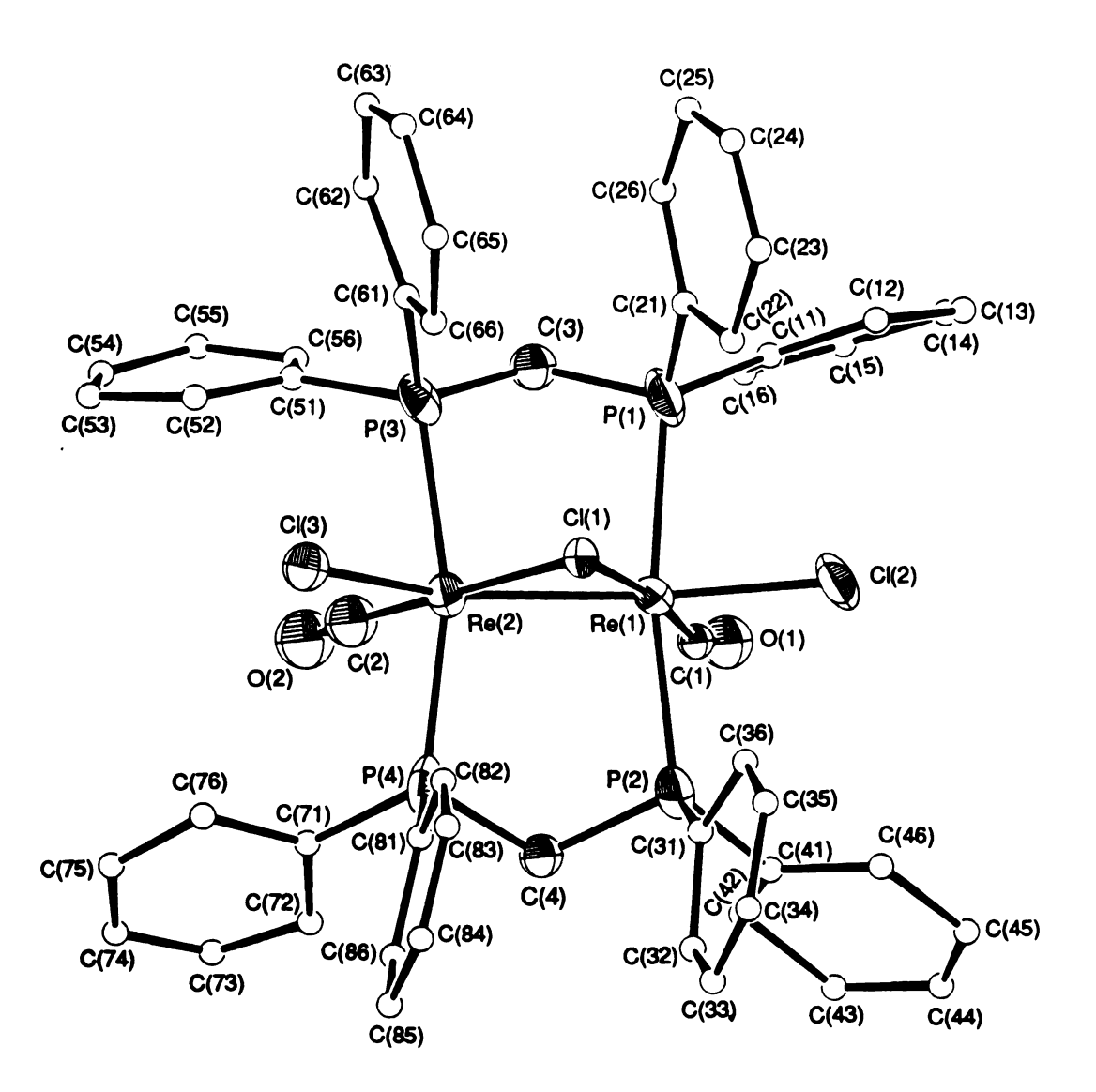


Figure 17

 $\label{eq:condition} \begin{table} \textbf{Table 5.} & Crystal\ Data\ for\ [Re_2(\mu-H)(\mu-Cl)Cl_2(CO)_2(dppm)_2](BF_4)\ \textbf{(3)}\ and \\ & [Re_2(\mu-CO)(\mu-Cl)Cl_2(CO)(NO)(dppm)_2](BF_4)\ \textbf{(4)} \\ \end{table}$

	(3)	(4)
Formula	$Re_2Cl_3P_4O_2C_{52}B_1F_4H_{45}$	Re ₂ Cl ₃ P ₄ O ₃ C ₅₂ B ₁ F ₄ H ₁ H ₄₄
Formula weight		
Crystal system	Triclinic	Monoclinic
Space group	P-1	P2 ₁ / n
a, Å	13.729 (7)	14.347 (3)
b, Å	14.420 (6)	27.934 (6)
с, Å	15.936 (8)	16.864 (4)
α, deg	90.17 (3)	90
β, deg	110.03 (4)	92.92 (2)
γ, deg	112.29 (3)	90
V, Å ³	2710 (2)	6750 (2)
Z	2	4
d _{calc} , g/cm ³	1.705	1.398
Crystal size, mm	0.31 x 0.14 x 0.05	0.20 x 0.18 x 0.05
Radiation	Cu $K_{\alpha}(\lambda = 1.54184 \text{ Å})$	Cu $K_{\alpha}(\lambda = 1.54184 \text{ Å})$
μ , cm ⁻¹	112.510	90.628
Data collection instrument	Siemens P3/v	Siemens P3/v
Temperature, °C	-95 ± 2	-95 ± 2
Scan method	$\omega - 2\theta$	ω – 2θ
Data col. range, 20, deg.	4 – 106	4 – 106
Ra	0.161	0.167
R _w ^b	0.146	0.214

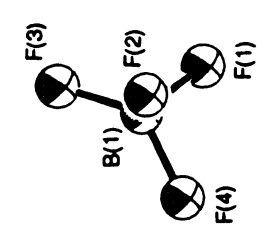
 $aR = \Sigma ||F_o| - |F_c||/\Sigma |F_o|$

 $b R_w = [\Sigma w | F_o | - | F_c |)^2 / \Sigma w | F_o |^2]^{1/2}; w = 1/\sigma^2 (| F_o |)$

Table 6. Selected Bond Distances (Å) and Angles (deg) for [Re₂(μ-H)(μ-Cl)Cl₂(CO)₂(dppm)₂](BF₄).

Atom 1	Atom 2		Distance	Atom 1	Atom 2	1 2	Distance
Re(1)	Re(2)	7	2.552 (3)	Re(2)	CI(3)		2.402 (9)
Re(1)	CI(1)	(1	2.45 (1)	Re(2)	C(2)		1.95 (6)
Re(1)	CI(2)	(7	2.37 (1)	Re(2)	P(3)		2.48 (1)
Re(1)	C(1)	-	1.97 (4)	Re(2)	P(4)		2.41 (1)
Re(1)	P(1)	(4	2.47 (1)	C(1)	0(1)		1.10 (4)
Re(1)	P(2)	(4	2.51 (1)	C(2)	0(2)		1.18 (6)
Re(2)	CI(1)	7	2.49 (1)				
Atom 1	Atom 2	Atom 3	Angle	Atom 1	Atom 2	Atom 3	Angle
Re(2)	Re(1)	Cl(1)	59.6 (2)	Re(1)	Re(2)	C(2)	118 (1)
Re(2)	Re(1)	Cl(2)	151.1 (3)	Re(1)	Re(2)	P(3)	96.0 (2)
Re(2)	Re(1)	C(1)	115(1)	Re(1)	Re(2)	P(4)	97.5 (3)
Re(2)	Re(1)	P(1)	94.8 (3)	Cl(1)	Re(2)	CI(3)	87.0 (4)
Re(2)	Re(1)	P(2)	93.8 (3)	Cl(1)	Re(2)	C(2)	177 (1)
CI(1)	Re(1)	Cl(2)	91.5 (4)	Cl(3)	Re(2)	C(2)	96 (1)
Cl(1)	Re(1)	C(1)	173 (1)	Re(1)	Cl(1)	Re(2)	62.3 (3)
CI(2)	Re(1)	C(1)	93 (1)	Re(1)	C(1)	0(1)	164 (3)
Re(1)	Re(2)	Cl(1)	58.1 (2)	Re(2)	C(2)	0(2)	169 (4)
Re(1)	Re(2)	Cl(3)	145.1 (3)				

Figure 18. ORTEP drawing of $[Re_2(\mu\text{-CO})(\mu\text{-Cl})Cl_2(CO)(NO)(dppm)_2][BF_4]$. showing the atom labeling scheme. All phenyl-group carbon atoms are represented as small circles for clarity.



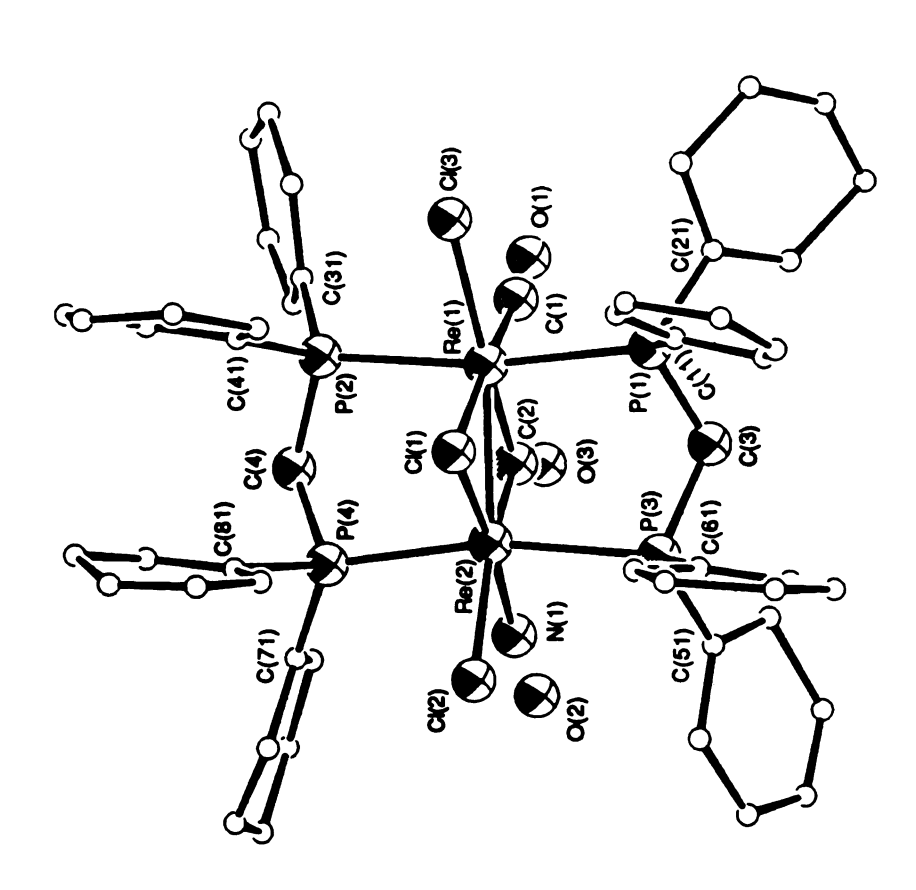


Figure 18

Figure 19. Stereoview of the unit cell of the molecule $[Re_2(\mu\text{-CO})(\mu\text{-Cl})Cl_2(CO)(NO)(dppm)_2][BF_4]$ along the a axis.

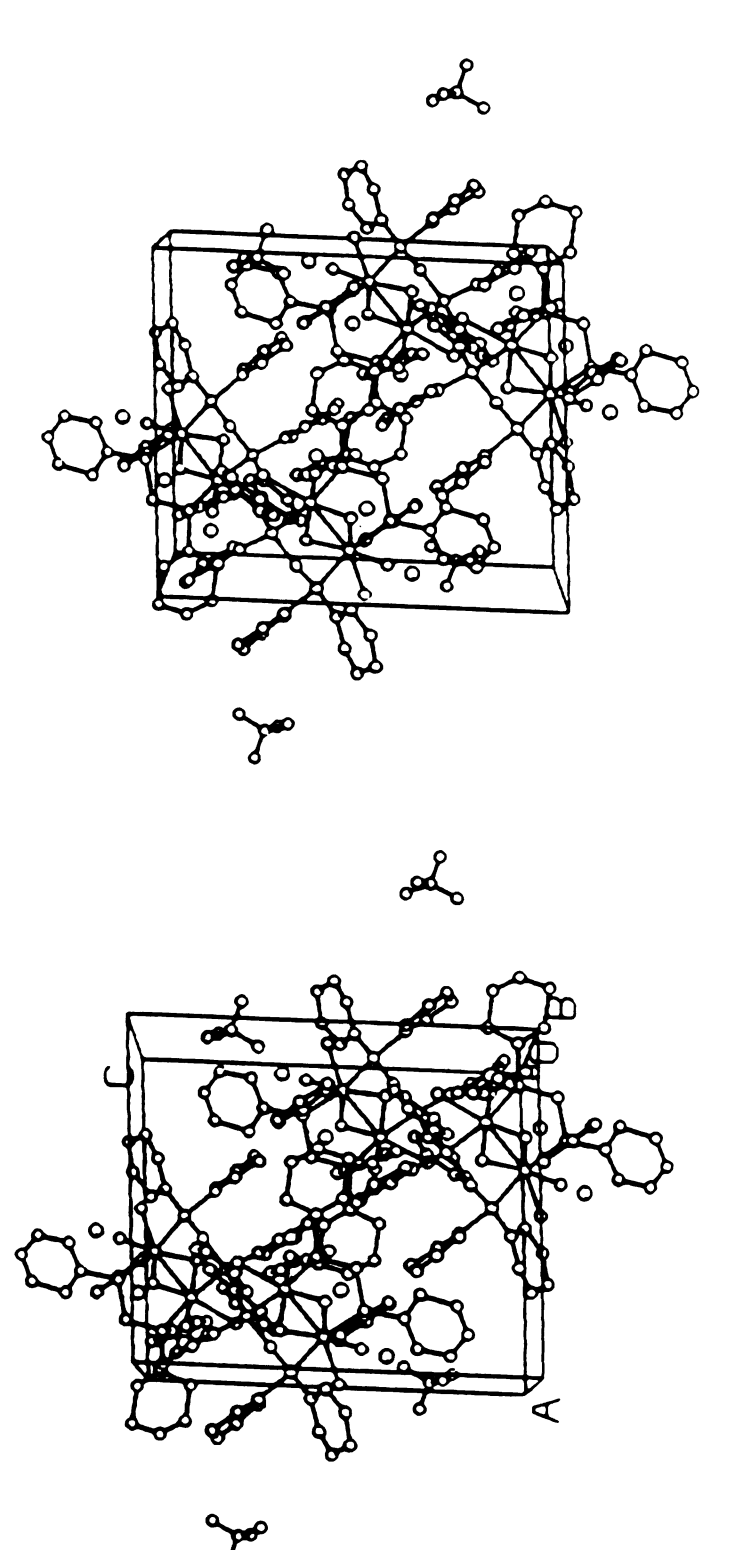
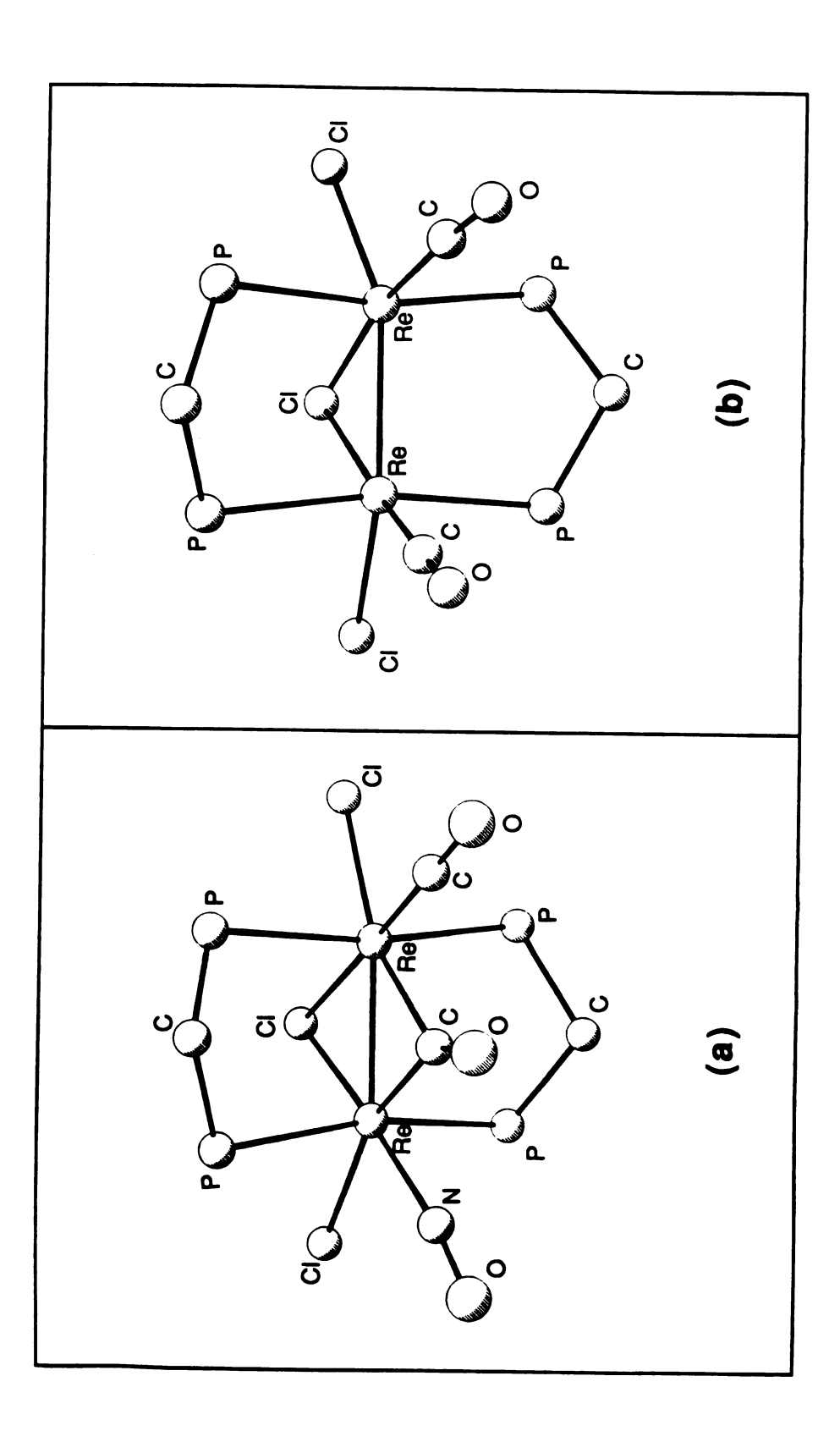


Figure 19

Figure 20. Pluto drawing emphasizing the main features of the cations in the structures of (a) $[Re_2(\mu\text{-CO})(\mu\text{-Cl})Cl_2(CO)(NO)(dppm)_2][BF_4]$ and (b) $[Re_2(\mu\text{-H})(\mu\text{-Cl})Cl_2(CO)_2(dppm)_2][BF_4]$.



cations in $[BF_4]$

Figure 20

84.5 (9) 63.8 (3) 75 (1)

N(1)
Re(2)
Re(2)
C(1)
O(2)

Cl(1) C(2) C(1)

Re(1)
Re(1)
Re(1)
Re(1)
Re(2)

Re(2)

94.7 (2) 92.2 (3) 178 (1) 89 (1)

> Cl(2) C(1) C(1) Cl(1)

> > Re(1)
> > Re(2)
> > Re(2)
> > Re(2)

Re(1)

Re(1)

Re(1)

Re(1) Re(1)

> Cl(1) Cl(2)

Re(1)

Re(2) Cl(1) 59 (1) 136 (2)

0(3)

59.0 (2) 147.7 (2)

Cl(3)

C(2)

Table 7. Selected Bond Distances (Å) and Angles (deg) for $[Re_2(\mu-CO)(\mu-CI)Cl_2(CO)(NO)(dppm)_2](BF_4)$.

Atom 1	Atom 2	2	Distance	Atom 1	Atom 2	2	Distance
Re(1)	Re(2)		2.593 (2)	Re(2)	CI(3)		2.395 (9)
Re(1)	Cl(1)		2.48 (1)	Re(2)	C(2)		2.04 (4)
Re(1)	CI(2)		2.42 (1)	Re(2)	N(1)		2.02 (3)
Re(1)	C(1)		1.92 (4)	Re(2)	P(3)		2.52 (1)
Re(1)	C(2)		2.20 (4)	Re(2)	P(4)		2.45 (1)
Re(1)	P(1)		2.50(1)	G(1)	0(1)		1.12 (4)
Re(1)	P(2)		2.49 (1)	C(2)	0(2)		1.15 (4)
Re(2)	Cl(1)		2.43 (1)	N(1)	0(3)		1.50 (6)
Atom 1	Atom 2	Atom 3	Angle	Atom 1	Atom 2	Atom 3	Angle
Re(2)	Re(1)	Cl(1)	57.2 (2)	Re(1)	Re(2)	N(1)	127.8 (8)
Re(2)	Re(1)	CI(2)	149.2 (3)	Re(1)	Re(2)	P(3)	96.1 (2)
Re(2)	Re(1)	C(1)	122 (1)	Re(1)	Re(2)	P(4)	95.1 (2)
Re(2)	Re(1)	C(2)	50 (1)	CI(1)	Re(2)	CI(3)	88.6 (3)
Re(2)	Re(1)	P(1)	93.7 (2)	Cl(1)	Re(2)	N(1)	172.8 (9)

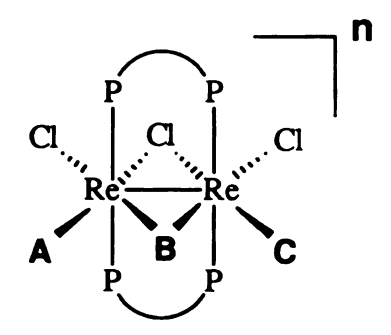
Table 8. Crystal data for the disordered structure formulated as ${}^{\circ}\text{Re}_2\text{Cl}_4(\text{CO})_2(\text{dppm})_2$ ".

Formula	$Re_2Cl_4P_4O_2C_{52}H_{44}$
Formula weight	
Crystal system	Monoclinic
Space group	C2/c
a, Å	22.945 (5)
b, Å	11.322 (3)
с, Å	23.406 (8)
α, deg	90
β, deg	100.96 (2)
γ, deg	90
V, Å ³	5968 (3)
Z	4
d _{calc} , g/cm ³	
Crystal size, mm	0.26 x 0.13 x 0.06
Radiation	Mo $K_{\alpha}(\lambda = 0.71073 \text{ Å})$
μ , cm ⁻¹	43.996
Data collection instrument	Siemens P3/V
Temperature, °C	-95 ± 2
Scan method	ω
Data col. range, 20, deg.	4 – 45
R ^a	
R _w b	

 $aR = \Sigma | |F_o| - |F_c| |/\Sigma| F_o|$

$$b R_w = [\Sigma w | F_o| - |F_c|)^2 / \Sigma w |F_o|^2]^{1/2}; w = 1/\sigma^2 (|F_o|)$$

Figure 21. Comparison of a series of edge-sharing bioctahedral dirhenium complexes with the syn-Re₂Cl₃(dppm)₂ core.



_						
	A	В	С	n	Re—Re	Reference
	Cl	Cl	Cl	0	2.616(1)	[1]
	Cl	Cl	Cl	+1	2.682(1)	[2]
	CO	Н	СО	0	2.605 (0)	this work
	СО	Н	CO	+1		this work
	NO	СО	CO	+1	2.591 (3)	this work
	СО	Cl	CO	0	2.70	this work
	Cl	СО	CO	0		[3]
	СО	СО	CO	0	2.583	[4]
	СО	CO	CO	+1		[5]
	СО	CO	СО	-1		[6]
	СО	CO	PMe ₃	0		[7]
	СО	СО	PMe ₃	+1		[8]

Figure 21

CHAPTER III

REACTIONS OF QUADRUPLY BONDED DINUCLEAR HALIDE
COMPLEXES WITH TRINUCLEAR CARBONYL CLUSTERS

1. Introduction

Ligand transfer reactions between two different metal systems have been explored in recent years [55], and this type of reaction provides an alternate synthetic route for many desired compounds which can not be simply achieved by ligand substitution reactions. Different pathways for reactions can occur due to interactions between both metal complexes to form thermally and/or kinetically unstable intermediates which may play a key role in the outcome of a desired reaction.

Over the past decade, the chemistry of carbonyl halide clusters has attracted much research interest because facile CO dissociation reactions in these complexes provide a good opportunity to study catalytic applications under mild conditions. Traditionally, carbonyl halide clusters are synthesized from simple ligand substitution reactions of metal carbonyl clusters with halides, but unfortunately this method is not very selective. We postulated that an alternative approach to such compounds via ligand transfer reactions between 'classical' organometallic compounds, namely metal carbonyl clusters, and metal halide complexes might be useful. In this respect, multiply bonded metal—metal dinuclear complexes were considered to be suitable precursors as they have been shown to exhibit a tendency to undergo halide substitution.

In this study, a new class of halide carbonyl clusters were successfully synthesized via the reactions between Re⁴Re halide complexes with metal carbonyl clusters. Detailed structural information for these complexes revealed by X-ray diffraction are reported.

2. Experimental

A. Reaction of $Ru_3(CO)_{12}$ with $Re_2Cl_6(PBu_3^n)_2$

Re₂Cl₆(PBu₃ⁿ)₂ was prepared from the reaction of Re₂Cl₄(dppm)₂ with PBu_3^n as reported in the literature [57]. A solution of $Ru_3(CO)_{12}$ (0.100 g, 0.154 mmol) and $\text{Re}_2\text{Cl}_6(\text{PBu}_3^n)_2$ (0.155 g, 0.154 mmol) in THF (20 mL) was refluxed under argon, and the reaction was monitored by infrared spectroscopy and stopped after 2 h on the basis of the disappearance of the v(CO) stretch at 2060 cm⁻¹ for Ru₃(CO)₁₂. The solvent was then removed to leave a dark brown residue which was extracted with hexane. The hexane extract was purified by silica gel column chromatography and eluted with a 3:2 (v/v) mixture of hexane/CH₂Cl₂. Three bands were observed in the order of light yellow, yellow, and orange. The light yellow fraction was collected and identified as Ru₃(CO)₁₂ based on infrared spectroscopy. The second band was not characterized due to the small quantity. The orange band was collected and the product was crystallized from hexane at -20 °C for several days to give X-ray quality single crystals. A crystallographic study revealed the compound to be $Ru_3(CO)_8(\mu-Cl)_2(PBu_3^n)_2$. The infrared spectrum of the product exhibits characteristic v(CO) bands at 2078(s), 2020(vs), 2005(vs), 1974(w), and 1952(s) cm⁻¹.

B. Reaction of $(\mu-H)_2Os_3(CO)_{10}$ with $(n-Bu_4N)_2Re_2Cl_8$

The compound $(\mu-H)_2Os_3(CO)_{10}$ [40] and $(n-Bu_4N)_2Re_2Cl_8$ [58] were prepared by literature methods. A suspension of $(\mu-H)_2Os_3(CO)_{10}$ (0.100 g, 0.154 mmol) and $(n-Bu_4N)_2Re_2Cl_8$ (0.178 g, 0.154 mmol) in CH₃CN (20 mL) was refluxed under argon for 15 h after which time the solvent was removed in vacuo to leave a dark brown residue which was extracted with Et₂O. The

hexane extract was purified by silica gel column chromatography and a major yellow band was collected with a mixture of hexane/CH₂Cl₂ (3:1, v/v). The product was crystallized from hexane at -20 °C for several days to give X-ray quality single crystals and identified as the known cluster $Os_3(\mu-H)(\mu-Cl)(CO)_{10}$ by an X-ray diffraction study [59].

B. X-ray Crystal Structures

(1) $Ru_3(CO)_8(\mu-Cl)_2(PBu_3^n)_2$

(1) Data Collection and Reduction

A brown crystal with approximate dimensions of 0.45 x 0.30 x 0.08 mm³ was mounted on a glass fiber. All measurements were made on a Nicolet P3/F diffractometer equipped with graphite—monochromated MoK α radiation and a low temperature device. A rotation photograph was used to locate 16 reflections from which a preliminary cell was indexed. Accurate cell constants and an orientation matrix for data collection, obtained from a least–squares refinement using the setting angles of 25 reflections in the range of $20 \le 20 \le 25^{\circ}$, corresponded to a monoclinic cell with dimensions: a = 11.093 (2) Å, b = 20.959 (3) Å, c = 19.221 (2) Å and V = 4451 (3) Å³. The data were collected at room temperature by using an ω -20 scan mode in the range of $4.5 \le 20 \le 55^{\circ}$ with a scan speed of 4 min^{-1} .

Three standard reflections were measured at constant intervals, and no significant loss in intensity was observed. However, the decay correction program CHORT was still applied as a routine procedure. An empirical absorption correction, based on azimuthal scans of three reflections with χ

near 90° was also applied; and the linear absorption coefficient for MoK α was 12.187° cm⁻¹. The data were corrected for Lorentz and polarization effects.

(2) Structure Solution and Refinement

The three ruthenium atoms were located by direct methods, and the remaining non-hydrogen atoms were located by subsequent difference Fourier maps and least-squares cycles. The final cycle of full-matrix least-squares refinement involved 419 variable parameters and 4231 observed reflections with $F_o^2 > 3\sigma(F_o^2)$. The refinement converged with residuals of R = 0.0395 and $R_w = 0.0563$.

3. Results and Discussion

A. Synthetic Methods

The thermal reaction between $Ru_3(CO)_{12}$ and $Re_2Cl_6(PBu_3^n)_2$ led to the isolation of a double halide-bridged trinuclear carbonyl phosphine cluster $Ru_3(CO)_8(\mu\text{-Cl})_2(PBu_3^n)_2$ which was confirmed by an X-ray diffraction study. It is obvious that the compound results from a ligand transfer reaction, a situation that was also observed for the reaction between $Os_3(\mu\text{-H})_2(CO)_{10}$ and $(n\text{-Bu}_4N)Re_2Cl_8$ to give the known edge doubly-bridged trinuclear carbonyl clusters $Os_3(\mu\text{-H})(\mu\text{-Cl})(CO)_{10}$ [59]. It is well established that multiply metal-metal bonded dinuclear complexes undergo facile metal-metal bond cleavage upon the reaction with π -acceptor ligands such as carbon monoxide, and isocyanides. It is reasonable to predict that the intractable brown residue contains mononuclear carbonyl halide complexes of Re.

The original synthesis of $Os_3(\mu-H)(\mu-Cl)(CO)_{10}$ involves the reaction of $Os_3(\mu-H)_2(CO)_{10}$ with Cl_2 . This study simply serves to demonstrate that an alternative source of Cl^- for the preparation of the edge doubly-bridged trinuclear carbonyl cluster $Os_3(\mu-H)(\mu-Cl)(CO)_{10}$ can be a dinuclear chlorophosphine complex.

Among the edge doubly–bridged trinuclear carbonyl clusters (Group 8), the three most common are of the types $M_3(\mu-H)_2(CO)_{10}$, $M_3(\mu-H)(\mu-X)(CO)_{10}$ and $M_3(\mu-X)_2(CO)_{10}$ (X = halide); these are illustrated below.

These three structural types also exhibit different electronic properties and reactivities. In the first class, $Os_3(\mu-H)_2(CO)_{10}$ is the only known dihydride—bridged species of its kind, as the ruthenium analogue has not yet been observed. The molecule $Os_3(\mu-H)_2(CO)_{10}$ is a 46—electron unsaturated molecule, and it exhibits a high reactivity with great potential for catalytic applications owing to its inherent coordinative unsaturation. The second class of edge doubly—bridged clusters, $M_3(\mu-H)(\mu-X)(CO)_{10}$ (M = Os, Ru), comprises the 48—electron saturated clusters which show only moderate reactivity [60, 61]. Additionally, another type of cluster, $M_3(\mu-X)_2(CO)_{10}$ contains an open edge in the molecule with no metal—metal interaction [61]. Although the species has a relatively high stability, the presence of two bridging chlorides results in a labilizing effect on the CO

groups in the trans positions. For example, the reaction of $Os_3(\mu-Cl)_2(CO)_{10}$ with triphenylphosphine leads to a disubstituted cluster $Os_3(CO)_8(PPh_3)_2(\mu-Cl)_2$ which is formed via CO exchange with triphenylphosphine; the exchange reaction does not occur with $Os_3(CO)_{12}$ under the same mild conditions.

B. Molecular Structure

The structural data for $\mathrm{Ru}_3(\mathrm{CO})_8(\mu\text{-Cl})_2(\mathrm{PBu}_3^n)_2$ are listed in Table 9; selected bond distances and angles are given in Table 10. An Ortep drawing including the labeling scheme is shown in Figure 22. The cluster possesses approximate C_{2v} symmetry with a triruthenium framework involving two metal-metal bonds [$\mathrm{Ru}(1)$ — $\mathrm{Ru}(3) = 2.859$ (1)Å; $\mathrm{Ru}(2)$ — $\mathrm{Ru}(3) = 2.871$ (1) Å] and one open edge $\mathrm{Ru}(1)$ ···Ru(2) supported by two bridging chlorides $\mathrm{Cl}(1)$ and $\mathrm{Cl}(2)$. The metal-metal separation between $\mathrm{Ru}(1)$ and $\mathrm{Ru}(2)$ is 3.230 (1) Å, which is in agreement with the prediction for a zero bond order. Similar non-bonding distances have been found in closely related edge double-bridged species such as $\mathrm{Ru}_3(\mu\text{-NO})_2(\mathrm{CO})_{10}$ (3.150 (2) Å) and $\mathrm{Ru}_3(\mu\text{-I})_2(\mathrm{CO})_{10}$ (3.301(1)Å).

Atoms Ru(1) and Ru (2) are coordinated to two CO groups and one PBu₃ⁿ ligand, respectively. Both PBu₃ⁿ ligands occupy nearly equivalent equatorial sites which are trans to the unique ruthenium atom Ru(2). Carbonyl ligands are located in the positions opposite to the bridging chloride atoms. The trans influence of the Cl atoms results in an average value of metal-carbon bonds trans to Cl of 1.816 (1) Å, significantly shorter than the corresponding value found for metal-carbon bonds to Ru(2) (average 1.909Å).

Table 9. Crystal Data for $Ru_3(\mu-Cl)_2(\mu-PBu_3^n)_2(CO)_8$

Formula	Ru ₃ Cl ₂ P ₂ O ₈ C ₃₂ H ₅₄
Formula weight	1002.8
Crystal system	Monoclinic
Space group	P2 ₁ /n
a, Å	11.093 (2)
b, Å	20.959 (3)
c, Å	19.221 (2)
α, deg	90
β, deg	95.092 (2)
γ, deg	90
V, Å ³	4451 (3)
Z	4
d _{calc} , g/cm ³	1.532
Crystal size, mm	0.50 x 0.45 x 0.38
Radiation	Mo K_{α} (λ = 0.71073 Å)
μ , cm ⁻¹	12.187
Data collection instrument	Nicolet P3/F
Temperature, °C	22 ± 2
Scan method	$\omega - 2\theta$
Data col. range, 20, deg.	4.5 – 55
Ra	0.039
R _w b	0.056

 $aR = \Sigma | |F_o| - |F_c| |/\Sigma| F_o|$

$$b R_w = [\Sigma w | F_o | - | F_c |)^2 / \Sigma w | F_o |^2]^{1/2}; w = 1/\sigma^2 (| F_o |)$$

Table 10. Selected Bond Distances (Å) and Angles (deg) for Ru₃(μ-Cl)₂(CO)₈(PBu₃ⁿ)₂.

Atom 1	Atom 2		Distance	Atom 1	Atom 2	1 2	Distance
Ru(1)	Ru(2)	3.	3.230 (1)	Ru(2)	P(2)		2.383 (2)
Ru(1)	Ru(3)	2.	2.859 (1)	P(1)	C(9)		1.846 (7)
Ru(2)	Ru(3)	2.	2.871 (1)	P(1)	C(17)		1.836 (9)
Ru(1)	P(1)	2.	2.477 (2)	P(2)	C(21)		1.838 (8)
Ru(1)	CI(1)	2.	2.472 (2)	P(2)	C(25)		1.839 (7)
Ru(1)	CI(2)	2.	2.378 (2)	Ru(1)	C(1)		1.865 (8)
Ru(2)	Cl(1)	2.	2.467 (2)	Ru(1)	C(2)		1.834 (7)
Ru(2)	Cl(2)	2.	2.474 (2)				
Atom 1	Atom 2	Atom 3	Angle	Atom 1	Atom 2	Atom 3	Angle
Ru(2)	Ru(1)	Ru(3)	55.86 (2)	CI(1)	Ru(1)	C(1)	172.3 (2)
Ru(1)	Ru(2)	Ru(3)	55.51 (2)	Cl(2)	Ru(1)	C(2)	174.4 (2)
Ru(1)	Ru(3)	Ru(2)	68.63 (2)	Cl(1)	Ru(1)	P(1)	90.94 (6)
Ru(3)	Ru(2)	P(2)	177.69 (6)	Cl(2)	Ru(1)	P(1)	91.08 (7)
Ru(3)	Ru(1)	Cl(1)	87.01 (5)	Cl(1)	Ru(2)	P(2)	91.25 (7)
Ru(3)	Ru(1)	CI(2)	87.64 (5)	Cl(2)	Ru(2)	P(2)	90.98 (7)
Ru(3)	Ru(2)	Cl(1)	86.93 (5)	Cl(1)	Ru(2)	C(4)	173.8 (3)
Ru(3)	Ru(2)	Cl(2)	87.34 (5)	Cl(2)	Ru(2)	C(4)	94.8 (2)
Ru(3)	Ru(1)	P(1)	177.72 (5)				

Figure 22. ORTEP drawing of $Ru_3(\mu-Cl)_2(PBu_3^n)_2(CO)_8$ showing the atom labeling scheme. All *n*-butyl carbon atoms are represented as small circles for clarity, and all other atoms are represented by their 50% propability ellipsoids.

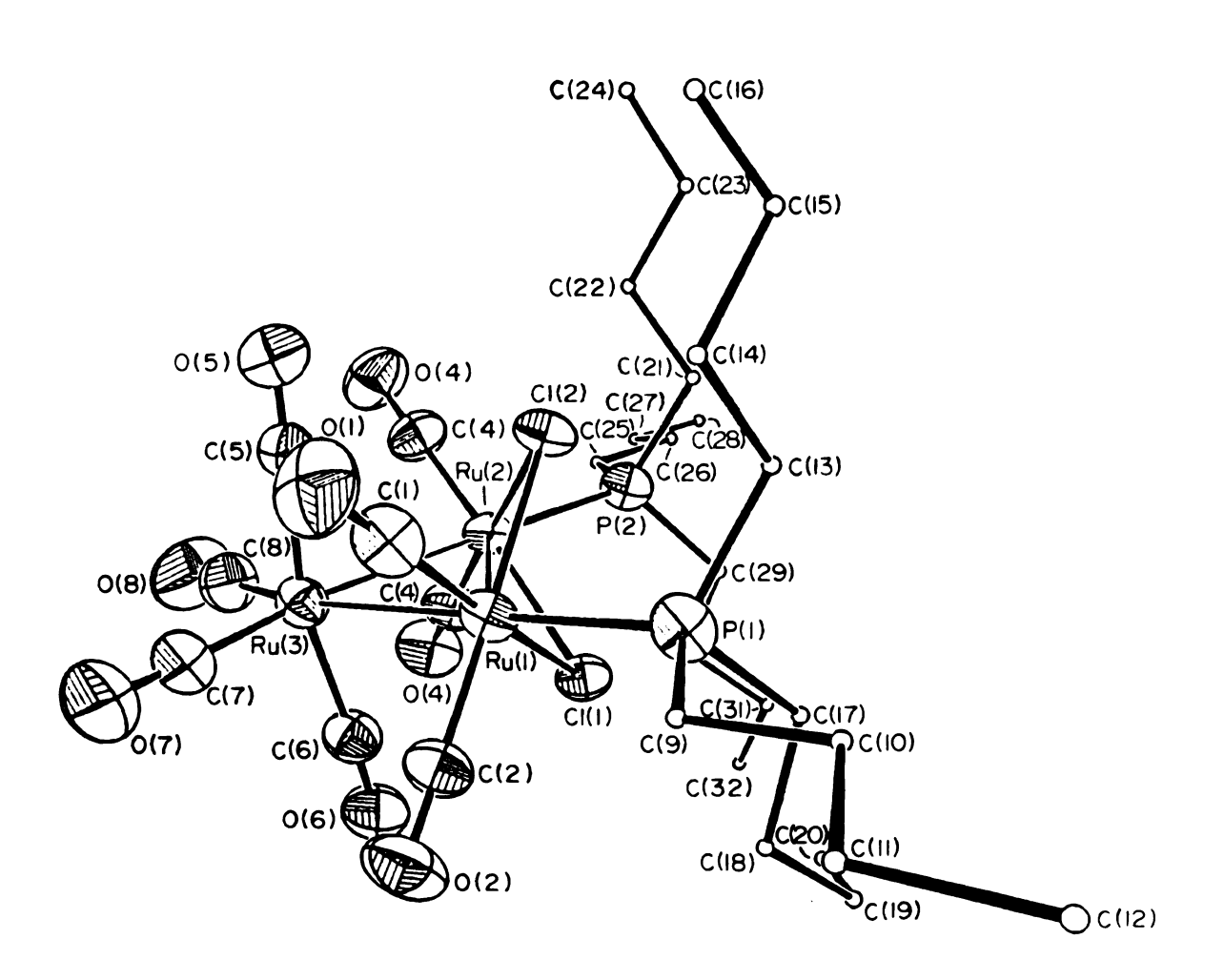


Figure 22

4. Summary

The work describes a possible route for bridging the area of 'classical' organometallic and coordination chemistry. The halide carbonyl clusters derived from the reactions between Re⁴Re halide complexes with metal carbonyl clusters demonstrate a promising approach toward the syntheses of a new class of reactive mixed-ligand compounds which may exhibit unique electronic properties induced by the combined presence of the dramatically different donor ligands.

CHAPTER IV

REACTIONS OF THE MULTIFUNCTIONALIZED PHOSPHINE LIGAND
TRIS(2,4,6-TRIMETHOXYPHENYL)PHOSPHINE WITH DINUCLEAR
CARBOXYLATE AND SOLVATED METAL COMPLEXES

1. Introduction

It is well-known that metal phosphine complexes are good catalyst precursors in important reactions such as hydrogenation, hydroformylation, and polymerization. The investigation of bulky and labile phosphine ligands is especially interesting due to the formation of reactive coordinatively unsaturated molecules. One of our recent research interests is to explore the chemistry of the unusually large and basic phosphine ligand tris(2,4,6-trimethoxyphenyl)phosphine (TMPP) with a wide variety of transition metal complexes. The first TMPP metal complex that was prepared in our laboratories is $[Rh(TMPP)_2](BF_4)_2$, a novel Rh(II)monoclear compound possessing a chelating tridentate arrangement for the PR₃ ligand. Since both oxygen and phosphorous atoms are good donors, one may envision a variety of possible multidentate coordination modes for the ligand involving either chelates or bridges. The use of this highly flexible ligand in the series of complexes $[Rh(TMPP)_2]^{n+}$ (n =1, 2, 3) afforded us the rare opportunity to probe the geometrical preferences of a metal center as a function of the electronic configuration. We were intrigued by these results in mononuclear chemistry, and our research interest was further extended to exploring the possibilities that this ligand might have in higher nuclearity metal compounds.

It has been known that bidentate phosphine ligands with bridging coordination tendencies are very useful for studying the reactivites of complexes that contain metal-metal bonds because of the variety of structural types that result from binding these molecules. In this respect, one of our research efforts thus focuses on the investigation of the multifunctionalized phosphine TMPP with metal-metal bonded species. Among them, carboxylate-bridged metal complexes $M_2(O_2CCH_3)_4$ (M =

Rh(II), Mo(II)) were chosen as precursors in this study because they have been extensively studied in the past two decades [62]. The intense research interest in rhodium(II) and molybdenum(II) carboxylates has continued to grow in recent years, as more researchers explore structural and spectroscopic properties, ligand substitution, redox reactions [66] in solution and potential practical applications [64-65] of these complexes.

In early investigations, we found the low solubility of $M_2(O_2CCH_3)_4$ to be a main drawback for the study of its reactivity toward a nucleophile. The solubility of these systems can be dramatically improved by the use of Trifluoroacetate metal complexes fluorinated carboxylate ligands. M₂(O₂CCF₃)₄ with 'paddlewheel' structures [63] are isostructural to M₂(O₂CCH₃)₄, but they demonstrate more facile ligand substitution in many reactions due mainly to their great ligand lability. A series of reactions between trifluoroacetate molybdenum (II) complexes Mo₂(O₂CCF₃)₄ and tertiary phosphines were carried out by Anderson and co-workers who concluded that two main types of reactions were occurring, depending on the combined influences of phosphine basicity and their steric bulk. A graph of ligand size versus basicity for various phosphine ligands is given in Figure 23. In general, larger phosphine ligands with low basicity prefer to form bis-adducts in axial positions, and smaller ones with high basicity occupy the equatorial positions along with two bridging and two monodentate dangling trifluoroacetates. Since the TMPP ligand exhibits unique electronic and steric properties with multidentate functionality, namely high basicity and large steric bulk, we explored the reactivity TMPP with trifluoroacetate metal complexes.

Figure 23. A graph of ligand size versus basicity. The ligand size and basicity are expressed by the cone angle and $\nu(CO)$ value, respectively. The cone angles and $\nu(CO)$ values (smaller values indicating greater σ -donor and poorer π -acceptor properties) were taken from Tolman's work [22].

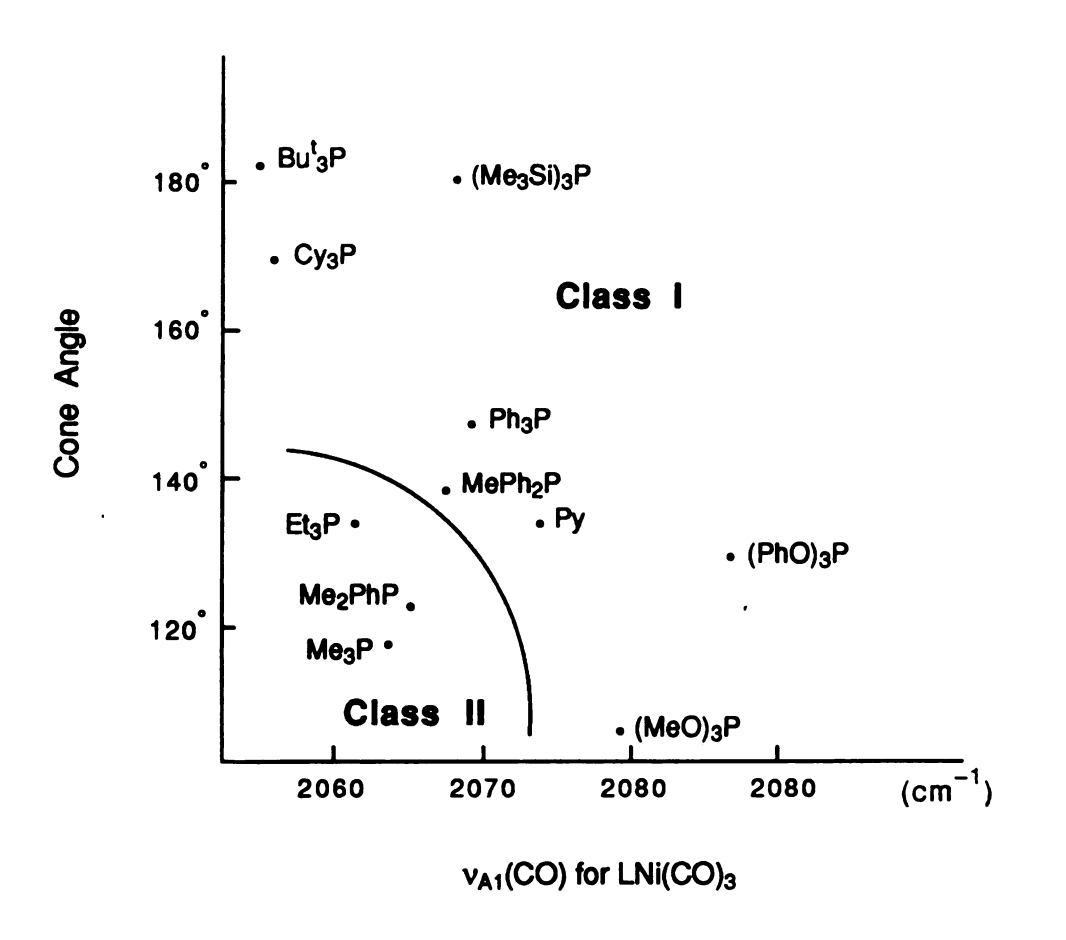


Figure 23

2. Experimental

A. Synthesis

(1) Reaction of Rh₂(O₂CCH₃)₄ (MeOH) ₂with TMPP

(i) Synthesis of Rh₂(O₂CCH₃)₂(TMPP-O)(MeOH) (1)

Rh₂(O₂CCH₃)₄(MeOH)₂ was prepared according to a literature method [67]. A suspension of $Rh_2(O_2CCH_3)_4(MeOH)_2$ (0.100 g, 0.198 mmol) and TMPP (0.211 g, 0.397 mmol) in ethanol (20 mL) was refluxed for 12 h to give a dark green-brown solution. The solvent was removed in vacuo to ca. 3 mL, and then chromatographed on a silica gel column with CH2Cl2 as eluent to remove a yellow band. The yellow product was characterized as the [MeTMPP][CH₃COO] phosphonium salt. ¹H NMR (CDCl₃): $\delta = 6.13$ (d, $J_{HP} = 5 \text{ Hz}, m-H$, 3.89 (s, p-OMe), 3.58 (s, o-OMe), 2.45 (d, $J_{HP} = 15 \text{ Hz}, Me-Me$ TMPP) ppm. A second green band was collected with acetone as eluent, and the product was spectroscopically and structurally characterized as the compound $Rh_2(O_2CCH_3)_3(TMPP-O)(MeOH)$ (1). Yield: 0.118 g (64%). Recrystallization was carried out by slow diffusion of diethyl ether into a methanol solution of (1), and a crop of green crystals was obtained at room temperature after several days. UV-vis (CH₃CN): $\lambda_{max} = 600$ nm ($\epsilon = 174.84$ $M^{-1}cm^{-1}$). IR (Nujol): $v_{as}(COO) = 1590 \text{ cm}^{-1}$. ³¹P NMR (CD₃CN): $\delta = 9.8$ ppm (d, J_{P-Rh} = 158.9 Hz). Crystalline samples that are subjected to a static vacuum for 24 h lose interstitial ethanol of crystallization and the labile axial methanol ligand, as evidenced by ¹H NMR spectroscopy and FABMS spectrum: parent ion, m/z = 900.1 (103Rh) corresponding to $Rh_2(O_2CCH_3)_3(TMPP-O)$. Anal. Calcd for $C_{32}H_{39}O_{15}P_1Rh_2$: C, 42.51; H, 4.65. Found: C, 42.68; H, 4.37.

(ii) Chemical Oxidation of Rh₂(O₂CCH₃)₃(TMPP-O)(MeOH)

A solution of NOPF₆ (0.0188 g, 0.107 mmol) in CH₃CN (5 mL) was slowly added to Rh₂(O₂CCH₃)₃(TMPP-O)(MeOH) (0.100 g, 0.107 mmol) in CH₃CN (10 mL). The green solution turned brown immediately, and after the mixture was stirred for ca. 5 min, the solvent was removed *in vacuo*. The dark greenish-brown residue was extracted with 10 mL of CH₂Cl₂ after which time diethyl ether (10 mL) was added to induce precipitation. A brown microcrystalline solid was collected on a medium-porosity frit under argon and dried *in vacuo*. The product was recrystallized by slow diffusion of diethyl ether into a CH₂Cl₂ solution of the compound. UV-vis (CH₃CN): $\lambda_{max} = 330$ (sh), 295 nm. IR (Nujol): ν_{as} (COO) = 1590 cm⁻¹. ν (P—F) = 845 cm⁻¹. ¹H NMR: broad and featureless. When an excess of NOPF₆ (0.0250 g, 0.143 mmol) was used, a different brown product was obtained. IR (Nujol): ν_{as} (COO) = 1590 cm⁻¹. ν (NO) = 1720 cm⁻¹. ¹H NMR: broad and featureless. FABMS spectrum: parent ion, m/z = 915 (¹⁰³Rh) corresponding to the nitrosyl product Rh₂(O₂CCH₃)₃(TMPP-2O)(NO).

(2) Preparation of $Mo_2(O_2CCF_3)_4$

The method is a slight modification of the synthesis reported in the literature [68]. A suspension of $Mo_2(O_2CCH_3)_4$ (1.00 g, 2.336 mmol) in CF_3COOH (30 mL) and $(CF_3COO)_2O$ (5 mL) was refluxed to give a clear yellow solution, and the reaction was stopped after ca. 20 min. The hot solution was immediately filtered by suction through a medium porosity frit, and the yellow filtrate was subsequently reduced by using a water

aspirator to 5 mL. From this procedure, a crop of yellow crystalline solid was obtained. Further purification was carried out by sublimation to give a finely divided sample of $Mo_2(O_2CCF_3)_4$. IR (Nujol): $v_{as}(COO) = 1590$ cm⁻¹. ¹⁹F NMR (CDCl₃): $\delta = -73.45$ ppm.

(3) Reaction of Mo₂(O₂CCF₃)₄ with TMPP

A yellow solution of $Mo_2(O_2CCF_3)_4$ (0.100 g, 0.155 mmol) and TMPP (0.165 g, 0.310 mmol) in THF or acetone (20 mL) was stirred at room temperature with no apparent color change after ca. 30 min. After the solvent had been reduced in volume, the yellow solution turned reddishyellow, and a red residue was obtained after complete evaporation of the solvent. The residue was extracted with diethyl ether to give a red solution, leaving behind a pale yellow-brown solid. The yellow-brown product was investigated as a [MeTMPP]⁺ phosphonium salt with an unidentified counterion. IR (Nujol): $v_{as}(COO) = 1600$, 1680 cm⁻¹. ¹H NMR (CDCl₃): $\delta = 6.13$ (d, $J_{HP} = 5$ Hz, m-H), 3.89 (s, p-OMe), 3.58 (s, o-OMe), 2.45 (d, $J_{HP} = 15$ Hz, Me-TMPP) ppm. The red extract was treated with a mixture of toluene and hexane to give a red solid. The red product was investigated by various spectroscopic methods; IR (Nujol): $v_{as}(COO) = 1600$ cm⁻¹. UV-vis (CH₂Cl₂): $\lambda_{max} = 527$, 315 nm. FABMS spectrum: parent ion, m/z = 1452.8 (⁹⁶Mo).

(4) Preparation of Rh₂(O₂CCF₃)₄

The method used in our laboratories is a modification of the literature procedure [69]. A suspension of $Rh_2(O_2CCH_3)_4(MeOH)_2$ (0.200 g, 0.397 mmol) in CF_3COOH (20 mL) and $(CF_3COO)_2O$ (5 mL) was refluxed for 3 days to give a green solution. Filtration in air led to a clear green filtrate which was reduced in volume on a water aspirator to 5 mL to give a green

solid. Sublimation to remove trace amounts of CF_3COOH and $(CF_3COO)_2O$ was carried out, and a fine green powder was obtained. IR (Nujol): $v_{as}(COO) = 1650 \text{ cm}^{-1}$. UV-vis (CH_3CN) : $\lambda_{max} = 550$, 450 nm.

(5) Reaction of Rh₂(O₂CCF₃)₄ with TMPP

A suspension of $Rh_2(O_2CCF_3)_4$ (0.100 g, 0.165 mmol) and TMPP (0.275 g, 0.330 mmol) in THF (20 mL) was stirred at room temperature for 30 min to give a clear green solution. The solvent was removed *in vacuo* to 3 mL, and then chromatographed on a silica gel column with acetone as eluent to lead to a green band. The first green band (1) was collected with acetone as eluent, and a second green band (2) was removed with MeOH. UV-visible spectrum (CH₃CN): band (1), $\lambda_{max} = 586$ nm; band (2), $\lambda_{max} = 594$ nm.

B. X-ray Crystal Structure of $Rh_2(O_2CCH_3)_3(TMPP-O)(MeOH)$ (1)

(1) Data Collection and Reduction

A green crystal of approximate dimension $0.78 \times 0.52 \times 0.20 \text{ mm}^3$ was covered with epoxy cement and mounted at the end of a glass fiber. Geometric and intensity data were obtained on a Nicolet P3/F diffractometer equipped with graphite-monochromated MoK α radiation. A rotation photograph was used to locate 15 reflections from which a preliminary cell was indexed. The reduced cell dimensions indicated that the crystal was triclinic which was confirmed by axial photography. An accurate cell for data collection was calculated from 20 reflections in the range $20 \le 20 \le 30^\circ$. An ω -2 θ scan motion was used to scan 7053 data points in the range $4 \le 2\theta \le 50^\circ$. The structure factors were obtained after correction for Lorentz and

polarization effects. During data collection, three check reflections were measured every 100 reflections; no loss in intensity was observed.

(2) Structure Solution and Refinement

The positions of the Rh atoms were obtained from a Patterson Fourier map. A sequence of successive difference Fourier maps and least-squares cycles led to full development of the coordination sphere. The final full-matrix refinement involved 451 parameters and 6209 obsertvations with $F_0^2 > 3\sigma(F_0^2)$ for a data-to-parameter ratio of 11.3. The refinement converged with residuals of R = 0.0504 and $R_w = 0.0858$ and a quality-of-fit of 2.93. The largest shift/esd in the final cycle was 0.96.

3. Results and Discussion

(1) Reaction of Rh₂(O₂CCH₂)₄(MeOH)₂with TMPP

A. Synthesis

Reactions of the ether-phosphine ligand tris(2,4,6-trimethoxy-phenyl)phosphine (TMPP) with Rh₂(O₂CCH₃)₄(MeOH)₂ in refluxing alcohols yield the demethylation product Rh₂(O₂CCH₃)₃(TMPP-O)(MeOH). The excess TMPP in solution is methylated to form a phosponium salt as evidenced by ¹H NMR spectroscopic studies performed on residues retrieved from the filtrate. The reaction has been successfully carried out in methanol and ethanol with the latter solvent producing a higher yield of (1) (67% verus 40%) for a shorter reflux time (6 h verus 24 h). The identical experiment in THF results in no observed reaction for reflux times up to

several days. Further attempts to obtain analogous rhodium complexes in acetic acid proved to be unsuccessful. Since the highly basic TMPP (pKa ≈ 11) is a good nucleophile, it can easily form a phosphonium salt by either protonation or methylation. A summary of these reactions is shown in Figure 24.

B. Spectroscopic Studies

The room temperature 300 MHz 1 H NMR spectrum of (1) in CD $_3$ CN reveals that the TMPP ligand is ligated in a completely unsymmetrical fashion about the two metal centers. Four meta protons are well-resolved quartets, and resonate at $\delta = 6.52$, 5.96, 5.84, and 5.65 ppm; two ring protons, appear as virtual triplets at $\delta = 6.15$ and 5.93 ppm (Figure 25). After 31 P decoupling, all six meta protons are simplified into doublets (Figure 26). Eight methoxy group resonances were observed, with the most deshielded signal at $\delta = 2.57$ ppm being assigned to the ring that participates in an axial interaction with the metal center. The absence of a ninth methoxy group suggested that demethylation had occurred, which was subsequently confirmed by a solid state structrual determination.

The DQCOSY spectrum of (1) (Figure 27) clearly shows the J-coupling between H_1 and H_2 , H_3 and H_6 , H_4 and H_5 via their mutual crosspeaks. Due to the strong bonding between ring 1 and Rh(2) via a methoxide interaction, the most deshielded protons H_1 and H_2 were assigned to this ring. The two meta protons in the free phenyl ring have similar environments, thus we assign protons H_4 and H_5 to ring 2. Finally, H_3 and H_6 are in the same ring based on correlated crosspeaks, and a further study reveals that the chemical shift of H_3 is very solvent dependent. The meta proton region of (1) between 5.0 and 6.5 ppm, measured in five different

Figure 24. Schematic diagram of various approaches to the synthesis of $Rh_2(O_2CCH_3)_3(TMPP-O)(MeOH)$.

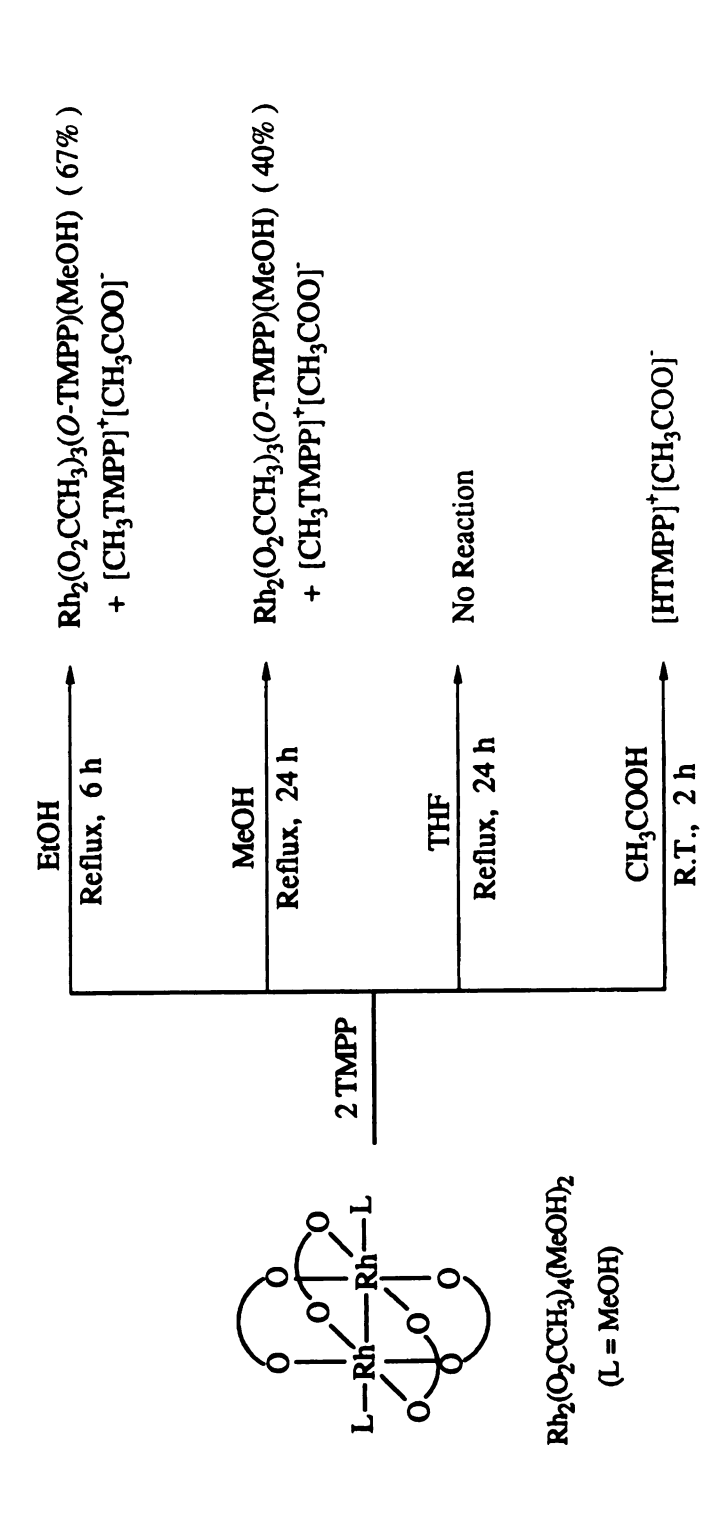


Figure 24

Figure 25. A 300 MHz 1 H NMR spectrum of $Rh_2(O_2CCH_3)_3(TMPP-O)(MeOH)$ in CD_3CN at 22 $^{\circ}C$.

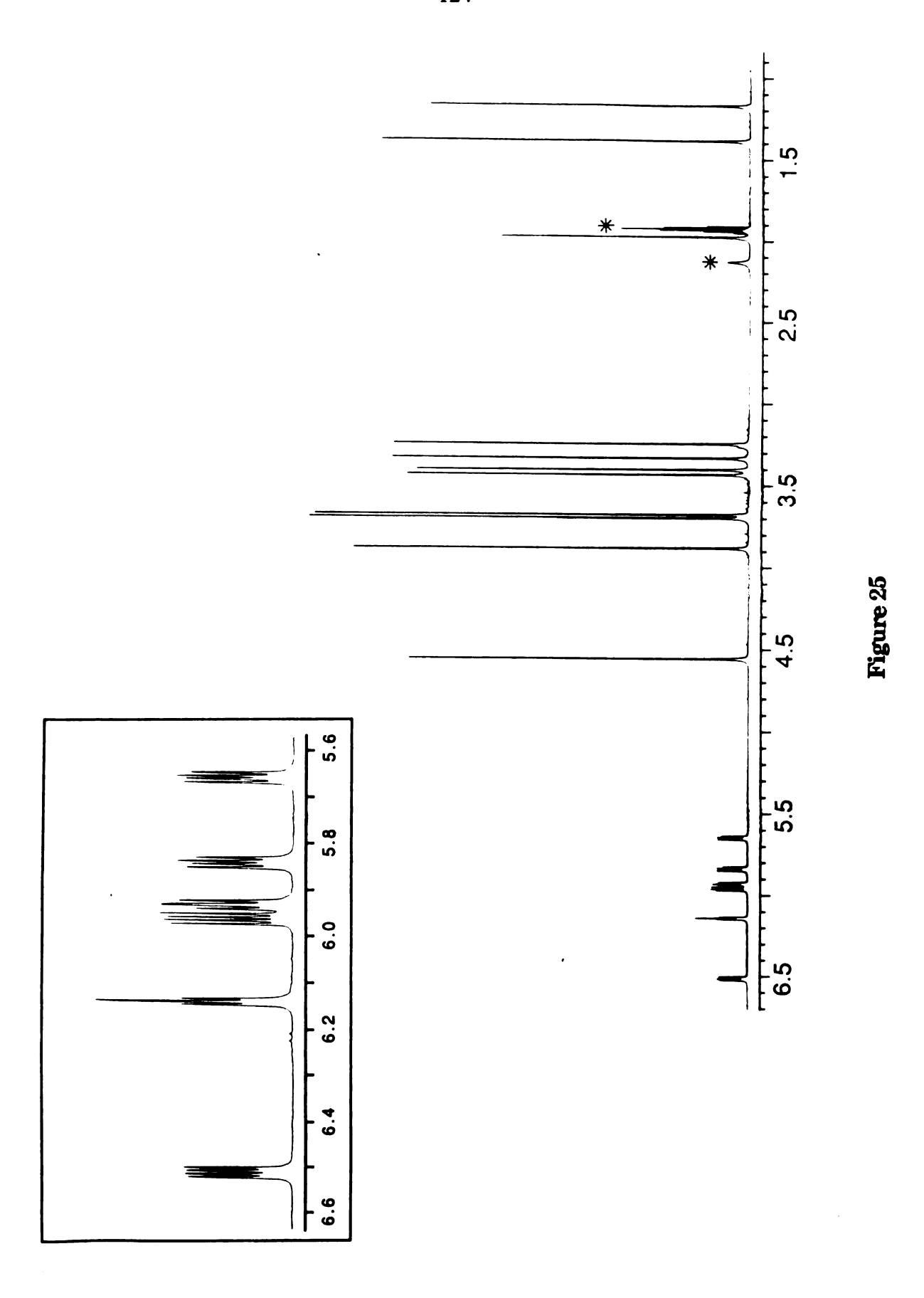
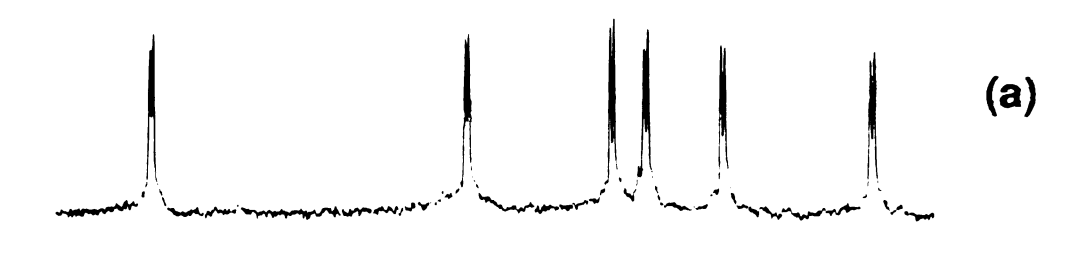


Figure 26. A 500 MHz ¹H NMR spectra of the meta proton region of Rh₂(O₂CCH₃)₃(TMPP-O)(MeOH) in CD₃CN at 22 °C with (a) ³¹P decoupling (b) ³¹P undecoupling.



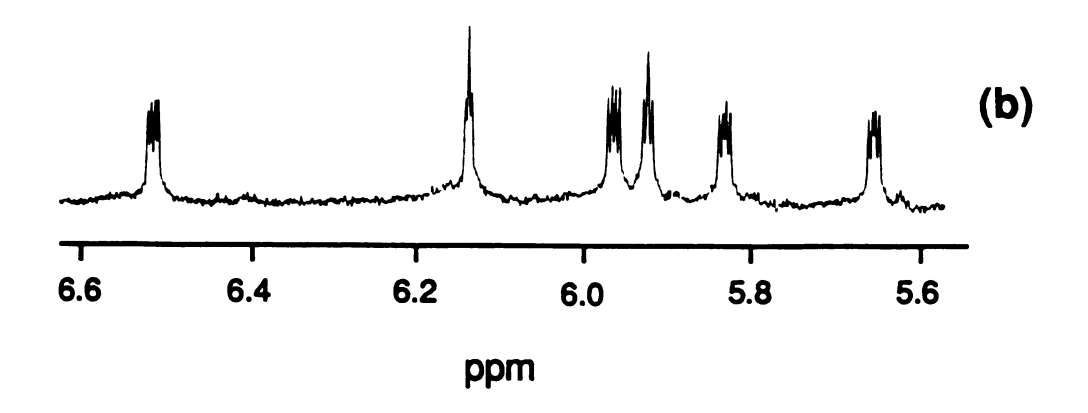


Figure 26

Figure 27. Two-dimentional DQCOSY spectrum of $Rh_2(O_2CCH_3)_3(TMPP-O)(MeOH)$.

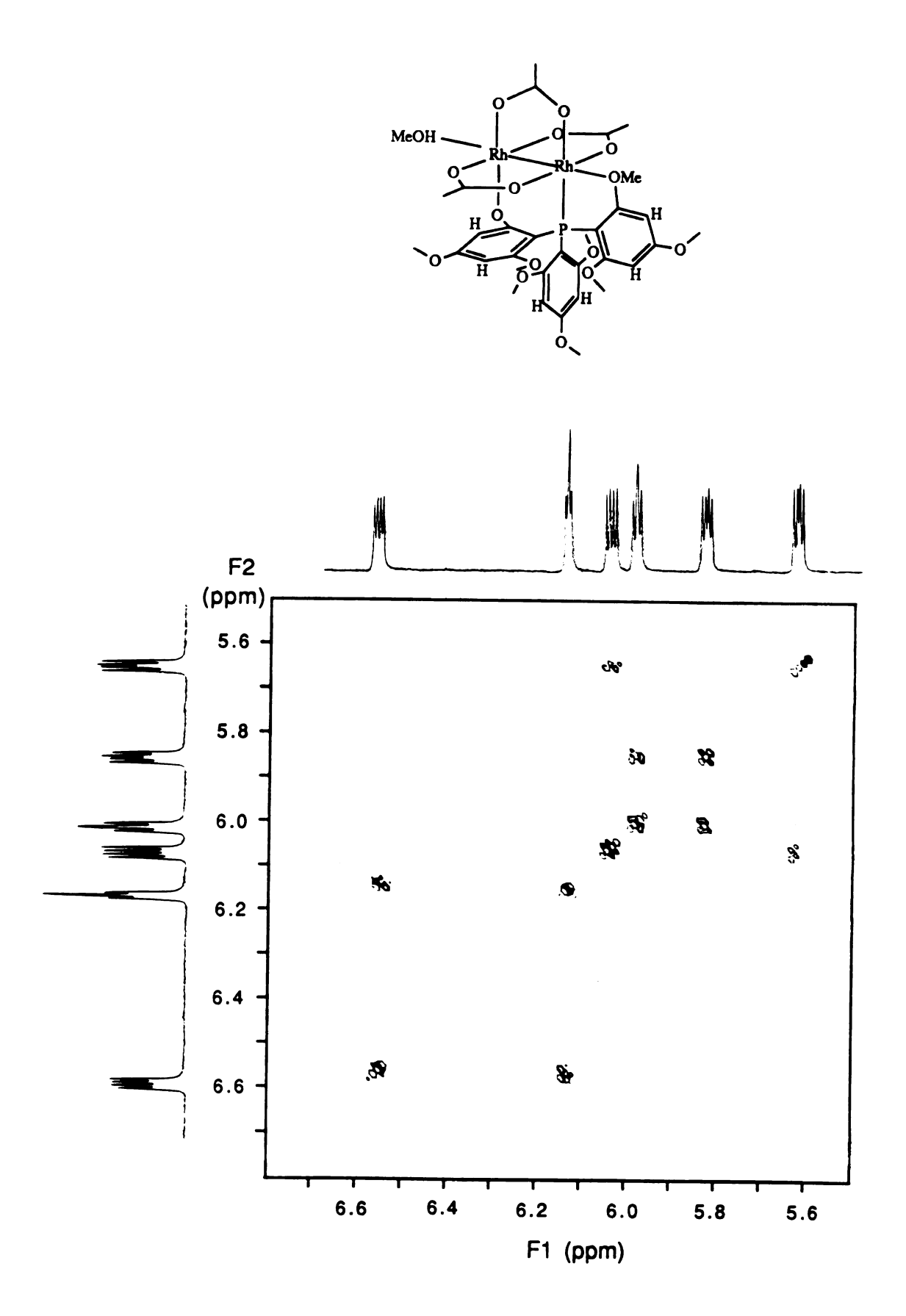


Figure 27

deuteriated solvents are shown in Figure 28. The quartet denoted by an asterisk symbol (H_3 in CD_3CN) shifts to an upfield position. These observations are consistent with axial ether group exchange with the solvent. The ring proton in close proximity to the axial methoxy ligand is expected to be most affected by the chemical environment of the position. The Brucker simulation program PANIC was utilized to obtain further coupling constant information (Figure 29): $J_{H1H2} = 1.94$ Hz, $J_{H1P} = 4.20$ Hz, $J_{H2P} = 2.15$ Hz, $J_{H3H6} = 2.37$ Hz, $J_{H3P} = 4.60$ Hz, $J_{H6P} = 4.00$ Hz, $J_{H4H5} = 2.15$ Hz, $J_{H4P} = 2.70$ Hz, and $J_{H5P} = 3.91$ Hz. The smaller coupling constants J_{H2P} and J_{H4P} are consistent with the observation that both triplets of H_2 and H_4 are due to a second order effect.

 ^{31}P (^{1}H) NMR studies in CD₃CN revealed a doublet at δ = 9.8 ppm with J_{P-Rh} = 159 Hz versus 85% $H_{3}PO_{4}$ (Figure 30).

A FABMS spectrum of the compound reveals the highest observed mass peak at m/z = 900.1 (103 Rh) corresponding to $Rh_2(O_2CCH_3)_3(TMPP-O)$. The result supports the idea that the axial ligand MeOH is quite labile (Figure 31).

C. Molecular Structure of Rh₂(O₂CCH₃)₃(TMPP-O)(MeOH) (1)

Compound (1) was recrystallized from MeOH and diethyl ether to give green crystals, one of which was examined by single crystal X-ray diffraction methods. The crystallographic data are shown in Table 11, and the important bond distances and angles for (1) are given in Table 12. An ORTEP plot of the molecular structure with the atom-labelling scheme is shown in Figure 32. The molecule contains an unusually bonded μ - η^3 -TMPP ligand. Of particular note in this structure, is the transformation of an ether group on the phosphine to an alkoxide thus allowing for a strong

Rh(1)—P(1)—C(7)—C(8)—O(7)—Rh(2) metallacycle to form. The Rh(2)—O(7) bond distance of 2.048 (2) Å is substantially shorter than the axial ether interaction Rh(1)—O(10) of 2.351 (2) Å. Other metric parameters within the molecule are within usual ranges for dirhodium(II,II) complexes. The Rh—Rh bond distance of 2.4228 (3) Å is slightly longer than that found for the complex $Rh_2(O_2CCH_3)_4(MeOH)_2$ in which the Rh—Rh distance is 2.377 (1) Å.

Although ortho-metallation is quite common among mononuclear complexes in which the ortho-metallated tertiary phosphine acts as a chelating ligand with a four-membered ring, it has not been well explored among metal-metal bonded complexes. Until recently, several reports showed that triarylphosphines such as triphenylphosphine can be transformed via ortho-metallation into an unusual tridentate mode of coordination as in $Os_2Cl_2(OAc)_2(Ph_2PC_6H_4)_2$ and $Rh_2(OAc)_2(Ph_2PC_6H_4)_2L$ (L = pyridine or CH_3COOH) [70].

D. Redox Chemisry

The cyclic voltammogram of $Rh_2(O_2CCH_3)_3(TMPP-O)(MeOH)$ in 0.1 M $[n-Bu_4N][PF_6]-CH_3CN$ exhibits a one-electron quasi-reversible oxidation at +0.78 V vs. Ag/AgCl with a peak-to-peak separation of 70 mV at 200 mV/sec which confirms that the reduction process is reversible (Figure 33). Further investigations at various scan speeds revealed a reversible couple at high scan speeds (100 to 10,000 mV/sec) but at slower scan speeds (20 to 100 mV/sec), the wave clearly becomes irreversible (Figure 34). These results suggest that the formation of (2) by the process $Rh_2(II,II) \rightarrow Rh_2(II,III)$ is immediately followed by a chemical reaction

which is most likely a ligand substitution reaction at the axial site as depicted below.

Oxidative bulk electrolysis of complex (1) in 0.1 M $[n\text{-Bu}_4N][PF_6]$ – CH_3CN , at an applied potential of +1.0 V, is accompanied by a color change from green to orange-brown. The orange-brown product was charcaterized to be an EPR-active species. The frozen solution EPR spectrum of the electrogenerated cation (Figure 35) in 0.1 M $[n\text{-Bu}_4N][PF_6]$ – CH_3CN is comprised of three relatively broad signals at $g_1 = 2.05$, $g_2 = 2.02$, and $g_3 = 1.996$ which are consistent with a metal-centered, unpaired electron; the rhombic nature of the spectrum is due to the low symmetry of $[Rh_2(O_2CCH_3)_3(TMPP-O)]^+$ (~ C_2) [71]. The electrolyzed species is quite unstable, and undergoes further decomposition evidenced by the disappearance of the EPR signal over longer periods of time.

Chemical oxidation of $Rh_2(O_2CCH_3)_3(TMPP-O)(MeOH)$ by reaction with one equivalent of $NOPF_6$ yields a brown EPR-active product (2), which was investigated by several spectroscopic methods. The broad and featureless ¹H NMR spectrum clearly indicated that the compound is paramagnetic, thus supporting the formulation as a Rh_2^{+5} species. The infrared spectrum of (2) exhibits an absorption at 790 cm⁻¹ which corresponds to the v(P-F) of the PF_6^- counterion. Additional evidence to support the formation of the product as a paramagnetic salt is the ³¹P NMR

spectrum which shows a resonance at ca -100 ppm due to the PF₆⁻ anion but no resonance for the phosphine ligand. Based on those spectroscopic investigations, the oxidation product is believed to be [Rh₂(O₂CCH₃)₃(TMPP-O)](PF₆); an exact formulation of the molecule is still not clear without a crystallographic study. If the oxidation reaction is carried out in an excess of NOPF₆, a brown product forms which is paramagnetic as evidenced by ¹H NMR spectroscopy. A FABMS spectrum of the compound exhibits the highest mass peak at m/z = 931 (103 Rh) which corresponds to the nitrosyl complex Rh₂(O₂CCH₃)₃(TMPP-2O)(NO) (Figure 36). Convincing evidence was further provided by both solution and solid-state EPR spectra (Figure 37) which showed signals at $g \approx 2.0$. The solution EPR spectrum with better resolution than the solid-state, clearly showed a triplet pattern with a small hyperfine coupling constant, indicating it might be due to an organic radical (NO⁺) which would be expected to exhibit a g value close to that of a free electron (= 2.0) [72]. Based on the previous cyclic voltammetric study, the assignment of the nitrosyl formula as Rh₂(O₂CCH₃)₃(TMPP-2O)(NO) $(TMPP-2O = P[(C_6H_2(OMe)_3]\{(C_6H_2(OMe)(O)_2)_2\})$ is consistent with the idea of ligand substitution at the axial site upon oxidation. The formation of the compound is postulated as below.

$$-\frac{e^{-}}{NO}$$

Rh₂(OAc)₃(TMPP-O)(L)

[Rh₂(OAc)₃(TMPP-O)(L)]⁺

Rh₂(OAc)₃(TMPP-2O)(NO)

Figure 28. ¹H NMR spectra of the meta proton of Rh₂(O₂CCH₃)₃(TMPP-O)(MeOH), measured in various solvents (a) THF-d₈ (b) CD₃CN (c) acetone-d₆ (d) CDCl₃ (e) CD₂Cl₂.

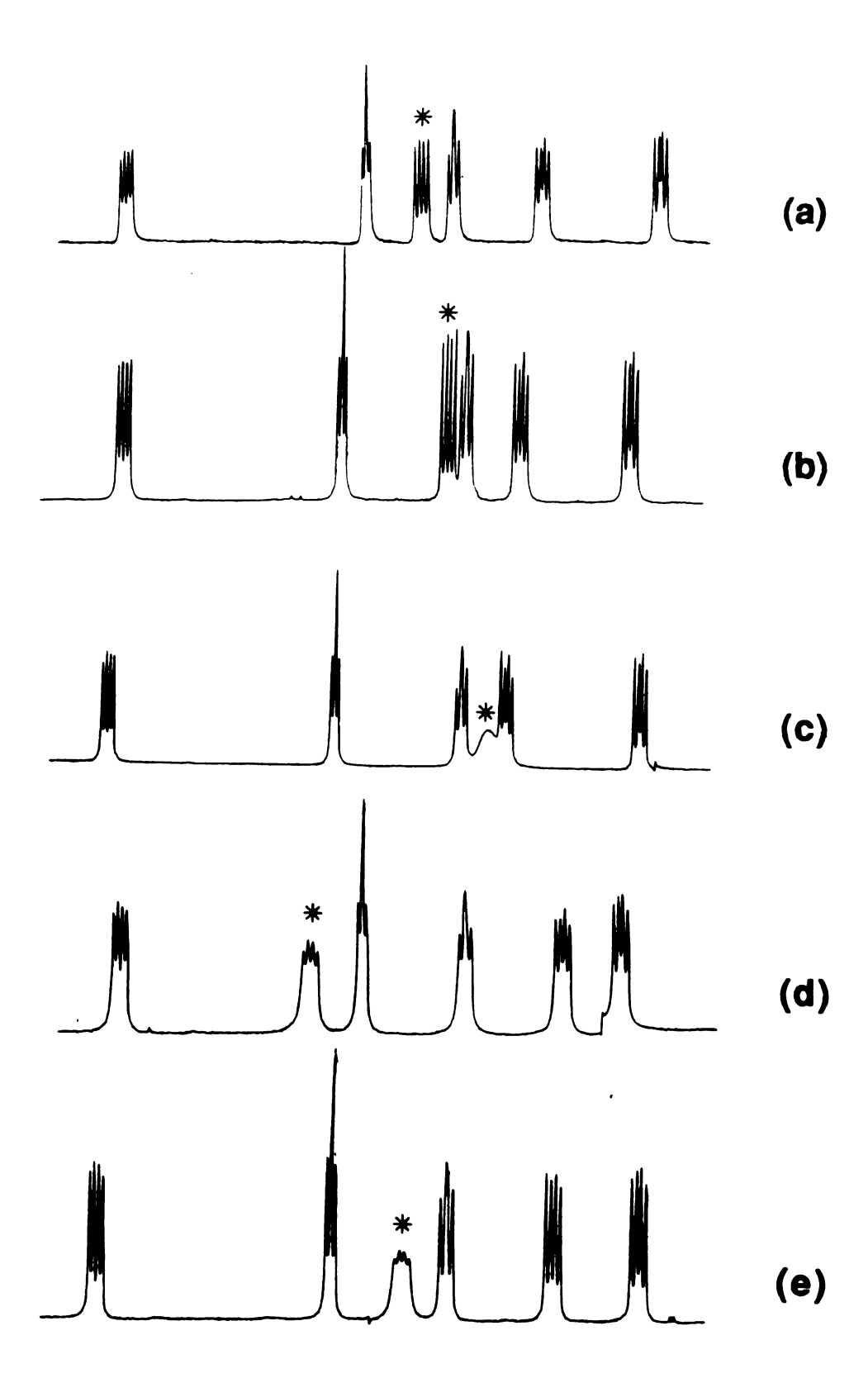
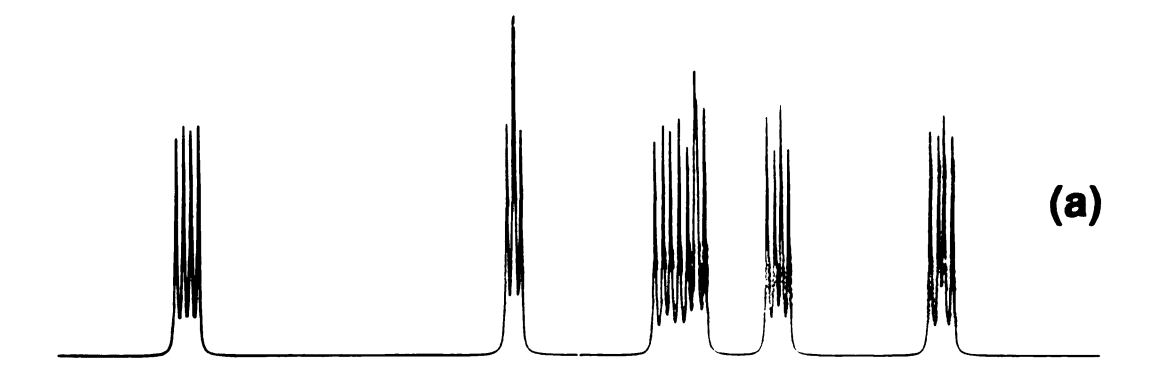


Figure 28

Figure 29. (a) Simulated and (b) experimental 1H NMR spectra of metaprotons of $Rh_2(O_2CCH_3)_3(TMPP-O)(MeOH)$.



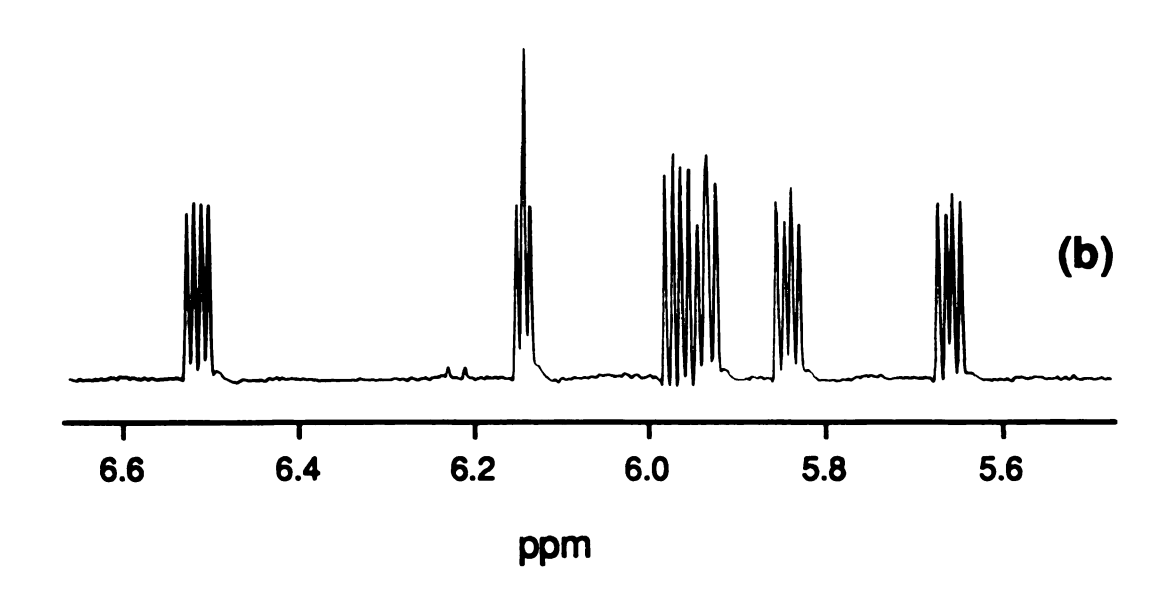


Figure 29

Figure 30. A $^{31}P\{^{1}H\}$ NMR spectrum of $Rh_{2}(O_{2}CCH_{3})_{3}(TMPP-O)(MeOH)$.

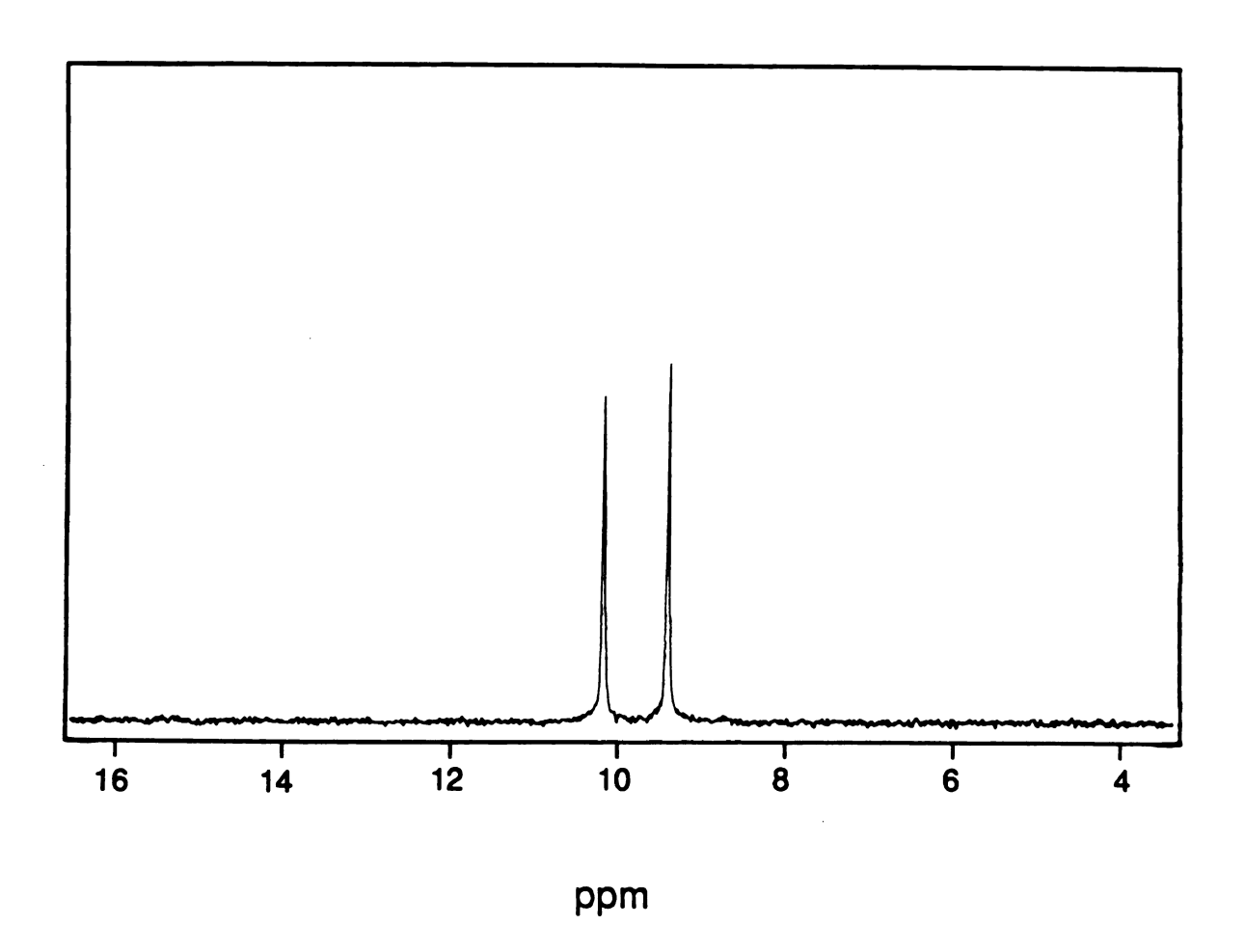
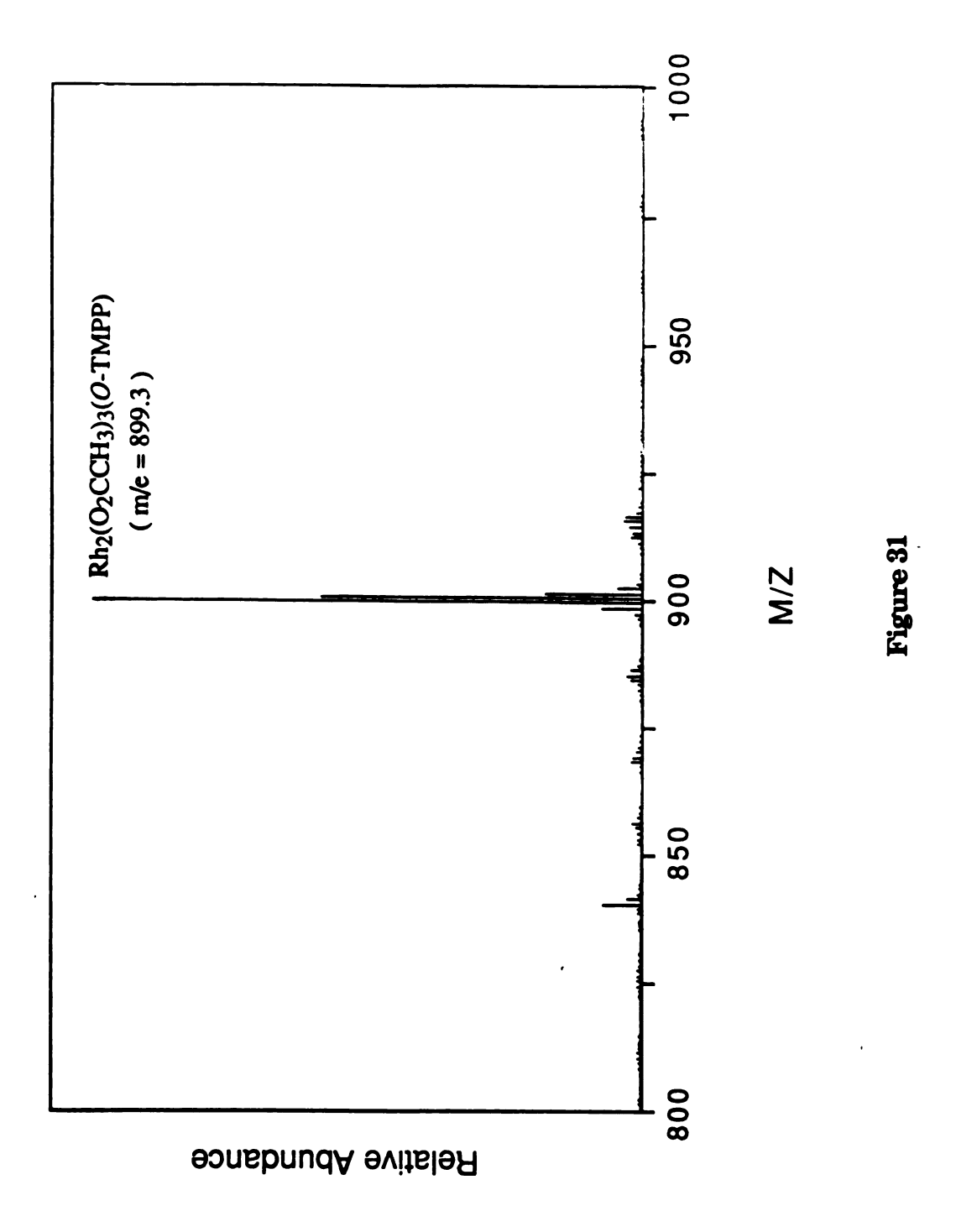


Figure 30

Figure 31. Positive ion FABMS spectrum of $Rh_2(O_2CCH_3)_3(TMPP-O)(MeOH)$.



MPP.

 $\textbf{Table 11.} \ \ \textbf{Crystal Data for } \ \textbf{Rh}_2(\textbf{O}_2\textbf{CCH}_3)_3(\textbf{TMPP-O})(\textbf{MeOH}) \cdot \textbf{EtOH}$

Formula	$Rh_2P_1O_{17}C_{35}H_{49}$
Formula weight	978.547
Crystal system	Triclinic
Space group	P-1
a, Å	13.730 (3)
b, Å	14.396 (5)
c, Å	11.921 (5)
α, deg	109.65 (2)
β, deg	95.65 (2)
γ, deg	64.32 (2)
V, Å ³	1997 (1)
Z	2
d _{calc} , g/cm ³	1.633
Crystal size, mm	0.78 x 0.52 x 0.02
Radiation	Mo $K_{\alpha}(\lambda = 0.71073 \text{ Å})$
μ , cm ⁻¹	9.251
Data collection instrument	Nicolet P3/F
Temperature, °C	22 ± 2
Scan method	$\omega - 2\theta$
Data col. range, 20, deg.	4.4 – 40
$R^{\mathbf{a}}$	0.030
R _w ^b	0.036

 $a R = \Sigma | |F_o| - |F_c| |/\Sigma| F_o|$

 $b R_w = [\Sigma w | F_o | - | F_c |)^2 / \Sigma w | F_o |^2]^{1/2}; w = 1/\sigma^2 (| F_o |)$

Table 12. Selected Bond Distances (Å) and Angles (deg) for Rh₂(O₂CCH₃)₃(TMPP-O)(MeOH)·EtOH.

Atom 1	Atom 2	~ 1	Distance	Atom 1	Atom 2	2	Distance
Rh(1)	Rh(2)		2.4228 (3)	P(1)	C(7)		1.793 (3)
Rh(1)	P(1)		2.2135 (8)	P(1)	C(15)		1.813 (3)
Rh(1)	0(2)		2.050 (2)	P(1)	C(24)		1.847 (3)
Rh(1)	0(4)		2.134 (2)	0(1)	C(1)		1.257 (4)
Rh(1)	(9)(2.038 (2)	0(2)	C(1)		1.280 (4)
Rh(2)	0(10)		2.351 (2)	0(3)	C(3)		1.227 (4)
Rh(2)	0(1)		2.049 (2)	0(4)	C(3)		1.258 (4)
Rh(2)	0(3)		2.034 (2)	0(5)	C(5)		1.262 (4)
Rh(2)	0(2)		2.030 (2)	(9)(0	C(5)		1.265 (4)
Rh(2)	0(1)		2.048 (2)	0(1)	C(8)		1.345 (4)
Rh(2)	0(16)		2.251 (2)	0(10)	C(16)		1.384 (4)
Atom 1	Atom 2	Atom 3	Angle	Atom 1	Atom 2	Atom 3	Angle
Rh(2)	Rh(1)	P(1)	95.92 (2)	Rh(1)	P(1)	C(15)	105.0 (1)
Rh(2)	Rh(1)	0(3)	(2) 89.98	Rh(1)	P(1)	C(7)	109.6 (1)
Rh(2)	Rh(1)	0(4)	86.51 (6)	Rh(2)	0(1)	C(8)	118.2 (2)
Rh(2)	Rh(1)	(9)(87.67 (6)	Rh(1)	0(10)	C(16)	117.8 (2)
Rh(2)	Rh(1)	0(10)	171.05 (6)	Rh(2)	0(16)	C(33)	116.2 (2)
P(1)	Rh(1)	0(10)	80.06 (6)	P(1)	C(7)	C(8)	114.0 (2)
Rh(1)	Rh(2)	0(1)	88.65 (7)	0(1)	C(8)	C(7)	118.1 (3)
Rh(1)	Rh(2)	0(1)	94.57 (6)	P(1)	C(15)	C(16)	120.5 (2)
0(1)	Rh(2)	0(16)	(6) 90:06	0(10)	C(16)	C(15)	116.1 (3)

Figure 32. An ORTEP drawing of Rh₂(O₂CCH₃)₃(TMPP-O)(MeOH), showing the atom labeling scheme. All phenyl-group and MeOH carbon atoms are represented as small circles for clarity, and all other atoms are represented by their 50% propability ellipsoids.

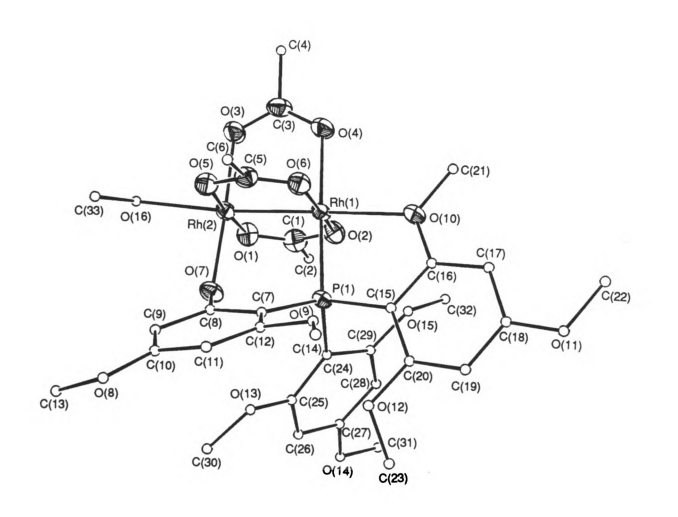
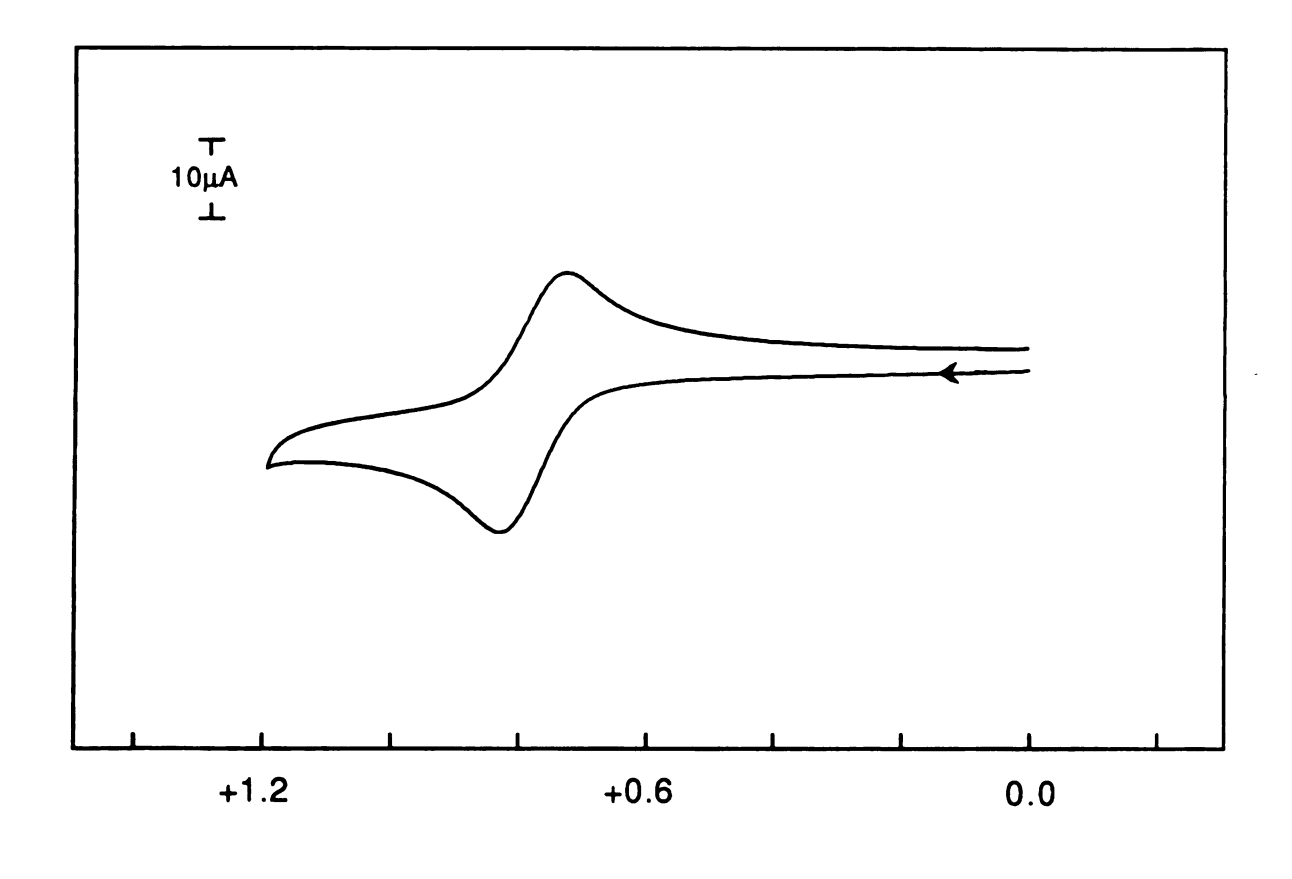


Figure 32

Figure 33. Cyclic voltammogram of $Rh_2(O_2CCH_3)_3(TMPP-O)(MeOH)$ in 0.2 M TBAPF₆—CH₃CN at 200 mV/s using a Pt-disk electrode.



VOLTS vs Ag/AgCI

Figure 33

)H) in rode.

Figure 34. Varible scan speed cyclic voltammograms of Rh₂(O₂CCH₃)₃(TMPP-O)(MeOH) in 0.2 M TBAH-CH₃CN.

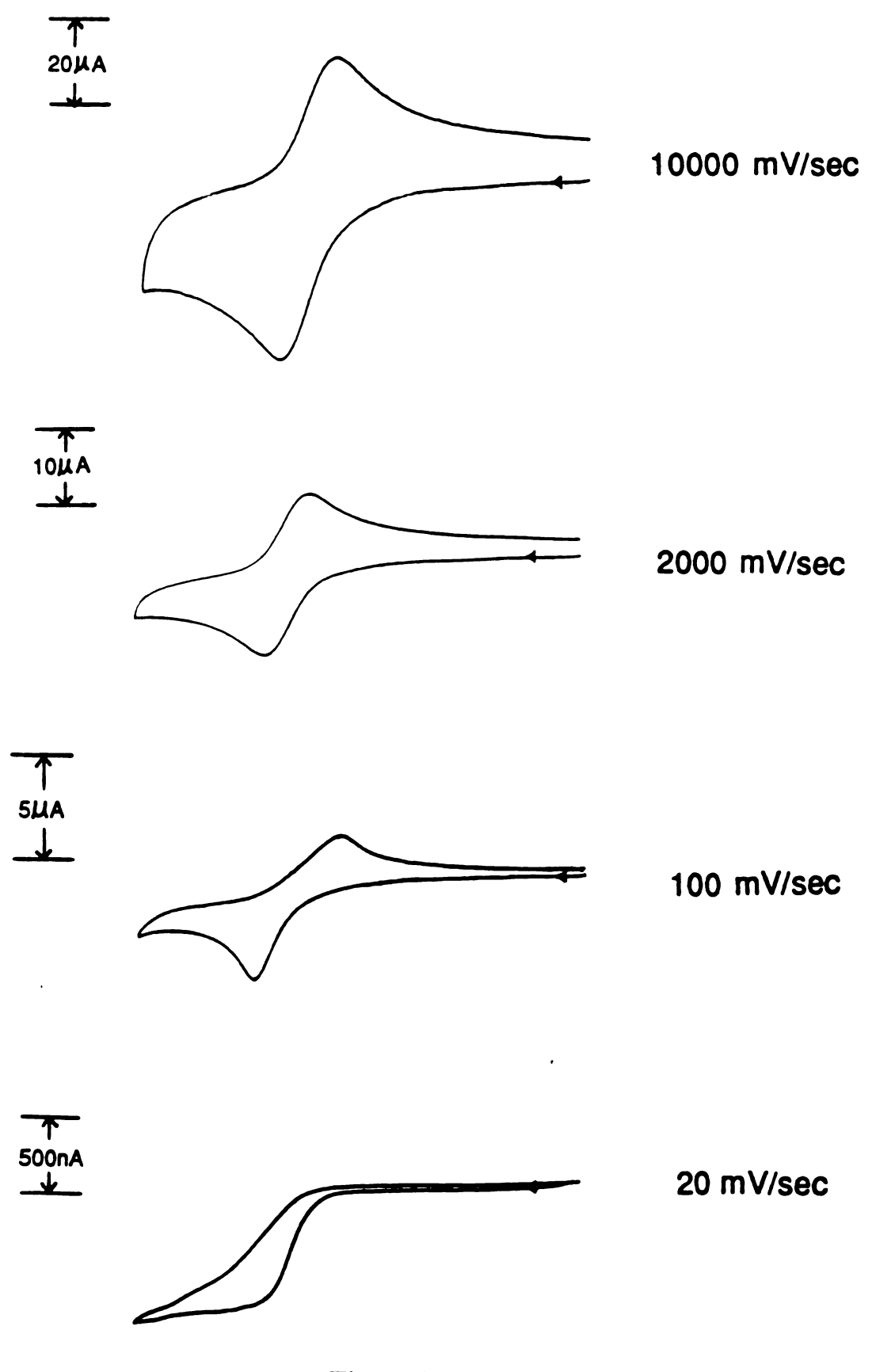
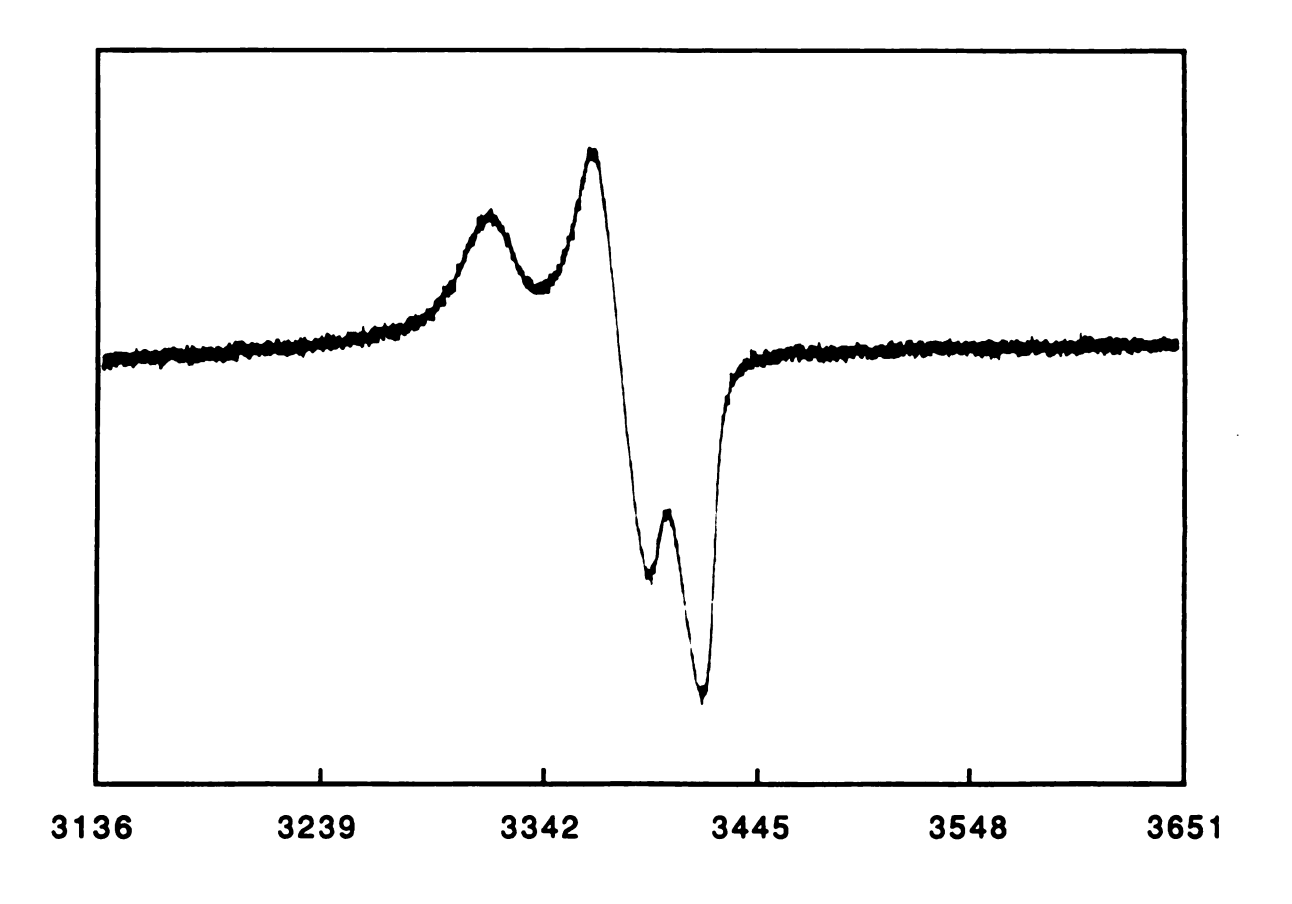


Figure 34

Figure 35. An X-band EPR spectrum (-150 °C) of a 2-MeTHF/CH $_3$ CN frozen solution containing 0.1 M TBAPF $_6$ of $Rh_2(O_2CCH_3)_3(TMPP-O)(MeOH).$



Field (Gauss)

Figure 35

Figure 36. Positive ion FABMS spectrum of $Rh_2(O_2CCH_3)_3(TMPP-2O)(NO)$.

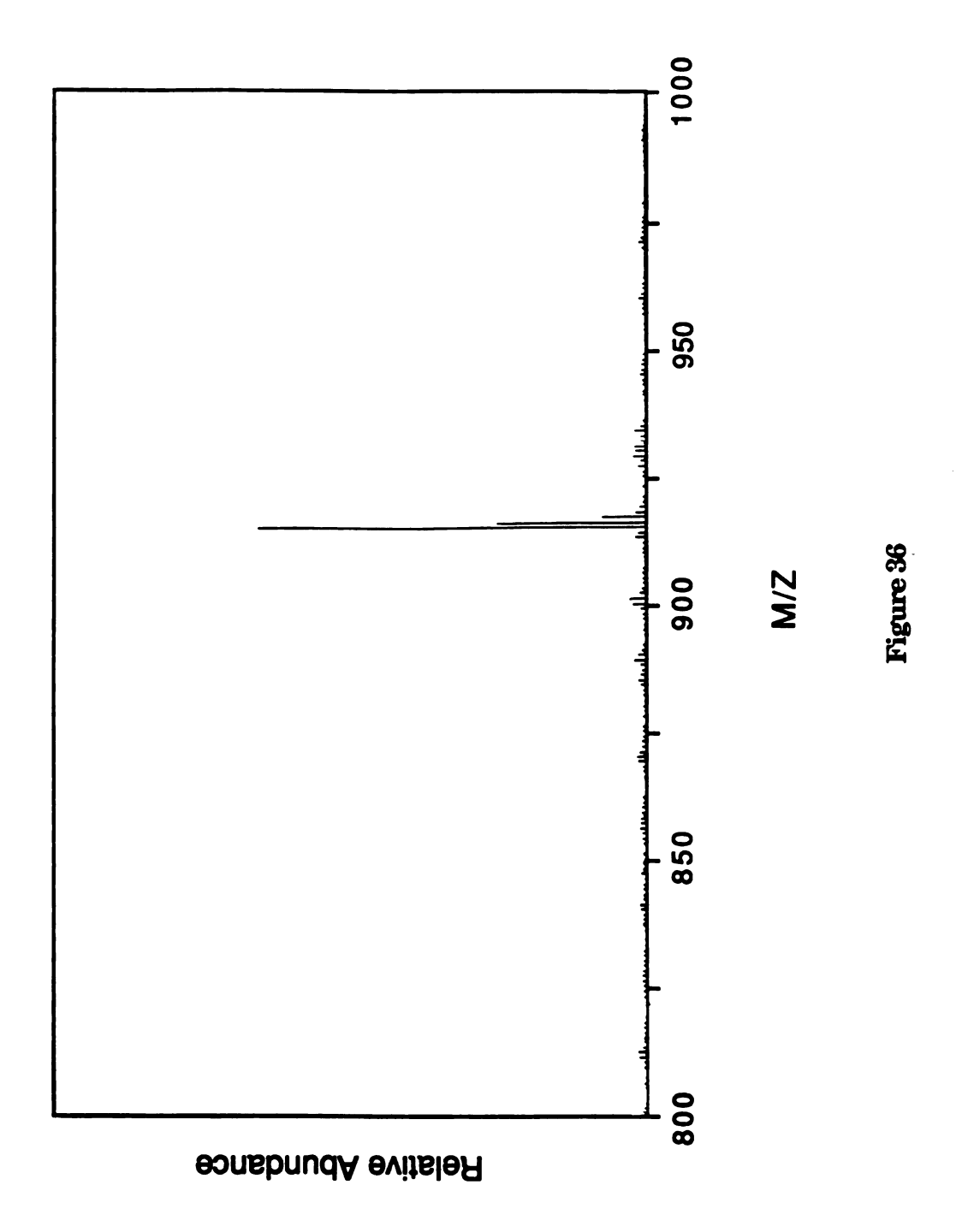


Figure 37. X-band EPR spectra in (a) the solid state and in (b) solution for $Rh_2(O_2CCH_3)_3(TMPP\text{-}2O)(NO).$

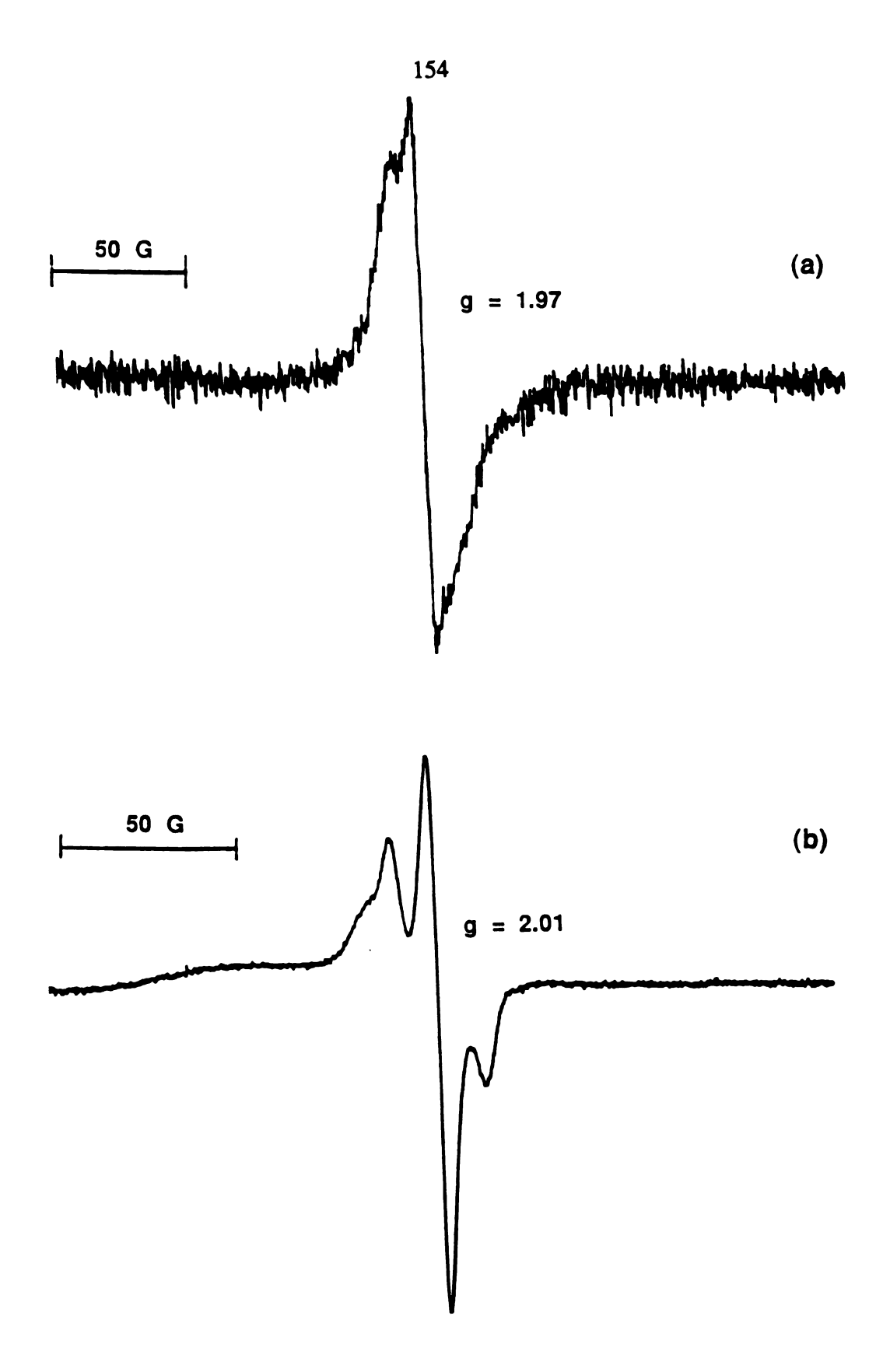


Figure 37

(2) Reaction of M₂(O₂CCF₃)₄ with TMPP

The low solubility of $M_2(O_2CCH_3)_4$ is a main drawback for the study of its reactivity toward a nucleophile. The solubility of metal complexes can be improved with use of fluorinated groups. The compound $M_2(O_2CCF_3)_4$ was synthesized by a carboxylate exchange of trifluoroacetate for the acetate ligands in $M_2(O_2CCH_3)_4$. The exchange reaction for $Mo_2(O_2CCF_3)_4$ is very facile, and is essentially complete after ca. 5 min of reflux. In direct contrast, the corresponding reaction of $Rh_2(O_2CCH_3)_4$ with CF_3COOH is stepwise and proceeds much slower; hence prolonged refluxing for one day is required for a complete exchange to give $Rh_2(O_2CCF_3)_4$.

A mixture of Mo₂(O₂CCF₃)₄ and TMPP in THF or acetone remained yellow after the solution was stirred for two hours at room temperature; however upon evacuation, the yellow solution gradually turned red, and a red product Mo₂(O₂CCF₃)₂(TMPP-O)₂ was isolated with extraction by using diethyl ether. The infrared spectrum of the red compound in Nujol shows the antisymmetric carboxylate stretch at 1650 cm⁻¹ which confirms the presence of the bridging acetate groups. Complicated solution behavior was revealed by ¹H and ¹⁹F NMR spectra. The 500 MHz ¹H NMR in CDCl₃ indicated a magnetically inequivalent environment for the three phenyl groups of the phosphine ligand (Figure 38); the meta proton region showed numerous multiplets at $\delta = 5.72$ (1H), 5.77 (1H), 5.83 (1H), 5.87 (1H), 5.92 (1H), 6.00 (3H), 6.08 (3H). The ortho and para methoxy groups displayed a complicated pattern in the region of 3.0-4.0 ppm. The ¹⁹F NMR spectrum in CDCl₃ indicated some association of free trifluoroacetate with the complexes (Figure 39). In the FABMS spectrum of the red compound, the highest observed peak was at m/z = 1452.8, in accordance with the molecular ion $[Mo_2(O_2CCF_3)_2(TMPP-O)_2]^+$ (Figure 40).

corresponding to the $[M-(CF_3COO)]^+$ fragment at m/z=1339.8 were also observed. According to the IR and NMR data, we propose the compound to be the bis-demethylated TMPP complex $Mo_2(O_2CCF_3)_2(TMPP-O)_2$. An electronic absorption spectrum (CH_3CN) shows λ_{max} values at 550 and 450 nm with the low energy absorption being assigned to the $\delta \to \delta^*$ transition normally observed at such energies for quadruply-bonded dimolybdenum complexes. Without a crystal structure determination, an exact geometric arrangement of ligands cannot be known, but it is logical to expect that the two bridging TMPP-O groups are situated in a trans orientation instead of cis based on steric considerations.

We postulated that a reasonable reaction pathway for the formation of Mo₂(O₂CCF₃)₂(TMPP-O)₂ is as shown in Figure 41. The first step of the reaction is expected to be axial coordination of both bulky phosphines, and in fact, the yellow color observed in the initial step supports this notion, as other bisphosphine adducts $Mo_2(O_2CCF_3)_4(L)_2$ (L = phosphine) are electronically similar [63(c)]. The step following axial ligation is believed to be an intramolecular transformation of the bis-axial phosphine adduct to a second isomer. With both phosphines in equatorial positions, there is a possibility for demethylation to give the volatile organic substrate CF₃COOMe. The trifluoroacetate dirhodium complex was also reacted with TMPP in an attempt to synthesize the dirhodium analogue of Mo₂(O₂CCF₃)₂(TMPP-O)₂. The reactions of Rh₂(O₂CCF₃)₄ with TMPP occurred under very mild conditions to give a green product which has been recrystallized from a mixture of hexane and CH₂Cl₂. The plate-like green crystal was investigated by a preliminary X-ray diffraction study which showed that the crystal was monoclinic with dimensions : a = 14.511 (9) Å, b = 23.63 (1) Å, c = 24.68 (1) Å, β = 99.52 (4) and V = 8350 (8) Å³.

Figure 38. A 300 MHz 1 H NMR spectrum of $Mo_{2}(O_{2}CCH_{3})_{2}(TMPP-O)_{2}$.

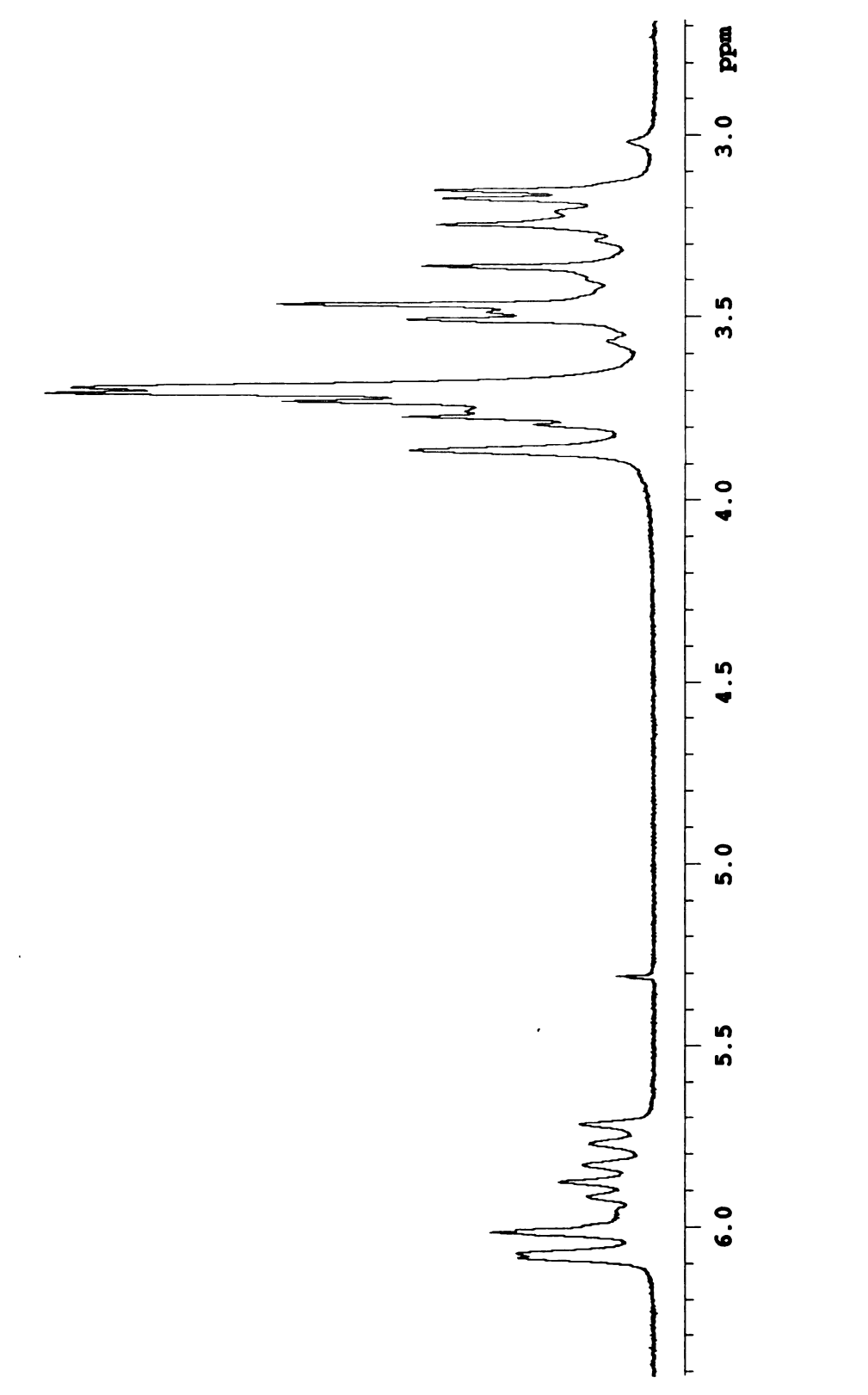


Figure 38

Figure 39. A 300 MHz 19 F NMR spectrum of $Mo_2(O_2CCH_3)_2(TMPP-O)_2$.

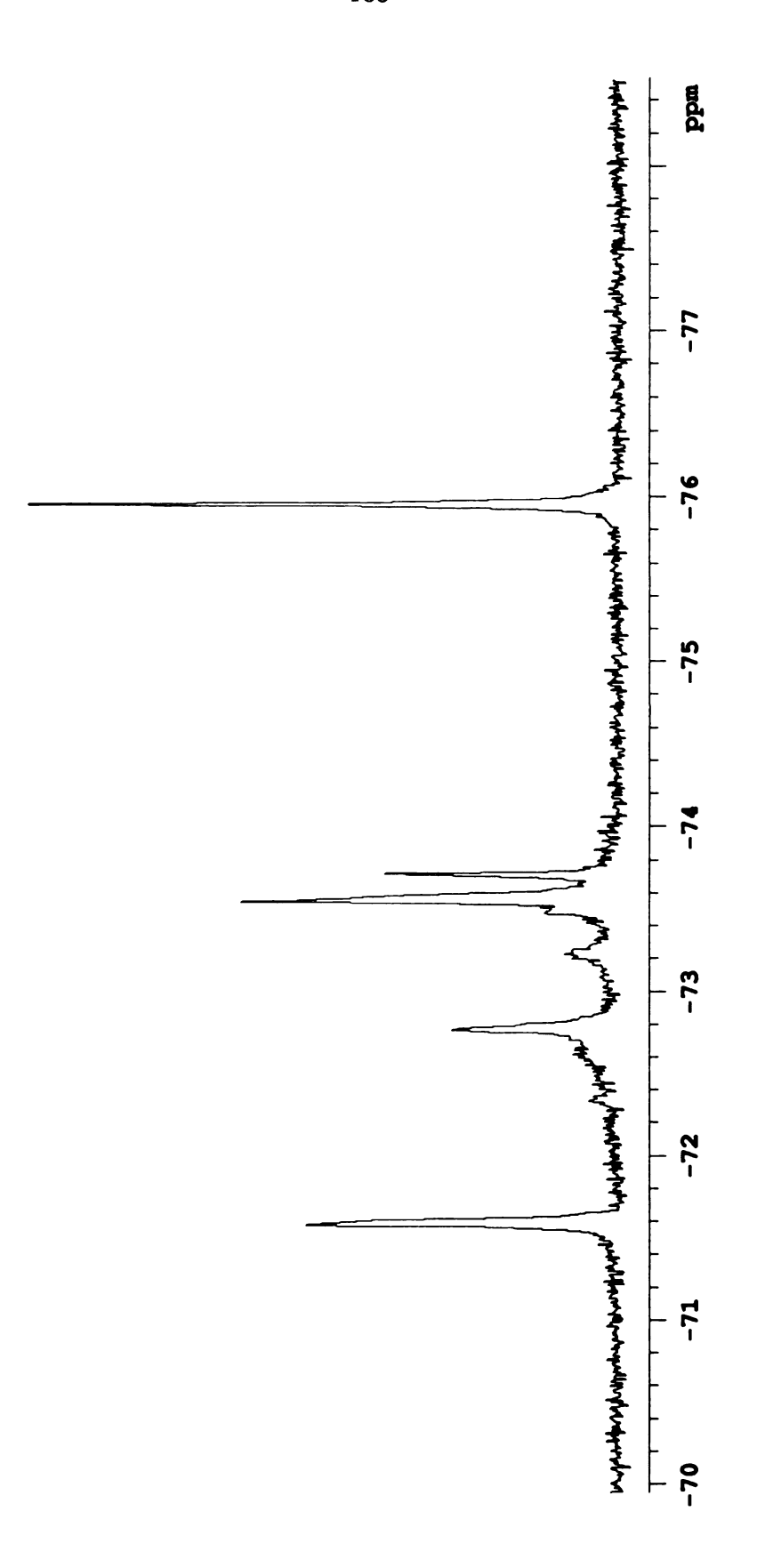
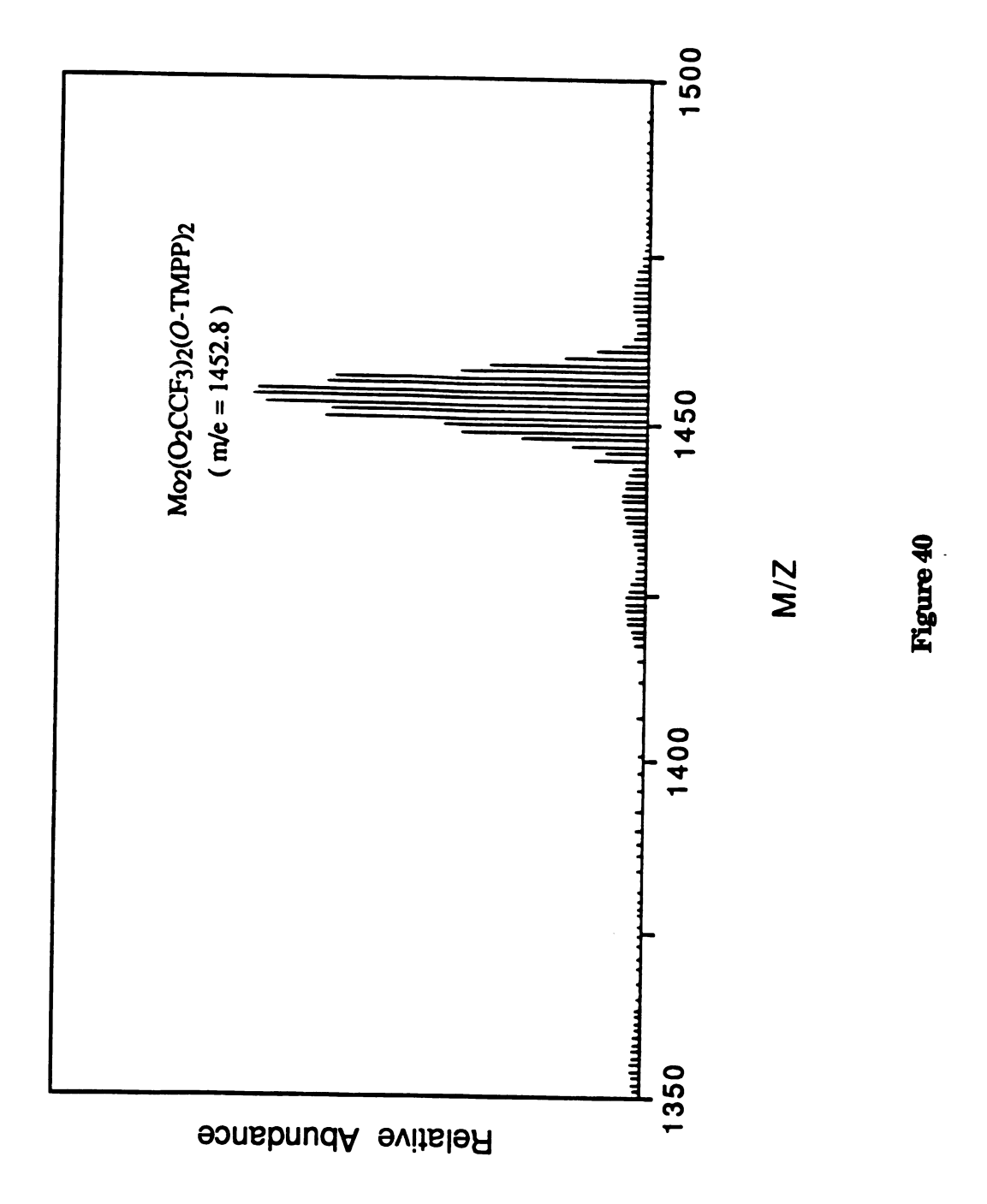


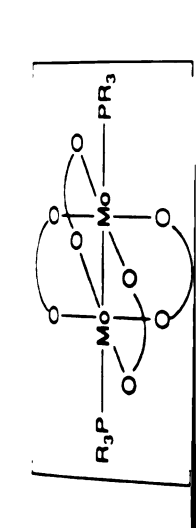
Figure 39

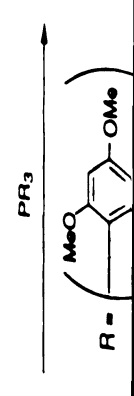
Figure 40. A positive ion FABMS spectrum of $Mo_2(O_2CCH_3)_2(TMPP-O)_2$.

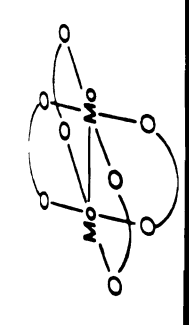


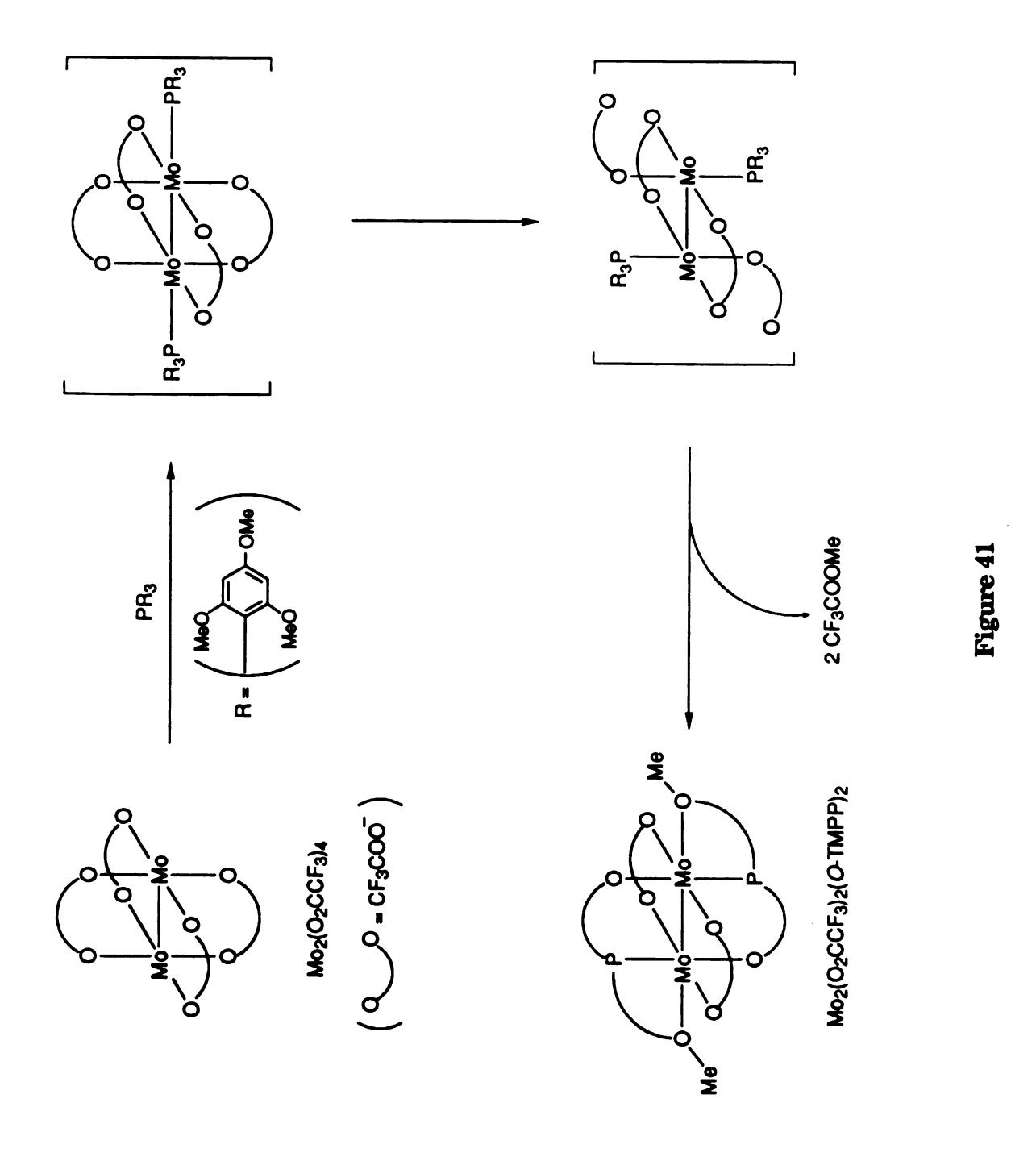
PP-0)2.

Figure 41. Schematic diagram of a proposed reaction scheme for the formation of $Mo_2(O_2CCH_3)_2(TMPP-O)_2$.









The cell volume corresponds well to a Z = 2 for molecules of $Rh_2(O_2CCF_3)_2(TMPP-O)_2$. These results suggest that reactions of TMPP with trifluoroacetate complexes such as $Rh_2(II,II)$ and $Mo_2(II,II)$ undergo ligand substitution reactions with to form stable doubly bridged-phenoxyphosphine metal complexes.

(3) Reaction of $[M_2(O_2CCH_3)_2(NCMe)_6](BF_4)_2$ (M = Mo and Rh) with TMPP

The synthesis of the solvated acetonitrile complexes $[M_2(O_2CCH_3)_2(NCMe)_6](BF_4)_2$ (M = Mo(II), Rh(II)) was carried out with the use of $[R_3O][BF_4]$ (R = Et or Me) as an esterification reagent.

The coordinated acetonitrile ligands result in a v(CN) shift to a higher energy (~2300 cm⁻¹) compared to free acetonitrile (v(CN) ~ 2260 cm⁻¹) which is in agreement with the σ -donating character of the nitrogen atom. The weak coordination ability of the acetonitrile ligands renders them easily displaced by strong nucleophiles. In agreement with this is a ¹H NMR study that has shown that both axial and equatorial acetonitrile ligands in [Mo₂(O₂CCH₃)₂(NCMe)₆](BF₄)₂ freely exchange with coordinated solvent . Corresponding reactions of [Mo₂(O₂CCH₃)₂(NCMe)₆](BF₄)₂ with TMPP in MeCN gave a red-purple product with a large amount of unidentified methylphosphonium salt [CH₃TMPP]⁺ observed by ¹H NMR spectroscopy.

Reactions of [Rh₂(O₂CCH₃)₂(NCMe)₆](BF₄)₂ with TMPP carried out in various solvents (THF, MeCN, MeOH) produced a similar result, yielding a green product along with a large amount of a methylphosphonium salt [CH₃TMPP]⁺ as judged by ¹H NMR spectroscopy.

(4) Reaction of [Mo₂(NCMe)₁₀](BF₄)₄with TMPP

The fully solvated dinuclear complexes $[M_2(NCMe)_{10}](BF_4)_4$ (M = Rh(II), Mo(II)) have been discovered recently. The reaction of TMPP with the fully solvated dirhodium compound led to a facile metal-metal bond cleavage to give a mononuclear complex $[Rh(TMPP)_2](BF_4)_2$. The reaction of $[Mo_2(NCMe)_{10}](BF_4)_4$ with TMPP turned brown immediately with MeOH as the solvent, suggesting a Mo/oxo species is being formed. Without the support of bridging ligands in the complex, a metal-metal bond cleavage reaction as was found in $[Rh_2(NCMe)_{10}](BF_4)_4$ also must be considered. If so, a paramagnetic Mo(II) mononuclear complex would form, and indeed, a green product that was isolated from the reaction performed in CH₃CN was shown to be paramagnetic by 1 H NMR spectroscopy.

4. SUMMARY

The aforementioned work resulted in the isolation of the unusual dirhodium compound $Rh_2(O_2CCH_3)_3(TMPP-O)(MeOH)$. The identity of the compound was confirmed by an X-ray diffraction study which revealed that the molecule consists of a dirhodium unit bridged by three acetate ligands and one demethylated TMPP ligand that forms two separate metallacycle rings with the rhodium atoms. In this arrangement, the phosphorus atom occupies an equatorial position, and one methoxy group in the ortho position has demethylated to form an alkoxide group. Similar reactions to yield bis-demethylated TMPP complexes are also observed in the chemistry of $M_2(O_2CCF_3)_4$ (M = Mo, Rh) with TMPP.

CHAPTER V

REACTIONS OF TRIS(2,4,6-TRIMETHOXYPHENYL)PHOSPHINE WITH TRINUCLEAR CARBONYL CLUSTERS

1. Introduction

Chemistry of metal carbonyl clusters complexes has received much attention in inorganic chemistry [73], and major developments are still emerging in this field. Many of these clusters have been found to act as good catalytic precursors in a great variety of industrial processes, thus their use as homogeneous catalysts has been an active area of research for many years. The clusters under investigation for homogeneous catalysis generally consist of multinuclear metal centers surrounded by carbonyls and ancillary ligands, with the crucial role of the secondary groups being to modify the steric and electronic environment of the active species. Along this line, a central theme of organometallic chemistry is to design ligands, especially multifunctionalized ligands, and use their versatile coordination abilities to influence the activity, selectivity and stability of catalytic systems.

Traditional organometallic chemistry has developed largely through the use of soft π -acceptor ligands such as carbon monoxide, tertiary phosphines, π -olefins, and cyclopentadiene ligands. The use of ancillary hard π -donor ligands such as oxo, imido and alkoxo ligands has only recently attracted attention. It is now well established that polynuclear metal carbonyl complexes may be attached to metal oxide supports with retention of the essential framework of the metal cluster, and in certain cases, catalytic activity of the supported cluster has been observed. For instance, it has been shown that the oxygen-bound triosmium cluster is an efficient catalyst for the hydrogenation of ethylene. Furthermore, the surface oxygen atoms are capable of functioning as either one or three electron donors, with interconversions occurring between these two

different coordination modes. One example of this process from a recent literature report is shown below [88].

In our earlier studies of the reactivity of tris(2,4,6-trimethoxyphenyl)phosphine, we demonstrated that TMPP exhibits a wide variety of bonding modes with various mononuclear and dinuclear metal complexes. Based on this framework of knowledge, we endeavored to extend our research to higher nuclearity systems, namely trinuclear carbonyl clusters. Chemistry of phosphines with trinuclear carbonyl clusters has been well explored, especially in Group 8 metal systems [74-76]. Since the tertiary phosphine TMPP is very basic, high reactivity toward metal carbonyl clusters is therefore expected. We postulated that the functionalized nature of the phosphine with its hard and soft donors would provide a promising opportunity for facilitating cluster transformations in multinuclear complexes.

2. E

A. S

 $0s_3($ are

prep

by K

(1) F

clear redis

mmo

unde

be u

band

a red Vello

ident

Fe₁P₂

=3 H

4.26 I

Was s

THE

2. Experimental

A. Synthesis

The syntheses of $Ru_3(CO)_{11}(NCMe)$, $Ru_3(CO)_{10}(NCMe)_2$, $Os_3(CO)_{11}(NCMe)$, and $Os_3(CO)_{10}(NCMe)_2$ described in the following section are modifications of those reported by Johnson and Lewis [77]. The preparation of $(\mu$ -H)₂Os₃(CO)₁₀ is a modified version of the literature report by Kaesz [78].

(1) Reaction of Fe₃(CO)₁₂ with TMPP

A solution of $Fe_3(CO)_{12}$ (0.100 g, 0.198 mmol) and TMPP (0.211 g, 0.397 mmol) in THF (20 mL) was stirred at room temperature for 12 h to give a clear red solution. After the solvent was removed, the red residue was redissolved in THF (ca. 3 mL) and chromatographed on a silica gel column under argon. Three bands were observed; the first green band was found to be unreacted starting material Fe₃(CO)₁₂; this was followed by a yellow band which was collected with THF/hexane (1:3, v/v) as the eluent. Finally, a red product was eluted with THF/hexane (1:1, v/v). The TMPP-containing yellow product was investigated by various spectroscopic methods, and identified to be the mononuclear cluster Fe(CO)₅(TMPP). Anal. Calcd for $Fe_1P_1O_{14}C_{32}H_{33}$: C, 52.76; H, 4.57. Found: C, 53.04; H, 4.75. IR (THF): v(CO)= 2023 (s), 1934 (s), 1916 (vs), 1940 (s) cm⁻¹. 1 H NMR (CDCl₃): δ = 6.03 (d, J_{HP} = 3 Hz, m-H), 3.78 (s, p-OMe), 3.48 (s, o-OMe). ³¹P (¹H) NMR (CDCl₃): δ = 4.26 ppm. FABMS spectrum: parent ion, m/z = 728 (⁵⁶Fe). The red product was structurally characterized to be the salt [HFe₃(CO)₁₁][HTMPP]. IR (THF): ν (CO) = 1998 (vs), 1974 (s), 1952 (w), 1940 (w), 1748 (w). ¹H NMR

((

(2

sl

(1: m

TO:

20

m] so]

sol

(3)

(10 sol

ins red

abs 配上

con

(CD)

 Ru_{3}

(CDCl₃, -50 °C): $\delta = 6.08$ (d, $J_{HP} = 3$ Hz, m-H), 3.86 (s, p-OMe), 3.69 (s, o-OMe).

(2) Preparation of Ru₃(CO)₁₁(NCMe)

A solution of Me_3NO (0.017 g, 0.220 mmol) in CH_3CN (10 mL) was slowly added to a suspension of $Ru_3(CO)_{12}$ (0.072 g, 0.110 mmol) in CH_2Cl_2 (100 mL) and CH_3CN (10 mL) at r.t.. The progress of the reaction was monitored by infrared spectroscopy, and stopped after 5 h of stirring at room temperature according to the disappearance of the v(CO) stretch at 2060 cm⁻¹ due to $Ru_3(CO)_{12}$. The solvent was then removed *in vacuo* to ca. 5 mL, filtered through a silica gel column, and eluted with CH_3CN . The solvent was removed under reduced pressure, leaving behind an orange solid; yield $\approx 80\%$. IR (cyclohexane): v(CO) = 2045(s), 2037(s), 2021(m), 2001(s) and 1994(s) cm⁻¹.

(3) Reaction of Ru₃(CO)₁₁(NCMe) with TMPP

A yellow solution of $Ru_3(CO)_{11}(NCMe)$ (0.100 g, 0.142 mmol) in THF (10 mL) was placed in a 100-mL Schlenk flask and treated with a THF solution (10 mL) of TMPP (0.121 g, 0.142 mmol) whereupon an instantaneous reaction occurred as evidenced by the formation of a clear red solution. The infrared spectrum of the reaction solution revealed the absence of a bridging v(CO) band. The solvent was removed in vacuo to ca. 5 mL, and a red solid precipitated out after hexane was added to the concentrated solution. The red compound was characterized by ¹H NMR (CDCl₃): $\delta = 6.03$ (d, $J_{HP} = 3$ Hz, m-H), 3.78 (s, p-OMe), 3.48 (s, o-OMe) which indicated the product was a monodentate TMPP product, formulated as $Ru_3(CO)_{11}(TMPP)$ derived from a ligand substitution of TMPP for a labile

Cl an

sta

TI

wl P{

(4)

an -78

ha rer

ten

bri bri

bro

drie solu

the v(C

(5)]

(10)

THE

CH₃CN ligand. The red product is quite thermally unstable both in solution and in the solid state, and decomposed to an orange solution in THF after standing overnight at room temperature. Separation of the resulting mixture of transformed products by column chromatography with THF/hexane (1/2) as an eluent led to an isolation of a stable orange product which was characterized to be $Ru_3(\mu\text{-CO})_2(CO)_6[\mu_3-\eta^2\text{-C}_6H_2(OMe)_3][\mu\text{-P}(C_6H_2(OMe)_3)_2]$ based on an X-ray crystallographic study.

(4) Preparation of Ru₃(CO)₁₀(NCMe)₂

A suspension of $Ru_3(CO)_{12}$ (0.100 g, 0.156 mmol) in CH_2Cl_2 (100 mL) and CH_3CN (10 mL) was stirred and chilled in a dry ice/acetone bath at $-78^{\circ}C$. After a solution of Me_3NO (0.030 g, 0.32 mmol) in CH_3CN (10 mL) had been added to the stirred suspension, the dry ice/acetone bath was removed, and the reaction mixture was slowly warmed to room temperature. This was accompanied by a color change from orange to bright yellow. The solvent was then removed in vacuo to ca. 3 mL, and a bright yellow solid precipitated from a yellow-brown solution. After the brownish-yellow solution was decanted off, the bright yellow solid was dried in vacuo for ca. 30 min. (Note: Prolonged stirring of the reaction solution at room temperature for several hours results in decomposition of the yellow compound to an uncharacterized brown product.) IR (THF): v(CO) = 2055(sh), 2018(vs), 1999(s), 1987(sh) and 1954(m) cm⁻¹.

(5) Reaction of Ru₃(CO)₁₀(NCMe)₂ with TMPP

A yellow solution of $Ru_3(CO)_{10}(NCMe)_2$ (0.100 g, 0.148 mmol) in THF (10 mL) was prepared in a 100-mL Schlenk flask, and then treated with a THF solution (10 mL) of TMPP (0.136 g, 0.148 mmol). The solvent was then

re by

an

CT

Rı

sp

cm

(6)

ref hyd

sol

the

res

(≈ 8

(7)

nl An

clea

out

v/v) plat

iden

metl

removed in vacuo to ca. 5 mL, and chromatographed on a silica gel column by elution with THF/hexane (1:5; v/v). A major orange band was collected and recrystallized from THF/hexane at r.t. to give thin plate-like orange crystals after 2 days. A crystallographic study revealed the compound to be $Ru_3(\mu-CO)_2(CO)_6[\mu_3-\eta^2-C_6H_2(OMe)_3][\mu-P\{C_6H_2(OMe)_3\}_2]$. The infrared spectrum of the product exhibits bridging v(CO) bands at 1807 and 1866 cm⁻¹.

(6) Preparation of $(\mu-H)_2Os_3(CO)_{10}$

A suspension of $Os_3(CO)_{12}$ (1.0 g, 1.10 mmol) in 200 mL of toluene was refluxed for 6 h in a 500-mL three-necked round-bottom flask while hydrogen gas was continuously bubbled through the solution. As the yellow solution turned purple, the reaction was monitored by TLC with hexane as the eluent. The solvent was removed on a rotary evaporator, and the resulting purple solid was recrystallized from hexane; yield = 0.77 g (\approx 82%).

(7) Reaction of $(\mu-H)_2Os_3(CO)_{10}$ with TMPP

A purple solution of $(\mu\text{-H})_2\text{Os}_3(\text{CO})_{10}$ (0.100 g, 0.117 mmol) in THF (10 mL) was added to a solution of TMPP (0.06 g, 0.117 mmol) in THF (10 mL). An instantaneous reaction occurred as evidenced by the formation of a clear yellow solution. After removal of the solvent, purification was carried out by preparative thin layer chromography by using hexane/acetone (10:1, v/v) as the liquid phase. A yellow band was collected, removed from the plate and extracted with hexane to give a yellow solution. The product was identified as $Os_3(\mu\text{-H})(H)(CO)_{10}(TMPP)$ based on various spectroscopic methods of characterization as well as by comparison to a series of related

compounds [87]; yield = 0.15g (\approx 90%). FABMS spectrum: parent ion, m/z = 1385 (192 Os).

(8) Preparation of Os₃(CO)₁₁(NCMe)

A solution of Me₃NO (0.017 g, 0.220 mmol) in CH₃CN (10 mL) was slowly added to a suspension of Os₃(CO)₁₂ (0.100 g, 0.110 mmol) in CH₂Cl₂ (100 mL) and CH₃CN (10 mL) at r.t. The progress of the reaction was monitored by infrared spectroscopy, and stopped after ca. 5 h stirring at room temperature according to the disappearance of the v(CO) stretch at 2068 cm⁻¹ due to Os₃(CO)₁₂. The solvent was then removed *in vacuo* to ca. 5 mL, and filtered through a silica gel column and eluted with CH₃CN. The solvent was removed under reduced pressure, leaving behind a yellow solid; yield = 0.082 g (\approx 80%). IR (CH₂Cl₂): v(CO) = 2107 (sh), 2054 (vs), 2040 (vs), 2017 (s, sh), 2008 (vs) and 1981 (m) cm⁻¹.

(9) Reaction of Os₃(CO)₁₁(NCMe) with TMPP

A light yellow solution of $Os_3(CO)_{11}(NCMe)$ (0.100 g, 0.105 mmol) in THF (10 mL) was prepared in a 100-mL Schlenk flask, and then treated with a THF solution (10 mL) of TMPP (0.068 g, 0.105 mmol) whereupon an instantaneous reaction occurred as evidenced by the formation of an orange solution. The reaction mixture was evaporated to dryness *in vacuo*, the residue was redissolved in 20 mL of THF/hexanes (1:4; v/v) and concentracted until an orange precipitate began to form. The reaction mixture was cooled to ca. -10 °C to effect complete crystallization of the orange complex, which was isolated by removing the supernatant by cannula into another flask. The orange solid was washed with hexanes (20 mL), and then dried *in vacuo* for 2 h; yield = 0.122 g (\approx 82%). FABMS

spectrum: parent ion, m/z = 1411 corresponding to $Os_3P_1C_{37}O_{19}H_{35}$, and a lower mass peak at m/z = 1385 due to $[M-CO]^+$.

(10) Preparation of $Os_3(CO)_{10}(NCMe)_2$

A suspension of $Os_3(CO)_{12}$ (0.100 g, 0.110 mmol) in CH_2Cl_2 (100 mL) and CH_3CN (10 mL) was stirred and kept in a dry ice/acetone bath (-78°C). A solution of Me_3NO (0.0017 g, 0.220 mmol) in CH_3CN (10 mL) was slowly added to the stirred suspension, while the reaction mixture was slowly warmed to room temperature. The reaction was monitored by infrared spectroscopy, and stopped after ca. 5 h of stirring at room temperature on the basis of the disappearance of the v(CO) stretches at 2054 and 2040 cm⁻¹ due to $Os_3(CO)_{11}(NCMe)$. The solvent was then removed in vacuo to ca. 5 mL, filtered through a silica gel column, and eluted with CH_3CN . A bright yellow band was collected, and the solvent was removed to give a yellow solid; yield = 0.084 g (\approx 80%). IR (CH_3CN): v(CO) = 2021 (vs), 1983 (s) 1959 (m) cm⁻¹.

(11) Reaction of Os₃(CO)₁₀(NCMe)₂ with TMPP

A yellow solution of $Os_3(CO)_{10}(NCMe)_2$ (0.100 g, 0.095 mmol) in THF (10 mL) was prepared in a 100-mL Schlenk flask, and then treated with a THF solution (10 mL) of TMPP (0.0525 g, 0.095 mmol). The progress of the subsequent reaction was periodically monitored by infrared spectroscopy, the diminishing of the starting material v(CO) at 2021 cm⁻¹ occurring with the concomitant appearance of a new band at v(CO) = 2005 cm⁻¹. The reaction mixture was evaporated to a small volume (5 mL), and then chromatographed on a silica gel column with THF/hexane (1:2, v/v) as an eluent. An orange band was collected, and recrystallized from

CH₂Cl₂/hexane at r.t. to give yellow crystals after two days. A yellow crystal was structurally characterized to be $Os_3(\mu-OH)(CO)_9(\mu-\eta^2-TMPP-O)$.

B. X-ray Crystal Structure

(1) $[HFe_3(CO)_{11}][HTMPP]$

(i) Data Collection and Reduction

A red crystal with approximate dimensions of 0.30 x 0.05 x 0.16 mm³ was mounted on a glass fiber. All measurements were made on a Nicolet P3/F diffractometer with graphite monochromated MoKa radiation and a low temperature device. A rotation photograph was used to locate 16 reflections from which a preliminary cell was indexed. Accurate cell constants and an orientation matrix for data collection, obtained from a least-squares refinement using the setting angles of 25 reflections in the range of $20 \le 20 \le 25^{\circ}$ corresponded to a triclinic cell with dimensions : a = 8.342(5) Å, b = 16.43(1) Å, c = 17.36(1) Å and V = 2149(3) Å³. The data were collected at $-110 \pm 2^{\circ}$ C by using an ω -20 scan mode in a range of $4 \le 20 \le 45^{\circ}$ with a scan speed 4° min⁻¹. Three standard reflections collected at constant intervals. Although no significant decrease in intensity was observed, a decay correction (program CHORT) was applied. The linear absorption coefficient for MoKa was 11.366 cm⁻¹. An absorption correction (program DIFABS) was applied. The data were corrected for Lorentz and polarization effects.

(ii) Structure Solution and Refinement

All calculations were performed on a VAX 11/750 computer using the program from SDP/VAX. The structure was solved by direct methods using the program MULTAN to give the positions of the heavy atoms. The remaining non-hydrogen atoms were located by a sequence of successive difference Fourier maps and least–squares cycles which led to full development of the coordination sphere. The final cycle of full–matrix least–squares refinement involved 554 variable parameters and 3581 observed reflections with $F_o^2 > 3\sigma(F_o^2)$. The refinement converged with residuals of R = 0.0551 and $R_w = 0.0633$.

(2) $Ru_3(\mu-CO)_2(CO)_6[\mu_3-\eta^2-C_6H_2(OMe)_3][\mu-P\{C_6H_2(OMe)_3\}_2]$

(i) Data Collection and Reduction

A plate-like red crystal with approximate dimensions of $0.05 \times 0.15 \times 0.08 \text{ mm}^3$ was mounted on the end of a glass fiber and covered with epoxy cement. Geometric and intensity data were collected on a Nicolet P3/F diffractometer with graphite-monochromated MoK α radiation and a low temperature device. The crystal was indexed on 25 intense reflections in the range of $20 \le 20 \le 25^{\circ}$ which gave a triclinic cell with dimensions : a = 11.209 (7) Å, b = 15.60 (1) Å, c = 24.73 (2) Å and V = 4244 (6) Å³. The symmetry and lattice dimensions were verified by axial photography. Least-square analysis was used to refine the cell dimensions and the orientation matrix.

The intensity data, gathered by the ω -20 scan technique at -110 \pm 2° C, were reduced by routine procedures. Absorption corrections were applied, based on azimuthal scans of three reflections with diffractometer angle χ near 90°. The linear absorption coefficient for MoK α was 11.366 cm⁻

1. An absorption correction (program DIFABS) was applied. The data were corrected for Lorentz and polarization effects.

(ii) Structure Solution and Refinement

Crystallographic computing was performed on a VAX-11/750 computer with programs from the Enraf-Nonius SDP package. The six unique ruthenium atoms in the structure were located from a Patterson map. The subsequent development of the coordination spheres of the two separate triruthenium molecules was routine. All non-hydrogen atoms were located with an alternating sequence of least-squares refinements and difference Fourier maps. The refinement was completed in two units, with each unit comprising one of the crystallographically independent molecules. The final cycle of full-matrix least-squares refinement converged with residuals of R=0.0759 and $R_{\rm w}=0.084$.

(3) $Os_2(\mu\text{-OH})_2(CO)_9(TMPP)$

(i) Data Collection and Reduction

A yellow crystal with approximate dimensions of 0.10 x 0.08 x 0.15 mm³ was mounted on the end of a glass fiber. All measurements were made on a Nicolet P3/F diffractometer with graphite-monochromated MoK α radiation and a low temperature device. A rotation photograph was used to locate 16 reflections from which a preliminary cell was indexed. Accurate cell constants and an orientation matrix for data collection, obtained from a least-squares refinement using the setting angles of 25 reflections in the range of $20 \le 20 \le 25^{\circ}$ corresponded to a triclinic cell with dimensions: a = 11.435 (5) Å, b = 13.079 (8) Å, c = 14.116 (9) Å and V = 2085

(2) Å³. The data were collected using a ω -2 θ scan mode in the range of $4 \le 2\theta \le 40^{\circ}$ with a scan speed 3° min⁻¹. The diameter of the incident beam collimator was 1.5 mm. Three standard reflections were measured at constant intervals with no observable decay. The linear absorption coefficient for MoK α was 92.491 cm⁻¹. An empirical absorption correction, based on azimuthal scans of three reflections with χ near 90°, was applied. The data were corrected for Lorentz and polarization effects.

(ii) Structure Solution and Refinement

All calculations were performed on a VAXSTATION 2000 computer using the programs from SDP. The heavy atoms were located by direct methods (MULTAN) a sequence of difference Fourier maps and least-squares cycles resulted in the location of all non-hydrogen atoms. The final cycle of full-matrix least-squares refinement involved 241 variable parameters and 2806 reflections with $F_o^2 > 3\sigma(F_o^2)$. The refinement converged with residuals of R = 0.038 and $R_w = 0.046$.

(4) $Os_3(\mu\text{-OH})(CO)_9(\mu\text{-}\eta^2\text{-TMPP-}O)$

(i) Data Collection and Reduction

A yellow crystal with approximate dimensions of $0.45 \times 0.30 \times 0.08$ mm³ was mounted on the end of a glass fiber. All measurements were made on a Nicolet P3/F diffractometer upgraded to a Siemens P3/V with graphite monochromated CuK α radiation and a low temperature device. A rotation photograph was applied to locate 16 reflections from which a preliminary cell was indexed. Accurate cell constants and an orientation matrix for data collection, obtained from a least-squares refinement using

tl a

1

SC in

al aŗ

li

T

(ii

re F₀

inv 3σ

0.0

3.]

(I)

A s

nuc] A ye

the setting angles of 25 reflections in the range $20 \le 20 \le 25^{\circ}$ corresponded to an monoclinic cell with dimensions: a = 16.088 (2) Å, b = 13.108 (2) Å, c = 19.601 (2) Å and V = 4133.5 (9) Å³. The data were collected using a ω -20 scan mode in the range $4 \le 20 \le 106^{\circ}$ with a variable scan speed of 3° min⁻¹ (in omega). The diameter of the incident beam collimator was 1.5 mm. The linear absorption coefficient for CuK α was 180.610 cm⁻¹. An empirical absorption correction, based on azimuthal scans of three reflections, was applied which resulted in transmission factors ranging from 1.00 to 0.0988. The data were corrected for Lorentz and polarization effects.

(ii) Structure Solution and Refinement

The three osmium atoms were located by direct methods, and the remaining non-hydrogen atoms were located by subsequent difference Fourier maps. The final cycle of full-matrix least-squares refinement involved 253 variable parameters and 2980 observed reflections with $F_o^2 > 3\sigma(F_o^2)$. The refinement converged with residuals of R = 0.089 and $R_w = 0.061$.

3. Results and Discussion

(I) Triiron carbonyl clusters with TMPP

A. Synthesis and Characterization

Our investigation of the reaction between $Fe_3(CO)_{12}$ and the highly nucleophilic phosphine TMPP led to the isolation of two TMPP derivatives. A yellow compound was identified as $Fe(CO)_5(TMPP)$ based on the evidence

from several methods of characterization including an elemental analysis (Anal. Calcd. C: 52.76 %, H: 4.57 %; Found: 53.04 %, H: 4.75 %). A FABMS spectrum of the compound revealed the highest mass peak at m/z = 726 (⁵⁶Fe) which is in close agreement with an analysis of isotope distributions for $Fe(CO)_5(TMPP)$ (m/z = 728, (⁵⁶Fe)). Some structural information was afforded by the ¹H NMR spectrum which indicated a symmetrical magnetic environment for the three phenyl groups of the phosphine ligand, as evidenced by the presence of only three resonances corresponding to the ortho and the para methoxy groups; $\delta = 6.03$ (d) (d, $J_{HP} = 3$ Hz, m-H), 3.78 (s, p-OMe), 3.48 (s, o-OMe) ppm. ³¹P{¹H} NMR spectroscopy showed a singlet for the product at $\delta = 4.26$ ppm with a downfield shift from free TMPP which occurs at $\delta = -68$ ppm. Recrystallization of the yellow compound from a mixture of hexane and THF yielded yellow crystals whose preliminary cell revealed the crystal system to be triclinic with dimensions : a = 15.27 (1) Å, b = 16.09 (1) Å, c = 13.45 (1) Å, α = 90.34 (7), β = 99.52 (4), γ = 96.78 (7) and V = 3241 (4) Å³; no further data collection was carried out due to severe twinning problems with the crystals.

The second product isolated from the reaction and purified by column chromatography is the red salt [HTMPP][HFe₃(CO)₁₁] characterized by an X-ray diffraction study as well as by solution spectroscopy. The hydride resonance of [HFe₃(CO)₁₁]⁻, located at $\delta = -15.8$ ppm, is close to the values for other [HFe₃(CO)₁₁]⁻ salts reported in the literature. The chemistry of metal carbonyl anions is of special interest in part because they have been discovered to promote hydride migration in the formation of stable metal formyl complexes. This finding has prompted a number of research groups to investigate the reactivity of metal carbonyl hydrides with various Lewis acids [79]. The extent of ion-pairing in salts of metal carbonyl

si p ca h tŀ tŀ bı pa aı W de pa io fu CO

h

R

ar

lię

43

hydrides has been correlated to the reactivity of these species. In general, a site on the anion that interacts with the cation is dependent on the charge polarization in the molecule. For example, the interaction of mononuclear carbonyl hydride complexes with Lewis acids usually occurs through the hydride ligands with the degree of interaction depending on the extent of the hydride basicity. On the other hand, in metal cluster anions such as [HFe₃(CO)₁₁]⁻, the more basic center is a bridging CO group that dominates the ion-pairing interaction. It has been demonstrated that the v(CO) of the bridging CO group provides a characteristic feature for the study of the ion pair interactions in these cluster anions [80-81]. The "free" [HFe₃(CO)₁₁] anion exhibits a v(CO) at ca. 1740 cm⁻¹, but an interaction of $[HFe_3(CO)_{11}]^$ with the counter-cation results in a v(CO) shift to lower energies, with the degree of the shift significantly depending on the strength of the ion-In our particular study, the v(CO) for the pairing interaction. [HFe₃(CO)₁₁] anion occurrs at 1780 cm⁻¹ (Figure 42), indicating there is no ion-pairing interaction present in the salt [HTMPP][HFe₃(CO)₁₁]; this was further confirmed in the solid state by a crystallographic study. A comparsion of several [HFe₃(CO)₁₁] salts with various extents of cation anion interactions represented by the different absorptions of bridging CO ligands is given in Table 13.

B. Molecular Stucture

A molecular structure of [HTMPP][HFe₃(CO)₁₁] is shown in Figure 43, and a stereoview of the salt is shown in Figure 44. Crystallographic

Table 13. Bridging carbonyl stretches of various $[HFe_3(CO)_{11}]^-$ salts.

	solid	CHCl ₃	C_6H_6	THF	CH ₃ CN
[H ₂ Et ₂ N]	1550	1656	1640	1745	1725
$[\mathrm{H_2}(n\mathrm{-Bu})_2\mathrm{N}]$	1550		1641	1745	
$[\mathrm{H_2}(i\text{-}\mathrm{Pr})_2\mathrm{N}]$	1650	1665	1645	1745	1725
[HEt ₃ N]	1660	1640	1642		
PPN	1720				
TMPP	1740			1748	

Figure 42. Infrared spectrum in the v(CO) region for $[HTMPP][HFe_3(CO)_{11}]. \ \ The \ v(CO) \ \ stretch \ \ at \ 1748 \ cm^{-1} \ is \ a$ bridging mode.

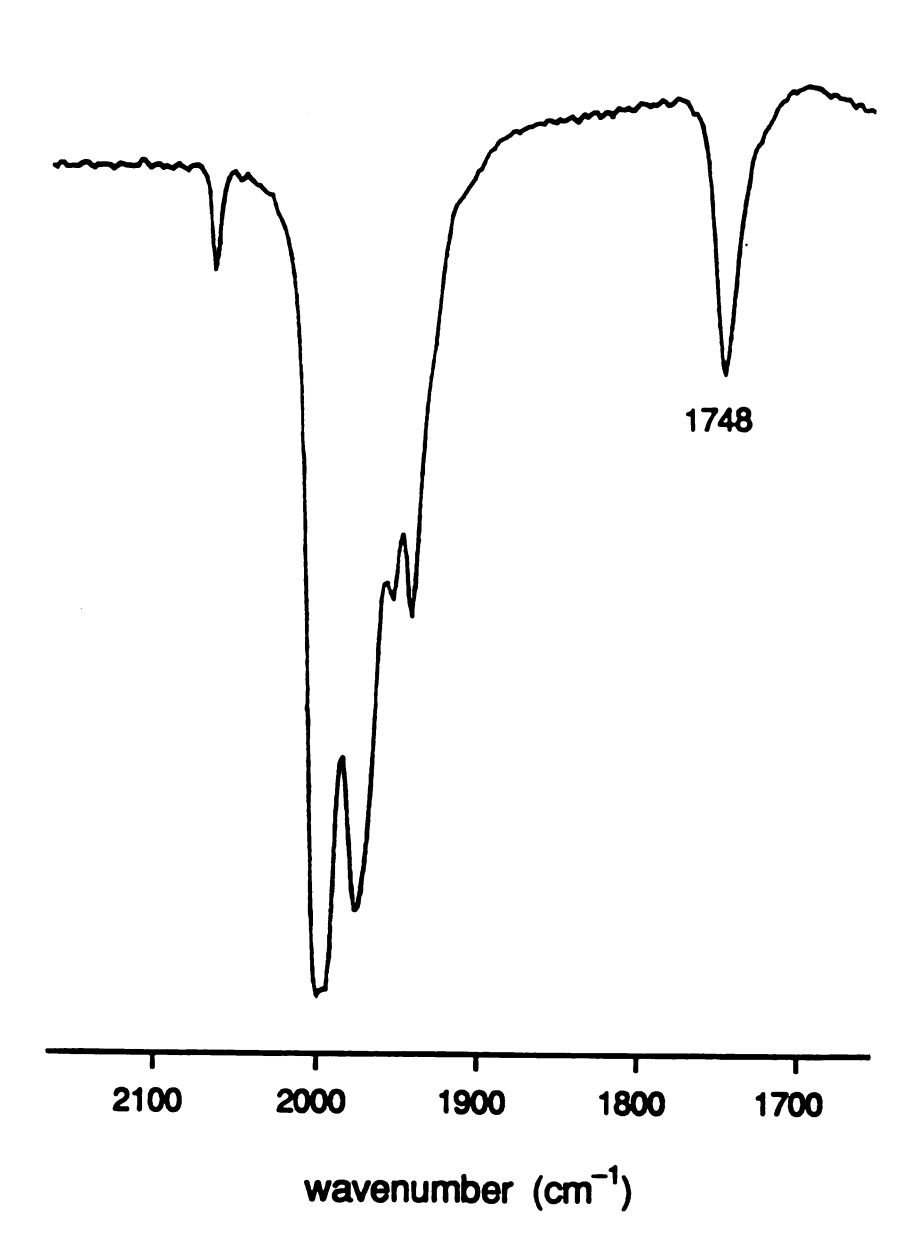


Figure 42

data for the compound are given in Table 14, and selected bond distances and angles are listed in Table 15. The packing diagram clearly shows that the anion [HFe₃(CO)₁₁] and the cation [HTMPP] are separated by normal van der Waals interactions without any contact ion-pairing. The anion consists of an isosceles triangular framework (Fe(1)—Fe(2) = 2.683 (1) Å, Fe(2)—Fe(3) = 2.590 (1) Å, <math>Fe(1)—Fe(3) = 2.680 (2) Å), wherein the shorter edge between Fe(2) and Fe(3) is symmetrically bridged by a carbonyl group (Fe(2)-C(11) = 1.924 (7) Å, Fe(3)-C(11) = 1.946 (7) Å) and one hydride ligand; these are located on opposite sides of the trianglar framework. (Note: The hydride is not structurally located, and appears in a calculated position with the use of the "HYDRIDE" program). The symmetrically bridging nature of the carbonyl group suggests that there is an equivalent electronic environment around both iron atoms Fe(2) and Fe(3). Three terminal carbonyl groups are bonded to atoms Fe(2) and Fe(3), respectively, and atom Fe(1) has four terminal carbonyl groups. The molecule is of approximate C_s symmetry; a mirror plane passes through Fe(1), C(1), O(1), C(2), O(2), C(11), O(11) and H(1), and bisects the Fe(2)—Fe(3) vector. It is noteworthy that the bond distance of C(11)—O(11) is significantly longer than the value for the bridging CO ligands in the neutral species Fe₃(CO)₁₂. The bond-lengthening feature indicates that there is a localization of anionic charge on O(11). This observation is actually quite consistent with the literature reports that the bridging CO group is the nucleophilic center of cation—anion coupling in anion clusters.

Table 14. Crystal Data for [HTMPP][$Fe_3(\mu-H)(\mu-CO)(CO)_{10}$]

Formula	$Fe_3P_1O_{20}C_{38}H_{35}$
Formula weight	1008.19
Crystal system	Triclinic
Space group	P-1
a, Å	8.342 (5)
b, Å	16.43 (1)
с, Å	17.36 (1)
α, deg	114.85 (6)
β, deg	91.95 (5)
γ, deg	93.69 (5)
V, Å ³	2149 (3)
${f z}$	2
d _{calc} , g/cm ³	1.558
Crystal size, mm	0.30 x 0.05 x 0.16
Radiation	Mo $K_{\alpha}(\lambda = 0.71073 \text{ Å})$
μ , cm ⁻¹	11.114
Data collection instrument	Nicolet P3/F
Temperature, °C	-110 ± 2
Scan method	$\omega - 2\theta$
Data col. range, 2θ, deg.	4 – 45
R ^a	0.055
$R_{\mathbf{w}}^{}}^{}}$	0.063

 $a R = \Sigma | |F_o| - |F_c| |/\Sigma| F_o|$

b $R_w = [\Sigma w | F_o| - |F_c|)^2 / \Sigma w |F_o|^2]^{1/2}; w = 1/\sigma^2 (|F_o|)$

Table 15. Selected Bond Distances (Å) and Angles (deg) for [HTMPP][Fe $_3(\mu\text{-H})(\mu\text{-CO})(CO)_{10}].$

T IIIMU	Atom 2		Distance	Atom 1	Atom 2	1.2	Distance
Fe(1)	Fe(2)		2.683 (1)	Fe(2)	C(7)		1.755 (8)
Fe(1)	Fe(3)	•	2.680 (2)	Fe(2)	C(11)		1.924 (7)
Fe(2)	Fe(3)		2.590 (1)	Fe(3)	C(8)		1.797 (9)
Fe(1)	Q(1)		1.776 (9)	Fe(3)	(6)O		1.76 (1)
Fe(1)	C(2)		1.772 (9)	Fe(3)	C(10)		1.764 (8)
Fe(1)	C(3)		1.793 (9)	Fe(3)	C(11)		1.946 (7)
Fe(1)	C(4)		1.816 (9)	P(1)	C21		1.769 (7)
Fe(2)	C(5)		1.756 (9)	P(1)	C31		1.786 (7)
Fe(2)	C(6)		1.815 (8)	P(1)	<u>2</u>		1.785 (6)
Atom 1	Atom 2	Atom 3	Angle	Atom 1	Atom 2	Atom 3	Angle
Fe(2)	Fe(1)	Fe(3)	57.76 (4)	Fe(3)	Fe(2)	C(6)	118.2 (2)
Fe(1)	Fe(2)	Fe(3)	61.05 (4)	Fe(3)	Fe(2)	C(7)	113.5 (3)
Fe(1)	Fe(3)	Fe(2)	61.20 (4)	Fe(2)	Fe(3)	C(8)	120.3 (3)
Fe(2)	Fe(1)	C(1)	159.3 (3)	Fe(2)	Fe(3)	(6))	108.1 (3)
Fe(2)	Fe(1)	C(2)	97.2 (3)	Fe(2)	Fe(3)	C(10)	127.7 (2)
Fe(2)	Fe(1)	C(3)	81.1 (2)	P(1)	C21	C22	123.6 (5)
Fe(2)	Fe(1)	C(4)	89.4 (2)	P(1)	C31	C32	125.2 (5)
Fe(2)	α_{11}	Fe(3)	84.0 (3)	P(1)	C41	C42	118.3 (5)
Fe(3)	Fe(2)	C(5)	128.2 (2)	Fe(2)	C(11)	0(11)	138.4 (5)

Figure 43. An ORTEP diagram of [HTMPP][HFe $_3$ (CO) $_{11}$], showing the atom labeling scheme. All atoms are represented by their 40% probability ellipsoids.

the

40F

Figure 43

Figure 44. A packing diagram of $[HTMPP][HFe_3(CO)_{11}]$, showing there is no ion-pairing interaction present in the molecule.

Figure 44

there is

(II) Triruthenium carbonyl clusters with TMPP

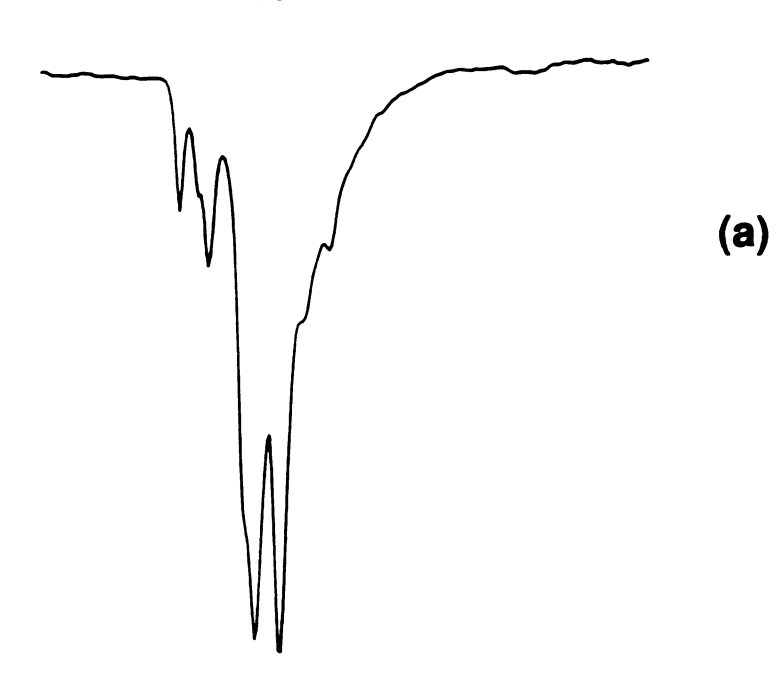
A. Synthesis and Characterization

Reactions of $Ru_3(CO)_{12}$ with the strong nucleophile TMPP in refluxing THF yields the red product $Ru_3(CO)_{11}(TMPP)$ as identified by NMR studies and infrared spectroscopy. The ¹H NMR spectrum showed a symmetrical magnetic environment for the three phenyl groups of the phosphine ligand in $Ru_3(CO)_{11}(TMPP)$, as evidenced by the presence of one resonance in the meta region at $\delta = 6.02$ (d, $J_{HP} = 3$ Hz, m-H) ppm, and two singlets for the ortho and the para methoxy groups located at $\delta = 3.32$ and 3.23 ppm, respectively. ³¹P {¹H} NMR spectroscopy showed a singlet for the product at $\delta = -15.6$ ppm with a downfield shift from free TMPP ($\delta = -68$ ppm). The infrared spectrum revealed v(CO) bands at 2003 and 2023 cm⁻¹, but no stretches that may be attributed to a bridging CO group (Figure 45(a)). These spectroscopic data support compound (1) as being a monodentate TMPP—containing cluster in which the phosphine most likely occupies an equatorial position based on streic bulk considerations.

With $Ru_3(CO)_{11}(NCMe)$ as the cluster precursor, the nucleophilic reaction with TMPP proceeds much faster, and yields the same monodentate TMPP product, $Ru_3(CO)_{11}(TMPP)$, as in the previous reaction. However, this product is highly thermally unstable both in solution and in the solid state, and undergoes transformation as evidenced by the observation of a color change which is accompanied by spectral changes in the infrared carbonyl region. As the spectra in Figure 45(b) clearly demonstrate, two new bridging v(CO) bands at 1790 and 1800 cm⁻¹ appear after several hours at room temperature.

Figure 45. Infrared spectral changes in the $\nu(CO)$ region for (a) initial product $Ru_3(CO)_{11}(TMPP)$ and (b) transformed product with bridging $\nu(CO)$ bands observed at 1790 and 1800 cm⁻¹.







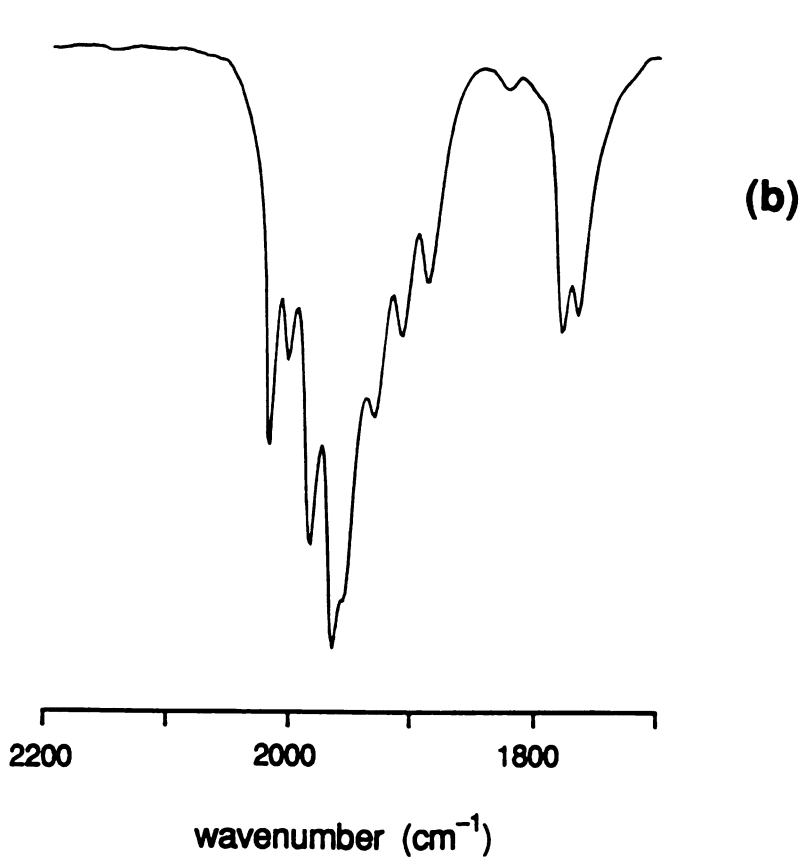


Figure 45

Figure 46. Infrared spectrum in THF for the molecule $Ru_3(\mu - CO)_2(CO)_6\{\mu_3-\eta^2-C_6H_2(OMe)_3\}[\mu-P\{C_6H_2(OMe)_3\}_2]$. The $\nu(CO)$ stretches at 1807 and 1866 cm⁻¹ are bridging modes.

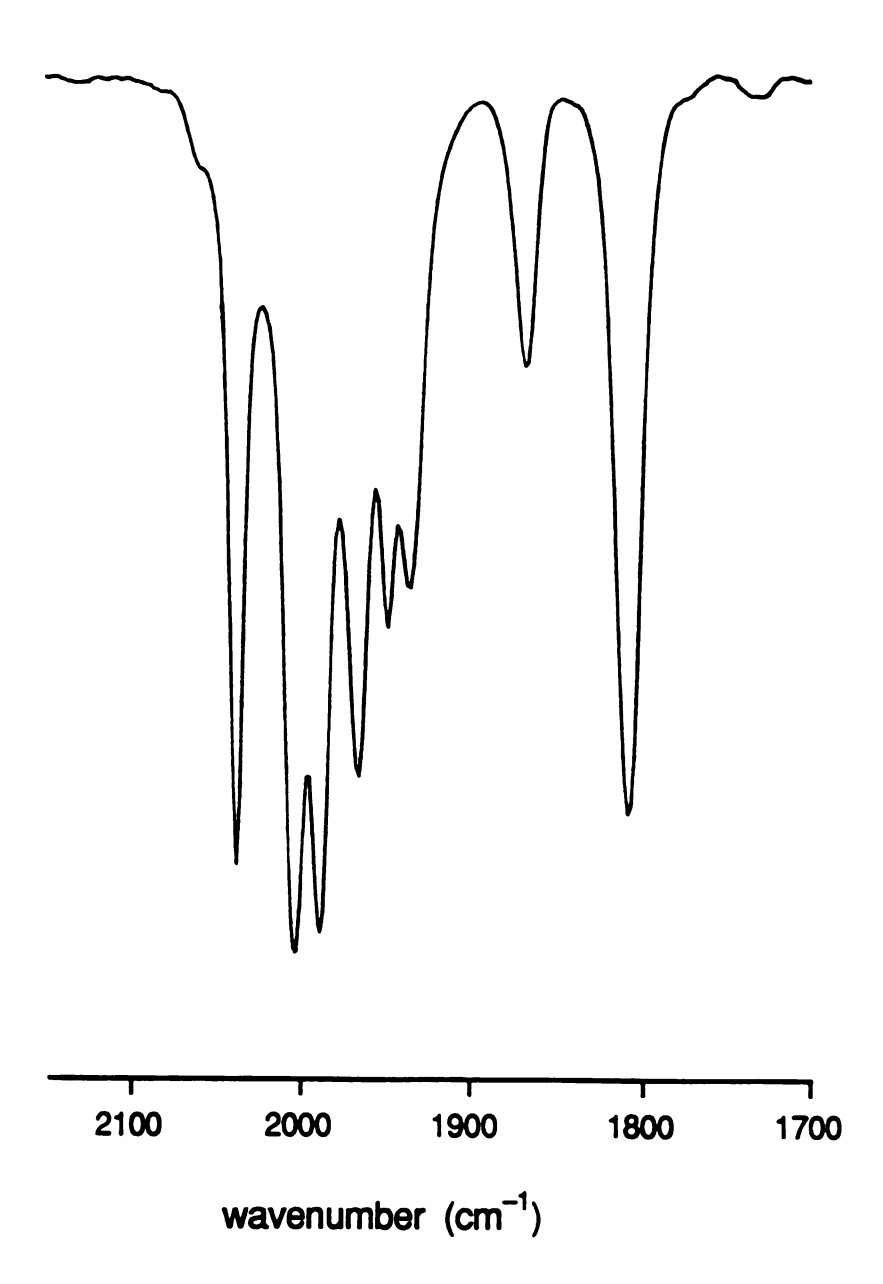


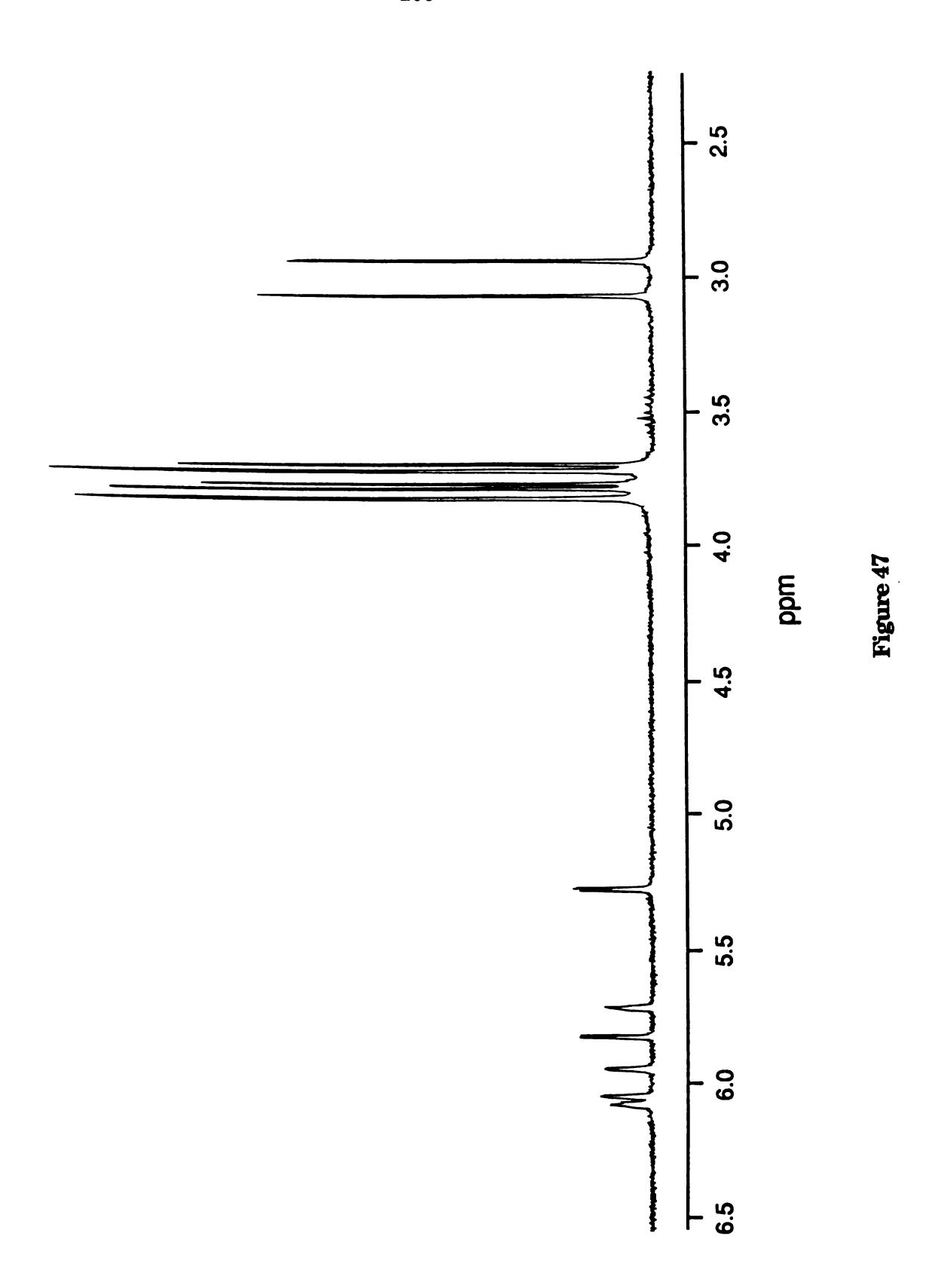
Figure 46

le Ru $_3$ μ .
The v(CO)

Separation of the decomposition products by column chromatography led to the isolation of a stable red product which exhibits two bridging v(CO)stretches at 1807 and 1866 cm⁻¹ in the infrared spectrum (Figure 46). An X-ray diffraction study of the compound revealed the compound to be $Ru_3(\mu-CO)_2(CO)_6(\mu_3-\eta^2-R)(\mu-PR_2)$ (R = 2,4,6-C₆H₂(OMe)₃) which consists of a bridging-phosphido group and a triply-bonded cyclometallated trimethoxyphenyl ring. The room temperature 300 MHz ¹H NMR spectrum of (2) in CD₃CN confirms that the TMPP ligand is ligated in a completely unsymmetrical fashion (Figure 47). Four meta protons are multiplets and resonate at $\delta = 5.84$ (1H), 6.07 (1H) and 6.17 (2H); two additional signals are doublets at $\delta = 5.43$ (1H, $J_{HH} = 2$ Hz) and 5.84 (1H, $J_{HH} = 2$ Hz) ppm. Both doublets are assigned to the meta protons in the cyclometalled phenyl ring due to the absence of a coupling to the phosphorus nuclei. Seven methoxy group resonances were observed at $\delta \approx 3.80$ ppm, with two signals being shifted to the upfield region; these are centered at $\delta = 2.98$ and 3.10 ppm. Both shielded methoxy resonances are assigned to the ortho-methoxy groups in the cyclometallated ring because the free 2,4,6-trimethoxyphenyl group is expected to exhibit less significant chemical shift deviations from (2,4,6-trimethoxyphenyl)phosphine.

The formation of the phosphido-bridged cluster $Ru_3(\mu\text{-CO})_2(CO)_6(\mu_3-\eta^2\text{-R})(\mu\text{-PR}_2)$ (R = 2,4,6-C₆H₂(OMe)₃) is a result of an intramolecular oxidative addition via P—C bond cleavage. Numerous phosphido bridged polynuclear complexes have been explored due to the possibility that $\mu\text{-PR}_2$ bridges might function as strongly bound, flexible but inert ligands. For example, a recent study revealed that $\mu\text{-PR}_2$ bridges have the capability of allowing interconversion between "open" (50-electron) and "closed" (48-electron) shell clusters [85].

Figure 47. A 300 MHz 1 H NMR spectrum in THF-d₈ at 22 $^{\circ}$ C for Ru₃(μ -CO)₂(CO)₆{ μ ₃- η ²-C₆H₂(OMe)₃}[μ -P{C₆H₂(OMe)₃}₂]. Resonances denoted by (a) and (b) are assigned to both ortho-methoxy groups and two meta protons, respectively, in the cyclometallated ring.



2 °C for Rust.

]. Resonance

ortho-methor

vely, in the

The reaction pathway to prepare many phosphido-bridged polynuclear complexes involves a transition metal mediated P-C bond cleavage which usually occurs for the corresponding tertiary phosphine complexes only under forcing conditions [82]. The first example of cluster-assisted phosphorous ligand transformation via P—C bond cleavage was observed in the course of a prolonged thermal reaction of Os₃(CO)₁₂ with triphenylphosphine [83]; similar reactions with different tertiary phosphines, but parallel ligand transformations of $\mathrm{Ru}_3(\mathrm{CO})_{12}$ were also observed [84]. Mechanistic studies of transition metal mediated P—C bond cleavage are not conclusive, but it appears that the formation of a coordinatively unsaturated intermediate often occurs prior to oxidative addition [ref]. Based on that, we propose a possible reaction pathway for the formation of the molecule $Ru_3(\mu\text{-CO})_2(CO)_6(\mu_3-\eta^2-R)(\mu\text{-PR}_2)$ (R = 2,4,6-C₆H₂(OMe)₃) (Figure 48). In this reaction scheme, the reaction of $Ru_3(CO)_{11}(NCMe)$ (I) with PR_3 (R = 2,4,6-C₆H₂(OMe)₃) initially produces a monodentate product Ru₃(CO)₁₁(PR₃) (II) which then further transforms into a didentate product "Ru₃(CO)₁₀(μ -PR₃)" (III) which can further transform, via P—C bond cleavage, into the phosphido-bridged cluster $Ru_3(\mu-CO)_2(CO)_6(\mu_3-\eta^2-R)(\mu-PR_2)$ (V) with a cyclometallated phenyl ring and a phosphido bridge. The intermediate (IV) is expected to be very unstable.

We consider the most significant result obtained from this work to be the synthesis of the 46-electron unsaturated phosphido bridged cluster $Ru_3(\mu\text{-CO})_2(CO)_6(\mu_3-\eta^2\text{-R})(\mu\text{-PR}_2)$ (R = 2,4,6-C₆H₂(OMe)₃). The inherent unsaturation of the molecule is revealed by its space filling model in Figure 49.

Figure 48. Proposed reaction pathway for the formation of $Ru_3(\mu\text{-CO})_2(CO)_6\{\mu_3-\eta^2\text{-}C_6H_2(OMe)_3\}[\mu\text{-P}\{C_6H_2(OMe)_3\}_2].$

Figure 48

Figure 49. Computer generated space–filling model of molecule B of $Ru_3(\mu\text{-CO})_2(CO)_6\{\mu_3\text{-}\eta^2\text{-}C_6H_2(OMe)_3\}[\mu\text{-P}\{C_6H_2(OMe)_3\}_2].$ The Ru atoms are denoted by the black balls.

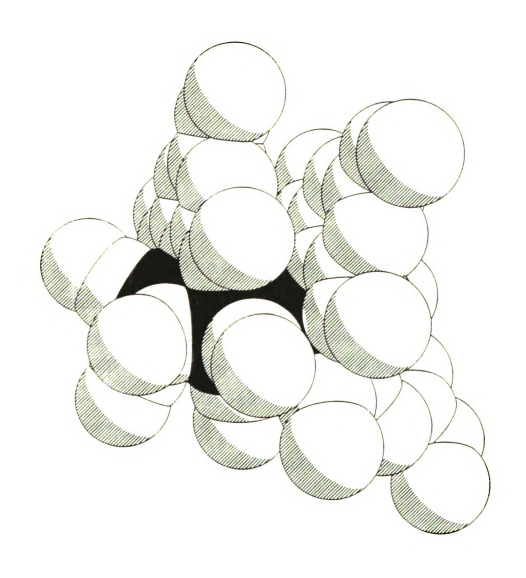


Figure 49

A number of unsaturated cluster complexes have been prepared [86], and, in general, they are able to undergo associative reactions with a variety of reagents under mild conditions. Based on this consideration, we expect the molecule $Ru_3(\mu\text{-CO})_2(CO)_6(\mu_3-\eta^2-R)(\mu\text{-PR}_2)$ to have similar reactivity to give a saturated molecule. It is reasonable to expect that one possible addition reaction of the molecule involves the opening of the weak ether interaction as shown in the reaction scheme (I).

$$(CO)_{2} Ru = CO)_{2} Ru(CO)_{2}$$

$$Ru(CO)_{2} Ru = CO)_{2} Ru(CO)_{2}$$

Another consideration that is worth mentioning is that the Ru—Ru bond with the bridging carbon atom exhibits the shortest bond distance (Ru(1)—Ru(2) = 2.669 (3) Å in molecule A; Ru(4)—Ru(5) = 2.668 (4) Å in molecule B); based on these facts, a second possibility for the nucleophilic addition is the opening of one longer C—Ru bonding (Ru(2)—C56 = 2.34 (2) Å in molecule A; Ru(5)—C66 = 2.32 (2) Å) as shown in the reaction scheme (II).

$$(\infty)_{2} \text{ Ru} \xrightarrow{C} (\infty)_{2} \text{ Ru}(\infty)_{2} + L \qquad (\infty)_{2} \text{ Ru}(\infty)_{2}$$

$$(\infty)_{2} \text{ Ru} \xrightarrow{C} (\infty)_{2} \text{ Ru}(\infty)_{2}$$

$$(\infty)_{2} \text{ Ru} \xrightarrow{C} (\infty)_{2} \text{ Ru}(\infty)_{2}$$

$$(\infty)_{3} \text{ Ru}(\infty)_{4} \text{ Ru}(\infty)_{5}$$

$$(\infty)_{4} \text{ Ru}(\infty)_{5} \text{ Ru}(\infty)_{6} \text{ Ru}(\infty)_{6}$$

$$(\infty)_{5} \text{ Ru}(\infty)_{6} \text{ Ru}(\infty)_{7} \text{$$

B. Molecular Structure

A crystallographic study of $Ru_3(\mu\text{-CO})_2(CO)_6(\mu_3-\eta^2\text{-R})(\mu\text{-PR}_2)$ (R = 2,4,6-C₆H₂(OMe)₃) reveals a triclinic space group P-1 with Z = 4. Each asymmetric unit contains two independent molecules A and B which are enantiomers that exhibit chiral centers at the bridging carbon atoms C(56) and C(66), respectively, in the cyclometallated phenyl ring. Crystallographic data are summarized in Table 16; important bond distances and angles for this cluster are given in Table 17. The ORTEP plots of both molecules A and B with the atom-labeling schemes are presented in Figure 50. A comparison of the main features of these two molecules is given in Figure 51.

Compound (2) consists of a triruthenium framework with a symmetrically disposed phosphido bridge between atoms Ru(1) and Ru(2). Two bridging carbonyl groups are located on the other two edges of the trinuclear framework. Some important distances in molecule A are Ru(2)-P(1) = 2.334 (8) Å, Ru(3)-P(1) = 2.348 (8), and in molecule B; Ru(5)-P(1) = 2.348P(2) = 2.367 (7) Å, Ru(6)-P(2) = 2.353 (8) Å. By considering the electrondonating characteristics of bridging ligands in metal clusters, an edgebridging phosphido group PR2 is treated as a three-electron donor as are Additionally, one cyclometallated (2,4,6-SR and OR ligands. trimethoxy) phenyl ring functions as a capping ligand that is triply bonded to three ruthenium metal centers. The coordination mode is $\mu_3\text{-}\eta^2\text{-}2\text{,}4\text{,}6\text{-}$ $C_6H_2(OMe)_3$ wherein the carbon atom doubly bridges two ruthenium atoms (Ru(1)-C(56) = 2.24 (2) Å, Ru(2)-C(56) = 2.34 (2) Å in molecule A; Ru(4)-C(56) = 2.34 (2) A in molecule A; Ru(4)-C(5C(66) = 2.77 (2) Å, Ru(5)—C(66) = 2.32 (2) Å in molecule B). The oxygen atom of a methoxy group in the ortho position is bound to the third metal center (Ru(3)—O(51) = 2.20 (2) Å in molecule A; Ru(6)—O(61) = 2.19 (2) Å in

molecule B). The cyclometallated phenyl ring which functions as a one electron donor is clearly aromatic with all C—C distances in the range of 1.39–1.49 Å as shown in Figure 52. The group, then, functions as a three electron donor in the formation of two five-membered metallacycles which are observed in both molecules: (Ru(1)-Ru(2)-C(51)-C(52)-O(51), Ru(3)-Ru(2)-C(51)-C(52)-O(51) in molecule A, and Ru(4)-Ru(5)-C(61)-C(62)-O(61), Ru(6)-Ru(5)-C(61)-C(62)-O(61) in molecule B). Electron counting, by treating both the edge-bridging phosphido group and the cyclometallated trimethoxyphenyl ligand as three-electron donors, gives the compound $Ru_3(\mu-CO)_2(CO)_6(\mu_3-\eta^2-R)(\mu-PR_2)$ (R = 2,4,6- $C_6H_2(OMe)_3$) a total of 46 electrons, a count which is in good agreement with the presence of one short metal-metal i.e. Ru(1)-Ru(2) and Ru(4)-Ru(5) in the molecules A and B, respectively.

Table 16. Crystal Data for $Ru_3(\mu-CO)_2(CO)_6\{\mu_3-\eta^2-C_6H_2(OMe)_3\}[\mu-P\{C_6H_2(OMe)_3\}_2]$

Formula	$Ru_3P_1O_{17}C_{15}H_{33}$
Formula weight	1059.83
Crystal system	Triclinic
Space group	P-1
a, Å	11.209 (7)
b, Å	15.60 (1)
c, Å	24.73 (2)
α, deg	85.48 (8)
β, deg	86.83 (6)
γ, deg	80.16 (7)
v, Å ³	4244 (6)
Z	4
d _{calc} , g/cm ³	1.658
Crystal size, mm	0.10 x 0.12 x 0.08
Radiation	Mo $K_{\alpha}(\lambda = 0.71073 \text{ Å})$
μ , cm ⁻¹	11.366
Data collection instrument	Nicolet P3/F
Temperature, °C	-95 ± 2
Scan method	ω .
Data col. range, 20, deg.	4 – 35
R ^a	0.075
R _w b	0.084

 $aR = \Sigma | |F_o| - |F_c||/\Sigma |F_o|$

$$b R_w = [\Sigma w | F_o | - | F_c |)^2 / \Sigma w | F_o |^2]^{1/2}; w = 1/\sigma^2 (| F_o |)$$

Table 17. Selected Bond Distances (Å) and Angles (deg) for $Ru_3(\mu - CO)_2(CO)_6[\mu_3 - \eta^2 - C_6H_2(OMe)_3][\mu - P\{C_6H_2(OMe)_3\}_2]$.

Atom 1	Atom 2	Distance	Atom 1	Atom 2	Distance
Ru(1)	Ru(2)	2.669 (3)	Ru(4)	Ru(5)	2.668 (4)
Ru(1)	Ru(3)	2.742 (3)	Ru(4)	Ru(6)	2.756 (3)
Ru(2)	Ru(3)	2.781 (3)	Ru(5)	Ru(6)	2.780 (3)
Ru(2)	P(1)	2.334 (8)	Ru(5)	P(2)	2.367 (7)
Ru(3)	P(1)	2.348 (8)	Ru(6)	P(2)	2.353 (8)
Ru(1)	C56	2.24 (2)	Ru(4)	990	2.77 (2)
Ru(2)	C56	2.34 (2)	Ru(5)	990 Cee	2.32 (2)
Ru(3)	051	2.20 (2)	Ru(6)	061	2.19 (2)
P(1)	C11	1.84 (3)	P(2)	C31	1.86 (2)
P(1)	C21	1.86 (3)	P(2)	C41	1.86 (3)

Atom 1	Atom 1 Atom 2 Atom 3	Atom 3	Angle	Atom 1	Atom 2 Atom 3	Atom 3	Angle
Ru(2)	Ru(1)	Ru(3)	61.83 (9)	Ru(5)	Ru(4)	Ru(6)	(6) 59.19
Ru(1)	Ru(2)	Ru(3)	60.39 (9)	Ru(4)	Ru(5)	Ru(6)	60.72 (9)
Ru(1)	Ru(3)	Ru(2)	57.78 (9)	Ru(4)	Ru(6)	Ru(5)	57.63 (9)
Ru(2)	P(1)	Ru(3)	72.9 (2)	Ru(5)	P(2)	Ru(6)	72.2 (2)
Ru(1)	C56	Ru(2)	71.3 (7)	Ru(4)	990	Ru(5)	(1) 6.02
Ru(3)	061	C51	118.0 (2)	Ru(6)	061	C61	119.0 (2)
C56	C51	051	113.0 (2)	C66	C61	190	116.0 (2)

Figure 50. ORTEP drawings of (a) molecule A and (b) molecule B of $Ru_3(\mu\text{-CO})_2(CO)_6\{\mu_3-\eta^2\text{-}C_6H_2(OMe)_3\}[\mu\text{-P}\{C_6H_2(OMe)_3\}_2],$ showing the atom labeling scheme with all atoms represented by their 40% probability ellipsoids.

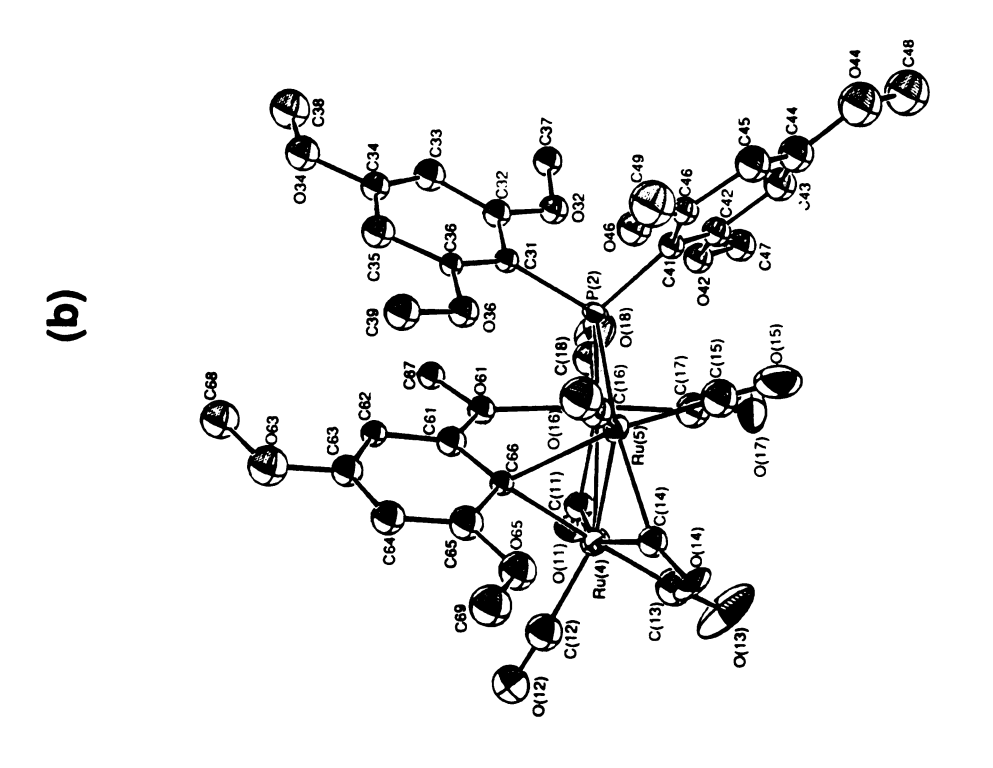
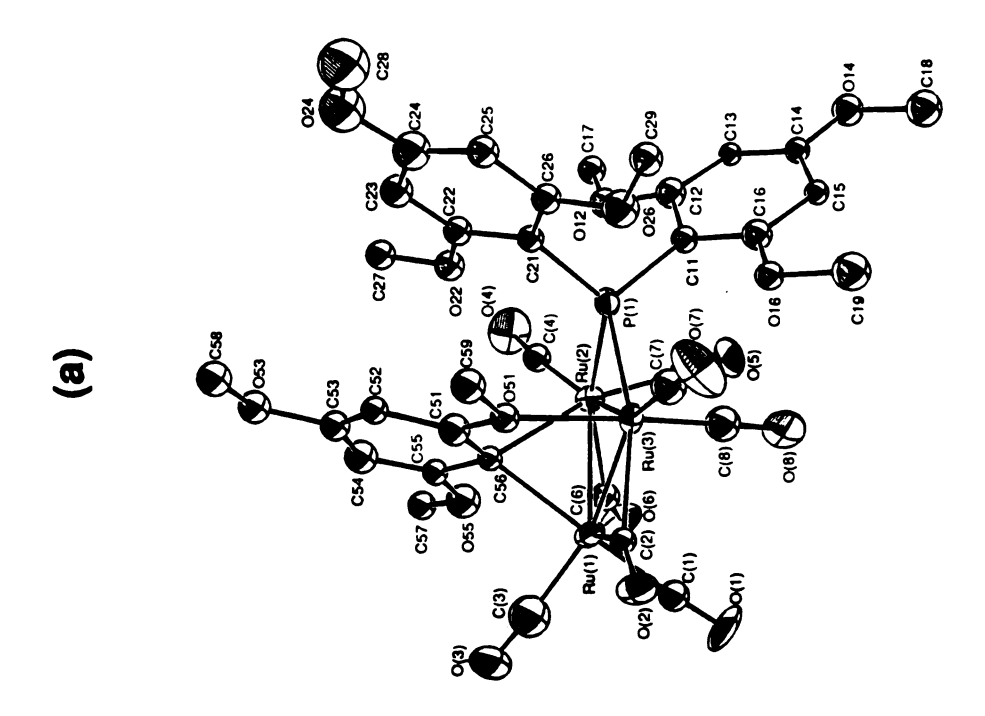


Figure 50



nolecule B of Me)3}2],

s represented

Figure 51. Main features of both enantiomers A and B in the structure of $Ru_3(\mu\text{-CO})_2(CO)_6\{\mu_3-\eta^2\text{-}C_6H_2(OMe)_3\}[\mu\text{-}P\{C_6H_2(OMe)_3\}_2].$ Chiral carbon atoms in both molecules are denoted by *.

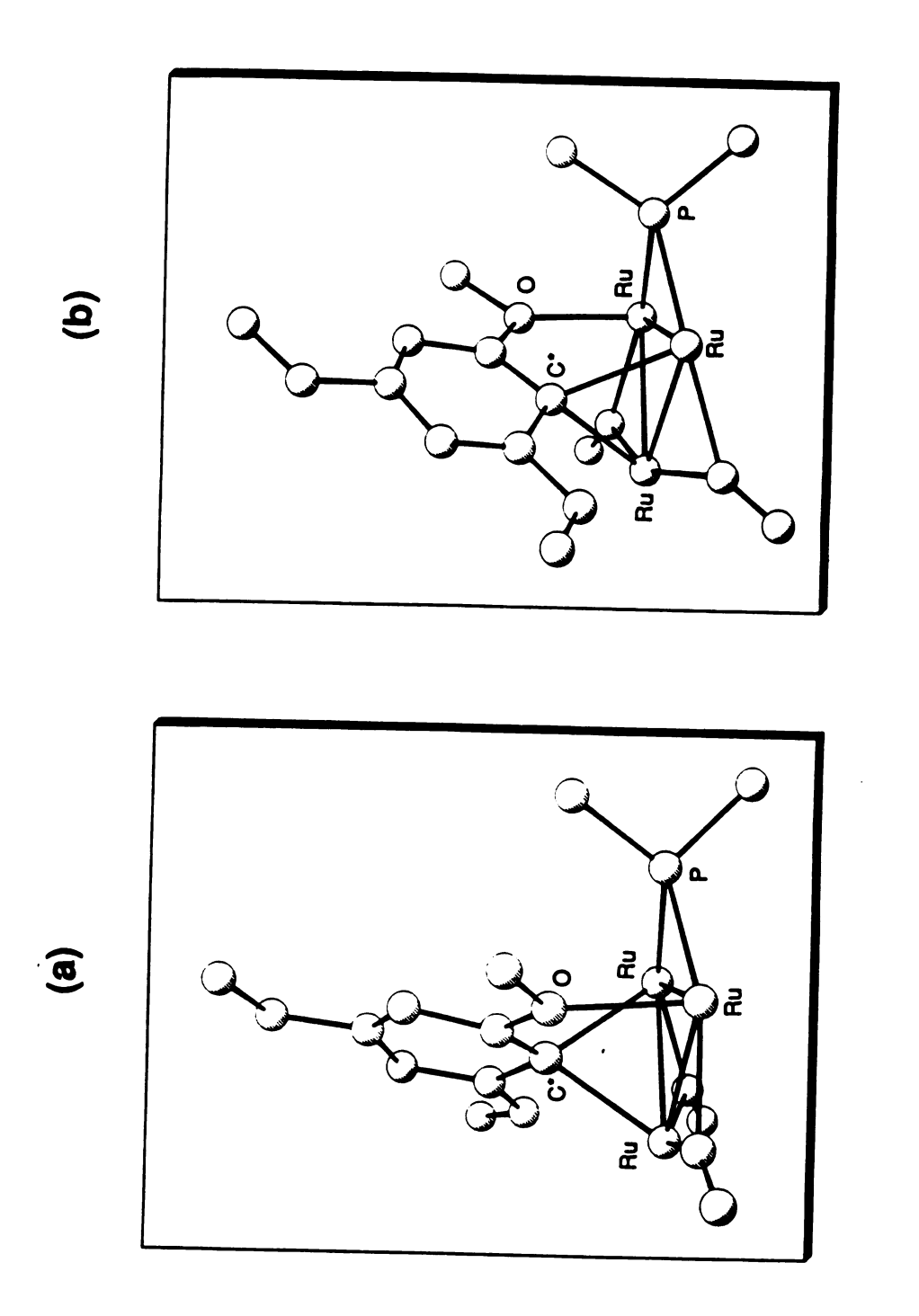


Figure 51

Figure 52. Selected bond distances for molecules A and B in the structure $of \ Ru_3(\mu\text{-CO})_2(CO)_6\{\mu_3\cdot\eta^2\text{-}C_6H_2(OMe)_3\}[\mu\text{-P}\{C_6H_2(OMe)_3\}_2].$

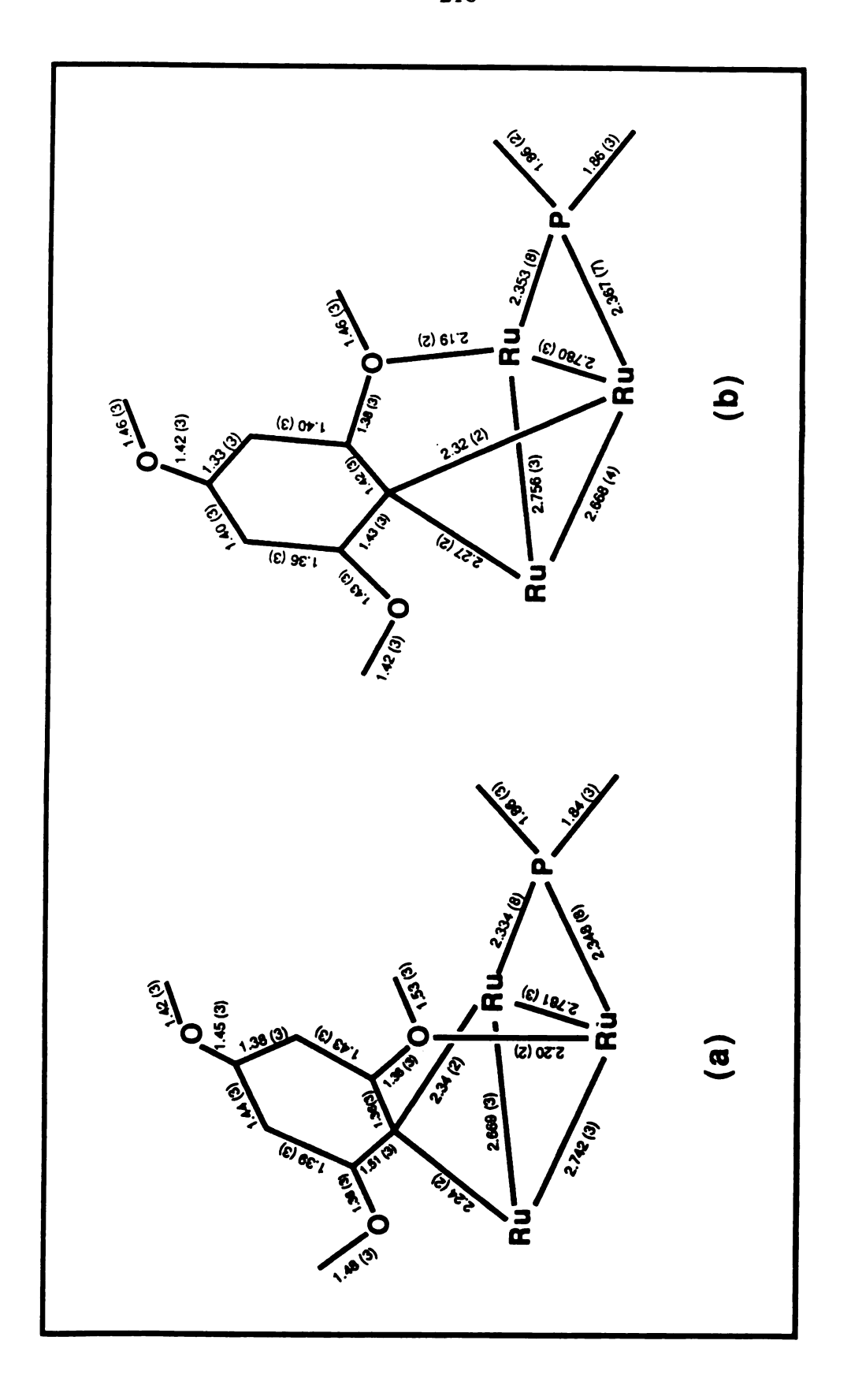


Figure 52

(III) Reactions of Triosmium Carbonyl Clusters with TMPP

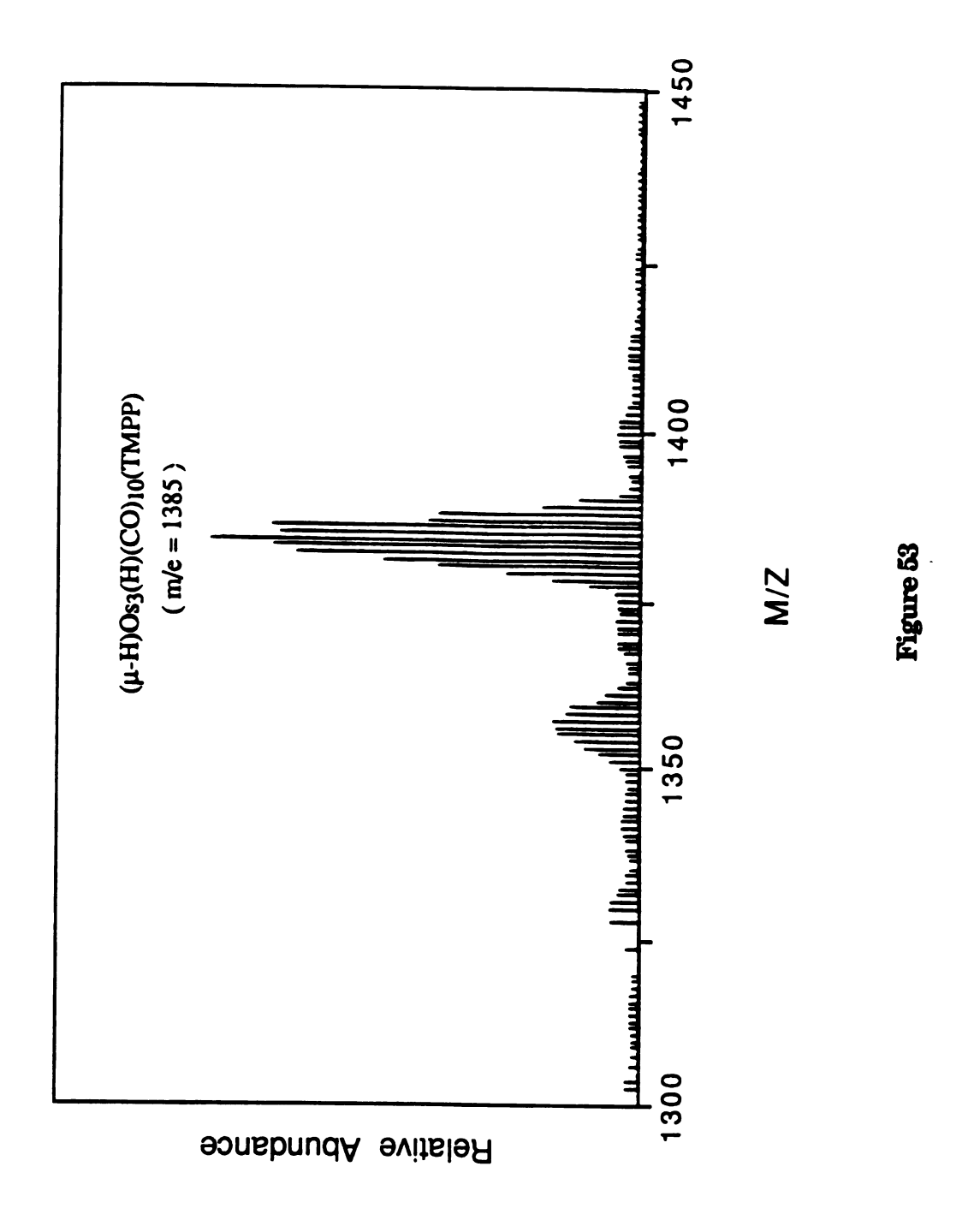
A. Synthesis and Discussion

The trinuclear cluster Os₃(CO)₁₂ is highly stable, and like reactions with other PR₃ ligands, chemistry with TMPP occurs only with a large excess of the phosphine or under forcing conditions with high boiling solvents. In either case, the reactions led to mixtures of products in low yields. Because of these observations, our initial experiments in this study were undertaken with the use of unsaturated molecules such as the 46electron molecule (µ-H)₂Os₃(CO)₁₀ which exhibits high reactivity due to the electronic unsaturation, and "lightly-stabilized" solvated molecules such as $Os_3(CO)_{12-n}(NCMe)_n$ (n = 1 or 2) wherein the labile acetonitriles are easily replaced in the presence of stronger nucleophiles. Reactions of Os₃(μ-H)₂(CO)₁₀ with TMPP in THF at room temperature showed an instantaneous color change from purple to yellow, similar to that reported for various other tertiary phosphines under the same conditions [87]. This indicated to us that a reaction occurred to form a 48-electron saturated molecule. Further work-up by thin-layer chromatography led to the isolation of a yellow product characterized as Os₃(μ-H)(H)(CO)₁₀(TMPP) on the basis of various spectroscopic methods. A FABMS spectrum of the compound gave the highest mass peak at m/z = 1385 corresponding to the molecular ion $[Os_3(H)_2(CO)_{10}(TMPP)]^+$, and a lower mass peak at m/z = 1357 due to the fragment [M-CO]⁺ (Figure 53). The molecule Os₃(µ- $H(H)(CO)_{10}(TMPP)$ exhibits dynamic behavior in solution as evidenced by a temperature-dependent 500 MHz ¹H NMR study in the hydride region. At room temperature, two broad unresolved resonances centered at -15 and -20 ppm were observed. Upon cooling, both resonances sharpened and then

collapsed into two well-resolved resonances by -50° C. A quartet centered at -20 ppm is assigned to the bridging hydride which is coupled to one phosphorus atom ($J_{HP} = 3Hz$) and one terminal hydride ligand ($J_{HH} = 3Hz$). The high-temperature limiting spectrum was not obtained due to the thermal instability of the complex. The 1 H NMR spectra in the hydride region at various temperatures are shown in Figure 54. The dynamic phenomenon in solution has also been observed in a series of related compounds such as $Os_{3}(\mu-H)(H)(CO)_{10}(L)$ ($L = PMe_{2}Ph$, PPh_{3} and PhCN [87(a)] and $^{t}Bu_{2}E'NSNE^{t}Bu_{2}$, (E , E' = P, As) [87(b)]). The behavior is interpreted as a hydride ligand-site exchange involving a bridging and a terminal hydride as well as one axial and one equatorial carbonyl in the molecule as shown below.

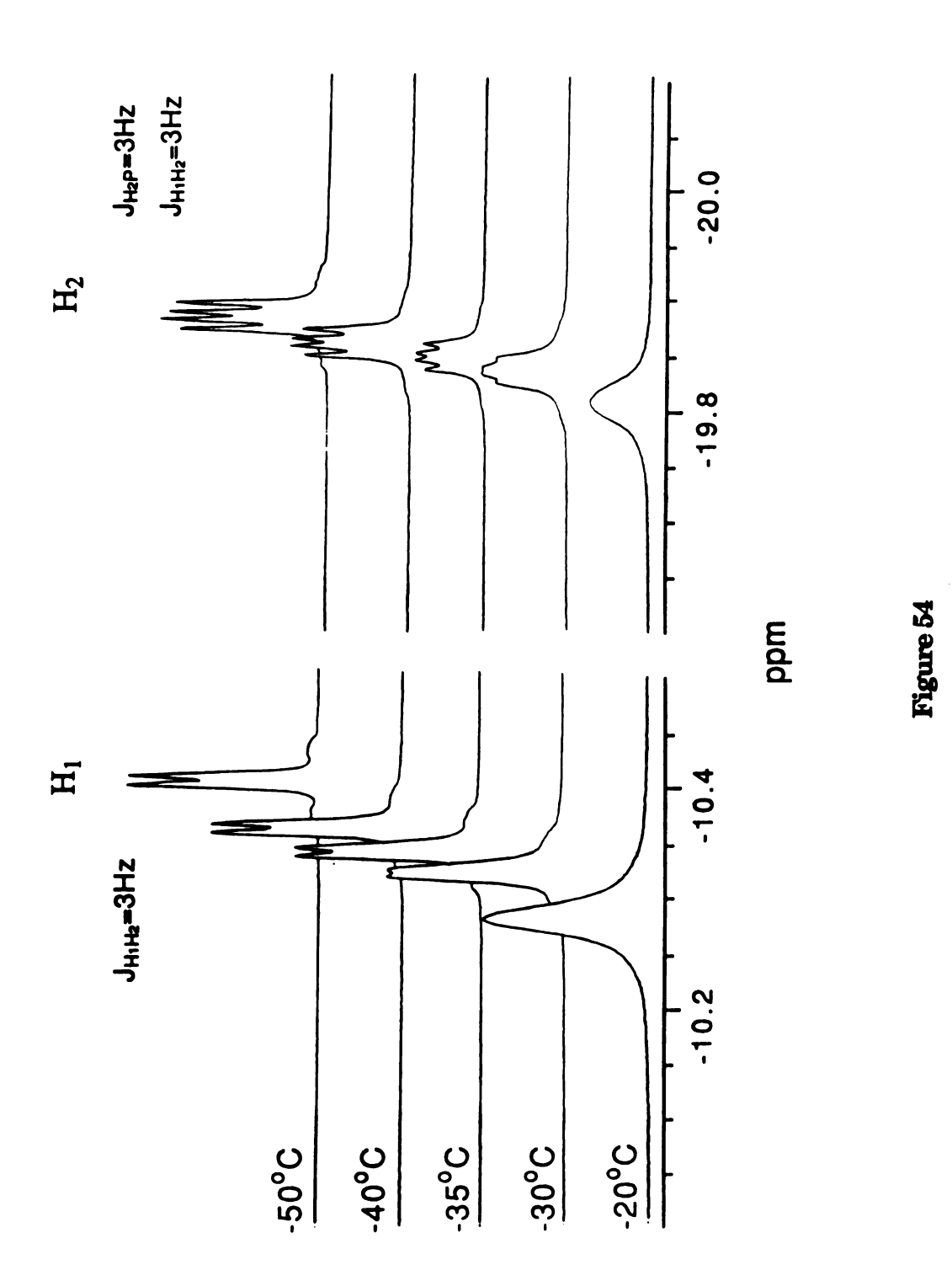
Recrystallization of the compound $Os_3(\mu-H)(H)(CO)_{10}(TMPP)$ from a mixture of hexane/THF led to the formation of yellow crystals. A preliminary cell of a single crystal grown from hexane/CH₂Cl₂ showed the crystal system to be monoclinic with dimensions : a = 22.33 (2) Å, b = 14.38 (1) Å, c = 27.59 (3) Å, $\beta = 102.38$ (9) and V = 8655 (16) Å³. A data set was not collected, however, due to the poor quality of the crystals.

Figure 53. Positive ion FABMS spectrum of $Os_3(\mu-H)(H)(CO)_{10}(TMPP)$.



))₁₀(TMPP).

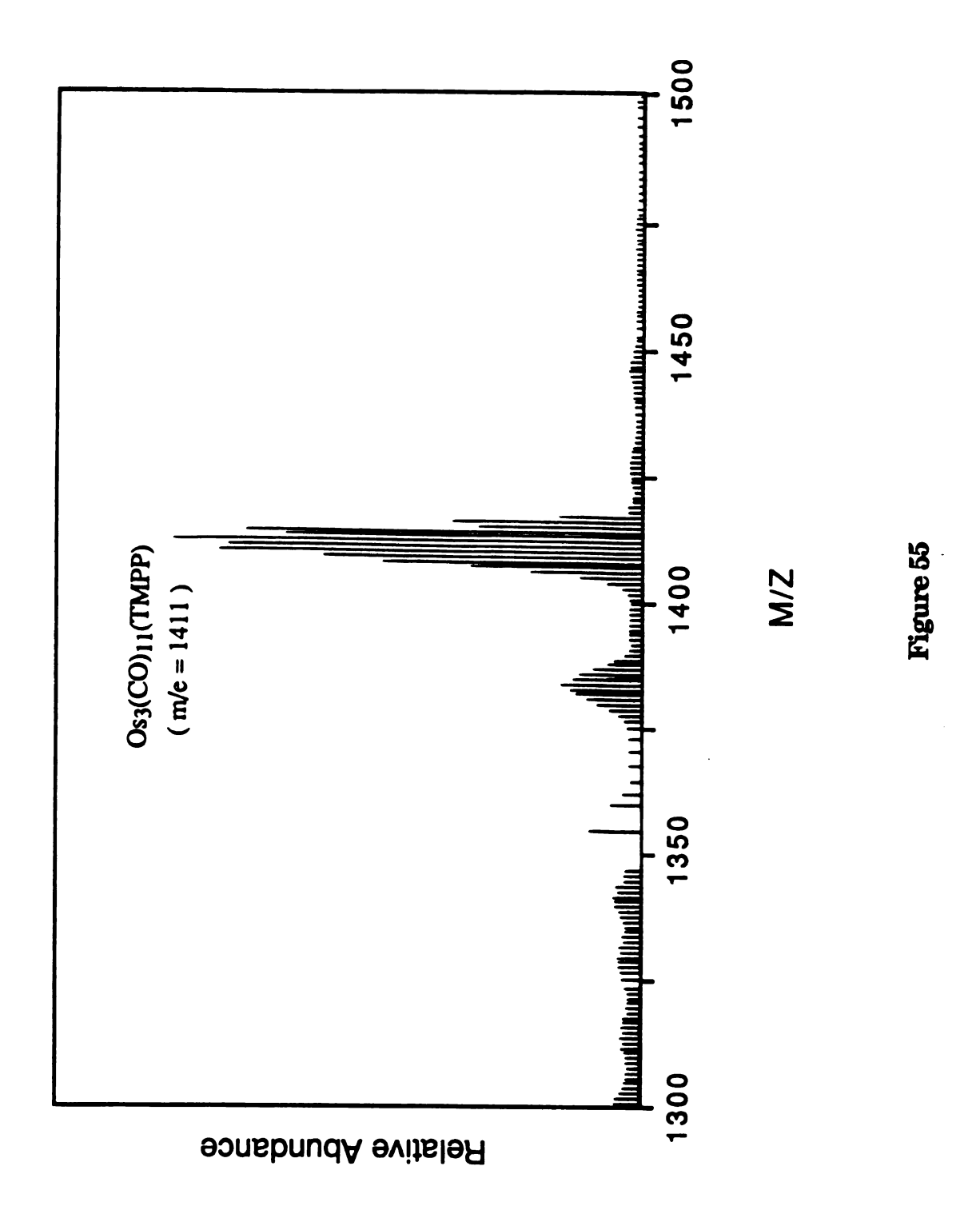
Figure 54. Variable–temperature 500 MHz 1 H NMR spectra of $Os_3(\mu\text{-H})(H)(CO)_{10}(TMPP) \ recorded \ in \ CDCl_3.$



Although a precise structure is not available, several structurally characterized triosmium clusters provide good background information for the compound. Based on the large steric bulk of the phosphine TMPP, it is reasonable to expect that the coordinated TMPP is located in an equatorial position.

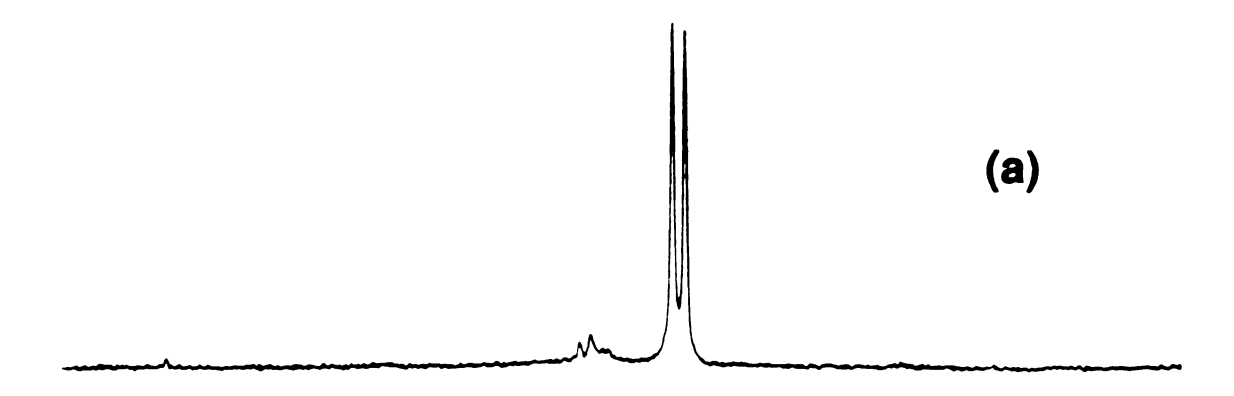
Reactions of Os₃(CO)₁₁(NCMe) with TMPP gave the yellow product Os₃(CO)₁₁(TMPP) (1) in quantitative yield. Characterization by FABMS showed a molecular peak at m/z = 1411 corresponding to $[Os_3(CO)_{11}(TMPP)]^+$, and a fragment at m/z = 1385 due to $[M-CO]^+$ (Figure 55). A ¹H NMR spectrum taken in CDCl₃ indicated a symmetrical magnetic environment for the three phenyl groups of the phosphine ligand, as evidenced by the presence of only three resonances arising from the ortho and the para methoxy groups; $\delta = 6.0$ (d) (d, $J_{HP} = 3$ Hz, $m-\underline{H}$), 3.5 (s, p-OMe), 3.8 (s, o-OMe) ppm. The transformation process was monitored by ¹H NMR spectroscopy in CD₃CN, and symmetrical meta proton resonances due to the initial product with a monodentate TMPP ligand were replaced by multiplets after ca. three days at room temperature. This result indicated that the compound containing monodentate TMPP transformed into a product with an unsymmetrical coordination mode for the phosphine (Figure 56). Unfortunately, in the course of recrystallizing $Os_3(CO)_{11}(TMPP)$ (1) from a mixture of hexane and CH_2Cl_2 , hydrolysis occurred, and the cluster transformed to a hydroxy-derivative cluster which was structurally characterized as $Os_3(\mu-OH)_2(CO)_9(TMPP)$ (3), a species which consists of doubly edge-bridging hydroxy groups similar to other known hydroxy clusters.

Figure 55. Positive ion FABMS spectrum of Os₃(CO)₁₁(TMPP).



Reactions of $Os_3(CO)_{10}(NCMe)_2$ with TMPP led to the isolation of two major products; $Os_3(CO)_{11}(TMPP)$ (1) and $Os_3(\mu\text{-OH})(CO)_9(\mu\text{-}\eta^2\text{-TMPP-}O)$ (2). The latter was confirmed by a crystallographic study. The room temperature 300 MHz ¹H NMR spectrum of (2) in CDCl₃ reveals that the TMPP ligand is bonded in a completely unsymmetrical fashion (Figure 57). Six meta protons appear as multiplets and resonate in the range of 5.80–6.18 ppm. Eight methoxy group resonances appear between 3.35 and 3.85 ppm. The absence of a ninth methoxy group suggested that demethylation had occurred, which was subsequently confirmed by a solid–state structural determination. A schematic diagram depicting the formation of molecule (1) and (2) is shown in Figure 58.

Figure 56. A 300 MHz 1 H NMR study depicting spectral changes during the transformation of $Os_3(CO)_{11}(TMPP)$. (a) Initial product $Os_3(CO)_{11}(TMPP)$ with terminal $\nu(CO)$ stretches only, and (b) transformed product with bridging $\nu(CO)$ stretches present.



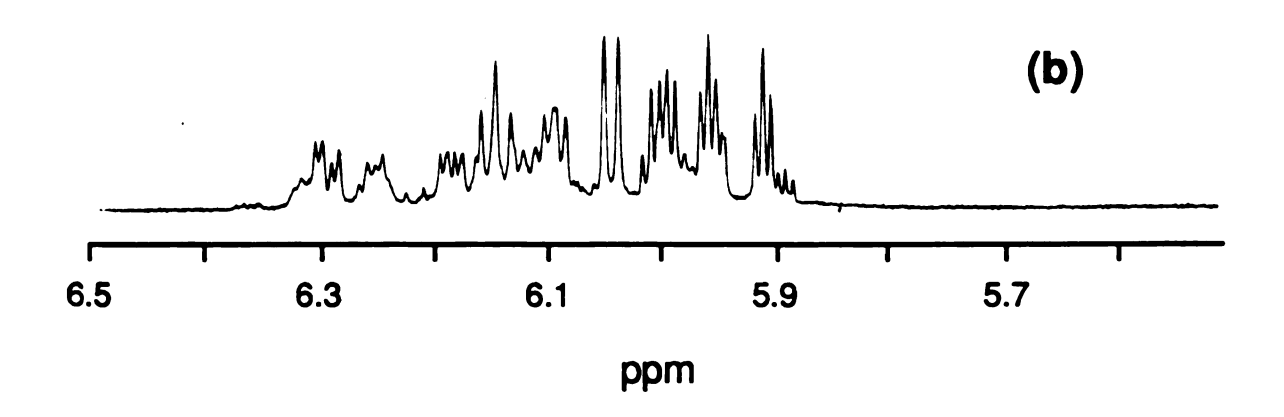


Figure 56

Figure 57. A 300 MHz 1 H NMR spectrum of $Os_3(\mu\text{-OH})(TMPP\text{-}O)(CO)_9$ in $CDCl_3$ at room temperature. The doublet denoted by * is due to an impurity of a methyl phosphonium salt.

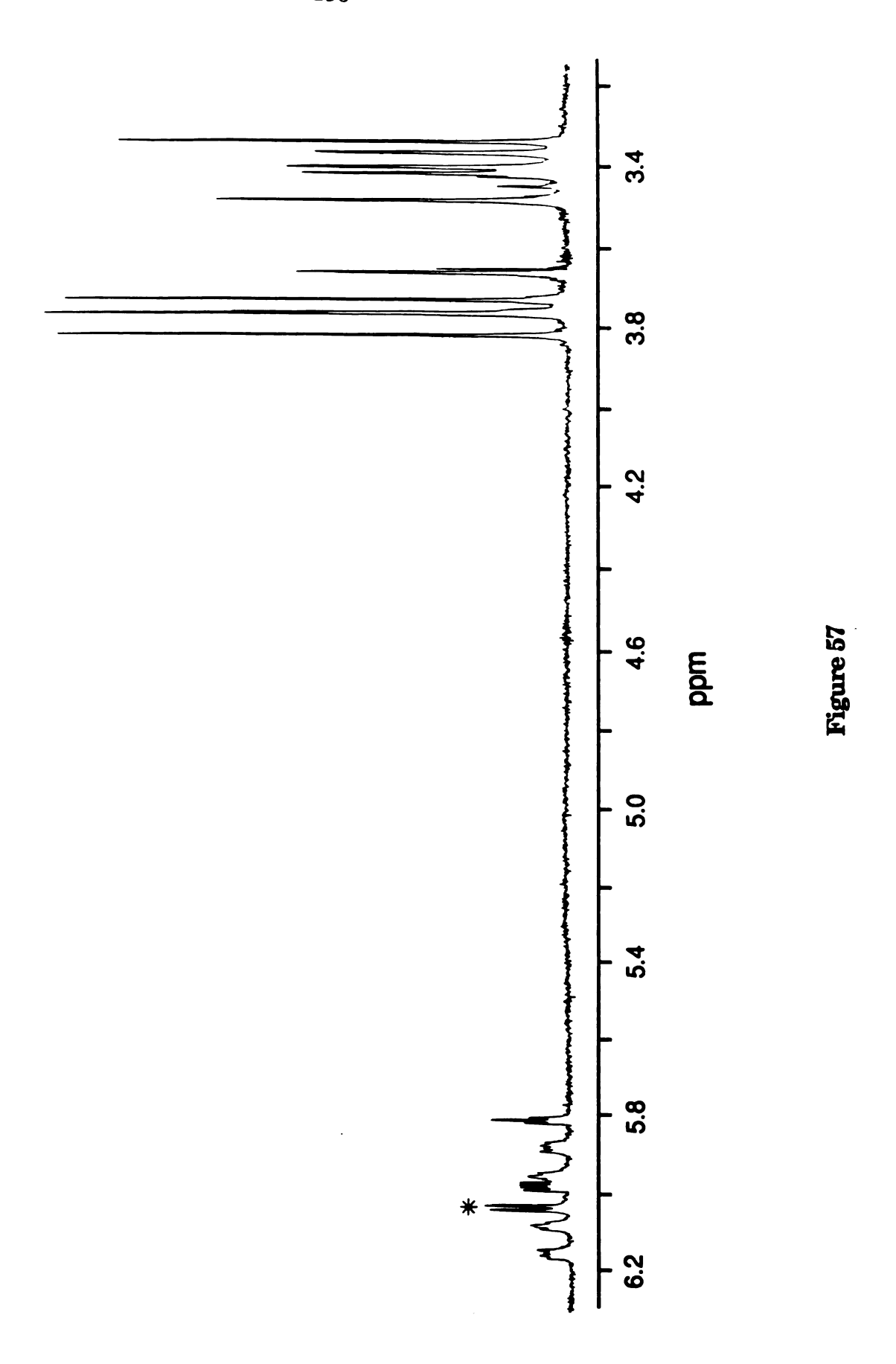


Figure 58. Schematic diagram outlining a proposed reaction sequence in the formation of $Os_3(\mu\text{-OH})_2(TMPP)CO)_9$ and $Os_3(\mu\text{-OH})(TMPP-O)(CO)_9$.

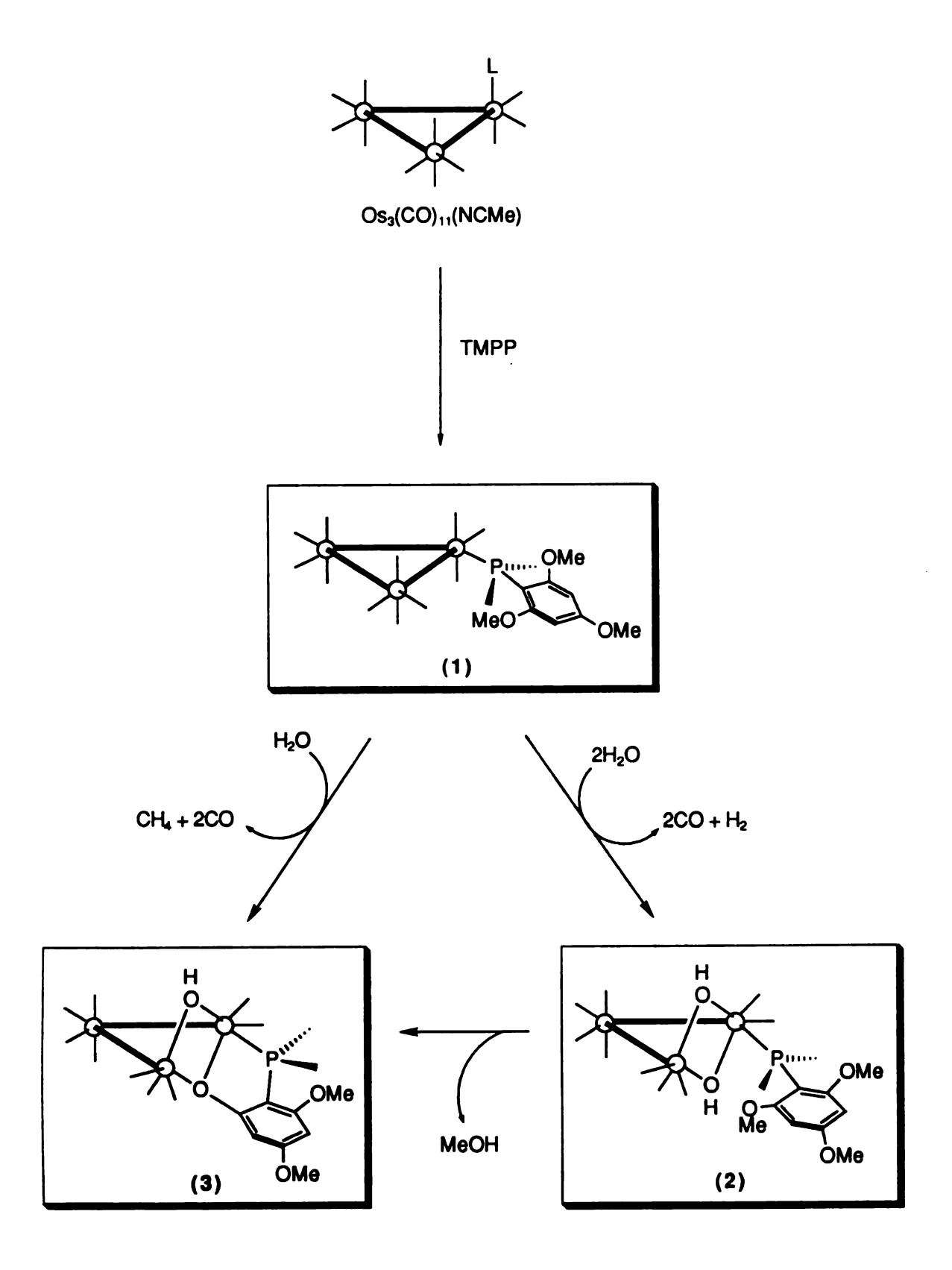


Figure 58

B. Molecular Structure

(1) $Os_3(\mu\text{-OH})_2(CO)_9(TMPP)$

The molecular structure of $Os_3(\mu-OH)_2(CO)_9(TMPP)$ is shown in Figure 59. Crystallographic data are given in Table 18, and selected bond distances and angles are listed in Table 19. The molecule contains a triangular arrangement of osmium atoms in which Os(2) is bonded to four terminal carbonyl ligands, Os(1) is attached to three terminal carbonyl groups, and Os(3) is bonded to two terminal carbonyl ligands and one phosphine group. Additionally, the edge Os(1) and Os(2) is bridged by two uhydroxide ligands. The unbridged metal-metal bond distances are Os(1)— Os(2) = 2.833(1) Å and Os(2) - Os(3) = 2.844(1) Å. The doubly-bridged edge with an Os(1)....Os(3) separation of 3.114 (2) Å would be expected to involve no significant metal-metal orbital overlap by distance considerations as well as electron count. The two hydroxide ligands form two pseudosymmetrical bridges across Os(1) and Os(2); the osmium-oxygen distances are Os(1)—O(10) = 2.10 (1) Å, <math>Os(3)—O(10) = 2.13 (1) Å, <math>Os(1)—O(11) = 2.06 (1)Å, Os(3)—O(11) = 2.09 (1) Å, and the angles Os(1)—O(10)—Os(3) and Os(1)— O(11)—Os(3) are 95.2 (5) and 97.1 (5)°, respectively. An angular distortion observed at the ortho-methoxy group may be explained by the involvement of hydrogen bonding between the hydrogen H[O(11)] and the lone-pair of electrons on the atom O(12). The ortho-methoxy group interacts significantly with one of the bridging hydroxy groups via hydrogen bonding. The hydrogen atoms were not located during the crystallography refinement, but the distance between the oxygen atom of the hydroxy group and methoxy group is only 2.521 (1) Å, clearly indicating the presence of a hydrogen bond.

Table 18. Crystal Data for $Os_3(\mu\text{-OH})_2(CO)_9(TMPP)$ (1) and $Os_3(\mu\text{-OH})(CO)_9(\mu\text{-}\eta^2\text{-TMPP-}O)$ (2)

	(1)	(2)
Formula	$Os_3P_1O_{20}C_{36}H_{35}$	$Os_3P_1O_{19}C_{35}H_{31}$
Formula weight	1389.24	1357.19
Crystal system	Triclinic	Monoclinic
Space group	P-1	P2 ₁ /n
a, Å	11.435 (5)	16.088 (2)
b, Å	13.079 (8)	13.108 (1)
c, Å	14.116 (9)	19.601 (2)
α, deg	96.44 (5)	90
β, deg	93.08 (5)	90.38 (1)
γ, deg	95.23 (4)	90
V, Å ³	2085 (2)	4133.5 (9)
\mathbf{z}	2	4
d _{calc} , g/cm ³	2.213	2.181
Crystal size, mm	0.10 x 0.08 x 0.15	0.30 x 0.15 x 0.10
Radiation	Mo K _α ($\lambda = 0.71073 \text{ Å}$)	Cu $K_{\alpha}(\lambda = 1.54184 \text{ Å})$
μ, cm ⁻¹	92.491	180.610
Data collection instrument	Nicolet P3/F	Siemens P3/V
Temperature, °C	-95 ± 2	-95 ± 2
Scan method	$\omega - 2\theta$	$\omega - 2\theta$
Data col. range, 20, deg.	4 – 40	4 – 106
R ^a	0.038	0.089
R _w ^b	0.046	0.061

 $a R = \Sigma | |F_o| - |F_c| |/\Sigma| F_o|$

 $b R_w = [\Sigma w | F_o | - | F_c |)^2 / \Sigma w | F_o |^2]^{1/2}; w = 1/\sigma^2 (| F_o |)$

Table 19. Selected Bond Distances (Å) and Angles (deg) for Os₃(μ-OH)₂(CO)₉(TMPP).

Atom 1	Atom 2	Distance	Atom 1	Atom 2	Distance
Os(1)	Os(3)	3.114 (2)	Os(2)	C(6)	1.97 (3)
Os(1)	Os(2)	2.833 (1)	Os(2)	C(7)	1.94 (3)
Os(2)	Os(3)	2.844 (1)	Os(3)	P(1)	2.477 (5)
Os(1)	C(1)	1.83 (3)	Os(3)	C(8)	1.91 (3)
Os(1)	C(2)	1.85 (3)	Os(3)	C(9)	1.97 (3)
Os(1)	C(3)	1.97 (3)	Os(3)	б	2.13 (1)
Os(1)	Ö	2.10 (1)	Os(3)	ප	2.09 (1)
Os(1)	ප	2.06 (1)	P(1)	C11	1.82 (2)
Os(2)	C(4)	1.99 (3)	P(1)	C21	1.82 (2)
Os(2)	C(5)	1.97 (3)	P(1)	C31	1.86 (2)

Atom 1	Atom 1 Atom 2 Atom 3	Atom 3	Angle	Atom 1	Atom 2 Atom 3	Atom 3	Angle
Os(2)	Os(1)	Ø	81.7 (3)	Os(2)	Os(3)	20	79.7 (3)
Os(2)	Os(1)	8	80.4 (3)	P(1)	Os(3)	Б	88.6 (4)
Os(1)	Os(2)	Os(3)	66.59 (3)	P(1)	Os(3)	8	94.3 (3)
Os(2)	Os(3)	P(1)	169.1 (1)	Os(1)	Ö	Os(3)	95.2 (5)
Os(2)	Os(3)	ಶ	80.8 (3)	Os(1)	8	Os(3)	97.1 (5)

Figure 59. An ORTEP diagram of $Os_3(\mu\text{-OH})_2(TMPP)(CO)_9$, showing the atom labeling scheme. All phenyl-group carbon atoms of TMPP are represented as small circles for clarity, and all other atoms are represented by their 40% propability ellipsoids.

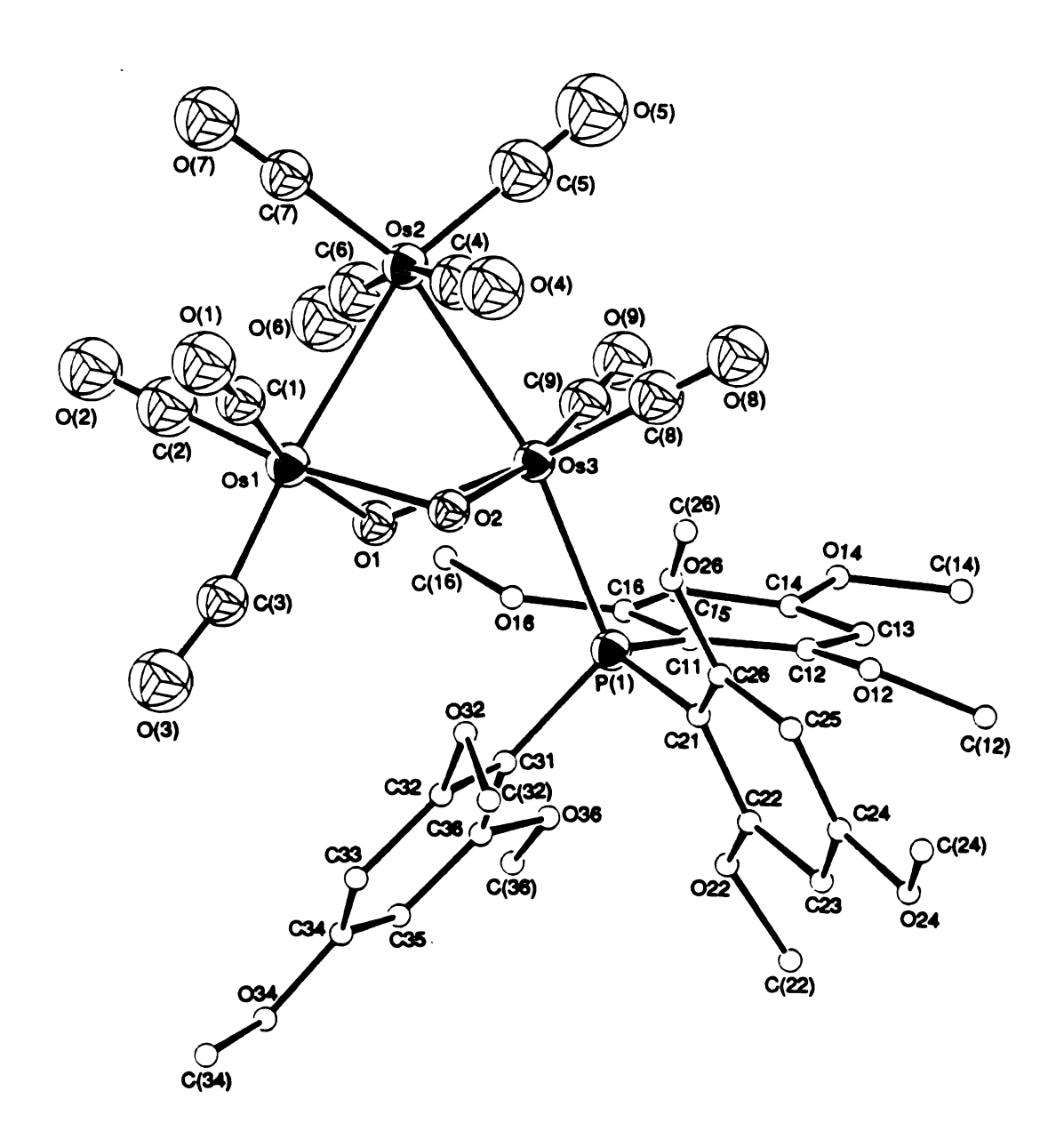


Figure 59

(2) $Os_3(\mu-OH)(CO)_9(\mu-\eta^2-TMPP-O)$

The molecular structure of $Os_3(\mu-OH)(CO)_9(\mu-\eta^2-TMPP-O)$ is shown in Figure 60. Crystallographic data are listed in Table 18, and selected bond distances and angles are given in Table 20. The cluster consists of a triosmium framework containing two metal-metal bonds, namely Os(1)-Os(2) = 2.835 (3) Å and Os(2)—Os(3) = 2.843 (2) Å, and one open edge [Os(1)...Os(3) = 3.099 (3) Å] supported by one hydroxy ligand [Os(1)...O(10) =2.12(2) Å; Os(3)—O(10) = 2.17(2) Å], and one phenoxide group [Os(1)—O(11) = 2.12 (2) Å; Os(3)—O(11) = 2.24 (2) Å]. The demethylated TMPP is triply bonded to two osimium atoms Os(1) and Os(3) with the oxygen atom O(11) as a bridging ligand among the edge of Os(1) and Os(3). The phosphorus atom is bound to Os(3) as a terminal group. The phenoxide group allows for the tridentate coordination mode of μ - η^2 -(TMPP-O) and provides a fivemembered metallacycle containing Os(3)—P(1)—C(32)—C(32)—O(11) as a chelating group. The main features of both molecular structures (1) and (2) are highlighted in Figure 61 where it can be seen that the molecules contain very similar trinuclear frameworks with one open Os...Os edge bridged by two oxygen atoms.

5. Summary

The versatile coordination ability of the tertiary phosphine TMPP has been well-demonstrated in the aforementioned reactions with Group 8 metal carbonyl clusters. In the reaction with $Fe_3(CO)_{12}$, the formation of a new salt [HTMPP][HFe₃(CO)₁₁] supports the previous literature report that ion-pair coupling in [HFe₃(CO)₁₁] salts is greatly influenced by the steric bulk of counter cation; in this case, the size of TMPP precludes any interaction. Both reactions of $Ru_3(CO)_{12}$ and also the activated species

Ru₃(CO)₁₁(NCMe) with TMPP proceed by oxidative addition of the P—C bond, leading to formation of a new 46-electron unsaturated cluster such as Ru₃(μ -CO)₂(CO)₆(μ ₃- η ²-R)(μ -PR₂) (R = 2,4,6-C₆H₂(OMe)₃). The cluster-mediated ligand transformation observed in this system is uncharacteristically facile, occurring under very mild conditions compared to previously reported reactions of this type. The reactions of triosmium carbonyl clusters with the phosphine TMPP gave two hydroxy-bridged triosmium carbonyl clusters, namely Os₃(μ -OH)₂(CO)₉(TMPP) and Os₃(μ -OH)(CO)₉(μ - η ²-TMPP-O). Structural determinations on the molecules revealed that both clusters consist of similar open frameworks with two oxygen atoms doubly-bridging one Os···Os open edge.

In this study, the phosphine, tris(2,4,6-trimethoxyphenyl)phosphine, exhibits great reactivity toward the low valent metal complexes with π -acceptors. The presence of mixed-donors, i.e. phosphorus and oxygen atoms, provides the ligand with good chelate tendencies. Reversible coordination of certain interactions, especially the M-ether bonds, of TMPP-containing cluster complexes is considered to be feasible based on the results of this work.

Table 20. Selected Bond Distances (Å) and Angles (deg) for $Os_3(\mu-OH)(CO)_9[\mu-\eta^2-(TMPP-O)]$.

Atom 1	Atom 2	Distance	Atom 1	Atom 2	Distance
Os(1)	Os(3)	3.099 (3)	Os(2)	C(6)	1.88 (4)
)s(1)	Os(2)	2.835 (3)	Os(2)	C(7)	2.06 (6)
(2)	Os(3)	2.843 (2)	Os(3)	P(1)	2.36 (1)
)s(1)	C(1)	1.94 (4)	Os(3)	C(8)	1.83 (6)
)s(1)	C(2)	1.84 (4)	Os(3)	C(9)	1.80 (3)
)s(1)	C(3)	1.75 (5)	Os(3)	0(10)	2.17 (2)
)a(1)	0(10)	2.14 (2)	Os(3)	0(11)	2.24 (2)
Os(1)	0(11)	2.12 (2)	P(1)	C(11)	1.80 (3)
) s (2)	C(4)	2.07 (4)	P(1)	C(21)	1.86 (3)
Os(2)	C(5)	2.96 (5)	P(1)	C(31)	1.85 (4)

Atom 1	Atom 2	Atom 3	Angle	Atom 1	Atom 1 Atom 2 Atom 3	Atom 3	Angle
Os(2)	Os(1)	O(10)	82.4 (6)	Os(2)	Os(3)	0(11)	82.0 (5)
Os(2)	Os(1)	0(11)	84.3 (6)	P(1)	Os(3)	O(10)	88.6 (5)
Os(1)	Os(2)	0s(3)	57.04 (6)	P(1)	Os(3)	0(11)	84.0 (6)
Os(2)	Os(3)	P(1)	164.6 (3)	Os(1)	O(10)	Os(3)	92.1(8)
0s(2)	0s(3)	O(10)	81.7 (5)	Os(1)	0(11)	Os(3)	90.7(9)

Figure 60. ORTEP diagram of $Os_3(\mu\text{-OH})(TMPP\text{-}O)(CO)_9$, showing the atom labeling scheme. All phenyl-group carbon atoms of TMPP are represented as small circles for clarity.

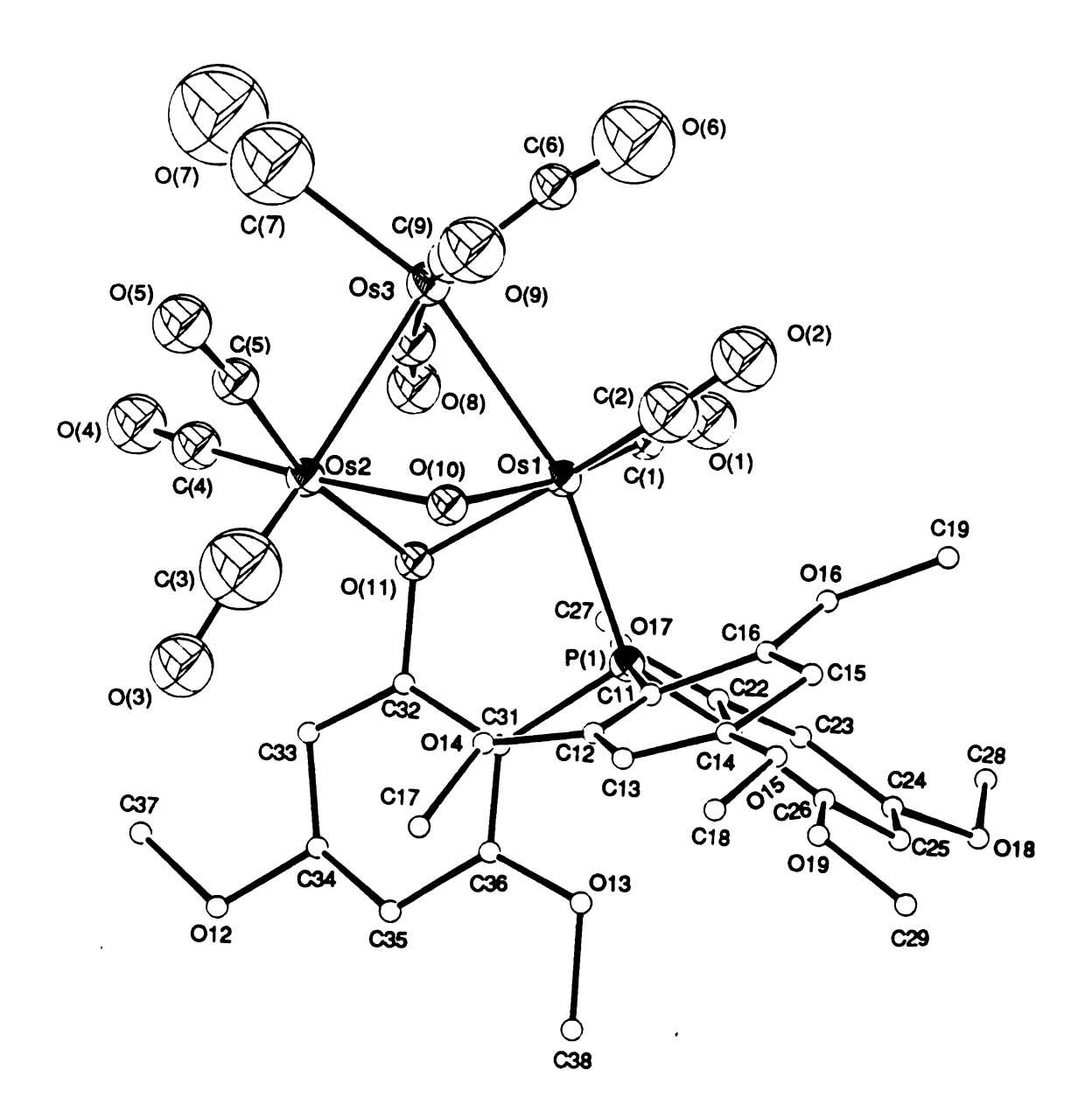


Figure 60

Figure 61. Main features of the molecular structures of (a) $Os_3(\mu - OH)_2(TMPP)(CO)_9$ and (b) $Os_3(\mu - OH)(TMPP-O)(CO)_9$.

Figure 61

CHAPTER VI

FINAL REMARKS

The aforementioned studies outline new directions in the syntheses of reactive mixed-ligand complexes at the interface of coordination and organometallic complexes.

In our initial project, we synthesized a novel bridging hydride dirhenium species Re₂(μ-H)(μ-Cl)Cl₂(CO)₂(dppm)₂ by the investigation of the reaction between $Re_2Cl_4(dppm)_2$ ($Re^{-3}Re$) ($dppm = Ph_2PCH_2PPh_2$) and the electronically and coordinatively unsaturated molecule $\mathrm{H_2Os_3(CO)_{10}}$ in the presence H₂. Further elucidations of various alternative reactions suggested the formation of the bridging hydride dirhenium complex might be achieved by different reaction pathways, namely, by hydride transfer reaction via a metal hydride coupling between the different metal system, or directly from an unprecedented H₂ activation reaction. Moreover, a new carbonyl halide cluster, Ru₃(CO)₈(Cl)₂(PBu₃ⁿ)₂, was synthesized from the reaction between the multiply bonded dirhenium complex Re₂Cl₆(PBu₃ⁿ)₂ (Re-Re) and Ru₃(CO)₁₂. Both results demonstrate the feasibility of preparing mixed ligand complexes by ligand transfer reactions between two entirely different metal systems; this new synthetic approach provides a promising opportunity for the syntheses of unusual coordination and organometallic compounds.

In a second area of investigation, we explored the chemistry of new transition metal phosphine complex with unusual properties. Our study of TMPP chemistry with dinuclear metal—metal bonded systems led to the discovery of unsymmetrical complexes containing an unusual bridging phenoxy—phosphine ligand. Furthermore, the phosphine ligand, TMPP was shown to exhibit novel chemistry with trinuclear cluster complexes. In the chemistry of Group 8 carbonyls of Fe, Ru and Os, we observed facile cluster transformations under extraordinarily mild conditions compared to

all previously reported phosphine reactions of these systems; some oxidative addition reactions were also discovered in the courses of the study of reactions with this highly nucleophilic phosphine. In particular, results such as facile P-C bond activation by intramolecular oxidative addition and cyclometallation in the triruthenium system, and demethylation of the phosphine to give an open trinuclear phenoxy-phosphine cluster in the triosmium system are promising for future organometallic chemistry.

Future directions for this research include mechanistic studies of H_2 reactions with triply bonded dinuclear complexes and further investigations of the role of steric versus electronic factors in dictating the chemistry of the ether-phosphine tris(2,4,6-trimethoxyphenyl)phosphine.

REDEPENDENCES

- Cotton, F. A.; Wilkinson, G. Advanced Inorganic Chemistry, 5th ed.;
 J. Wiley and Sons: New York, 1988.
- (a) Cotton, F. A.; Walton, R. A. Multiple Bonds Between Metal Atoms; Wiley-Intersience: New York, 1982. (b) Cotton, F. A.; Walton, R. A. Structure and Bonding, 1985, 62, 1. (c) Cotton, F. A.; Chisholm, M. H. Chem. Eng. News 1982. 60. 40.
- 3. Chisholm, M. H.; Huffman, J. C.; Koh, J. J. Polyhedron, 1989, 8, 127.
- (a) Moynihan, K. J.; Gao, X.; Boorman, P. M.; Fait, J. F.; Freeman, G. K. W.; Thronton, P.; Ironmonger, D. J. Inorg. Chem. 1990, 29, 1648.
 (b) Bott, S. G.; Clark, D. L.; Green, M. L. H.; Mountford, P. J. Chem. Soc., Chem. Commun. 1989, 418.
 (c) Cotton, F. A.; Luck, R. L. Inorg. Chem. 1989, 28, 182.
 (d) Cotton, F. A.; Poli, R. Inorg. Chem. 1987, 26, 3310.
 (e) Bergs, D. J.; Chisholm, M. H.; Folting, K.; Huffman, J. C.; Stahl, K. A. Inorg. Chem. 1988, 27, 2950.
 (f) Nocera, D. G.; Gray, H. B. Inorg. Chem. 1984, 23, 3686.
- (a) Cotton, F. A.; Eglin, J. L.; Luck, R. L.; Son, K. Inorg. Chem. 1990, 29, 1802.
 (b) Mui, H. D.; Poli, R. Inorg. Chem. 1989, 28, 3609.
 (c) Chacon, S. T.; Chisholm, M. H.; Streib, W. E.; Van der Sluys, W. Inorg. Chem. 1989, 28, 5.
 (d) Schrock, R. R.; Sturgeoff, L. G.; Sharp, P. R. Inorg. Chem. 1983, 22, 2801.
 (e) Jackson, R. B.; Streib. W. E. Inorg. Chem. 1971, 10, 1760.
- 6. Chisholm, M. H. Acc. Chem. Res. 1990, 23, 419.
- 7. Braydich, M. D.; Bursten, B. E.; Chisholm, M. H.; Clark, D. L. J. Am. Chem. Soc. 1985, 107, 4450.
- 8. Chisholm, M. H. Organometallics 1989, 8, 67.

- 9. Chisholm, M. H. Pure & Appl. Chem. 1989, 61, 1707.
- M—M bond cleavage in multiply bonded dinuclear complexes:
 (a) Bakir, M.; Cotton, F. A.; Cudahy, M. M.; Simpson, C. Q.; Smith, T. J.; Vogel, E. F.; Walton, R. A. Inorg. Chem. 1988, 27, 2608. (b) Bucknor, S.; Cotton, F. A.; Falvello, L. R.; Reid, A. H. Jr.; Schmulbach, C. D. Inorg. Chem. 1986, 25, 1021. (c) Hertzer, C. A.; Myers, R. E.; Brant, P.; Walton, R. A. Inorg. Chem. 1978, 17, 2383.
- Edge-sharing bioctohedral Re₂ complexes with π -acceptor ligands: 11. (a) Cotton, F. A. Polyhedron 1987, 6, 667. (b) Price, A. C.; Walton, R. A. Polyhedron 1987, 6, 729. (c) Anderson, L. B.; Cotton, F. A.; Dunbar, K. R.; Falvello, L. R.; Price, A. C.; Reid, A. H.; Walton, R. A. Inorg. Chem. 1987, 26, 2717. (d) Fanwick, P. E.; Price, A. C.; Walton, R. A. *Inorg. Chem.* **1987**, *26*, 3920. (e) Anderson, L. B.; Barder, T. J.; Cotton, F. A.; Dunbar, K. R.; Falvello, L. R.; Walton, R. A. Inorg. Chem. 1986, 25, 3629. (f) Anderson, L. B.; Barder, T. J.; Esjornson, D.; Walton, R. A. J. Chem. Soc., Dalton Trans. 1986, 2607. (g) Cotton, F. A.; Dunbar, K. R.; Price, A. C.; Schwotzer, W.; Walton, R. A. J. Am. Chem. Soc. 1986, 108, 4843. (i) Cotton, F. A.; Dunbar, K. R.; Falvello, L. R.; Walton, R. A. Inorg. Chem. 1985, 24, 4180. (j) Anderson, L. B.; Barder, T. J.; Walton, R. A. Inorg. Chem. 1985, 24, 1421. (k) Barder, T. J.; Cotton, F. A.; Falvello, L. R.; Walton, R. A. Inorg. Chem. 1985, 24, 1258. (1) Cotton, F. A.; Daniels, L. M.; Dunbar, K. R.; Falvello, L. R.; Tetrick, S. M.; Walton, R. A. J. Am. Chem. Soc. 1985, 107, 3524. ($Re_2Cl_4(CO)_2(dppm)_2$)
- 12. Cotton, F. A.; Daniels, L. M.; Dunbar, K. R.; Falvello, L. R.; Tetrick, S. M.; Walton, R. A. J. Am. Chem. Soc. 1985, 107, 3524.
- (a) Price, A. C.; Walton, R. A. Polyhedron 1987, 6, 729. (b) Anderson,
 L. B.; Cotton, F. A.; Dunbar, K. R.; Falvello, L. R.; Price, A. C.; Reid,
 A. H.; Walton, R. A. Inorg. Chem. 1987, 26, 2717.
- 14. Recent work on the heteroatomic chelate metal complexes:

- (a) Pottier, Y.; Mortreux, A.; Petit, F. J. Organomet. Chem. 1990, 370, 333. (b) Stephan, D. W. Coor. Chem. Revs. 1989, 95, 41. (c) Park, S.; Johnson, M. P.; Roundhill, D. M. Organometallics 1989, 8, 1700. (d) Kraft, M. E.; Wilson, L. J.; Onan, K. D. Organometallics 1988, 7, 2528. (e) Ferguson, G. S.; Wolczanski, P. T.; Parkanyi, L.; Zonnevylle, M. C. Organometallics 1988, 11, 531. (f) Anderson, P. M.; Casalnuovo, A. L.; Johnson, B. J.; Mattson, B. M.; Mueting, A. M.; Pignolet, L. H. Inorg. Chem. 1988, 27, 1649. (g) Wang, H. H.; Casalnuovo, A. L.; Johnson, B. J.; Mueting, A. M.; Pignolet, L. H. Inorg. Chem. 1988, 27, 325. (i) Bullock, R. M.; Casey, C. P. Acc. Chem. Res. 1987, 20, 167.
- 15. Keim, W.; Behr, A.; Gruber, B.; Hoffman, B.; Kowaldt, F. H.; Kurschner, U.; Limbacker, B.; Sistig, F. P. Organometallics 1986, 5, 2356.
- Reviews on transition metal phosphine complexes:

 (a) McAuliffe, C. A. Comprehensive Coordination Chemistry;
 Pergamon Press: Oxford, 1987, Vol. 2, Ch. 14, p. 989. (b) Casey, C. P. J. Chem. Ed. 1986, 63, 189. (c) Pibnolet, L. H. Homogeneous Catalysts with Metal Phosphine Complexes; Plenum Press: New York, 1983.
 (d) Alyea, E. C.; Meek, D. W. Catalytic Aspects of Metal Phosphine Complexes; Advances in Chemistry, 196; American Chemical Society: Washington, DC, 1982. (e) Kagan, H. B. Comprehensive Organometallic Chemistry; Pergamon Press: Oxford, England, 1982, Vol 8, p. 464. (f) Parshall, G. W. Homogeneous Catalysts: The Applications and Chemistry of Catalysts by Soluble Transition Metal Complexes; Wiley: New York, 1980. (g) Stelzer, O. Top. Phosphorus Chem. 1977, 9, 1.
- 17. Functionalized phosphine complexes with P~N donors:
 (a) Katti, K. V.; Cavell, R. G. Comments Inorg. Chem. 1990, 10, 53.
 (b) Cooper, M. K.; Organ, G. J. J. Chem. Soc., Dalton Trans. 1988, 2287.
 (c) Organ, G. J.; Cooper, M. K.; Henrick, K.; McPartlin, M. J. Chem. Soc., Dalton Trans. 1984, 2377.

- Functionalized phosphine complexes with P~O donors:
 (a) Bader, A.; Linder, E. Coord. Chem. Rev. 1991, 108, 1. (b) Linder, E.; et al. Chem. Ber. 1990, 123, 459. (c) Linder, E.; et al. Chem. Ber. 1990, 123, 1469. (d) Linder, E.; et al. J. Chem. Soc., Dalton Trans. 1990, 3107. (e) Linder, E.; et al. Chem. Ber. 1988, 121, 829. (f) Rauchfuss, T. B.; et al. Inorg. Chem. 1979, 18, 2656. (g) Rauchfuss, T. B.; et al. J. Am. Chem. Soc. 1979, 101, 1045. (i) Rauchfuss, T. B.; et al. Inorg. Chem. 1977, 16, 2966. (j) Rauchfuss, T. B.; et al. J. Am. Chem. Soc. 1975, 14, 652. (k) Empsall, H. D.; Mentzer, E.; Shaw, B. J. J. Chem. Soc., Chem. Commun. 1975, 861. (l) Mason, R.; Tomas, K. M.; Empsall, H. D.; Fletcher, S. R.; Heys, P. N.; Hyde, E. M.; Johns, C. E.; Shaw, B. J. J. Chem. Soc., Chem. Commun. 1974, 615.
- 19. Rahman, M. M.; Liu, H. Y.; Eriks, K.; Prock, A.; Giering, W. P. Organometallics 1989, 8, 1.
- 20. Wada, M.; Higashizaki, S. J. Chem. Soc. Chem. Commun. 1984, 482.
- (a) Bowmaker, G. A.; Cotton, J. D.; Healy, P. C.; Kildea, J. D.; Silong, S. B.; Skelton, B. W.; White, A. H. Inorg. Chem. 1989, 28, 1462. (b)
 Wada, M. J. Synthetic Organic Chemistry, Japan. 1986, 44, 957. (c)
 Wada, M.; Higashizaki, S.; Tsuboi, A. J. Chem. Res. Synop. 1985, 38;
 J. Chem. Res. Miniprint 1985, 467.
- 22. Tolman, C. A. J. Am. Chem. Soc. 1970, 92. 2956.
- 23. Otsuka, S.; Yoshida, T.; Matsumoto, M.; Nakatsu, K. J. Am. Chem. Soc. 1976, 98, 5850.
- Recent work on steric and electronic effects on M—P bonding:
 (a) Dunne, B. J.; Morris, R. B.; Orpen, A. G. J. Chem. Soc., Daiton Trans. 1991, 653.
 (b) Orpen, A. G.; Salter, I. D. Organometallics, 1991, 10, 111.
 (c) Rahman, M. M.; Liu, H. Y.; Eriks, K.; Prock, A.; Giering, W. P. Organometallics 1989, 8, 1.
 (d) Rahman, M. M.; Liu, H. Y.; Prock, A.; Giering, W. P. Organometallics 1987, 6, 650.
 (e)

- Golovin, M. N.; Rahman, M. M.; Belmonte, J. E.; Giering, W. P. Organometallics 1985, 4, 1981.
- 25. (a) Dunbar, K. R.; Haefner, S. C.; Pence, L. E. J. Am. Chem. Soc.
 1989, 111, 5504. (b) Dunbar, K. R.; Haefner, S. C. Organometallics
 1992, 113, 0000. (c) Haefner, S. C.; Dunbar, K. R.; Bender, C. J. Am. Chem. Soc. 1991, 113, 0000. (d) Dunbar, K. R.; Haefner, S. C.;
 Swepston, P. N. J. Chem. Soc., Chem. Commun. 1991, 460.
- 26. Dunbar, K. R.; Quillevere, A. to be published.
- (a) Rardin, R. L.; Tolman, W. B.; Lippard, S. J. New J. Chem. 1991, 15, 417.
 (b) Mehrotra, R. C.; Bohra, R. Metal Carboxylates; Academic: New York, 1983.
 (c) Catterick, J.; Thronton, P. Adv. Inorg. Chem. Radiochem. 1977, 20, 291.
 (d) Oldham C.; Prog. Inorg. Chem. 1968, 10, 223.
- (a) Cotton, F. A.; Walton, R. A. Multiple Bonds Between Metal Atoms, Wiley-Intersience: New York, 1982 and references therein.
 (b) Boyer, E. B.; Robinson, S. D. Coord. Chem. Rev. 1983, 50, 109. (c) Felthouse, T. R. Prog. Inorg. Chem. 1982, 29, 73.
- (a) Creutz, C. Prog. Inorg. Chem. 1983, 30, 1. (b) Richarson, D. E.;
 Taube, H. Coord. Chem. Rev. 1984, 60, 107. (c) Meyer, T. J. Acc.
 Chem. Res. 1978, 1, 94. (d) Clark, R. J. H. Chem. Soc. Rev. 1984, 13, 219.
- 30. Rardin, R. L.; Tolman, W. B.; Lippard, S. J. New J. Chem. 1991, 15.
- (a) Deeming, A. J. Adv. Organomet. Chem. 1986, 26, 1. (b)
 Dahlinger, K.; Poe, A. J.; Sayal, P. K.; Sekhar, V. K. J. Chem. Soc.,
 Dalton Trans. 1986, 2145. (c) Foulds, G. A.; Johnson, B. F. G.; Lewis,
 J. Organomet. Chem. 1985, 294, 123. (d) Burgress, K. Polyhedron
 1984, 3, 1175.
- 32. Hydrogen transfer reaction:

- James, B. R. Comprehensive Organometallic Chemistry; Wilkinson, G., Stone, F. G. A., Abel, E. W. (Eds.); A. Wheaton & Co. Ltd.: Exeter, 1982; Vol. 8, Chapter 51, p 285.
- Cis stabilizing interaction of hydride and hydrogen:
 Van der Sluys, L. S.; Eckert, J.; Eisenstein, O.; Hall, J. H.; Huffman, J. C.; Jackson, S. A.; Kostzle, T. F.; Kubas, G. J.; Vergamini, P. J.; Caulton, K. G. J. Am. Chem. Soc. 1990, 112, 4831.
- 34. Interconversion of hydride and dihydrogen:
 Luo, X. L.; Crabtree, R. H. J. Am. Chem. Soc. 1990, 112, 6912.
- 35. Reactions of H₂ with multiply bonded dinuclear complexes:

 (a) Bucknor, S.; Cotton, F. A.; Falvello, L. R.; Reid, A. H.;

 Schmulbach, C. D. *Inorg. Chem.* 1987, 26, 2954. (b) Bucknor, S.;

 Cotton, F. A.; Falvello, L. R.; Reid, A. H.; Schmulbach, C. D. *Inorg. Chem.* 1986, 25, 1021.
- 36. Redox reactions of dirhenium complexes:
 (a) Walton, R. A. Polyhedron 1989, 8, 1689. (b) Esjornson, D.;
 Derringer, D. R.; Fanwick, P. E.; Walton, R. A. Inorg. Chem. 1989, 28, 2821.
- 37. Chemistry of mixed metal clusters:
 (a) Braunstein, P. Nouv. J. Chim. 1986, 10, 365. (b) Sappa, E.;
 Tiripicchio, A.; Braunstein, P. Coord. Chem. Rev. 1985, 65, 219. (c)
 Geoffroy, G. L. Acc. Chem. Res. 1980, 13, 469.
- Mixed-metal clusters synthesized from H₂Os₃(CO)₁₀:
 (a) Adams, R. D.; Babin, J. E.; Tasi, M. Organometallics 1988, 7, 219.
 (b) Jan, D. Y.; Hsu, L. Y.; Hsu, W. L.; Shore, G. S. Organometallics 1987, 6, 274.
 (c) Hsu, L. Y.; Hsu, W. L.; Jan, D. Y. Organometallics 1986, 5, 1041.
 (d) Trirpicchio, A.; Camellimi, M. T.; Sappa, E. J. Chem. Soc. Dalton Trans. 1984, 627.
 (e) Hsu, L. Y.; Hsu, W. L.; Jan, D. Y.; Marshall, A. G.; Shore, S. G. Organometallics 1984, 3, 591.
 (f) Shore, S. G.; Hsu, W. L.; Churchill, M. R.; Bueno, C. J. Am. Chem.

- Soc. 1983, 105, 655. (g) Shore, S. G.; Hsu, W. L.; Weisenberger, C. R.; Caste, M. L.; Churchill, M. R.; Bueno, C. Organometallics 1982, 1, 1405. (h) Churchill, M. R.; Bueno, C.; Kennedy, S.; Bricker, J. C.; Plotkin, J. S.; Shore, S. G. Inorg. Chem. 1982, 21, 627. (i) Churchill, M. R.; Bueno, C.; Hsu, W. L.; Plotkin, J. S.; Shore, S. G. Inorg. Chem. 1982, 21, 1958. (j) Plotkin, J. S.; Alway, D. G.; Weisenberger, C. R.; Shore, S. G. Inorg. Chem. 1980, 102, 6157.
- Bucknor, S.; Cotton, F. A.; Falvello, L. R.; Reid, A. H.; Schmulbach,
 C. D. *Inorg. Chem.* 1987, 26, 2954.
- 40. Synthesis of H₂Os₃(CO)₁₀:
 (a) Johnson, B. F. G.; Lewis, J.; Kilty, P. A. J. Chem. Soc. A. 1968,
 2859. (b) Knox, S. A. R.; Koepke, J. W.; Andrews, M. A.; Kaesz, H. D. J. Am. Chem. Soc. 1975, 97, 3942.
- Churchill, M. R.; Bueno, C.; Kennedy, S.; Bricker, J. C.; Plotkin, J. S.; Shore, S. G. *Inorg. Chem.* 1982, 21, 627.
- 42. Synthesis of H₄Ru₄(CO)₁₂:
 (a) Johnson, B. F. G.; Lewis, J.; Kilty, P. A. J. Chem. Soc. A . 1968,
 2859. (b) Knox, S. A. R.; Koepke, J. W.; Andrews, M. A.; Kaesz, H. D. J. Am. Chem. Soc. 1975, 97, 3942.
- 43. Metal hydride coupling:
 - (a) Shapley, J. R.; Pearson, G. A.; Tachikawa, M.; Schmidt, G. E.;
 Churchill, M. R.; Hollander, F. J. J. Am. Chem. Soc. 1977, 99, 8064.
 (b) Churchill, M. R.; Hollander, F. J.; Lashewycz, R. A.; Pearson, G. A.; Shapley, J. R. J. Am. Chem. Soc. 1981, 103, 2430.
- 44. Bridging hydride complexes with unusual chemical shifts:
 (a) Chisholm, M. H.; Eichhorn, B. W.; Huffman, J. C.; Smith, C. A. Organometallics 1986, 8, 67. (b) Chisholm, M. H.; Huffman, J. C.; Smith, C. A. J. Am. Chem. Soc. 1986, 108, 222. (c) Chisholm, M. H.; Eichhorn, B. W.; Huffman, J. C.; Smith, C. A. J. Chem. Soc., Chem.

Commun. 1985, 861. (d) Wilson, R. B.; Sattelberger, A. P.; Huffman, J. C. J. Am. Chem. Soc. 1982, 104, 858.

45. Evans methods:

- (a) Evans, D. F. J. Chem. Soc. 1959, 2003.(b) Deutsch, J. L.; Poling, S. M. J. Chem. Educ. 1969, 46, 167.
- 46 Chisholm, M. H.; Huffman, J. C.; Smith, C. A. J. Am. Chem. Soc. 1986, 108, 222.
- Anderson, L. B.; Cotton, F. A.; Dunbar, K. R.; Falvello, L. R.; Price,
 A. C.; Reid, A. H.; Walton, R. A. Inorg. Chem. 1987, 26, 2717.
- 48. Diamagnetic anisotropy in multiply bonded dinuclear complexes: McGlinchey, M. J. Inorg. Chem. 1980, 19, 1392.
- 49. T₁ criterion for transition metal hydrides:
 (a) Desrosiers, P. J.; Cai, L.; Lin, Z.; Richards, R.; Halpern, J. J. Am. Chem. Soc. 1991, 113, 4173. (b) Luo, X.-L.; Crabtree, R. H. J. Am. Chem. Soc. 1990, 112, 4813. (c) Crabtree, R. H. Acc. Chem. Res. 1990, 23, 95. (d) Cotton, F. A.; Luck, R. L.; Root, D. R.; Walton, R. A. Inorg. Chem. 1990, 29, 43. (e) Luo, X.-L.; Crabtree, R. H. Inorg. Chem. 1989, 28, 3775. (f) Cotton, F. A.; Luck, R. L. Inorg. Chem. 1989, 28, 2128. (h) Cotton, F. A.; Luck, R. L. Inorg. Chem. 1989, 28, 2128. (h) Cotton, F. A.; Luck, R. L. J. Am. Chem. Soc. 1989, 111, 5757. (i) Hamilton, D. G.; Crabtree, R. H. J. Am. Chem. Soc. 1988, 110, 4126.
- 50. FABMS for organometallic and coordination compounds:
 (a) Miller, J. M. Mass. Spec. Rev. 1990, 9, 319. (b) Bruce, M. I.;
 Liddell, M. J. Appl. Organometallic. Chem. 1987, 1, 191. (c) Miller,
 J. M. Adv. Inorg. Chem. Radiochem. 1984, 28, 1.
- 51. (a) Cotton, F. A. Polyhedron 1987, 6, 667. (b) Price, A. C.; Walton, R. A. Polyhedron 1987, 6, 729. (c) Anderson, L. B.; Cotton, F. A.;
 Dunbar, K. R.; Falvello, L. R.; Price, A. C.; Reid, A. H.; Walton, R. A. Inorg. Chem. 1987, 26, 2717. (d) Fanwick, P. E.; Price, A. C.;

- Walton, R. A. Inorg. Chem. 1987, 26, 3920. (e) Anderson, L. B.; Barder, T. J.; Cotton, F. A.; Dunbar, K. R.; Falvello, L. R.; Walton, R. A. Inorg. Chem. 1986, 25, 3629. (f) Anderson, L. B.; Barder, T. J.; Esjornson, D.; Walton, R. A. J. Chem. Soc., Dalton Trans. 1986, 2607. (g) Cotton, F. A.; Dunbar, K. R.; Price, A. C.; Schwotzer, W.; Walton, R. A. J. Am. Chem. Soc. 1986, 108, 4843. (i) Cotton, F. A.; Dunbar, K. R.; Falvello, L. R.; Walton, R. A. Inorg. Chem. 1985, 24, 4180. (j) Anderson, L. B.; Barder, T. J.; Walton, R. A. Inorg. Chem. 1985, 24, 1421. (k) Barder, T. J.; Cotton, F. A.; Falvello, L. R.; Walton, R. A. Inorg. Chem. 1985, 24, 1258. (l) Cotton, F. A.; Daniels, L. M.; Dunbar, K. R.; Falvello, L. R.; Tetrick, S. M.; Walton, R. A. J. Am. Chem. Soc. 1985, 107, 3524.
- 52. (a) Cotton, F. A.; Daniels, L. M.; Dunbar, K. R.; Falvello, L. R.;
 Tetrick, S. M.; Walton, R. A. J. Am. Chem. Soc. 1985, 107, 3524. (b)
 Barder, T. J.; Cotton, F. A.; Lewis, D.; Schwotzer, W.; Tetrick, S. M.;
 Walton, R. A. J. Am. Chem. Soc. 1984, 106, 2882.
- 53. EPR of dirhenium phosphine complexes:
 Anderson, L. B.; Barder, T. J.; Cotton, F. A.; Dunbar, K. R.; Falvello, L. R.; Walton, R. A. *Inorg. Chem.* 1986, 25, 3629.
- 54. Examples of molecular structures with Cl/CO disorder: Cotton, F. A.; Dunbar, K. R.; Price, A. C.; Schwotzer, W.; Walton, R. A. J. Am. Chem. Soc. 1986, 108, 4843.
- Examples for ligand transfer reactions:
 (a) Petillon, F. Y. Rumin, R. Talarmin, J. J. Organomet. Chem.
 1988, 346, 111. (b) Rumin, R.; Manojlovic-Muir, L.; Muir, K. W.;
 Petillon, F. Y. Organometallics 1988, 7, 375. (c) Rumin, R.; Courtot,
 P.; Guerchais, J. E.; Petillon, F. Y.; Manojlovic-Muir, L.; Muir, K.
 W. J. Organomet. Chem. 1986, 301, C1. (d) Fenske, D.; Merzweiler,
 K. Angew. Chem., Int. Ed. Engl. 1986, 25, 338. (e) Pregosin, P. S.;
 Togni, A.; Venanzi, L. M. Angew. Chem., Int. Ed. Engl. 1986, 25,
 734.

- 56. Carbonyl halide phosphine clusters:
 Bonnet, J-J, Lavigne, G. Papageorgiou F. J. Crystallographic and
 Spectroscopic Research, 1986, 16, 4, 475.
- 57. Rumin, R.; Manojlovic-Muir, L.; Muir, K. W.; Petillon, F. Y. Organometallics 1988, 7, 375.
- 58. Barder, T.; Walton, R. A. Inorg. Chem. 1982, 21, 2510.
- 59. Synthesis and characterization of Os₃(μ-H)(μ-Cl)(CO)₁₀:
 Deeming, A. J.; Hasso, S. J. Organomet. Chem. 1976, 114, 313.
- 60. Chemistry of Os₃(μ-H)(μ-X)(CO)₁₀:
 (a) Johnson, B. F. G.; Lewis, J.; Pippard, D. J. Chem. Soc., Dalton Trans. 1981, 407. (b) Deeming, A. J.; Hasso, S. J. Organomet. Chem. 1976, 114, 313.
- 61. Chemistry of $Ru_3(\mu-H)(\mu-X)(CO)_{10}$ and $Ru_3(\mu-X)_2(CO)_{10}$:

 (a) Kampe, C. E.; Boag, N. M.; Knobler, C. B.; Kaesz, H. D. *Inorg. Chem.* **1984**, 23, 1390.
- Chemistry of metal carboxylate complexes:
 (a) Rardin, R. L.; Tolman, W. B.; Lippard, S. J. New J. Chem. 1991, 15, 417.
 (b) Mehrotra, R. C.; Bohra, R. Metal Carboxylates; Academic: New York, 1983.
 (c) Catterick, J.; Thronton, P. Adv. Inorg. Chem. Radiochem. 1977, 20, 291.
 (d) Oldham C.; Prog. Inorg. Chem. 1968, 10, 223.
- Chemistry of trifluoroacetate metal complexes:
 (a) Santure, D. J.; Huffman, J. C.; Sattelberger, A. P. Inorg. Chem.
 1984, 23, 938. (b) Santure, D. J.; McLaughlin, K. W.; Huffman, J. C.; Sattelberger, A. P. Inorg. Chem. 1983, 22, 1877. (c) Girolami, G. S.; Anderson, R. A. Inorg. Chem. 1982, 21, 1318. (d) Cotton, F. A.; Lay, D. G. Inorg. Chem. 1981, 20, 935. (e) Girolami, G. S.; Mainz, V. V.; Anderson, R. A. Inorg. Chem. 1980, 19, 805. (f) Garner, C. D.;

- Hughes, C. D. Adv. Inorg. Chem. Radiochem. 1975, 17, 1. (g)
 Garner, C. D.; Senior, R. G. J. Chem. Soc., Dalton Trans. 1976, 1041.
- 64. Santure, D. J.; McLaughlin, K. W.; Huffman, J. C.; Sattelberger, A. P. Inorg. Chem. 1983, 22, 1877.
- 65. Rardin, R. L.; Tolman, W. B.; Lippard, S. J. New J. Chem. 1991, 15, 417.
- Redox chemistry of Rh₂(II,II) complexes:
 (a) McCarthy, H. J.; Tocher, D. A. Inorg. Chim. Acta. 1988, 145, 171.
 (b) Tocher, D. A.; Tocher, J. H. Inorg. Chim. Acta. 1987, 131, 69. (c)
 Tocher, D. A.; Tocher, J. H. Polyhedron, 1986, 5, 1615. (d) Tocher, D. A.; Tocher, J. H. Inorg. Chim. Acta. 1985, 104, L15.
- 67. Synthesis of Rh₂(O₂CCH₃)₄(MeOH)₂:

 Jofnson, S. A.; Hunt, H. R.; Neumann, H. M. *Inorg. Chem.* **1963**, 2, 960.
- 68. Synthesis of Mo₂(O₂CCF₃)₄:
 Cotton, F. A.; Norman, J. G., Jr. J. Coord. Chem. 1971, 1, 161.
- 69. Synthesis of Rh₂(O₂CCF₃)₄:
 (a) Bear, J. L.; Kitchens, J.; Willcott, M. R. J. *Inorg. Nucl. Chem.* 1971, 11, 3479. (b) Jofnson, S. A.; Hunt, H. R.; Neumann, H. M. *Inorg. Chem.* 1963, 2, 960.
- Ortho-metallated dirhodium complexes:
 (a) Morrison, E. C.; Tocher, D. A. Inorg. Chim. Acta. 1989, 157, 139.
 (b) Barcelo, F.; Cotton, F. A.; Lahuerta, P.; Sanau, M.; Schwotzer, W.; Ubeda, M. A. Organometallics 1987, 6, 1105. (c) Cotton, F. A.; Dunbar, K. R.; Verbruggen, M. G. J. Am. Chem. Soc. 1987, 109, 5498.
 (d) Cotton, F. A.; Dunbar, K. R. J. Am. Chem. Soc. 1987, 109, 3142. (e) Chakravarty, A. R.; Cotton, F. A.; Tocher, D. A.; Tocher, J. H. Organometallics 1985, 4, 8. (f) Chakravarty, A. R.; Cotton, F. A.; Tocher, D. A. J. Chem. Soc., Chem. Commun. 1984, 501.

- Recent work on EPR studies of Rh₂(II,III) complexes:

 (a) Yao, C. -L.; Park, K. H.; Khokhar, A. R.; Jun, M. -J.;l Bear, J. L.
 Inorg. Chem. 1990, 29, 4033.
 (b) Bear, J. L.; Yao, C. -L.; Capdevielle, F. J.; Korp, J. D.; Albright, T. A.; Kang, S. -K.; Kadish, K. M. Inorg. Chem. 1989, 28, 1254.
 (c) Lifsey, R. S.; Chavan, M. Y.; Chau, L. K.; Ahsan, M. Q.; Kadish, K. M.; Bear, J. L. Inorg. Chem. 1987, 26, 822.
 (d) Bear, J. L.; Liu, L. M.; Kadish, K. M. Inorg. Chem. 1987, 26, 2927.
 (e) Chavan, M. Y.; Ahsan, M. Q.; Lifsey, R. S.; Bear, J. L.; Kadish, K. M. Inorg. Chem. 1986, 25, 3218.
 (f) Ahsan, M. Q.; Bear, J. L.
 Inorg. Chem. 1986, 25, 260.
 (g) Chavan, M. Y.; Lin, X. Q.; Ahsan, M. Q.; Bernal, I.; Bear, J. L.; Kadish, K. M. Inorg. Chem. 1986, 25, 1281.
 (h) Kawamura, T.; Katayama, H.; Yamabe, T. Chem. Phys. Lett.
 1986, 130, 20.
 (i) Le, J. C.; Chavan, M. Y.; Chau, L. K.; Bear, J. L.; Kadish, K. M. J. Am. Chem. Soc. 1985, 107, 7195.
- 72. EPR studies of NO⁺ complexes:
 Richter-Addo, G. B.; Legzdins, P. Chem. Rev. 1988, 88, 991.
- Chemistry of metal carbonyl clusters complexes:
 (a) Shriver, D. F.; Kasez. H. D.; Adams. R. D. The Chemistry of Metal Cluster Complexes; VCH Publishers: New York, 1990. (b)
 Atwood, J. D.; Wovkulich, M. J.; Sonnenberger, D. C. Acc. Chem. Res. 1983, 16, 350. (c) Johnson, B. F. G. Transition Metal Clusters; Wiley: New York, 1980, p. 418. (d) Chisholm, M. H.; Rothwell, I. P. Prog. Inorg. Chem. 1982, 29, 1.
- 74. Foulds, G. A.; Jognson, B. F. G.; Lewis, J. J. Organomet. Chem. 1985, 296, 147.
- 75. Chemistry of triruthenium carbonyl clusters with phosphines:
 (a) Bruce, M. I. Coord. Chem. Rev. 1987, 76, 1. (b) Bruce, M. I.

 Comprehensive Organometallic Chemistry; Wilkinson, G.; Stine, F.
 G. A.; Abel, E. W. (Eds.) Pergamen: Oxford, 1982, Vol. 4, p. 843.

- 76. Atwood, J. D.; Wovkulich, M. J.; Sonnenberger, D. C. Acc. Chem. Res. 1983, 16, 350.
- 77. Syntheses of M₃(CO)_{12-n}(NCMe)_n (M=Os, Ru, n=1, 2; M=Fe, n=1):
 (a) Cardin, C. J.; Cardin, D. J.; Kelly, N. B.; Lawless, G. A.; Power, M. B. J. Organomet. Chem. 1988, 341, 447. (b) Foulds, G. A.; Jognson, B. F. G.; Lewis, J. J. Organomet. Chem. 1985, 296, 147.
- 78. Synthesis of H₂Os₃(CO)₁₀:
 (a) Johnson, B. F. G.; Lewis, J.; Kilty, P. A. J. Chem. Soc. A. 1968,
 2859. (b) Knox, S. A. R.; Koepke, J. W.; Andrews, M. A.; Kaesz, H. D. J. Am. Chem. Soc. 1975, 97, 3942.
- Ion-pairing of mononuclear metal carbonylates:
 (a) Kao, S. C.; Darensbourg, M. Y.; Schenk, W. Organometallics
 1984, 3, 871. (c) Mclain, S. J. J. Am. Chem. Soc. 1983, 105, 6355. (c)
 Powell, J.; Gregg, M.; Kuksis, A.; Meindl, P. J. Am. Chem. Soc.
 1983, 105, 1064. (d) Powell, J.; Kuksis, A.; May, C. J.; Nyburg, S. C.;
 Smith, S. J. J. Am. Chem. Soc. 1981, 103, 5941. (e) Collman, J. P.;
 Finke, R. G.; Gawse, J. N.; Branman, J. I. J. Am. Chem. Soc. 1978, 100, 4766. (f) Darensbourg, M.; Barros, H.; Borman, C. J. Am. Chem. Soc. 1977, 99, 1647.
- 80. Interactions of metal carbonyl hydrides with Lewis acids: Richmond, T. G.; Basolo, F.; Shriver, D. F. Organometallics 1982, 1, 1624.
- Ion-pairing of metal cluster anions:
 (a) Chen, C. K.; Cheng, C. H.; Hseu, T. H. Organometallics 1987, 6, 868.
 (b) Schick, K. -P.; Johns, N. L.; Sekula, P.; Boag, N. M.; Labinger, J. A.; Kasez, H. D. Inorg. Chem. 1984, 23, 2204.
 (c) Chen, C. K.; Cheng, C. H. Inorg. Chem. 1983, 22, 3378.
 (d) Collman, J. P.; Finke, R. G.; Matlock, P. L.; Wahren, R.; Komoto, R. G.; Brauman, J. I. J. Am. Chem. Soc. 1978, 100, 1119.
 (e) Wilkinson, J.; Todd, L. J. J. Organomet. Chem. 1976, 118, 199.

- Chemistry of bridging phosphido polynuclear complexes:
 (a) Lavigne, G. The Chemistry of Metal Cluster Complexes; Shriver,
 D. F.; Kasez. H. D.; Adams. R. D. (Eds.) VCH Publishers: New York,
 1990, Ch. 5. (b) Lagan, N.; Lavigne, G.; Bonnet, J. -J.; Reau, R.;
 Neiberker, D.; Tkatchenko, I. J. J. Am. Chem. Soc. 1988, 110, 5369.
 (c) Nucciarone, D. N.; MacLaughlin, S. A.; Taylor, N. J.; Carty, A. J.
 Organometallics 1988, 7, 106. (d) Carty, A. J.; MacLaughlin, S. A.;
 Nucciarone, D. Phosphorus-31 NMR Spectroscopy in Stereochemical Analysis: Organic Compounds and Metal Complexes; Verkade, J.
 G.; Quin, L. D. (Eds.) VCH Publishers: New York, 1986, Ch. 16, p.
 559. (e) Fehlhammer, W. P.; Stolzenberg, H. Comprehensive Organometallic Chemistry; Wilkinson, G.; Stone, F. G. A.; Abel, E.
 W. (Eds.) Pergamon: Oxford, 1982, Vol. 4, Ch. 31, p. 513.
- P—C bond cleavage in the reactions of Os₃(CO)₁₂ with PR₃:

 (a) Bradford, C. W.; Nyholm, R. S. J. Chem. Soc., Dalton Trans. 1973, 529. (b) Gainsford, G. J.; Guss, J. M.; Ireland, P. R.; Mason, R.; Bradford, C. W.; Nyholm, R. S. J. Organometal. Chem. 1972, 40, C70. (c) Deeming, A. J.; Rothwell, I. P.; Hursthouse, M. B.; Backer-Dirks, J. D. J. Chem. Soc., Dalton Trans. 1981, 1879. (d) Deeming, A. J.; Underhill, M. J. Chem. Soc., Dalton Trans. 1973, 2727. (e) Deeming, A. J.; Kimber, R. E.; Underhill, M. J. Chem. Soc., Dalton Trans. 1973, 2727.
- P—C bond cleavage in the reaction of Ru₃(CO)₁₂ with PR₃:
 Bruce, M. I.; Shaw, G. Stone, F. G. A. J. Chem. Soc., Dalton Trans.
 1972, 2094.
- Recent work on reactions with P—C bond cleavage:

 (a) Elliot, D. J.; Holah, D. G.; Hughes, A. N.; Mirza, H. A.; Zawada, E. J. Chem. Soc., Chem. Commun. 1990, 32. (b) Lugan, N.; Lavigne, G.; Bonnet, J. J. Inorg. Chem. 1987, 26, 585. (c) Dubois, R. A.; Garrou, P. E. Organometallics 1986, 5, 466. (d) Dubois, R. A.; Garrou, P. E.; Lavin, K.; Allock, H. R. Organometallics 1986, 5, 473. (e) Garrou, P. E. Chem. Rev. 1985, 85, 171. (f) Garrou, P. E.; Dubois,

- R. A.; Jung, C. W. CHEMTECH 1985, 123. (g) Dubois, R. A.; Garrou, P. E.; Lavin, K.; Allock, H. R. Organometallics 1984, 3, 649.
- 86. Unsaturated trinuclear carbonyl clusters:

 Lavigne, G.; Kasez, H. D. Metal Clusters in Catalysis; Amsterdam:
 Elsevier, 1986, Ch. IV, p. 43.
- 87. Reactions of H₂Os₃(CO)₁₀ with phosphines:
 (a) Ehrenreich, W.; Herberhold, M.; Herrmann, G.; Suss-Fink, G. J.
 Organomet. Chem. 1985, 294, 183. (b) Deeming, A. J.; Hasso, S. J.
 Organomet. Chem. 1976, 114, 313.
- 88. Recent work on alkoxide and phenoxide complexes: (a) Krafft, T. E.; Heina, C. I.; Smith, J. S. Inorg. Chem. 1990, 29, 2682. (b) Green, L. M.; Meek, D. W. Organometallics 1989, 8, 659. (c) Kim, Y.; Osakada, K.; Sugita, K.; Yamamoto, T.; Yamamoto, A. Organometallics 1989, 7, 2181. (c) Bryndza, H. E.; Fong, L. K.; Paciello, R. A.; Tam, W.; Bercaw, J. E. J. Am. Chem. Soc. 1987, 109, 1444. (d) Kegley, S. E.; Schaverien, C. J.; Freudenberger, J. H.; Bergman, R. G.; Nolan, S. P.; Hoff, C. D. J. Am. Chem. Soc. 1987, 109, 6563. (e) Bryndza, H. E.; Calabrese, J. C.; Marsi, M.; Roe, D. C.; Tam, W.; Bercaw, J. E. J. Am. Chem. Soc. 1986, 108, 4805. (f) Rees, W. M.; CHurchill, M. R.; Fettinger, J. C.; Atwood, J. D. Organomatallics 1985, 4, 2179. (g) Komiya, S.; Akai, Y.; Tanaka, K.; Yamamoto, T.; Yamamoto, A. Organometallics 1985, 4, 1130. (h) Bryndza, H. E. Organometallics 1985, 4, 1686. (i) Newman, L. J.; Bergman, R. G. J. Am. Chem. Soc. 1985, 107, 5314. (j) Collman, J. P.; Barnes, C. E.; Brothers, P. J. Collins, T. J.; Ozawa, T.; Gallucci, J. C.; Ibers, J. A. J. Am. Chem. Soc. 1984, 106, 5151. (k) Monaghan. P. K.; Puddephatt, R. J. Organomatallics 1984, 3, 444.

APPENDICES

PHYSICAL MEASUREMENTS

- (1) Infrared Spectroscopy Infrared spectra were recorded on a Perkin-Elmer 599 or a Nicolet 740 FT-IR spectrophotometer.
- (2) Electronic Absorption Spectroscopy Electronic absorption spectra were measured on a Hitachi U-2000 (1100–200 nm) or a Cary 17 (2000–200 nm) spectrophotometers.
- (3) Electrochemistry Electrochemical measurements were performed by using an EG&G Princeton Applied Research Model 352 scanning potentiostat in conjunction with a BAS Model RXY recorder. Cyclic voltammetry experiments were carried out at 22 ± 2 °C in dichloromethane solutions containing 0.1 M TBAH or TBABF₄ as supporting electrolyte. $E_{1/2}$ values $[(E_{p,a} + E_{p,c})/2]$ were referenced to the Ag/AgCl electrode and are uncorrected for junction potentials. The Cp₂Fe/Cp₂Fe⁺ couple occurs at $E_{1/2} = +0.46$ V under the same experimental conditions.
- (4) NMR Spectroscopy ¹H NMR spectra were recorded on a WM 250 Bruker spectrometer with an ASPECT 3000 computer; Gemini 300 MHz; Varian 300 MHz or Varian 500 MHz spectrometer. Resonances were referenced internally to the residual protons in the incompletely deuterated solvent. ³¹P{¹H} NMR spectra were recorded on a Varian 300 MHz spectrometer operating at 121.4 MHz with an internal deuterium lock using aqueous 85% H₃PO₄ as an external standard. Positive chemical shifts were

measured downfield from H₃PO₄. ¹⁹F NMR spectra were obtained on a Varian VXR 300 MHz spectrometer. An external standard of CF₃C₆H₅ at d -63.9 ppm was used to reference the ¹⁹F NMR spectrum.

- (5) ESR Spectroscopym X-Band ESR spectra of dichloromethane solutions were recorded with the use of a Bruker ER200D spectrometer. To obtain an accurate measure of g-values and line widths, a Bruker ER035M NMR Gaussmeter and a Hewlett-Packard 5245L frequency counter (with a 3-12 GHz adaptor) were used to measure magnetic field strength and the microwave frequency, respectively.
- (6) Mass Spectrometry Fast atom bombardment (FAB) mass spectrometry studies were performed on a JEOL HX 110 double-focusing mass spectrometer housed in the National Institutes of Health/Michigan State University Mass Spectrometry Facility; samples were dissolved in a 3-nitrobenzyl alcohol matrix.
- (7) Elemental Analyses Elemental analyses were performed at Galbraith Laboratories, Inc.

Table 21. Atomic positional parameters (Å²) and their estimated standard deviations for $Re_2(\mu-H)(\mu-Cl)Cl_2(CO)_2(dppm)_2$.

Atom	x -	у -	z -	B(A2)
Re(1) C1(1) C1(2) P(1) P(2) O(1) C(1) C(12) C(13) C(14) C(15) C(16) C(21) C(22) C(23) C(24) C(25) C(24) C(25) C(31) C(32) C(33) C(34) C(35) C(36) C(36) C(36)	0.13688(2) 0.2770(2) 0.1321(2) 0.2249(1) 0.0277(1) -0.0170(5) 0.0380(6) 0.2436(5) 0.1663(5) 0.1663(5) 0.1864(6) 0.1446(6) 0.0837(8) 0.0640(7) 0.1032(7) 0.3347(5) 0.3568(6) 0.4403(7) 0.4748(7) 0.4749(8) -0.1506(6) -0.2319(7) -0.2492(8) -0.1002(7) 0.0369(5)		0.04002(1) 0.000 0.09664(6) 0.10556(5) -0.01262(6) 0.0798(2) 0.0656(3) 0.0779(2) 0.1663(2) 0.1960(3) 0.2449(3) 0.2622(3) 0.2329(3) 0.1286(2) 0.1215(2) 0.1398(3) 0.1634(3) 0.1687(3) 0.1687(3) 0.1687(3) 0.1529(2) 0.0144(2) -0.0068(3) 0.0605(3) 0.0850(3) 0.0600(3) -0.0276(2)	2.290(3) 2.91(2) 3.46(3) 2.63(3) 2.70(3) 5.9(2) 3.9(1) 2.9(1) 4.0(2) 4.7(2) 5.2(2) 5.3(2) 5.1(2) 3.6(1) 3.9(1) 5.9(2) 6.7(3) 5.6(2) 4.2(2) 3.6(1) 4.4(2) 7.2(3) 7.5(3) 8.3(4) 5.5(2) 3.6(1)
C(36)	-0.1002(7)	0.3312(8)	0.0600(3)	5.5(2)

Anisotropically refined atoms are given in the form of the equivalent isotropic displacement parameter defined as $4/3[a^2\beta_{11} + b^2\beta_{22} + c^2\beta_{33} + ab(\cos\gamma)\beta_{12} + ac(\cos\beta)\beta_{13} + bc(\cos\alpha)\beta_{23}]$.

Table 22. Atomic positional parameters (Å²) and their estimated standard deviations for $[Re_2(\mu-H)(\mu-Cl)Cl_2(CO)_2-(dppm)_2](BF_4)$.

atom	1	¥	z	B(eq)
Re(1)	0. 3138(2)	0.1174(1)	0.2814(2)	2. 55(9)
Re(2)	0.3651(2)	0. 2711(1)	0. 2007(2)	2.55(9)
C1(1)	0 4605(9)	0 2815(7)	0. 3664(7)	2.4(4)
C1(2)	0.334(1)	0.041(1)	0.4150(9)	4.1(5)
C1(3)	0.486(1)	0. 4477(답)	0.2193(9)	3. 2(4)
P(1)	0.465(1)	0.069(1)	0. 272(1)	3.8(5)
P(2)	0.166(1)	0. 153(1)	0.316(1)	3.7(5)
P(3)	0.514(1)	0. 2414(9)	0.1654(8)	2.7(4)
P(4)	0. 225(1)	0. 329(1)	0. 2095(9)	3.4(5)
0(1)	0. 132(3)	-0.080(2)	0. 163(2)	3.6(7)
0(2)	0. 234(3)	0. 230(2)	-0.004(3)	4.4(7)
C(1)	0. 183(3)	-0.007(3)	0. 202(3)	1.6(8)
C(2)	0. 286(4)	0. 250(3)	0.069(3)	3(1)
C(3)	0. 473(4)	0. 105(3)	0. 163(3)	2. 7(9)
C(4)	0. 113(4)	0. 222(3)	0. 226(3)	2(1)
C(11)	0. 428(4)	-0. 070(4)	0. 258(4)	5(1)
C(12)	0. 468(4)	-0. 111(3)	0. 341 (3)	3(1)
C(13)	0. 423(5)	-0. 215(4)	0. 337(4)	5(1)
C(14)	0. 362(4)	-0. 277(3)	0. 257(3)	3(1)
C(15)	0. 327(5)	-0. 237(4)	0. 178(4)	5(1)
C(16)	0. 355(4)	-0. 127(4)	0. 171(4)	4(1)
C(21)	0. 602(3)	0. 118(3)	0. 353(3)	1. 3(7)
C(22)	0. 617(4)	0. 1 58 (3)	0. 441 (3)	4(1)
C(23)	0. 740(4)	0. 187(3)	0. 511(3)	3(1)
C(24)	0. 824(4)	0. 181(3)	Q. 488 (4)	4(1)

Table 22. Continued.

C(25)	0 806(4)	0.142(4)	0.405(4)	4(1)
C(26)	o. 689 (4)	0.106(3)	0. 331 (3)	3(1)
C(31)	o. 203 (3)	0. 227(3)	0.415(3)	1.6(8)
C(35)	0 119(3)	0, 26 6 (3)	0.428(3)	2. 2(8)
C(33)	0 152(4)	0. 333(3)	0. 511(3)	2.5(9)
6(34)	0.252(4)	0. 354(3)	0. 581 (3)	3(1)
C(35)	୦ ଓଟ୍ଟ(4)	0.311(4)	0.572(4)	4(1)
C(36)	0 300(5)	0. 248(4)	0.472(4)	5(1)
3(41)	ତ. 039(4)	0, 045(3)	0.308(3)	3(1)
0(42)	-0 045(4)	0. 009(4)	0. 235(4)	4(1)
0(43)	-0.153(5)	-0. 079(5)	0. 243(5)	7(2)
C(44)	-0.146(5)	-0. 122(4)	0. 321 (4)	5(1)
C(45)	-0.054(4)	-0.085(4)	0. 393(4)	4(1)
C(46)	0.045(3)	-0. 001(3)	0. 387(3)	2.4(8)
C(51)	0. 512(4)	0. 272(4)	0.055(4)	4(1)
C(52)	0. 536 (3)	0. 367(3)	0. 037(3)	2. 3(9)
C(53)	0. 524(4)	0. 398 (3)	-0.050(3)	2.3(9)
C(54)	0. 478(5)	0. 314(4)	-0. 117(4)	5(1)
C(55)	0. 454(4)	0. 211(3)	-0. 108(3)	3(1)
C (56)	0.463(4)	0. 192(3)	-0. 018(3)	3(1)
C(61)	0. 662(3)	0. 308 (2)	0. 229(2)	0.9(7)
C(62)	0. 745(4)	0. 303(3)	0. 192(4)	4(1)
C(63)	0. 860(5)	0. 348(4)	0. 247(4)	5(1)
C(64)	0. 898 (4)	0. 399(4)	0. 336(4)	4(1)
C(65)	0. 822(5)	0.419(4)	0. 377(4)	6(1)

Table 22. Continued.

atom	x	v	2	B(eq)
C (56)	0 697(3)	0. 355(3)	0. 313(3)	2.3(8)
C(71)	0 (56(3)	0.345(3)	0.106(3)	1.9(日)
C(72)	0.043(5)	0.318(4)	0.052(4)	5(1)
C(73)	0.001(5)	0.347(4)	0. 033(4)	5(1)
C(74)	0.054(4)	0. 431(4)	··0. 056(4)	3(1)
C(75)	0. 163(5)	0.486(4)	0.002(4)	5(1)
C(76)	0. 224(5)	0.462(4)	0.087(4)	5(1)
C(81)	0. 258(3)	0. 429(3)	0. 295(3)	1 8(8)
C(82)	0. 356(4)	0. 472(3)	0. 371(4)	4(1)
C(83)	0. 373(4)	0. 542(3)	0.438(3)	3(1)
C(84)	0. 287(4)	0. 578(3)	0. 430(3)	4(1)
C(85)	0. 186(5)	0. 546(4)	0.356(4)	5(1)
C (86)	0. 171 (4)	0. 472(3)	0.292(3)	2 . 3 (9)
C1(4)	0. 979(2)	0. 298(2)	0. 731(2)	14. 5(7)
C1(5)	1. 223(2)	0.388(2)	0.804(2)	14. 5(7)
C(5)	1. 108(8)	0. 371(6)	0. 753(7)	14(3)

Table 23. Atomic positional parameters (Å²) and their estimated standard deviations for $[Re_2(\mu\text{-CO})(\mu\text{-Cl})Cl_2(CO)(NO)-(dppm)_2](BF_4)$.

atom	x	У	Z
Re((1)) Re((1)) P((1)) P((2)) P((1))	0.2501(1) 0.1133(1) 0.1317(7) -0.0221(6) 0.3245(7) 0.3523(7) 0.1635(7) 0.1995(7) 0.0938(7) 1.063(3) 0.971(3) 0.947(3) 0.947(3) 0.933(4) 0.398(2) 0.245(2) 0.059(4) 0.059(4) 0.075(3) 0.313(3) 0.313(3) 0.353(4) 0.376(3) 0.376(3) 0.376(3) 0.376(3) 0.376(3) 0.376(3) 0.376(3) 0.376(3) 0.376(3) 0.376(3) 0.376(3) 0.3641(4) 0.669(4) 0.669(4) 0.630(4) 0.630(4) 0.520(3) 0.232(2) 0.232(2) 0.293(2) 0.293(2) 0.293(2) 0.108(2) 0.068(3) 0.016(4) 0.058(4) 0.058(4) 0.058(4) 0.058(4) 0.058(4) 0.058(4) 0.058(4) 0.058(4) 0.058(4) 0.058(4)	0.31597(6) 0.32390(6) 0.3805(3) 0.3675(3) 0.3415(4) 0.3733(4) 0.2626(4) 0.2755(4) 0.2755(4) 0.091(2) 0.150(1) 0.073(2) 0.116(2) 0.248(2) 0.280(1) 0.248(2) 0.280(1) 0.267(1) 0.367(1) 0.367(1) 0.436(1) 0.452(2) 0.503(2) 0.515(2) 0.471(1) 0.361(2) 0.352(1) 0.347(2) 0.365(2) 0.357(2) 0.365(2) 0.184(1) 0.223(1) 0.129(2) 0.365(2) 0.137(2) 0.365(2) 0.137(2) 0.365(2) 0.365(2) 0.365(2) 0.365(2) 0.365(2) 0.365(2) 0.366(2) 0.37(2) 0.365(2)	0.3759(1) 0.4698(1) 0.3624(6) 0.3624(6) 0.5054(6) 0.2578(6) 0.4542(6) 0.2794(7) 0.5719(6) 0.3874(3) 0.225(2) 0.197(3) 0.319(4) 0.394(2) 0.512(1) 0.627(3) 0.560(2) 0.477(2) 0.388(2) 0.388(2) 0.431(3) 0.360(3) 0.384(3) 0.360(3) 0.384(3) 0.465(3) 0.465(3) 0.465(3) 0.465(3) 0.465(3) 0.465(3) 0.469(3) 0.384(3) 0.524(2) 0.541(3) 0.155(2) 0.182(3) 0.155(2) 0.182(3) 0.167(3) 0.171(3) 0.171(3) 0.171(3) 0.713(4)

Table 23. Continued.

atom	x	Å	2
C(53)	0.219(5)	0.325(3)	0.800(5)
C(54)	0.138(3)	0.334(2)	0.828(3)
C(55)	0.073(3)	0.354(2)	0.784(3)
C(56)	0.091(3)	0.368(2)	0.704(3)
C(61)	0.191(3)	0.438(1)	0.571(2)
C(62) C(63)	0.233(3) 0.231(3)	0.463(2) 0.518(1)	0.634(2) 0.639(2)
C(64)	0.231(3)	0.518(1)	0.537(3)
C(65)	0.121(3)	0.517(2)	0.510(3)
C(66)	0.129(3)	0.462(2)	0.514(2)
C(71)	-0.073(3)	0.239(1)	0.436(2)
c(72)	-0.168(3)	0.253(2)	0.456(3)
C(73)	-0.231(3)	0.226(2)	0.488(3)
C(74)	-0.209(4)	0.188(2)	0.529(3)
C(75)	-0.108(4)	0.164(2)	0.516(4)
C(76)	-0.041(3)	0.195(2)	0.473(3)
C(81)	-0.077(3)	0.303(1)	0.308(2)
C(82)	-0.086(3)	0.349(2)	0.309(3)
C(83)	-0.150(3)	0.370(1)	0.248(2)
C(84) C(85)	-0.195(3)	0.343(2) 0.298(2)	0.198(3)
C(86)	-0.174(4) -0.122(3)	0.274(1)	0.187(3) 0.254(2)
B(1)	0.981(3)	0.274(1)	0.257(3)
0(4)	0.690(2)	0.3709(9)	0.985(1)
0(5)	0.885(2)	0.044(1)	0.641(2)
0(6)	0.205(2)	0.436(1)	0.968(2)
- (- /	***************************************		

Table 24. Atomic positional parameters (\mathring{A}^2) and their estimated standard deviations for $Ru_3(\mu\text{-Cl})_2(PBu_3^n)_2(CO)_8$.

Atom	x -	Ā	z -	B(A2)
Ru(1) Ru(3) Cl(1) P(1) O(12) O(2) O(3) O(5) O(6) O(6) C(6) C(6) C(13) C(12) C(13) C(12) C(13) C(14) C(15) C(15) C(113) C(0.30145(5) 0.29631(5) 0.23734(5) 0.1833(2) 0.4630(1) 0.3538(2) 0.3463(2) 0.4564(6) 0.0932(5) 0.0773(5) 0.4405(6) 0.5092(5) -0.0198(5) 0.1950(6) 0.1796(7) 0.3979(7) 0.1719(7) 0.3860(7) 0.3979(7) 0.1627(7) 0.3860(7) 0.2105(7) 0.2026(8) 0.3365(7) 0.364(1) 0.364(1) 0.5098(7) 0.6057(7) 0.7283(9) 0.6057(7) 0.7283(9) 0.812(1) 0.055(1) 0.027(1) 0.5971(7) 0.5971(7) 0.5971(7) 0.5971(7) 0.5971(7) 0.3336(8) 0.3441(9) 0.328(1) 0.354(1) 0.354(1) 0.354(1) 0.354(1) 0.359(1)	0.22580(3) 0.23764(3) 0.33945(3) 0.16656(9) 0.1289(1) 0.1504(1) 0.3080(3) 0.2493(3) 0.2739(3) 0.3660(3) 0.3660(3) 0.4173(4) 0.4353(4) 0.2771(4) 0.22951(4) 0.2592(4) 0.3553(4) 0.3027(4) 0.3553(4) 0.3997(4) 0.3997(4) 0.3997(4) 0.1360(4) 0.0758(5) 0.0877(6) 0.1209(7) 0.1001(4) 0.1460(5) 0.1209(7) 0.1640(8) 0.0592(4) 0.1695(6) 0.1695(6) 0.1695(6) 0.1698(4) 0.1698(4) 0.1891(8) 0.1891(8) 0.1891(8) 0.1891(8) 0.1891(8) 0.1891(8) 0.1891(8) 0.1895(6) 0.0238(6) 0.0238(6) 0.0238(6) 0.0295(8)	0.39260(3) 0.22483(3) 0.31578(3) 0.29810(8) 0.31367(9) 0.45228(9) 0.15333(9) 0.4758(3) 0.1497(3) 0.3221(3) 0.3221(3) 0.4456(4) 0.3203(4) 0.4543(4) 0.4543(4) 0.1689(4) 0.1791(4) 0.3209(5) 0.3063(4) 0.3209(5) 0.3973(5) 0.3973(5) 0.4442(4) 0.4730(5) 0.4663(4) 0.4730(5) 0.4518(8) 0.4518(8) 0.4518(8) 0.4518(8) 0.4518(8) 0.4518(8) 0.4518(8) 0.1587(5) 0.1587(5) 0.1587(5) 0.1587(5) 0.1587(5) 0.1587(5) 0.1587(5) 0.1587(5) 0.1587(5) 0.1587(6) 0.1587(6) 0.1587(5) 0.1587(6) 0.1597(4) 0.0111(4) -0.0661(5) 0.1290(5) 0.1275(7) 0.093(1)	3.59(1) 3.68(1) 4.30(1) 4.30(4) 4.17(4) 4.26(4) 4.26(4) 4.50(2) 7.3(2) 7.3(2) 7.3(2) 7.3(2) 7.3(2) 7.3(2) 7.3(2) 7.3(2) 7.4(2) 7.5(2) 6.6(2) 6.5(2) 6.5(2) 7.1(4) 7.2(4) 13.6(5) 7.2(4) 13.6(5) 13.6(5) 14.3(5) 15.4(6) 8.1(2) 7.2(2) 11.2(4) 13.6(5) 14.3(5) 15.4(6) 8.1(2) 7.2(2) 11.2(4) 13.6(5) 14.3(5) 15.4(6) 8.1(2) 7.0(2) 11.2(4) 13.6(5) 14.3(5) 15.4(6) 8.1(2) 7.0(2) 11.2(4)

Table 25. Atomic positional parameters (\mathring{A}^2) and their estimated standard deviations for $Rh_2(O_2CCH_3)_3(TMPP-O)(MeOH)$.

Atom	x -	y -	2	B(A2)
Rh(1)	0.97704(3)	0.35229(3)	0.23068(3)	1.616(8)
Rh(2)	1.05222(3)	0.16371(3)	0.10063(3)	1.633(8)
P(1)	0.81147(9)	0.39684(9)	0.1656(1)	1.56(2)
0(1)	1.0160(3)	0.1217(3)	0.2341(3)	2.39(8)
0(2)	0.9526(3)	0.2964(3)	0.3578(3)	2.36(8)
0(3)	1.1992(3)	0.1453(3)	0.1673(3)	2.59(9)
0(4)	1.1367(3)	0.3189(3)	0.2908(3)	2.62(9)
0(5)	1.0850(3)	0.2156(2)	-0.0239(3)	2.09(8)
0(6)	1.0172(3)	0.3908(2)	0.0974(3)	2.10(7)
0(7)	0.9073(3)	0.1720(2)	0.0311(3)	2.13(8)
0(8)	0.7923(3)	0.1996(3)	-0.3559(3)	3.7(1)
0(9)	0.7551(3)	0.5140(3)	-0.0299(3)	2.60(8)
0(10)	0.8996(3)	0.5422(3)	0.3292(3)	2.37(8)
0(11)	0.5873(4)	0.8837(3)	0.3734(4)	4.2(1)
0(12)	0.5893(3)	0.5445(3)	0.1251(3)	2.72(9)
0(13)	0.6669(3)	0.2732(3)	0.0387(3)	2.37(8)
0(14)	0.5279(3)	0.2763(3)	0.3873(3)	3.81(9)
0(15)	0.7465(3)	0.4691(3)	0.4123(3)	2.25(8)
0(16)	1.1367(3)	-0.0100(3)	-0.0216(3)	2.46(8)
C(1)	0.9731(4)	0.1956(4)	0.3316(4)	2.4(1)
C(2)	0.9446(6)	0.1651(5)	0.4282(6)	4.0(2)
C(3)	1.2114(4)	0.2246(4)	0.2467(5)	2.5(1)
C(4)	1.3242(4)	0.2016(5)	0.2902(7)	4.3(2)
C(5)	1.0588(4)	0.3160(4)	-0.0009(5)	2.2(1)
C(6)	1.0794(5)	0.3496(4)	-0.1012(5)	3.0(1)

Table 25. Continued.

Atom	x -	у -	z -	B(A2)
C(7)	0.8189(3)	0.3459(3)	0.0054(4)	1.6(1)
C(8)	0.8645(4)	0.2302(4)	-0.0437(4)	1.8(1)
C(9)	0.8584(4)	0.1762(4)	-0.1651(4)	2.2(1)
C(10)	0.8120(4)	0.2400(4)	-0.2372(4)	2.4(1)
C(11)	0.7793(4)	0.3520(4)	-0.1969(4)	2.2(1)
C(12)	0.7836(4)	0.4054(4)	-0.0764(4)	2.0(1)
C(13)	0.8029(7)	0.0907(6)	-0.3968(6)	5.6(2)
C(14)	0.7219(5)	0.5767(4)	-0.1098(5)	3.8(1)
C(15)	0.7455(4)	0.5449(4)	0.2215(4)	1.8(1)
C(16)	0.7967(4)	0.6035(4)	0.3006(4)	1.9(1)
C(17)	0.7479(4)	0.7165(4)	0.3537(5)	2.5(1)
C(18)	0.6410(4)	0.7717(4)	0.3239(5)	2.8(1)
C(19)	0.5863(4)	0.7171(4)	0.2466(5)	2.6(1)
C(20)	0.6384(4)	0.6050(4)	0.1979(4)	2.0(1)
C(21)	0.9575(4)	0.5982(4)	0.4112(6)	3.6(1)
C(22)	0.6426(8)	0.9460(8)	0.4359(9)	4.9(2)*
C(22B)	0.490(2)	0.939(2)	0.350(3)	4.8(6)*
C(23)	0.4774(4)	0.5774(5)	0.1506(5)	3.2(1)
C(24)	0.7175(4)	0.3623(4)	0.2261(4)	1.8(1)
C(25)	0.6604(4)	0.3032(4)	0.1605(4)	2.1(1)
C(26)	0.5961(4)	0.2759(4)	0.2170(5)	2.5(1)
C(27)	0.5885(4)	0.3106(4)	0.3404(5)	2.7(1)
C(28)	0.6378(4)	0.3735(4)	0.4100(5)	2.5(1)
C(29)	0.7009(4)	0.3997(4)	0.3493(4)	2.0(1)
C(30)	0.6285(4)	0.1932(4)	-0.0299(5)	2.9(1)*

/

Table 25. Continued.

Atom	x -	y -	z -	B(A2)
C(31)	0.5200(5)	0.3026(5)	0.5141(6)	3.7(1)*
C(32)	0.7495(4)	0.4954(4)	0.5390(5)	2.8(1)*
C(33)	1.1564(5)	-0.0244(4)	-0.1441(5)	3.2(1)*
C(34)	0.625	0.996	0.028	32(2) +
C(35)	0.625	0.916	0.082	13.1(5)+
0(17)	0.563	0.875	0.027	28.5(8) †

Starred atoms were refined isotropically.

Anisotropically refined atoms are given in the form of the equivalent isotropic displacement parameter defined as $4/3[a^28_{11} + b^28_{22} + c^28_{33} + ab(cosY)8_{12} + ac(cos8)8_{13} + bc(cos\alpha)8_{23}]$.

† Lattice ethanol which was placed in fixed positions

Table 26. Atomic positional parameters (Å²) and their estimated standard deviations for [HTMPP][Fe₃(μ -H)(μ -CO)(CO)₁₀].

Atom	x -	у -	z -	B(A2)
Fe(1)	0.4684(2)	0.16172(8)	0.09846(8)	2.92(3)
Fe(2)	0.3061(2)	0.23089(8)	0.23945(8)	2.45(3)
Fe(3)	0.6099(2)	0.28006(8)	0.24826(8)	2.79(3)
P(1)	0.0429(3)	0.2672(1)	0.7016(1)	1.91(5)
C(1)	0.634(1)	0.1370(6)	0.0328(6)	3.8(2)
C(2)	0.307(1)	0.0898(6)	0.0298(6)	3.3(2)
C(3)	0.509(1)	0.0829(6)	0.1418(5)	3.0(2)
C(4)	0.152(1)	0.2358(6)	0.1703(5)	3.0(2)
C(5)	0.758(1)	0.2024(6)	0.2402(6)	3.8(3)
C(6)	0.428(1)	0.2577(6)	0.0768(5)	3.3(2)
C(7)	0.249(1)	0.1226(6)	0.2397(6)	3.1(2)
C(8)	0.668(1)	0.3560(6)	0.3540(6)	3.7(3)
C(9)	0.706(1)	0.3393(6)	0.1957(6)	3.6(2)
C(10)	0.212(1)	0.2924(6)	0.3327(5)	3.1(2)
C(11)	0.418(1)	0.3414(5)	0.2492(5)	2.4(2)
012	-0.1715(7)	0.2842(4)	0.8400(3)	2.8(1)
014	0.2108(7)	0.4721(4)	1.0695(3)	2.5(1)
016	0.3366(7)	0.3761(4)	0.7840(3)	2.9(2)
C11	0.084(1)	0.3296(5)	0.8127(5)	1.8(2)
C12	-0.0262(9)	0.3306(5)	0.8738(5)	2.0(2)
C13	0.010(1)	0.3754(5)	0.9611(5)	2.0(2)
C14	0.1616(9)	0.4233(5)	0.9872(5)	1.8(2)*
C15	0.273(1)	0.4266(5)	0.9300(5)	2.1(2)
C16	0.2352(9)	0.3787(5)	0.8450(5)	2.1(2)

Table 26. Continued.

Atom	x -	у -	z -	B(A2)
C17	-0.287(1)	0.2789(7)	0.8992(6)	4.9(3)
C18	0.109(1)	0.4649(6)	1.1349(5)	2.9(2)
C19	0.487(1)	0.4336(6)	0.8141(6)	3.5(3)
022	0.0731(7)	0.1438(4)	0.7903(3)	3.0(1)
024	0.3016(8)	-0.0895(4)	0.5544(4)	4.1(2)
026	0.1033(7)	0.1643(4)	0.5325(3)	2.8(1)
C21	0.0981(9)	0.1542(5)	0.6615(5)	1.9(2)
C22	0.122(1)	0.1053(5)	0.7107(5)	2.3(2)
C23	0.189(1)	0.0220(5)	0.6770(5)	2.4(2)
C24	0.229(1)	-0.0102(5)	0.5929(6)	2.7(2)
C25	0.204(1)	0.0332(5)	0.5402(5)	2.4(2)
C26	0.1365(9)	0.1137(5)	0.5753(5)	2.1(2)
C27	0.118(1)	0.1064(6)	0.8499(5)	3.6(2)
C28	0.327(1)	-0.1434(6)	0.6002(6)	5.0(3)
C29	0.162(1)	0.1347(6)	0.4472(5)	3.6(2)
032	-0.0383(6)	0.4076(4)	0.6550(3)	2.7(1)
034	-0.6022(7)	0.3111(4)	0.5789(4)	3.5(2)
036	-0.2574(7)	0.1471(4)	0.6718(4)	2.9(1)
C31	-0.1519(9)	0.2776(5)	0.6627(5)	1.7(2)
C32	-0.1722(9)	0.3502(5)	0.6428(5)	2.0(2)
C33	-0.320(1)	0.3642(6)	0.6126(5)	2.4(2)
C34	-0.449(1)	0.3025(6)	0.6050(5)	2.8(2)
C35	-0.436(1)	0.2283(6)	0.6246(5)	2.6(2)
C36	-0.285(1)	0.2162(5)	0.6526(5)	2.2(2)

Table 26. Continued.

Atom	x -	у -	z -	B(A2)
C37	-0.051(1)	0.4851(5)	0.6350(6)	3.5(2)
C38	-0.631(1)	0.3932(6)	0.5703(6)	4.5(3)
C39	-0.395(1)	0.0883(6)	0.6725(6)	3.8(3)
0(1)	0.7397(8)	0.1237(4)	-0.0106(4)	5.1(2)
0(2)	0.2002(9)	0.0451(4)	-0.0151(4)	4.7(2)
0(3)	0.5378(8)	0.0277(4)	0.1632(4)	4.1(2)
0(4)	0.0498(7)	0.2414(4)	0.1266(4)	4.2(2)
0(5)	0.8584(8)	0.1563(4)	0.2368(4)	5.2(2)
0(6)	0.4042(9)	0.3128(4)	0.0555(4)	5.2(2)
0(7)	0.2017(8)	0.0579(4)	0.2438(4)	4.4(2)
0(8)	0.7054(9)	0.4069(5)	0.4230(4)	5.8(2)
0(9)	0.7667(8)	0.3813(4)	0.1636(4)	5.6(2)
0(10)	0.1404(8)	0.3338(4)	0.3898(4)	4.6(2)
0(11)	0.3861(7)	0.4141(4)	0.2569(4)	3.4(2)

Table 27. Atomic positional parameters (Ų) and their estimated standard deviations for $Ru_3(\mu\text{-CO})_2(CO)_6\{\mu_3-\eta^2-C_6H_2(OMe)_3\}[\mu\text{-P}\{C_6H_2(OMe)_3\}_2]$.

Atom	x -	у -	z -	B(A2)
Ru(1)	0.2403(3)	0.3305(2)	0.5471(1)	2.73(8)
Ru(2)	0.3566(3)	0.1731(2)	0.5808(1)	2.27(8)
Ru(3)	0.1125(3)	0.2214(2)	0.6097(1)	2.14(8)
P(1)	0.2438(8)	0.0979(6)	0.6443(4)	2.3(3)
0(1)	0.133(3)	0.355(2)	0.437(1)	7.2(9)
0(2)	-0.031(2)	0.402(1)	0.5693(9)	4.2(7)
0(3)	0.315(2)	0.507(1)	0.532(1)	5.3(8)
0(4)	0.618(2)	0.102(2)	0.605(1)	5.8(8)
0(5)	0.356(2)	0.032(1)	0.5019(9)	4.7(7)
0(6)	0.451(2)	0.254(2)	0.4710(9)	4.7(7)
0(7)	-0.139(2)	0.198(2)	0.660(1)	6.5(8)
0(8)	0.071(2)	0.139(1)	0.513(1)	4.8(7)
012	0.436(2)	-0.049(1)	0.6465(8)	2.7(5)*
014	0.244(2)	-0.261(1)	0.5724(9)	3.1(5)*
016	0.020(2)	0.025(1)	0.6107(8)	2.3(5)*
022	0.457(2)	0.117(1)	0.7136(8)	2.9(5)*
024	0.254(2)	0.098(2)	0.885(1)	5.3(7)*
026	0.065(2)	0.055(1)	0.7226(9)	3.7(6)*
051	0.166(2)	0.289(1)	0.6770(8)	2.3(5)*
053	0.502(2)	0.371(1)	0.7628(8)	3.2(5)*
055	0.523(2)	0.328(1)	0.5751(9)	4.0(6)*
C(1)	0.171(3)	0.349(2)	0.478(1)	2.9(8)*
C(2)	0.060(3)	0.350(2)	0.574(1)	1.9(8)*
C(3)	0.279(4)	0.442(3)	0.538(2)	5(1)*
C(4)	0.524(3)	0.131(2)	0.595(1)	2.6(8)*
C(5)	0.352(3)	0.084(2)	0.530(1)	1.8(7)*

Table 27. Continued.

	Atom	x -	у -	z -	B(A2)
•	C(6)	0.395(3)	0.252(2)	0.511(1)	2.8(8)*
	C(7)	-0.046(3)	0.208(2)	0.644(1)	3.3(9)*
	C(8)	0.086(3)	0.172(2)	0.554(1)	3.6(9)*
	C11	0.227(3)	-0.011(2)	0.627(1)	2.1(8)*
	C12	0.339(3)	-0.079(2)	0.630(1)	2.9(8)*
	C13	0.337(3)	-0.160(2)	0.608(1)	1.5(7)*
	C14	0.233(3)	-0.180(2)	0.591(1)	1.9(8)*
	C15	0.124(3)	-0.118(2)	0.588(1)	1.7(7)*
	C16	0.127(3)	-0.037(2)	0.608(1)	2.6(8)*
	C17	0.555(3)	-0.107(2)	0.643(1)	2.6(8)*
	C18	0.137(3)	-0.284(2)	0.549(1)	4.1(9)*
	C19	-0.091(3)	0.000(2)	0.591(1)	4.1(9)*
	C21	0.259(3)	0.087(2)	0.719(1)	1.9(8)*
	C22	0.357(3)	0.103(2)	0.746(1)	2.4(8)*
	C23	0.357(3)	0.108(2)	0.801(1)	2.9(8)*
	C24	0.251(3)	0.090(2)	0.830(1)	3.9(9)*
	C25	0.152(3)	0.072(2)	0.808(1)	2.5(8)*
	C26	0.155(3)	0.069(2)	0.750(1)	2.4(8)*
	C27	0.570(3)	0.127(2)	0.740(1)	2.8(8)*
	C28	0.149(4)	0.088(3)	0.920(2)	6(1)*
	C29	-0.044(3)	0.030(2)	0.754(1)	2.6(8)*
	C 51	0.280(3)	0.308(2)	0.675(1)	2.9(8)*
	C 52	0.324(3)	0.331(2)	0.724(1)	2.0(8)*
	c53	0.441(3)	0.350(2)	0.717(1)	2.6(8)*
	C 54	0.518(3)	0.351(2)	0.668(1)	3.5(9)*
	C 55	0.461(3)	0.328(2)	0.625(1)	2.2(8)*

Table 27. Continued.

Atom	x -	у -	z -	B(A2)
C56	0.337(3)	0.302(2)	0.625(1)	1.8(8)*
C57	0.652(3)	0.339(2)	0.570(1)	2.9(8)*
C58	0.434(3)	0.380(2)	0.813(1)	3.4(9)*
C59	0.093(3)	0.298(2)	0.731(1)	3.0(8)*
Ru(4)	-0.1518(3)	-0.1609(2)	0.8740(1)	2.75(8)
Ru(5)	-0.0280(3)	-0.3217(2)	0.8919(1)	2.35(8)
Ru(6)	-0.1233(3)	-0.2710(2)	0.7907(1)	1.97(7)
P(2)	0.0166(8)	-0.3980(6)	0.8123(4)	1.9(2)
C66	0.053(3)	-0.198(2)	0.862(1)	1.7(7)*
061	0.038(2)	-0.212(1)	0.7685(8)	2.4(5)*
C(11)	-0.205(3)	-0.138(2)	0.795(1)	3.1(8)*
C(12)	-0.135(3)	-0.050(2)	0.897(2)	4(1)*
C(13)	-0.312(3)	-0.144(2)	0.894(2)	5(1)*
C(14)	-0.124(3)	-0.241(2)	0.950(1)	2.7(8)*
C(15)	-0.121(3)	-0.409(2)	0.919(1)	4(1)*
C(16)	0.095(3)	-0.369(2)	0.939(1)	2.2(8)*
C(17)	-0.261(3)	-0.314(2)	0.813(1)	4.0(9)*
C(18)	-0.160(3)	-0.279(2)	0.717(1)	4.1(9)*
C31	0.165(3)	-0.407(2)	0.774(1)	1.7(7)*
C41	-0.024(3)	-0.509(2)	0.818(1)	2.1(8)*
032	0.057(2)	-0.446(1)	0.7042(8)	2.7(5)*
034	0.474(2)	-0.401(1)	0.6741(9)	3.4(6)*
036	0.271(2)	-0.379(1)	0.8482(8)	2.6(5)*
042	-0.179(2)	-0.469(1)	0.7537(8)	3.0(5)*
044	-0.123(2)	-0.753(2)	0.852(1)	5.3(7)*
046	0.134(2)	-0.547(1)	0.8758(9)	. 3.5(6)*

Table 27. Continued.

Atom	x -	у -	z -	B(A2)
063	0.393(2)	-0.128(2)	0.832(1)	4.6(6)*
065	0.071(2)	-0.175(1)	0.9558(9)	4.1(6)*
C32	0.166(3)	-0.427(2)	0.720(1)	2.6(8)*
C33	0.269(3)	-0.428(2)	0.684(1)	3.1(8)*
C34	0.367(3)	-0.407(2)	0.707(1)	2.4(8)*
C35	0.374(3)	-0.388(2)	0.760(1)	3.0(8)*
C36	0.270(3)	-0.394(2)	0.794(1)	1.6(7)*
C37	0.053(3)	-0.474(2)	0.650(1)	3.0(8)*
C38	0.481(3)	-0.417(2)	0.617(2)	5(1)*
C39	0.386(3)	-0.372(2)	0.869(1)	3.5(9)*
C42	-0.123(3)	-0.528(2)	0.791(1)	2.6(8)*
C43	-0.162(3)	-0.613(2)	0.799(1)	3.3(9)*
C44	-0.091(3)	-0.669(2)	0.840(1)	3.7(9)*
C45	0.003(3)	-0.654(2)	0.865(1)	3.5(9)*
C46	0.044(3)	-0.573(2)	0.854(1)	2.2(8)*
C47	-0.282(3)	-0.486(2)	0.724(1)	3.8(9)*
C48	-0.228(4)	-0.774(3)	0.826(2)	6(1)*
C49	0.193(4)	-0.602(3)	0.920(2)	6(1)*
C61	0.107(3)	-0.193(2)	0.809(1)	2.5(8)*
C62	0.220(3)	-0.169(2)	0.795(1)	2.2(8)*
C63	0.275(3)	-0.148(2)	0.837(1)	3.0(8)*
C64	0.235(3)	-0.148(2)	0.892(1)	3.2(9)*
C65	0.125(3)	-0.173(2)	0.902(1)	3.4(9)*
C67	0.088(3)	-0.199(2)	0.713(1)	2.4(8)*
C68	0.452(3)	-0.128(2)	0.778(1)	4(1)*
C69	0.143(3)	-0.165(2)	1.000(2)	5(1)*

Table 27. Continued.

atom	x	У	z	B(eq)
C(31)	0.235(2)	0.373(3)	0.452(2)	2.3(8)
C(32)	0.285(2)	0.425(3)	0.509(2)	3.5(9)
C(33)	0.287(2)	0.529(3)	0.522(2)	4(1)
C(34)	0.238(3)	0.584(4)	0.474(2)	6(1)
C(35)	0.181(2)	0.544(3)	0.425(2)	4(1)
C(36)	0.191(2)	0.434(3)	0.413(2)	2.5(8)
C(37)	0.272(3)	0.726(4)	0.542(3)	10(2)
C(38)	0.102(2)	0.447(3)	0.314(2)	4(1)

Table 28. Atomic positional parameters (\mathring{A}^2) and their estimated standard deviations for $Os_3(\mu\text{-OH})_2(TMPP)(CO)_9$.

Atom	x -	у -	2 -	B(A2)
0s1	0.31334(8)	0.50187(8)	0.68184(7)	2.76(2)
0s2	0.29534(9)	0.49045(8)	0.87981(7)	2.95(2)
0s3	0.19481(8)	0.66307(7)	0.81475(7)	2.41(2)
P1	0.1314(5)	0.8080(5)	0.7321(4)	2.4(1)
01	0.342(1)	0.660(1)	0.729(1)	3.0(3)*
02	0.148(1)	0.551(1)	0.697(1)	2.2(3)*
C(1)	0.267(2)	0.363(2)	0.660(2)	6.1(7)
C(2)	0.468(2)	0.472(2)	0.695(2)	7.0(7)
C(3)	0.326(2)	0.523(2)	0.547(2)	6.3(7)
C(4)	0.136(2)	0.419(2)	0.839(1)	5.5(6)
C(5)	0.265(2)	0.531(2)	1.014(2)	8.3(8)
C(6)	0.439(2)	0.588(2)	0.895(2)	7.1(7)
C(7)	0.377(2)	0.367(2)	0.880(1)	5.9(7)
C(8)	0.063(2)	0.640(2)	0.889(2)	6.3(7)
C(9)	0.265(2)	0.752(2)	0.929(2)	5.7(6)
0(1)	0.231(2)	0.270(1)	0.643(1)	6.4(5)
0(2)	0.567(1)	0.453(2)	0.711(1)	6.9(6)
0(3)	0.348(2)	0.526(2)	0.467(1)	6.4(6)
0(4)	0.048(1)	0.376(1)	0.818(2)	6.6(6)
0(5)	0.245(2)	0.553(2)	1.093(1)	8.6(7)
0(6)	0.523(1)	0.642(1)	0.898(1)	5.6(5)
0(7)	0.426(2)	0.292(1)	0.877(2)	7.4(6)
0(8)	-0.017(1)	0.630(2)	0.935(1)	6.8(6)

Table 28. Continued.

Atom	x -	у -	z -	B(A2)
0(9)	0.305(2)	0.798(1)	0.996(1)	6.1(5)
012	-0.024(1)	0.965(1)	0.843(1)	3.5(4)
014	0.302(1)	1.170(1)	1.025(1)	4.5(4)
016	0.366(1)	0.882(1)	0.799(1)	3.0(4)
022	0.031(1)	0.976(1)	0.643(1)	3.1(4)
024	-0.365(1)	0.830(1)	0.580(1)	3.7(4)*
026	-0.073(1)	0.641(1)	0.724(1)	3.6(4)
032	0.092(1)	0.663(1)	0.555(1)	2.5(3)
034	0.334(1)	0.844(1)	0.344(1)	4.2(4)
036	0.293(1)	0.994(1)	0.664(1)	2.4(3)*
C11	0.172(2)	0.924(2)	0.816(1)	4.3(5)
C12	0.092(2)	0.991(2)	0.864(2)	5.6(6)
C13	0.130(2)	1.075(2)	0.931(2)	4.8(6)
C14	0.253(2)	1.094(2)	0.953(2)	5.4(6)
C15	0.336(2)	1.033(2)	0.915(2)	4.9(6)
C16	0.294(2)	0.949(2)	0.843(1)	4.2(5)
C(12)	-0.104(2)	1.046(2)	0.865(2)	7.1(7)
C(14)	0.218(2)	1.240(2)	1.073(2)	8.6(8)
C(16)	0.491(2)	0.899(2)	0.829(2)	7.3(8)
C21	-0.021(2)	0.807(2)	0.687(2)	5.3(6)
C22	-0.057(2)	0.897(2)	0.646(1)	4.8(6)
C23	-0.172(2)	0.904(2)	0.611(2)	5.7(6)
C24	-0.252(2)	0.822(2)	0.612(2)	5.2(6)

Table 28. Continued.

Atom	x -	у -	z -	B(A2)
C25	-0.227(2)	0.726(2)	0.652(2)	6.3(6)
C26	-0.108(2)	0.724(2)	0.687(2)	5.2(6)
C(22)	-0.002(2)	1.076(1)	0.620(2)	6.0(7)
C(24)	-0.451(2)	0.737(2)	0.567(2)	7.2(8)
C(26)	-0.159(2)	0.550(2)	0.723(2)	7.3(7)
C31	0.200(2)	0.824(1)	0.618(1)	4.1(5)
C32	0.169(2)	0.747(2)	0.537(1)	4.2(5)
C33	0.212(2)	0.743(2)	0.442(1)	4.3(5)
C34	0.287(2)	0.830(2)	0.429(2)	5.6(6)
C35	0.319(2)	0.916(2)	0.505(2)	4.5(6)
C36	0.273(2)	0.912(2)	0.595(1)	3.8(5)
C(32)	-0.008(2)	0.638(2)	0.482(2)	5.7(6)
C(34)	0.292(2)	0.764(2)	0.261(2)	6.8(7)
C(36)	0.391(2)	1.072(2)	0.653(2)	6.8(7)
H1	0.410	0.719	0.716	4.3*
H2	0.066	0.527	0.659	3.2*

Table 29. Atomic positional parameters (\mathring{A}^2) and their estimated standard deviations for $Os_3(\mu\text{-OH})(TMPP\text{-}O)(CO)_9$.

atom	x	У	z	B(eq)
Os(1)	0.2793(1)	0.3381(1)	0.65171(8)	2.70(9)
Os(2)	0.4076(1)	0.1918(2)	0.66854(8)	3.5(1)
Os(3)	0.3357(1)	0.1938(1)	0.53559(7)	2.32(9)
P(1)	0.2605(6)	0.2373(8)	0.4358(4)	2.4(5)
0((1))	0.216(2)	0.264(2)	0.790(1)	6.0(8)
0(11)	0.333(1)	0.362(2)	0.555(1)	2.8(5)
0((2))	0.388(2)	0.494(2)	0.719(1)	5.8(7)
0(10)	0.223(1)	0.218(2)	0.594(1)	2.6(5)
0((3))	0.140(2)	0.483(3)	0.637(1)	6.7(8)
0((4))	0.264(2)	0.035(3)	0.701(1)	6.9(8)
0((5))	0.519(2)	0.013(3)	0.632(2)	11(1)
0((6))	0.517(2)	0.357(2)	0.598(1)	4.8(6)
0((7))	0.444(2)	0.238(3)	0.821(2)	10(1)
0((8))	0.323(2)	-0.036(3)	0.526(1)	7.0(8)
0((9))	0.502(2)	0.161(2)	0.469(1)	5.3(6)
0(12)	0.220(2)	0.690(3)	0.486(1)	6.5(7)
0(13)	0.153(1)	0.379(2)	0.361(1)	3.8(6)
0(14)	0.087(1)	0.280(2)	0.494(1)	2.1(5)
0(15)	-0.042(2)	-0.011(2)	0.402(1)	4.7(7)
0(16)	0.245(2)	0.035(2)	0.391(1)	4.3(6)
0(17)	0.416(1)	0.336(2)	0.411(1)	4.6(6)
0(18)	0.444(2)	0.249(2)	0.169(1)	4.9(7)
0(19)	0.195(1)	0.187(2)	0.291(1)	3.5(5)
C((1))	0.237(2)	0.284(3)	0.737(2)	4(1)
C((2))	0.342(2)	0.436(3)	0.695(2)	4(1)

Table 29. Continued.

atom	x	У	z	B(eq)
C((3))	0.194(3)	0.425(4)	0.644(2)	5(1)
C((4))	0.314(2)	0.095(3)	0.694(2)	3.6(9)
C((5))	0.481(3)	0.078(4)	0.650(2)	4(1)
C((6))	0.474(2)	0.296(4)	0.631(2)	4.1(9)
C((7))	0.429(3)	0.216(5)	0.767(3)	9(2)
C((8))	0.320(3)	0.056(4)	0.531(2)	6(1)
C((9))	0.437(2)	0.178(3)	0.499(2)	3.1(8)
C(11)	0.163(2)	0.172(3)	0.435(1)	2.5(7)
C(12)	0.090(2)	0.195(3)	0.455(1)	1.7(6)
C(13)	0.016(2)	0.142(3)	0.447(2)	4(1)
C(14)	0.026(2)	0.054(3)	0.418(2)	2.8(8)
C(15)	0.103(2)	0.002(3)	0.394(2)	2.6(8)
C(16)	0.174(2)	0.067(3)	0.407(2)	3.0(8)
C(17)	0.009(2)	0.336(3)	0.496(2)	4(1)
C(18)	-0.121(3)	0.019(3)	0.418(2)	5(1)
C(19)	0.264(3)	-0.071(4)	0.359(2)	7(1)
C(21)	0.305(2)	0.246(3)	0.349(2)	2.2(7)
C(22)	0.386(2)	0.288(3)	0.351(2)	2.1(7)
C(23)	0.435(2)	0.292(3)	0.290(2)	3.0(8)
C(24)	0.390(3)	0.251(3)	0.229(2)	5(1)
C(25)	0.313(2)	0.216(3)	0.228(1)	2.1(7)
C(26)	0.273(2)	0.210(3)	0.286(2)	2.7(8)
C(27)	0.495(3)	0.384(4)	0.409(2)	6(1)
C(28)	0.534(2)	0.262(3)	0.173(2)	5(1)
C(29)	0.161(2)	0.153(3)	0.229(2)	4(1)

Table 29. Continued.

Atom	x -	у -	z -	B(A2)
0(11)	-0.258(2)	-0.082(1)	0.7677(9)	3.6(6)
0(12)	-0.125(2)	0.019(2)	0.907(1)	5.7(8)
0(13)	-0.417(2)	-0.137(2)	0.906(1)	10(1)
0(14)	-0.164(2)	-0.238(2)	0.9942(8)	4.0(7)
0(15)	-0.167(3)	-0.460(2)	0.937(1)	8.4(9)
0(16)	0.168(2)	-0.398(2)	0.9660(9)	5.0(7)
0(17)	-0.340(2)	-0.346(2)	0.830(1)	5.8(8)
0(18)	-0.197(2)	-0.288(2)	0.676(1)	6.5(8)

